

BULLETIN OF RUSSIAN STATE MEDICAL UNIVERSITY

BIOMEDICAL JOURNAL OF PIROGOV RUSSIAN NATIONAL RESEARCH MEDICAL UNIVERSITY

EDITOR-IN-CHIEF Denis Rebrikov, DSc, professor

DEPUTY EDITOR-IN-CHIEF Alexander Oettinger, DSc, professor

EDITORS Valentina Geidebrekht, Nadezda Tikhomirova

TECHNICAL EDITOR Evgeny Lukyanov

TRANSLATORS Natalia Usman

DESIGN AND LAYOUT Marina Doronina

EDITORIAL BOARD

Averin VI, DSc, professor (Minsk, Belarus)
Alipov NN, DSc, professor (Moscow, Russia)
Belousov VV, DSc, professor (Moscow, Russia)
Bogomilskiy MR, corr. member of RAS, DSc, professor (Moscow, Russia)
Bozhenko VK, DSc, CSc, professor (Moscow, Russia)
Bylova NA, CSc, docent (Moscow, Russia)
Gainetdinov RR, CSc (Saint-Petersburg, Russia)
Gendlin GYe, DSc, professor (Moscow, Russia)
Ginter EK, member of RAS, DSc (Moscow, Russia)
Gorbacheva LR, DSc, professor (Moscow, Russia)
Gordeev IG, DSc, professor (Moscow, Russia)
Gudkov AV, PhD, DSc (Buffalo, USA)
Gulyaeva NV, DSc, professor (Moscow, Russia)
Gusev EI, member of RAS, DSc, professor (Moscow, Russia)
Danilenko VN, DSc, professor (Moscow, Russia)
Zarubina TV, DSc, professor (Moscow, Russia)
Zatevakhin II, member of RAS, DSc, professor (Moscow, Russia)
Kagan VE, professor (Pittsburgh, USA)
Kzyzhkowska YuG, DSc, professor (Heidelberg, Germany)
Kobrinskii BA, DSc, professor (Moscow, Russia)
Kozlov AV, MD PhD (Vienna, Austria)
Kotelevtsev YuV, CSc (Moscow, Russia)
Lebedev MA, PhD (Darem, USA)
Manturova NE, DSc (Moscow, Russia)
Milushkina OYu, DSc, professor (Moscow, Russia)
Mitupov ZB, DSc, professor (Moscow, Russia)
Moshkovskii SA, DSc, professor (Moscow, Russia)
Munblit DB, MSc, PhD (London, Great Britain)

Negrebetsky VV, DSc, professor (Moscow, Russia)
Novikov AA, DSc (Moscow, Russia)
Pivovarov YuP, member of RAS, DSc, professor (Moscow, Russia)
Platonova AG, DSc (Kiev, Ukraine)
Polunina NV, corr. member of RAS, DSc, professor (Moscow, Russia)
Poryadin GV, corr. member of RAS, DSc, professor (Moscow, Russia)
Razumovskii AYU, corr. member of RAS, DSc, professor (Moscow, Russia)
Rebrova OYu, DSc (Moscow, Russia)
Rudoy AS, DSc, professor (Minsk, Belarus)
Rylova AK, DSc, professor (Moscow, Russia)
Savelieva GM, member of RAS, DSc, professor (Moscow, Russia)
Semiglazov VF, corr. member of RAS, DSc, professor (Saint-Petersburg, Russia)
Skobolina NA, DSc, professor (Moscow, Russia)
Slavyanskaya TA, DSc, professor (Moscow, Russia)
Smirnov VM, DSc, professor (Moscow, Russia)
Spallone A, DSc, professor (Rome, Italy)
Starodubov VI, member of RAS, DSc, professor (Moscow, Russia)
Stepanov VA, corr. member of RAS, DSc, professor (Tomsk, Russia)
Suchkov SV, DSc, professor (Moscow, Russia)
Takhchidi KhP, member of RAS, DSc, professor (Moscow, Russia)
Trufanov GE, DSc, professor (Saint-Petersburg, Russia)
Favorova OO, DSc, professor (Moscow, Russia)
Filipenko ML, CSc, leading researcher (Novosibirsk, Russia)
Khazipov RN, DSc (Marsel, France)
Chundukova MA, DSc, professor (Moscow, Russia)
Shimanovskii NL, corr. member of RAS, DSc, professor (Moscow, Russia)
Shishkina LN, DSc, senior researcher (Novosibirsk, Russia)
Yakubovskaya RI, DSc, professor (Moscow, Russia)

SUBMISSION <http://vestnikrgmu.ru/login?lang=en>

CORRESPONDENCE editor@vestnikrgmu.ru

COLLABORATION manager@vestnikrgmu.ru

ADDRESS ul. Ostrovityanova, d. 1, Moscow, Russia, 117997

Indexed in Scopus. CiteScore 2021: 0.5

Scopus[®]

SCImago Journal & Country Rank 2020: 0.14

SJR

Scimago Journal & Country Rank

Indexed in WoS. JCR 2021: 0.5

WEB OF SCIENCE[™]

Listed in HAC 31.01.2020 (№ 507)



ВЫСШАЯ
АТТЕСТАЦИОННАЯ
КОМИССИЯ (БАК)

Five-year h-index is 8

Google
scholar

Open access to archive

CYBERLENINKA

Issue DOI: 10.24075/brsmu.2022-02

The mass media registration certificate № 012769 issued on July 29, 1994

Founder and publisher is Pirogov Russian National Research Medical University (Moscow, Russia)

The journal is distributed under the terms of Creative Commons Attribution 4.0 International License www.creativecommons.org



Approved for print 30.04.2022
Circulation: 100 copies. Printed by Print.Formula
www.print-formula.ru

ВЕСТНИК РОССИЙСКОГО ГОСУДАРСТВЕННОГО МЕДИЦИНСКОГО УНИВЕРСИТЕТА

НАУЧНЫЙ МЕДИЦИНСКИЙ ЖУРНАЛ РНИМУ ИМ. Н. И. ПИРОГОВА

ГЛАВНЫЙ РЕДАКТОР Денис Ребриков, д. б. н., профессор

ЗАМЕСТИТЕЛЬ ГЛАВНОГО РЕДАКТОРА Александр Эттингер, д. м. н., профессор

РЕДАКТОРЫ Валентина Гейдебрехт, Надежда Тихомирова

ТЕХНИЧЕСКИЙ РЕДАКТОР Евгений Лукьянов

ПЕРЕВОДЧИКИ Наталия Усман

ДИЗАЙН И ВЕРСТКА Марины Дорониной

РЕДАКЦИОННАЯ КОЛЛЕГИЯ

В. И. Аверин, д. м. н., профессор (Минск, Белоруссия)
Н. Н. Алипов, д. м. н., профессор (Москва, Россия)
В. В. Белоусов, д. б. н., профессор (Москва, Россия)
М. Р. Богомилский, член-корр. РАН, д. м. н., профессор (Москва, Россия)
В. К. Боженко, д. м. н., к. б. н., профессор (Москва, Россия)
Н. А. Былова, к. м. н., доцент (Москва, Россия)
Р. Р. Гайнетдинов, к. м. н. (Санкт-Петербург, Россия)
Г. Е. Гендлин, д. м. н., профессор (Москва, Россия)
Е. К. Гинтер, академик РАН, д. б. н. (Москва, Россия)
Л. Р. Горбачева, д. б. н., профессор (Москва, Россия)
И. Г. Гордеев, д. м. н., профессор (Москва, Россия)
А. В. Гудков, PhD, DSc (Буффало, США)
Н. В. Гуляева, д. б. н., профессор (Москва, Россия)
Е. И. Гусев, академик РАН, д. м. н., профессор (Москва, Россия)
В. Н. Даниленко, д. б. н., профессор (Москва, Россия)
Т. В. Зарубина, д. м. н., профессор (Москва, Россия)
И. И. Затевакин, академик РАН, д. м. н., профессор (Москва, Россия)
В. Е. Каган, профессор (Питтсбург, США)
Ю. Г. Кжышковска, д. б. н., профессор (Гейдельберг, Германия)
Б. А. Кобринский, д. м. н., профессор (Москва, Россия)
А. В. Козлов, MD PhD (Вена, Австрия)
Ю. В. Котелевцев, к. х. н. (Москва, Россия)
М. А. Лебедев, PhD (Дарем, США)
Н. Е. Мантурова, д. м. н. (Москва, Россия)
О. Ю. Милушкина, д. м. н., доцент (Москва, Россия)
З. Б. Митупов, д. м. н., профессор (Москва, Россия)
С. А. Мошковский, д. б. н., профессор (Москва, Россия)
Д. Б. Мунблит, MSc, PhD (Лондон, Великобритания)

В. В. Негребский, д. х. н., профессор (Москва, Россия)
А. А. Новиков, д. б. н. (Москва, Россия)
Ю. П. Пивоваров, д. м. н., академик РАН, профессор (Москва, Россия)
А. Г. Платонова, д. м. н. (Киев, Украина)
Н. В. Полунина, член-корр. РАН, д. м. н., профессор (Москва, Россия)
Г. В. Порядин, член-корр. РАН, д. м. н., профессор (Москва, Россия)
А. Ю. Разумовский, член-корр., профессор (Москва, Россия)
О. Ю. Реброва, д. м. н. (Москва, Россия)
А. С. Рудой, д. м. н., профессор (Минск, Белоруссия)
А. К. Рылова, д. м. н., профессор (Москва, Россия)
Г. М. Савельева, академик РАН, д. м. н., профессор (Москва, Россия)
В. Ф. Семглазов, член-корр. РАН, д. м. н., профессор (Санкт-Петербург, Россия)
Н. А. Скоблина, д. м. н., профессор (Москва, Россия)
Т. А. Славянская, д. м. н., профессор (Москва, Россия)
В. М. Смирнов, д. б. н., профессор (Москва, Россия)
А. Спаллоне, д. м. н., профессор (Рим, Италия)
В. И. Стародубов, академик РАН, д. м. н., профессор (Москва, Россия)
В. А. Степанов, член-корр. РАН, д. б. н., профессор (Томск, Россия)
С. В. Сучков, д. м. н., профессор (Москва, Россия)
Х. П. Тахчиди, академик РАН, д. м. н., профессор (Москва, Россия)
Г. Е. Труфанов, д. м. н., профессор (Санкт-Петербург, Россия)
О. О. Фаворова, д. б. н., профессор (Москва, Россия)
М. Л. Филипенко, к. б. н. (Новосибирск, Россия)
Р. Н. Хазипов, д. м. н. (Марсель, Франция)
М. А. Чундокова, д. м. н., профессор (Москва, Россия)
Н. Л. Шимановский, член-корр. РАН, д. м. н., профессор (Москва, Россия)
Л. Н. Шишкина, д. б. н. (Новосибирск, Россия)
Р. И. Якубовская, д. б. н., профессор (Москва, Россия)

ПОДАЧА РУКОПИСЕЙ <http://vestnikrgmu.ru/login>

ПЕРЕПИСКА С РЕДАКЦИЕЙ editor@vestnikrgmu.ru

СОТРУДНИЧЕСТВО manager@vestnikrgmu.ru

АДРЕС РЕДАКЦИИ ул. Островитянова, д. 1, г. Москва, 117997

Журнал включен в Scopus. CiteScore 2021: 0,5

Журнал включен в WoS. JCR 2021: 0,5

Индекс Хирша (h²) журнала по оценке Google Scholar: 8

Scopus®

WEB OF SCIENCE™

Google
scholar

Scimago Journal & Country Rank 2020: 0,14

Журнал включен в Перечень 31.01.2020 (№ 507)

Здесь находится открытый архив журнала

SJR
Scimago Journal & Country Rank

ВЫСШАЯ
АТТЕСТАЦИОННАЯ
КОМИССИЯ (ВАК)

CYBERLENINKA

DOI выпуска: 10.24075/vrgmu.2022-02

Свидетельство о регистрации средства массовой информации № 012769 от 29 июля 1994 г.

Учредитель и издатель — Российский национальный исследовательский медицинский университет имени Н. И. Пирогова (Москва, Россия)

Журнал распространяется по лицензии Creative Commons Attribution 4.0 International www.creativecommons.org



Подписано в печать 30.04.2022
Тираж 100 экз. Отпечатано в типографии Print.Formula
www.print-formula.ru

ORIGINAL RESEARCH**5****Development of a recombinant oncolytic poliovirus type 3 strain with altered cell tropism**

Hamad A, Soboleva AV, Vorobyev PO, Mahmoud M, Vasilenko KV, Chumakov PM, Lipatova AV

Разработка рекомбинантного онколитического штамма полиовируса 3-го типа с измененным клеточным тропизмом

А. Н. Хамад, А. В. Соболева, П. О. Воробьев, М. А. Махмуд, К. В. Василенко, П. М. Чумаков, А. В. Липатова

ORIGINAL RESEARCH**11****Models of mitochondrial dysfunction with inducible expression of *Polg* pathogenic mutant variant**

Kubekina MV, Kalinina AA, Korshunova DS, Bruter AV, Silaeva YY

Модели митохондриальной дисфункции с индуцируемой экспрессией мутантного варианта гена *Polg*

М. В. Кубекина, А. А. Калинина, Д. С. Коршунова, А. В. Брутер, Ю. Ю. Силаева

ORIGINAL RESEARCH**18****Footprints of interaction among Finnic-speaking, Slavic, and Turkic-speaking populations in modern gene pool and their reflection in pharmacogenetics**

Balanovska EV, Gorin IO, Ponomarev GY, Pylev VY, Petrushenko VS, Markina NV, Mamaeva AD, Larin AK, Agdzhoyan AT

Следы взаимодействия финноязычного, славянского и тюркоязычного населения в современном генофонде и их отражение в фармакогенетике

Е. В. Балановская, И. О. Горин, Г. Ю. Пономарев, В. Ю. Пылёв, В. С. Петрушенко, Н. В. Маркина, А. Д. Мамаева, А. К. Ларин, А. Т. Агджоян

ORIGINAL RESEARCH**28****Activity of nuclear factor κ B in lymphocyte populations of children with psoriasis**

Kuptsova DG, Petrichuk SV, Murashkin NN, Kurbatova OV, Radygina TV, Khotko AA, Ivanov RA

Активность ядерного фактора транскрипции κ B в популяциях лимфоцитов у детей с псориазом

Д. Г. Купцова, С. В. Петричук, Н. Н. Мурашкин, О. В. Курбатова, Т. В. Радыхина, А. А. Хотко, Р. А. Иванов

ORIGINAL RESEARCH**36****Effects of COVID-19 vector vaccine on autoantibody profile in reproductive age women**

Dovgan AA, Drapkina YuS, Dolgushina NV, Menzhinskaya IV, Krechetova LV, Sukhikh GT

Влияние векторной вакцины от COVID-19 на профиль аутоантител у женщин репродуктивного возраста

А. А. Довгань, Ю. С. Драпкина, Н. В. Долгушина, И. В. Менжинская, Л. В. Кречетова, Г. Т. Сухих

ORIGINAL RESEARCH**43****Experience of tocilizumab in hospital patients with moderate COVID-19**

Burgasova OA, Dolinniy SV, Tetova VB, Ogarkova DA, Odnoralov MA, Bacalin VV, Smetanina SV, Antipyat NA, Taranova MV

Опыт применения тоцилизумаба у стационарных пациентов со среднетяжелым течением COVID-19

О. А. Бургасова, С. В. Долинный, В. Б. Тетова, Д. А. Огаркова, М. А. Оdnoralov, В. В. Бакалин, С. В. Сметанина, Н. А. Антипат, М. В. Таранова

ORIGINAL RESEARCH**50****Microglia and putative macrophages of the subfornical organ: structural and functional features**

Guselnikova VV, Razenkova VA, Sufieva DA, Korzhevskii DE

Микроглия и предполагаемые макрофаги субфорникального органа: структурно-функциональные особенности

В. В. Гусельникова, В. А. Разенкова, Д. А. Суфиева, Д. Э. Коржевский

ORIGINAL RESEARCH**58****Regenerative effects of Gly-His-Lys and Gly-His-Lys-D-Ala peptides in infected skin wounds**

Rakimova KK, Mishina ES, Vorvul AO, Bobyntsev II, Dolgintsev ME, Bezgin AI

Регенеративные эффекты пептидов Gly-His-Lys и Gly-His-Lys -D-Ala при кожной инфицированной ране

К. К. Рахметова, Е. С. Мишина, А. О. Ворвуль, И. И. Бобынцев, М. Е. Долгинцев, А. И. Бежин

ORIGINAL RESEARCH

65

Specific features of memory consolidation and reconsolidation in older individuals with vision and hearing impairments

Zakharova IA, Petrash EA, Nikishina VB, Razuvaeva TN, Shuteeva TV

Особенности процессов консолидации и реконсолидации памяти при зрительных и слуховых нарушениях в пожилом возрасте

И. А. Захарова, Е. А. Петраш, В. Б. Никишина, Т. Н. Разуваева, Т. В. Шутеева

ORIGINAL RESEARCH

73

Hemoperfusion and functional state of the macula after simultaneous pancreas and kidney transplantation

Vorobyeva IV, Bulava EV, Moshetova LK, Pinchuk AV

Гемоперфузия и функциональное состояние макулы после сочетанной трансплантации почки и поджелудочной железы

И. В. Воробьева, Е. В. Булава, Л. К. Мошетова, А. В. Пинчук

ORIGINAL RESEARCH

79

The influence of migration factor on the establishment of menstrual function in girls

Milushkina OYu, Popov VI, Skoblina NA, Bokareva NA, Astashkevich EV, Zakharova AA, Skoblina EV

Влияние фактора миграции на становление менструальной функции у девочек

О. Ю. Милушкина, В. И. Попов, Н. А. Скоблина, Н. А. Бокарева, Е. В. Асташкевич, А. А. Захарова, Е. В. Скоблина

CLINICAL CASE

84

Chronic non-treated posterior fracture-dislocation of the shoulder

Egiazaryan KA, Ershov DS, Badriev DA, Soshnikov DY

Застарелый задний переломовывих плеча

К. А. Егизарян, Д. С. Ершов, Д. А. Бадриев, Д. Ю. Сошников

ORIGINAL RESEARCH

88

The impact of image orientation on distribution of visual fixations while solving simple cognitive problems

Nikishina VB, Petrash EA, Prirodova OF, Akhramenko RS, Danilova AV, Kuznetsova AA

Влияние ориентационных характеристик изображения на распределение зрительных фиксаций при решении простых когнитивных задач

В. Б. Никишина, Е. А. Петраш, О. Ф. Природова, Р. С. Ахраменко, А. В. Данилова, А. А. Кузнецова

DEVELOPMENT OF A RECOMBINANT ONCOLYTIC POLIOVIRUS TYPE 3 STRAIN WITH ALTERED CELL TROPISM

Hamad A^{1,2,3}, Soboleva AV¹, Vorobyev PO¹, Mahmoud M^{1,2}, Vasilenko KV⁴, Chumakov PM¹, Lipatova AV¹✉

¹ Engelhardt Institute of Molecular Biology, Moscow, Russia

² Moscow Institute of Physics and Technology (MIPT), Moscow, Russia

³ Center for Precision Genome Editing and Genetic Technologies for Biomedicine, Engelhardt Institute of Molecular Biology, Moscow, Russia

⁴ Pirogov Russian National Research Medical University, Moscow, Russia

Diffuse gliomas are incurable, prevalent, and aggressive central nervous system tumors. Therefore, the development of selective oncolytic viral strains for malignant neoplasms is highly relevant. This study aimed to create an oncolytic virus based on a vaccine strain of poliovirus type 3 with natural antitumor activity. To achieve this goal, we replaced the internal ribosome entry site (IRES) of poliovirus with the corresponding fragment of human rhinovirus 30. The resulting recombinant oncolytic strain RVP3 retained the serotype of poliovirus type 3, as confirmed by virus neutralization micro-test with specific antiserum. In addition, the oncolytic efficacy of RVP3 was assessed *in vitro* on a broad panel of cell cultures. According to the results, RVP3 has changed its tropism, losing the ability to replicate in conditionally normal cell lines of embryonic astrocytes and embryonic fibroblasts while retaining the ability to replicate in tumor cells.

Keywords: oncolytic viral therapy, glioma, vaccine strain of poliovirus

Funding: the project was supported by the Russian Science Foundation (agreement number 20-75-10157 of 14 August 2020 "Research on the possibilities of obtaining recombinant strains of oncolytic viruses with tumor-specific replication and immunomodulatory protein expression").

Author contribution: Chumakov PM, Lipatova AV — study concept and planning, data analysis; Hamad A, Vorobyev PO, Soboleva AV, Mahmoud M, Vasilenko KV, and Lipatova AV — laboratory experimental work; Hamad A, Soboleva AV, and Lipatova AV — preparation of figures and data interpretation.

Compliance with ethical standards: the study was conducted per the requirements of the World Medical Association Declaration of Helsinki 2000 and its subsequent revisions; in compliance with the principles of the European Convention for the Protection of Vertebrate Animals used for Experimental and other Scientific Purposes.

✉ **Correspondence should be addressed:** Anastasia V. Lipatova
Vavilova, 32/1, Moscow, 119991, Russia; lipatovaanv@gmail.com

Received: 18.04.2022 **Accepted:** 28.04.2022 **Published online:** 30.04.2022

DOI: 10.24075/brsmu.2022.023

РАЗРАБОТКА РЕКОМБИНАНТНОГО ОНКОЛИТИЧЕСКОГО ШТАММА ПОЛИОВИРУСА 3-ГО ТИПА С ИЗМЕНЕННЫМ КЛЕТОЧНЫМ ТРОПИЗМОМ

А. Н. Хамад^{1,2,3}, А. В. Соболева¹, П. О. Воробьев¹, М. А. Махмуд^{1,2}, К. В. Василенко⁴, П. М. Чумаков¹, А. В. Липатова¹✉

¹ Московский физико-технический институт (МФТИ), Москва, Россия

² Институт молекулярной биологии имени В. А. Энгельгардта, Москва, Россия

³ Центр высокоточного редактирования и генетических технологий для биомедицины, Институт молекулярной биологии имени В. А. Энгельгардта, Москва, Россия

⁴ Российский национальный исследовательский медицинский университет имени Н. И. Пирогова, Москва, Россия

Диффузная глиома является неизлечимым заболеванием, наиболее распространенным и агрессивным типом опухолей ЦНС. Разработка высокоонкоселективных вирусных штаммов для терапии злокачественных новообразований является актуальной задачей. Целью работы было создание онколитического вируса на базе вакцинного штамма полиовируса 3-го типа, обладающего природной противоопухолевой активностью, путем замены IRES полиовируса соответствующим участком из риновируса человека 30 типа. В результате был успешно получен рекомбинантный онколитический штамм RVP3, сохранивший серотип полиовируса 3-го типа, что было подтверждено микрореакцией нейтрализации специфической антисывороткой. Онколитическая эффективность RVP3 была оценена *in vitro* на широкой панели клеточных культур. RVP3 изменил тропизм, потеряв способность эффективно реплицироваться в условно нормальных клеточных линиях эмбриональных астроцитов и эмбриональных фибробластов, сохранив способность эффективно реплицироваться в опухолевых клетках.

Ключевые слова: онколитическая виротерапия, глиома, вакцинный штамм полиовируса

Финансирование: проект был поддержан Российским научным фондом (Соглашение №20-75-10157 от 14 августа 2020 г. «Изучение возможностей получения рекомбинантных штаммов онколитических вирусов с опухоль-специфической репликацией и экспрессией иммуномодулирующих белков»).

Вклад авторов: П. М. Чумаков, А. В. Липатова — разработка концепции и плана экспериментов, анализ данных; А. Н. Хамад, П. О. Воробьев, А. В. Соболева, М. А. Махмуд, К. В. Василенко и А. В. Липатова — проведение лабораторных экспериментов; А. Н. Хамад, А. В. Соболева и А. В. Липатова — подготовка рисунков и интерпретация результатов.

Соблюдение этических стандартов: исследование проведено в соответствии с требованиями Хельсинкской декларации Всемирной медицинской ассоциации (2000 г.) и последующих ее пересмотров; с соблюдением принципов Европейской конвенции по защите позвоночных животных, используемых в экспериментальных исследованиях.

✉ **Для корреспонденции:** Анастасия Валерьевна Липатова
ул. Вавилова, д. 32/1, г. Москва, 119991, Россия; lipatovaanv@gmail.com

Статья получена: 18.04.2022 **Статья принята к печати:** 28.04.2022 **Опубликована онлайн:** 30.04.2022

DOI: 10.24075/vrgmu.2022.023

Table. Oligonucleotide sequences used for RVP3 DNA amplification

№	ID	Sequence	Melting temperature, °C
1	HRV30 IRES for	tttatactccctcccttagaagttttacataaagaccaataggt	56
2	HRV30 IRES rev	taagttaaggagtaaaacgcgaattgtctattacgact	56
3	P3vect for	ttttactccttaactattgaaattgtttgaagac	57
4	P3vect rev	gggaggaggagtataaaacaggcgta	57

Diffuse glioma (glioblastoma) is the most prevalent and aggressive type of primary central nervous system malignancies [1]. Relapses occur in almost 100% of the cases. Despite all standard treatment approaches, the average survival is 12–18 months post-diagnosis, including surgical resection, radiation, chemo- and targeted therapies [2]. Alternative treatment approaches include viral treatment based on non-pathogenic oncolytic strains. Such strains may show natural tropism to tumor cells; besides, the antitumor properties can be deliberately enhanced by modifying viral genomes. The development of productive viral infection in a tumor activates innate and adaptive antitumor response [3–5], facilitating the elimination of tumor cells.

A recombinant oncolytic strain PVS-RIPO was developed to treat glioblastoma [6]. Intratumor administration of PVS-RIPO combined with chemotherapy and radiotherapy afforded prolonged remissions (over three years) in 21% of the patients [7].

PVS-RIPO is an attenuated non-pathogenic oncolytic virus created based on poliovirus type 1 Sabin vaccine strain, where the internal ribosome entry site (IRES) is replaced with the corresponding sequence of human rhinovirus type 2 (HRV2). The antitumor efficacy of PVS-RIPO is due primarily to the natural tropism of polioviruses to tumor cells, notably in tumors of the nervous system. Polioviruses enter cells by binding the PVR/CD155 cellular receptor, which is significantly overexpressed in solid tumors and in the tumor microenvironment [7–9]. However, polioviruses may exhibit neurotoxicity when administered systemically or intratumorally that is related with their ability to infect normal neurons. Tropism of polioviruses is not only determined by cell surface receptors and the structure of the viral IRES, which mediates the interactions of viral RNA with some tissue-specific cytoplasmic factors that modulate translation initiation efficiency [10, 11]. For instance, cellular factor DRBP76 can specifically bind the 3'-region of IRES in the rhinovirus HRV2 RNA, thereby inhibiting its translation in cells of neuronal origin [12]. The high tropism of polioviruses to neurons can be partially explained by the low binding affinity between DRBP76 and IRES. The oncolytic PVS-RIPO contains chimeric 5' UTR combining the cloverleaf of polio- with IRES of rhinovirus, limiting the infection to cells originating from glia and some other tissues; most importantly, it spares neurons [13]. Apart from brain tumors, PVS-RIPO is undergoing clinical

trials for unresectable melanomas [14], and many other immunotherapy-sensitive tumors that may also respond to the viral therapy. In the context of the increasing incidence of malignant neoplasms, the development of oncolytic viral strains becomes particularly urgent. The use of heterologous IRESes allows deliberate customization of viral tropism depending on the individual characteristics. At the same time, the expanded arsenal of available oncolytic strains enables a personalized selection of antitumor medications. Here we report a new recombinant oncolytic virus derived from the poliovirus type 3 Sabin vaccine strain by replacing a large segment of polioviral IRES with the corresponding sequence of human rhinovirus 30.

METHODS

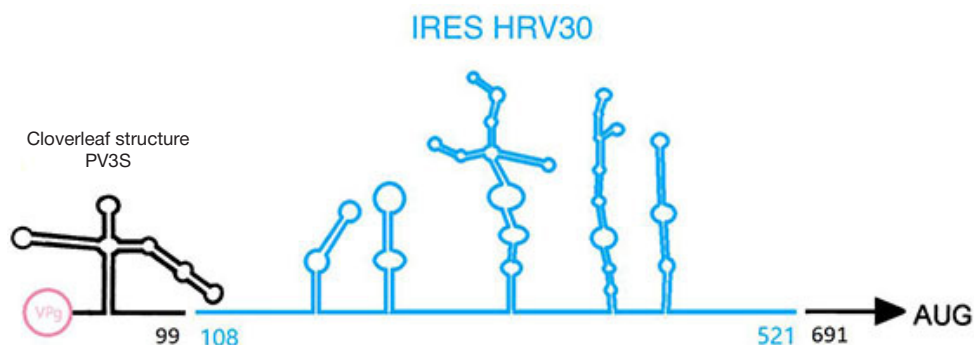
Development of recombinant viral strain RVP3

The recombinant viral strain RVP3 was created based on the poliovirus type 3 Sabin vaccine strain (PV3S). A pUC18 plasmid construct containing PV3S genome sequence under the control of T7 promoter was developed in the Laboratory of Cell Proliferation at Engelhardt Institute of Molecular Biology. The nucleotide sequence of the rhinovirus A30 (HRV30) 5'-noncoding region was accessed from the GenBank database (Human rhinovirus 30 strain ATCC VR-1140, FJ445179.1). The HRV30 genome fragment (nucleotides 108–521) was custom synthesized by IDT DNA (USA). The plasmid encompassing the final recombinant strain genome was obtained by ligase-free cloning of two fragments generated by PCR with primers listed in Table following a published protocol [15]. A scheme of the product is given in Fig. 1.

To obtain the infectious genomic RNA, the plasmid construct was transfected into HEK293T cells with a plasmid expressing codon-optimized T7 polymerase as described elsewhere [16]. At 36–48 h post-transfection, the medium was harvested and used for infection of fresh HEK293T cells to account for cytopathic foci and plaque formation.

Production of viral particles

The PV3S and RVP3 enteroviruses were produced in the RD and HEK293T cells. The cells were plated 24 h before the

**Fig. 1.** A scheme of 5' UTR in RVP3. The chimeric region combines sequences of rhinovirus and poliovirus type 3

infection at 70% confluence and MOI = 0.1. The cytopathic effect developed at 24 h post-transfection. The harvested medium was clarified from cell debris by centrifugation at +4 °C, 2500 rpm for 15 min. The virus-containing supernatant was stored in 0.5 mL aliquots at –80 °C.

Production of anti-PV3 sheep antiserum and virus neutralization micro tests

The study used a six-month-old lamb of the Dorper breed. The animal was obtained from the "Capri" breeding farm (Kaluga region, Russia) and housed under standard farming conditions with regular anthelmintic prophylaxis; the diet included hay, compound feed, and vitamin supplements.

For immunization, 1 mL of virus-containing supernatant (10^9 infectious units) was mixed with an equal volume of complete Freund's adjuvant (DIFCO; USA). The mixture was homogenized to a stable suspension and administered to the animal intradermally (0.1 mL on both sides in the hind thigh area) and intramuscularly (0.4 mL on both sides in the thigh muscles). Further injections were carried out similarly, but the virus was mixed with incomplete Freund's adjuvant (DIFCO; USA) 4 times at 7-day intervals. During the experiment, the lamb was housed separately from the herd. Seven days after the fifth injection, the blood was collected in several 9 mL vacuum tubes with coagulant — 40 mL from the jugular vein. The animal was not subject to slaughter and joined the herd. The collected blood was left for 4 h until the clot formation; the serum was clarified by centrifugation at 5000 rpm for 15 min. The serum was stored in aliquots at –70 °C.

Serotype of the new strain was verified by infectivity neutralization micro test using specific sheep antiserum to poliovirus type 3 in accordance with a published protocol [17]. The virus-containing supernatant was incubated for 2 hours with antiserum in 23 consecutive dilutions (1:10,000, 1:7,500, 1:5,000, 1:4,000, 1:3,500, 1:3,000, 1:2,500, 1:2,000, 1:1,500, 1:1,000, 1:750, 1:500, 1:200, 1:100, 1:75, 1:50, 1:30, 1:20, 1:15, 1:10, 1:7, 1:5, and 1:1). Apart from PV3S and RVP3, we tested other non-pathogenic oncolytic strains: Coxsackie B5 (CVB5, GenBank: MG642820.1), Coxsackie A7 (CVA7, GenBank: JQ041367.1) and prototype strain echovirus 12 Travis (ECHO12T, GenBank: X79047.1).

Cell line sensitivity and viral replication efficiency assays

To assess the sensitivity of cell lines to viral infections, the cells were plated in 96-well plates to 40% confluence (4×10^3 to 4×10^5 cells per well, depending on the culture). The next day, the cells were infected with the virus in serum-free DMEM at a wide multiplicity range (MOI = 0.001–100). After 1 h adsorption of the virus, the medium was replaced with DMEM supplemented with 1% fetal bovine serum (FBS). The viability was assessed by MTT test at 72 h. TCID₅₀ values were calculated for ease of interpretation by the Reed–Muench method [18]. The titrations were carried out in four technical parallels and three independent biological replicates.

To assess the replication efficiency, the cells were plated in 12-well plates to 50% confluence and infected by incubation with the virus (MOI = 0.1) in DMEM at 37 °C for 1 h. Then, the cells were washed from the virus and placed in a fresh medium with 0.5% FBS. The supernatants were harvested 48 h after infection. Viral replication capacity was determined by titration on HEK293T cells infected with serially diluted supernatants (Reed–Muench method).

RESULTS

RVP3 reconstitution and production in cell cultures

At 48 h after cotransfection of HEK293T cells with RVP3 genome-containing construct and codon-optimized T7 polymerase-expressing plasmid, accumulation of infectious particles in the supernatant was determined by measuring the cytopathic effect upon re-infection of fresh HEK293T monolayers. The virus was subjected to over 15 adaptation passages before its preparative production in HEK293T and RD cell lines. The titers were determined by Reed–Muench method; the results of the replication efficiency assay for RVP3 and PV3S are shown in Fig. 2. HEK293T cell line, which showed higher replication efficiency, was chosen for subsequent virus production.

RVP3 retains the serotype of poliovirus type 3

In virus neutralization micro tests, effective inactivation of PV3S was achieved at 1:3000–1:2500 dilutions of anti-PV3 sheep antiserum, whereas cross-inactivation of enteroviruses of another serotype (Coxsackie A7 and B5, and echovirus 12) was effective in 1:10–1:7 dilutions only, which confirmed high specificity of the serum. Effective inactivation of RVP3 was achieved at 1:2000–1:1500 dilutions of anti-PV3 sheep antiserum, indicating the retention of poliovirus type 3 serotype by RVP3 (Fig. 3).

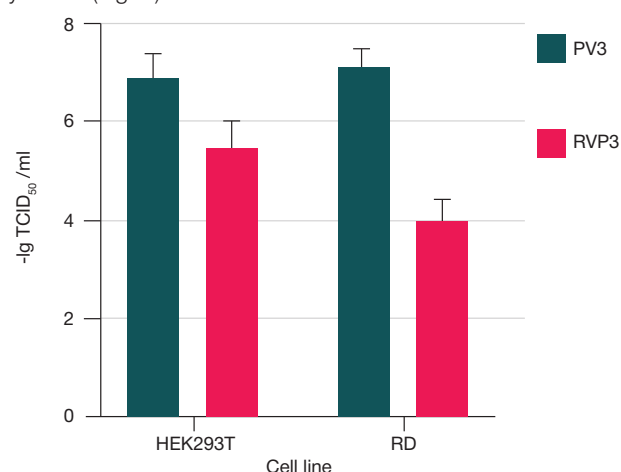


Fig. 2. Comparison of viral titers for enterovirus-sensitive cell cultures RD and HEK293T

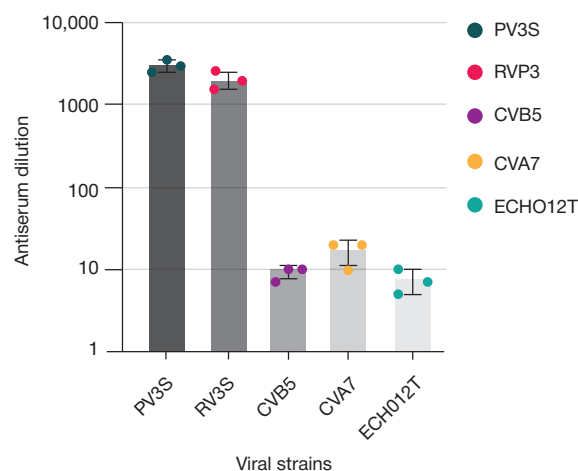


Fig. 3. Results of anti-poliovirus type 3 neutralization microtests for different viral strains

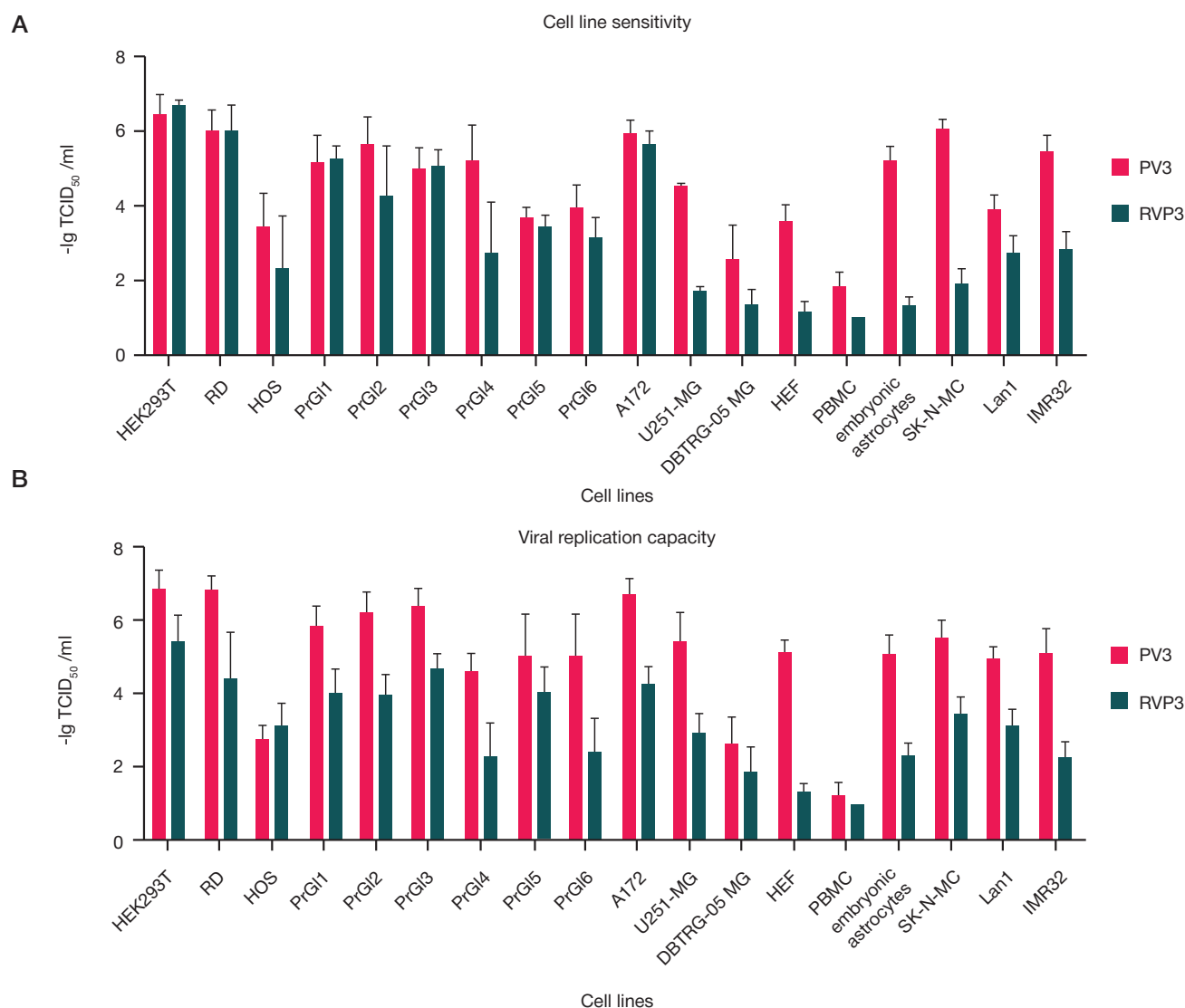


Fig. 4. *In vitro* functional tests for RVP3 and PV3S. A. Cell line sensitivity to infection. B. Viral replication capacity

Comparison of *in vitro* cytolytic activity for RVP3 and PV3S

Comparative assessment of cytolytic effects for the new RVP3 and the original PV3S viral strains involved the scope of tumor and conditionally normal cell lines; the results are shown in Fig. 4. The tumor cell lines included three model glioblastoma cultures DBTRG-05 MG, A-172, and U-251 MG (ATCC; USA); six low-passage glioblastoma cell lines PrGI1, PrGI2, PrGI3, PrGI4, PrGI5, and PrGI6 developed and characterized in Laboratory of Cell Proliferation at Engelhardt Institute of Molecular Biology [19]; three model neuroblastoma cell lines SK-N-MC, Lan1, and IMR-32 purchased from "Collection of vertebrate cell cultures" at the Institute of Cytology RAS (Russia); and two tumor cell lines RD and HOS from the collection of Laboratory of Cell Proliferation at Engelhardt Institute of Molecular Biology. The conditionally normal cells included human embryonic fibroblasts (HEF) and normal embryonic astrocytes from the Laboratory of Immunocytochemistry at Serbsky Research Center for Psychiatry and Narcology (Russia); and peripheral blood mononuclear cells (PBMC) from two patients.

Both viruses demonstrated high oncolytic activity against the studied panel of cultures. The RVP3 replication efficiency was significantly lower, with a profound decrease in HEF and embryonic astrocytes.

DISCUSSION

The development of selective oncolytic viral strains showing specific enhancement of replication efficiency in malignant neoplasms with negligible damage to normal cells is pivotal for the future of oncolytic viral strategies.

The differential tropism of enteroviruses toward cell type is determined by differential expression of specific cell surface proteins used as entry receptors and viral 5' UTR structure, notably its internal ribosome entry site (IRES). The efficiency of viral RNA translation largely depends on its binding with certain cellular regulatory factors, the availability of which varies in tissue- and tumor-specific manner. Accordingly, the same viral strain may show high antitumor efficacy in one patient. Still, it cannot replicate and kill tumor cells in another patient because of the difference in expression profiles of receptors or translation factors. Considering the considerable diversity of tumor cell types, the oncolytic viral strategies must involve a personalized selection of suitable therapeutic options from a large arsenal of viral strains with different cell tropisms. IRES modification provides an additional source of viral strain diversity and a tool for studying the effects of individual structural elements on the target cell specificity and replication efficiency of therapeutic viruses.

We constructed a recombinant variant based on the poliovirus type 3 Sabin (PV3S) vaccine strain using this concept. Of the three

available vaccine strains of polioviruses, PV3S showed the most effective lytic properties against primary glioblastoma cell lines. The IRES of PV3S differs by only one nucleotide substitution from the IRES of wild pathogenic PV3 Leon strain, from which it has been derived by lengthy passaging in monkey cells [20]. For this reason, PV3S is more susceptible to reversion causing vaccination-associated poliomyelitis than PV1S [21]. Replacement of the 5' regulatory region in PV3S with the corresponding sequence of rhinovirus prevents the possibility of reversion and enhances the safety of a candidate oncolytic construct.

Thanks to the global anti-polio vaccination campaign involving the trivalent live poliovirus vaccine, almost the entire population of the planet have lifelong immunity to polio. For PV3S, neutralization with vaccine-derived antibodies in vaccinated individuals is less effective compared with the other two variants of polioviruses [22], which may endow it with higher anticancer efficacy.

Functional tests using a panel of tumor and conditionally normal cell cultures (Fig. 4) revealed significantly altered cell tropism of RVP3 compared with PV3S. Despite the similar rates of RVP3 and PV3S replication in HOS osteosarcoma cells, in other cultures replication of the recombinant virus was 2–4 orders less productive. The relative replication efficiency changed accordingly: in cultures with top rates of PV3S replication (e.g., PrGl6 and U251MG), RVP3 replication was medium or low. We also observed no substantial differences for neuroblastoma cell lines. Despite the reduced replication efficiency of RVP3 in SK-N-MC, Lan1, and IMR-32 cells compared with PV3S, the infection still occurred and killed the cells. We can assume that neuroblastoma cells may have specific IRES-interacting protein expression signatures different from tumors and normal central nervous system neurons.

Moreover, the novel RVP3 strain revealed enhanced selectivity toward malignant cells: its replication efficiency in normal astrocytes and embryonic fibroblasts was, respectively, three and four orders of magnitude lower compared with PV3S, whereas its ability to replicate in peripheral blood mononuclear leukocytes were minimal.

The global experience of over a billion administrations of the live oral polio vaccines, entering the circulation via Peyer's patches and crossing the blood-brain barrier, confirms their safety in terms of neurological symptoms or emergence of the virus in the central nervous system. It should be noted that human cells propagated *in vitro* are usually more susceptible to viral infections than cells and tissues of the body. Continual passaging in artificial media significantly reorganize cell metabolism [23]. Therefore, *in vitro* cell sensitivity cannot be considered ultimate evidence of viral pathogenicity. However, the results of *in vitro* tests must not be discounted altogether: viruses with low *in vitro* replication efficiency are less likely to be pathogenic. For this reason, cell cultures provide essential test targets for the candidate therapeutic viral strains, which should be highly active in a tumor, but have minimal effect in normal tissues.

Further investigation of possibilities for targeting enteroviral replication within the human body by modifying IRES sequences will increase the availability of safe therapeutic viral strains for personalized anticancer therapy.

CONCLUSIONS

The recombinant oncolytic viral strain RVP3 was developed by replacement of the internal ribosome entry site (IRES) of poliovirus with the corresponding sequence of human rhinovirus 30. The developed strain retains the original serotype of poliovirus type 3 and can be successfully replicated in model cell cultures. The oncolytic activity of RVP3 was validated *in vitro* on a broad panel of cell cultures. The strain shows altered tropism, with a profoundly decreased efficiency to replicate in conditionally normal cell lines of embryonic astrocytes and embryonic fibroblasts. The enhanced target scope of the new recombinant virus with regard to tumor cell lines makes it an excellent oncolytic alternative to the prototype vaccine strain of poliovirus.

References

1. Louis DN, Perry A, Wesseling P, Brat DJ, Cree IA, Figarella-Branger D, et al. The 2021 WHO Classification of Tumors of the Central Nervous System: a summary. *Neuro Oncol.* 2021; 23: 1231–51.
2. Carpenter AB. Recombinant oncolytic poliovirus for glioblastoma: A current review of PVS (RIPO). *Georgetown Medical Review.* 2019; 3: 7789.
3. Brown MC, Dobrikova EY, Dobrikov MI, Walton RW, Gemberling SL, Nair SK, et al. Oncolytic polio virotherapy of cancer. *Cancer.* 2014; 120: 3277–86.
4. Ribas A, Dummer R, Puzanov I, VanderWalde A, Andtbacka RHI, Michielin O, et al. Oncolytic Virotherapy Promotes Intratumoral T Cell Infiltration and Improves Anti-PD-1 Immunotherapy. *Cell.* 2018; 174: 1031–2.
5. Twumasi-Boateng K, Pettigrew JL, Kwok YYE, Bell JC, Nelson BH. Oncolytic viruses as engineering platforms for combination immunotherapy. *Nat Rev Cancer.* 2018; 18: 419–32.
6. Gromeier M, Alexander L, Wimmer E. Internal ribosomal entry site substitution eliminates neurovirulence in intergeneric poliovirus recombinants. *Proceedings of the National Academy of Sciences.* 1996; 93: 2370–5.
7. Desjardins A, Gromeier M, Herndon JE, 2nd, Beaubier N, Bolognesi DP, Friedman AH, et al. Recurrent Glioblastoma Treated with Recombinant Poliovirus. *N Engl J Med.* 2018; 379: 150–61.
8. Sloan KE, Eustace BK, Stewart JK, Zehetmeier C, Torella C, Simeone M, et al. CD155/PVR plays a key role in cell motility during tumor cell invasion and migration. *BMC Cancer.* 2004; 4: 73.
9. Nishiwada S, Sho M, Yasuda S, Shimada K, Yamato I, Akahori T, et al. Clinical significance of CD155 expression in human pancreatic cancer. *Anticancer research.* 2015; 35: 2287–97.
10. Merrill MK, Gromeier M. The double-stranded RNA binding protein 76:NF45 heterodimer inhibits translation initiation at the rhinovirus type 2 internal ribosome entry site. *Journal of Virology.* 2006; 80: 6936–42.
11. López-Ulloa B, Fuentes Y, Pizarro-Ortega MS, López-Lastra M. RNA-Binding Proteins as Regulators of Internal Initiation of Viral mRNA Translation. *Viruses.* 2022; 14.
12. Merrill MK, Dobrikova EY, Gromeier M. Cell-type-specific repression of internal ribosome entry site activity by double-stranded RNA-binding protein 76. *J Virol.* 2006; 80: 3147–56.
13. Kauder SE, Racaniello VR. Poliovirus tropism and attenuation are determined after internal ribosome entry. *J Clin Invest.* 2004; 113: 1743–53.
14. Beasley GM, Nair SK, Farrow NE, Landa K, Selim MA, Wiggs CA, et al. Phase I trial of intratumoral PVSRIPO in patients with unresectable, treatment-refractory melanoma. *J Immunother Cancer.* 2021; 9.
15. Aslanidis C, de Jong PJ, Schmitz G. Minimal length requirement of the single-stranded tails for ligation-independent cloning (LIC)

- of PCR products. *PCR Methods Appl.* 1994; 4: 172–7.
16. Yun T, Park A, Hill TE, Pernet O, Beaty SM, Juelich TL, et al. Efficient reverse genetics reveals genetic determinants of budding and fusogenic differences between Nipah and Hendra viruses and enables real-time monitoring of viral spread in small animal models of henipavirus infection. *J Virol.* 2015; 89: 1242–53.
 17. Bewley KR, Coombes NS, Gagnon L, McInroy L, Baker N, Shaik I, et al. Quantification of SARS-CoV-2 neutralizing antibody by wild-type plaque reduction neutralization, microneutralization and pseudotyped virus neutralization assays. *Nature Protocols.* 2021; 16: 3114–40.
 18. Reed LJ, Muench H. A simple method of estimating fifty per cent endpoints. *American journal of epidemiology.* 1938; 27: 493–7.
 19. Lipatova AV, Soboleva AV, Gorshkov VA, Bubis JA, Solovyeva EM, Krasnov GS, et al. Multi-Omics Analysis of Glioblastoma Cells' Sensitivity to Oncolytic Viruses. *Cancers (Basel).* 2021; 13: 1–19.
 20. Sabin A. Oral poliovirus vaccine: History of its development and prospects for eradication of poliomyelitis. *JAMA.* 1965; 194: 130–4.
 21. Boulger L, Magrath D. Differing neurovirulence of three Sabin attenuated type 3 vaccine seed pools and their progeny. *Journal of Biological Standardization.* 1973; 1: 139–47.
 22. Bianchi FP, Larocca AMV, Bozzi A, Spinelli G, Germinario CA, Tafuri S, et al. Long-term persistence of poliovirus neutralizing antibodies in the era of polio elimination: An Italian retrospective cohort study. *Vaccine.* 2021; 39: 2989–94.
 23. Golikov MV, Karpenko IL, Lipatova AV, Ivanova ON, Fedyakina IT, Larichev VF, et al. Cultivation of Cells in a Physiological Plasmax Medium Increases Mitochondrial Respiratory Capacity and Reduces Replication Levels of RNA Viruses. *Antioxidants.* 2021; 11: 97.

Литература

1. Louis DN, Perry A, Wesseling P, Brat DJ, Cree IA, Figarella-Branger D, et al. The 2021 WHO Classification of Tumors of the Central Nervous System: a summary. *Neuro Oncol.* 2021; 23: 1231–51.
2. Carpenter AB. Recombinant oncolytic poliovirus for glioblastoma: A current review of PVS (RIPO). *Georgetown Medical Review.* 2019; 3: 7789.
3. Brown MC, Dobrikova EY, Dobrikov MI, Walton RW, Gemberling SL, Nair SK, et al. Oncolytic polio virotherapy of cancer. *Cancer.* 2014; 120: 3277–86.
4. Ribas A, Dummer R, Puzanov I, VanderWalde A, Andtbacka RHI, Michielin O, et al. Oncolytic Virotherapy Promotes Intratumoral T Cell Infiltration and Improves Anti-PD-1 Immunotherapy. *Cell.* 2018; 174: 1031–2.
5. Twumasi-Boateng K, Pettigrew JL, Kwok YYE, Bell JC, Nelson BH. Oncolytic viruses as engineering platforms for combination immunotherapy. *Nat Rev Cancer.* 2018; 18: 419–32.
6. Gromeier M, Alexander L, Wimmer E. Internal ribosomal entry site substitution eliminates neurovirulence in intergeneric poliovirus recombinants. *Proceedings of the National Academy of Sciences.* 1996; 93: 2370–5.
7. Desjardins A, Gromeier M, Herndon JE, 2nd, Beaubier N, Bolognesi DP, Friedman AH, et al. Recurrent Glioblastoma Treated with Recombinant Poliovirus. *N Engl J Med.* 2018; 379: 150–61.
8. Sloan KE, Eustace BK, Stewart JK, Zehetmeier C, Torella C, Simeone M, et al. CD155/PVR plays a key role in cell motility during tumor cell invasion and migration. *BMC Cancer.* 2004; 4: 73.
9. Nishiwada S, Sho M, Yasuda S, Shimada K, Yamato I, Akahori T, et al. Clinical significance of CD155 expression in human pancreatic cancer. *Anticancer research.* 2015; 35: 2287–97.
10. Merrill MK, Gromeier M. The double-stranded RNA binding protein 76:NF45 heterodimer inhibits translation initiation at the rhinovirus type 2 internal ribosome entry site. *Journal of Virology.* 2006; 80: 6936–42.
11. López-Ulloa B, Fuentes Y, Pizarro-Ortega MS, López-Lastra M. RNA-Binding Proteins as Regulators of Internal Initiation of Viral mRNA Translation. *Viruses.* 2022; 14.
12. Merrill MK, Dobrikova EY, Gromeier M. Cell-type-specific repression of internal ribosome entry site activity by double-stranded RNA-binding protein 76. *J Virol.* 2006; 80: 3147–56.
13. Kauder SE, Racaniello VR. Poliovirus tropism and attenuation are determined after internal ribosome entry. *J Clin Invest.* 2004; 113: 1743–53.
14. Beasley GM, Nair SK, Farrow NE, Landa K, Selim MA, Wiggs CA, et al. Phase I trial of intratumoral PVSRIPO in patients with unresectable, treatment-refractory melanoma. *J Immunother Cancer.* 2021; 9.
15. Aslanidis C, de Jong PJ, Schmitz G. Minimal length requirement of the single-stranded tails for ligation-independent cloning (LIC) of PCR products. *PCR Methods Appl.* 1994; 4: 172–7.
16. Yun T, Park A, Hill TE, Pernet O, Beaty SM, Juelich TL, et al. Efficient reverse genetics reveals genetic determinants of budding and fusogenic differences between Nipah and Hendra viruses and enables real-time monitoring of viral spread in small animal models of henipavirus infection. *J Virol.* 2015; 89: 1242–53.
17. Bewley KR, Coombes NS, Gagnon L, McInroy L, Baker N, Shaik I, et al. Quantification of SARS-CoV-2 neutralizing antibody by wild-type plaque reduction neutralization, microneutralization and pseudotyped virus neutralization assays. *Nature Protocols.* 2021; 16: 3114–40.
18. Reed LJ, Muench H. A simple method of estimating fifty per cent endpoints. *American journal of epidemiology.* 1938; 27: 493–7.
19. Lipatova AV, Soboleva AV, Gorshkov VA, Bubis JA, Solovyeva EM, Krasnov GS, et al. Multi-Omics Analysis of Glioblastoma Cells' Sensitivity to Oncolytic Viruses. *Cancers (Basel).* 2021; 13: 1–19.
20. Sabin A. Oral poliovirus vaccine: History of its development and prospects for eradication of poliomyelitis. *JAMA.* 1965; 194: 130–4.
21. Boulger L, Magrath D. Differing neurovirulence of three Sabin attenuated type 3 vaccine seed pools and their progeny. *Journal of Biological Standardization.* 1973; 1: 139–47.
22. Bianchi FP, Larocca AMV, Bozzi A, Spinelli G, Germinario CA, Tafuri S, et al. Long-term persistence of poliovirus neutralizing antibodies in the era of polio elimination: An Italian retrospective cohort study. *Vaccine.* 2021; 39: 2989–94.
23. Golikov MV, Karpenko IL, Lipatova AV, Ivanova ON, Fedyakina IT, Larichev VF, et al. Cultivation of Cells in a Physiological Plasmax Medium Increases Mitochondrial Respiratory Capacity and Reduces Replication Levels of RNA Viruses. *Antioxidants.* 2021; 11: 97.

MODELS OF MITOCHONDRIAL DYSFUNCTION WITH INDUCIBLE EXPRESSION OF *POLG* PATHOGENIC MUTANT VARIANT

Kubekina MV¹✉, Kalinina AA², Korshunova DS¹, Bruter AV¹, Silaeva YY¹

¹ Institute of Gene Biology, Moscow, Russia

² Blokhin Russian Cancer Research Center, Moscow, Russia

Mitochondrial dysfunctions, which underlie many systemic diseases in animals and humans, may arise from accumulation of mutations in the mitochondrial genome. PolG- α enzyme encoded by *Polg* gene is crucial for replication and repair of the mitochondrial genome. The aim of this study was to assess the possible role of *Polg* mutations in mitochondrial dysfunctions using *in vitro* and *in vivo* animal models. The experiments involved transgenic mice with inducible expression of *Polg* mutant variant; the methods included cell culture, real time PCR assay, fluorescence flow cytometry, and skeletal muscle functional tests. The results indicate that mouse embryonic fibroblasts (MEFs) expressing *Polg* pathogenic mutant variant have decreased mitochondrial membrane potential and increased expression of mitophagy markers compared with control cultures. Transgenic animals with systemic expression of the pathogenic variant develop mitochondrial dysfunction which significantly affects muscular performance. In addition, systemic expression of mutated *Polg* in transgenic animals significantly inhibits expression of TCR subunit α and CD3 coreceptor complex subunits δ and ϵ in total splenocyte populations and significantly affects cellularity of the thymus without altering its CD4/CD8 subpopulation ratio. Thus, inducible expression of mutated *Polg* in transgenic animals provides a relevant model for studying mitochondrial dysfunction and its treatment *in vitro* and *in vivo*.

Keywords: mitochondrial dysfunction, PolG- α enzyme, transgenic animals, genome editing, mitochondrial membrane potential, mitophagy

Funding: the study was supported by Russian Foundation for Basic Research, RFBR Project № 19-34-90073.

Author contribution: Kubekina MV — literature analysis, experimental research, data analysis and interpretation, oligo design, manuscript writing; Kalinina AA, Korshunova DS — experimental research; Bruter AV — literature analysis, research planning, data analysis and interpretation; Silaeva YY — literature analysis, research planning, data analysis and interpretation, scientific editing of the manuscript.

Compliance with ethical standards: the study was approved by Ethical Review board at the Institute of Gene Biology (Protocol of 05 December 2021) and carried out in strict compliance with the Directive 2010/63/EU of the European Parliament and of the Council of 22 September 2010 on the protection of animals used for scientific purposes.

✉ **Correspondence should be addressed:** Marina V. Kubekina
Beskudnikovskiy bulvar, 32, korpus 1, Moscow, 127474, Russia; marykumy@gmail.com

Received: 14.04.2022 **Accepted:** 28.04.2022 **Published online:** 27.04.2022

DOI: 10.24075/brsmu.2022.021

МОДЕЛИ МИТОХОНДРИАЛЬНОЙ ДИСФУНКЦИИ С ИНДУЦИРУЕМОЙ ЭКСПРЕССИЕЙ МУТАНТНОГО ВАРИАНТА ГЕНА *POLG*

М. В. Кубекина¹✉, А. А. Калинина², Д. С. Коршунова¹, А. В. Брутер¹, Ю. Ю. Силаева¹

¹ Институт биологии гена, Москва, Россия

² Национальный медицинский исследовательский центр онкологии имени Н. Н. Блохина, Москва, Россия

Митохондриальные дисфункции ответственны за развитие большого числа патологий различных органов и их систем у животных и человека. Наиболее часто они развиваются вследствие накопления мутаций в митохондриальном геноме. За репликацию и репарацию митохондриального генома отвечает продукт гена *Polg* фермент PolG- α . Целью данной работы было оценить влияние экспрессии мутантного гена *Polg* на развитие митохондриальных нарушений в *in vivo*- и *in vitro*-моделях. Исследование проводили на трансгенных животных и первичных культурах MEF с применением ПЦР-РВ, флуоресцентного окрашивания на проточном цитофлуориметре, тестов на функциональное состояние мышечной системы. Показано, что в эмбриональных фибробластах трансгенных животных с индуцируемой экспрессией мутантной формы гена *Polg*, созданных нами ранее, наблюдаются снижение митохондриального потенциала и увеличение уровня экспрессии маркеров митофагии по сравнению с контрольными эмбриональными фибробластами. Кроме того, в клетках организма этих животных развивается митохондриальная дисфункция, приводящая к снижению показателей выносливости животных и силы хвата, снижению экспрессии субъединиц ϵ и δ комплекса CD3 и α -цепи T-клеточного рецептора в тотальной популяции спленоцитов по сравнению с животными дикого типа. Экспрессия мутантной формы гена *Polg* приводит к снижению клеточности тимуса трансгенных животных, однако не меняет его субпопуляционный состав. Таким образом, трансгенные животные с индуцируемой экспрессией мутантной формы *Polg* могут служить релевантной моделью для изучения процесса развития митохондриальной дисфункции и разработки терапевтических подходов *in vitro* и *in vivo*.

Ключевые слова: митохондриальная дисфункция, фермент PolG- α , трансгенные животные, митохондриальный мембранный потенциал, митофагия

Финансирование: исследование выполнено при финансовой поддержке РФФИ в рамках научного проекта 19-34-90073.

Вклад авторов: М. В. Кубекина — анализ литературы, проведение всех экспериментов, анализ и интерпретация результатов, подбор олигонуклеотидов, написание рукописи; А. А. Калинина, Д. С. Коршунова — проведение экспериментов; А. В. Брутер — анализ литературы, планирование исследования, анализ и интерпретация результатов; Ю. Ю. Силаева — анализ литературы, планирование исследования, анализ и интерпретация результатов, научное редактирование рукописи.

Соблюдение этических стандартов: исследование одобрено этическим комитетом ИБГ РАН (протокол № от 5 декабря 2021 г.) и проведено в строгом соответствии с положениями Директивы 2010/63/EU Европейского Парламента и Совета Европейского Союза от 22 сентября 2010 г. по охране животных, используемых в научных целях.

✉ **Для корреспонденции:** Марина Владиславовна Кубекина
Бескудниковский бульвар, д. 32, корпус 1, г. Москва, 127474, Россия; marykumy@gmail.com

Статья получена: 14.04.2022 **Статья принята к печати:** 28.04.2022 **Опубликована онлайн:** 27.04.2022

DOI: 10.24075/vrgmu.2022.021

Mitochondrial dysfunctions constitute a diverse group of pathological conditions, including hereditary ones; their diagnosis is complicated by variable age at manifestation and diverse symptomatology [1]. Many mitochondrial dysfunctions have been associated with mutations in mitochondrial DNA (mtDNA) [2]. Increased rates of mitochondrial mutagenesis may reflect abnormal functioning of the nuclear *Polg* gene responsible for mtDNA replication and repair [3]. For instance, *Polg* D257A genetic variant promotes accumulation of random mutations in the mitochondrial genome [4]. In fact, mitochondrial genome is generally more vulnerable than nuclear genome due to its lack of histones, authentic repair mechanisms, and increased exposure to reactive oxygen species released as by-products of aerobic respiration [5], which explains the existence of specific cellular mechanisms for the maintenance of mitochondrial genome stability. One of such mechanisms is mitophagy [6] — a type of autophagy that ensures elimination of dysfunctional mitochondria [7].

Studies on the development of mitochondrial dysfunctions and associated pathologies require appropriate models. One of the simplest *in vivo* modeling strategies involves creation of transgenic animals expressing a pathogenic mutant form of *Polg* causing disruption of mtDNA repair processes and accumulation of mitochondrial mutations. A universal model comprising genetically modified mice with inducible tissue-specific and systemic expression of the *Polg* D257A variant has been created to study the onset and development of mitochondrial dysfunction in various organs and tissues [8]. The design is extremely convenient, as the pathogenic mutant allele is silent unless capacitated by crossing with another transgenic line carrying activator elements, which prevents spontaneous development of the phenotype and vertical transmission of defective mitochondria.

This study aimed to evaluate the possibility of using transgenic cultures of mouse embryonic fibroblasts (MEFs) derived from *Polg**Cre-CMV (*Polg**B6.C-Tg(CMV-cre)1Cgn/J mice [https://www.jax.org/strain/006054], subsequently referred to as *Polg**Cre-CMV MEFs, as *in vitro* model of mitochondrial dysfunction caused by accumulation of mutations in mitochondrial genome promoted by expression of the mutant *Polg* gene. Additional goals were to evaluate the effect of systemic expression of the transgene on muscular system and various pools of T cells.

METHODS

MEF primary cultures were derived from E13.5 embryos produced by crossing *Polg* females with Cre-CMV males in accordance with the published protocol [9]. All cultures used in the experiment were genotyped by PCR with primer pairs P1/P2 (STOP-cassette, 292 bp), P3/P4 (terminator, 417 bp), P5/P6 (internal control, 324 bp), and P7/P8 (CMV 100 bp); the oligonucleotide structures are listed in Table.

The embryonic fibroblasts were cultured for 5 weeks (10 passages). The culture medium contained 450 mL DMEM with L-glutamine (PanEco; Russia) supplemented with 50 mL fetal calf serum (BioSera; France), penicillin-streptomycin (100X lyophilized by PanEco; Russia), and MEM non-essential amino acids (100X solution by PanEco; Russia). The mitochondrial functionalities and mitophagy levels in the studied MEF cultures were determined by serial measurements of the mitochondrial membrane potentials by fluorescence flow cytometry assay with MitoTracker Orange (Thermo Fisher Scientific; USA) and real-time PCR measurements of mitophagy marker expression levels at 7 day intervals. To measure the mitochondrial

membrane potentials, the cells (10^5 per culture) were washed from medium in PBS (Paneco; Russia) and incubated with 100 nM MitoTracker Orange (excitation/emission = 550/580 nm) at 37 °C for 30 min, then washed from reagents, pelleted by centrifugation at 300 g for 5 min, resuspended in fresh PBS, and analyzed in a CytoFLEX flow cytometer (Beckman Coulter; USA). The results were plotted in histograms with normalization by the number of events.

Expression levels of mutated *Polg* in MEF cultures were determined by real time PCR assay with qPCRMix-HS (Evrogen; Russia) and primers P9/P10, using fluorescent probes P11 and P12 for the detection of wild-type and mutant variants, respectively.

During the culture period, fractions of cells (about 2×10^5 per culture) were collected weekly for RNA extraction with ExtractRNA reagent (Evrogen; Russia), reverse transcription with MMLV RT kit (Evrogen; Russia), and subsequent mitophagy gene expression assay with qPCRMix-HS SYBR kit (Evrogen; Russia) and gene-specific primers. The panel of mitophagy markers included Map1lc3a, Lamp2, Pink1, Parkin, and Nix [10]. The real-time PCR assay used gene-specific primers to a reference gene *Hprt* (P13/P14) and

Table. The list of primer sequences used in the study

Primer ID	Sequence 5→ to 3'
P1	GTTAGATCTGCTGCCACCGT
P2	AGGTGGCAAGTGGTATTCCG
P3	GCGAGTCCATGTCACTCAGG
P4	GTGTTGCCCTTTGGAGCTTG
P5	CTAGGCCACAGAATTGAAGATCT
P6	GTAGGTGGAAATTCTAGCATCATCC
P7	GCGGTCTGGCAGTAAAACTATC
P8	GTGAACAGCATTGCTGTCACTT
P9	CGGCTGACCTAATCCCTTTGG
P10	ATCGAGAAAACGCATCCGGG
P11	FAM-TGTTTCCTTTGACCGAGCCCATATC-BHQ1
P12	ROX-TGTTTCCTTTGCTCGAGCCCATATC-BHQ2
P13	GCAGTACAGCCCCAAATGG
P14	GGTCCTTTTACCAGCAAGCT
P15	CGACCGGCCTTTCAAGCA
P16	CACCTTTGTAGCGCTCGAT
P17	GTGCTTTCTGTGTCTAGAGCGT
P18	GGGCACAAGGAAGTTGTCTTCA
P19	GTGGGACTCAGATGGCTGTC
P20	CGCTCTACACTGGAGCTGTT
P21	AGTGTTTGCTAAGCGACAGG
P22	TGACTTCTCCTCCGTGGTCT
P23	GTGGCGATTTCACATGCAGC
P24	TGAGGTCTGACTGACCCTGG
P25	CAGGACATGAGACCGGAAGG
P26	TTCCCTCCAAGACGGCTGTA
P27	CCTCCTAGCTGTTGGCACTT
P28	ACTGTCTAGAGGGCACGTCA
P29	AGACAAGCTTCACCTGCCAA
P30	AGGAGGATTCGGAGTCCCAT

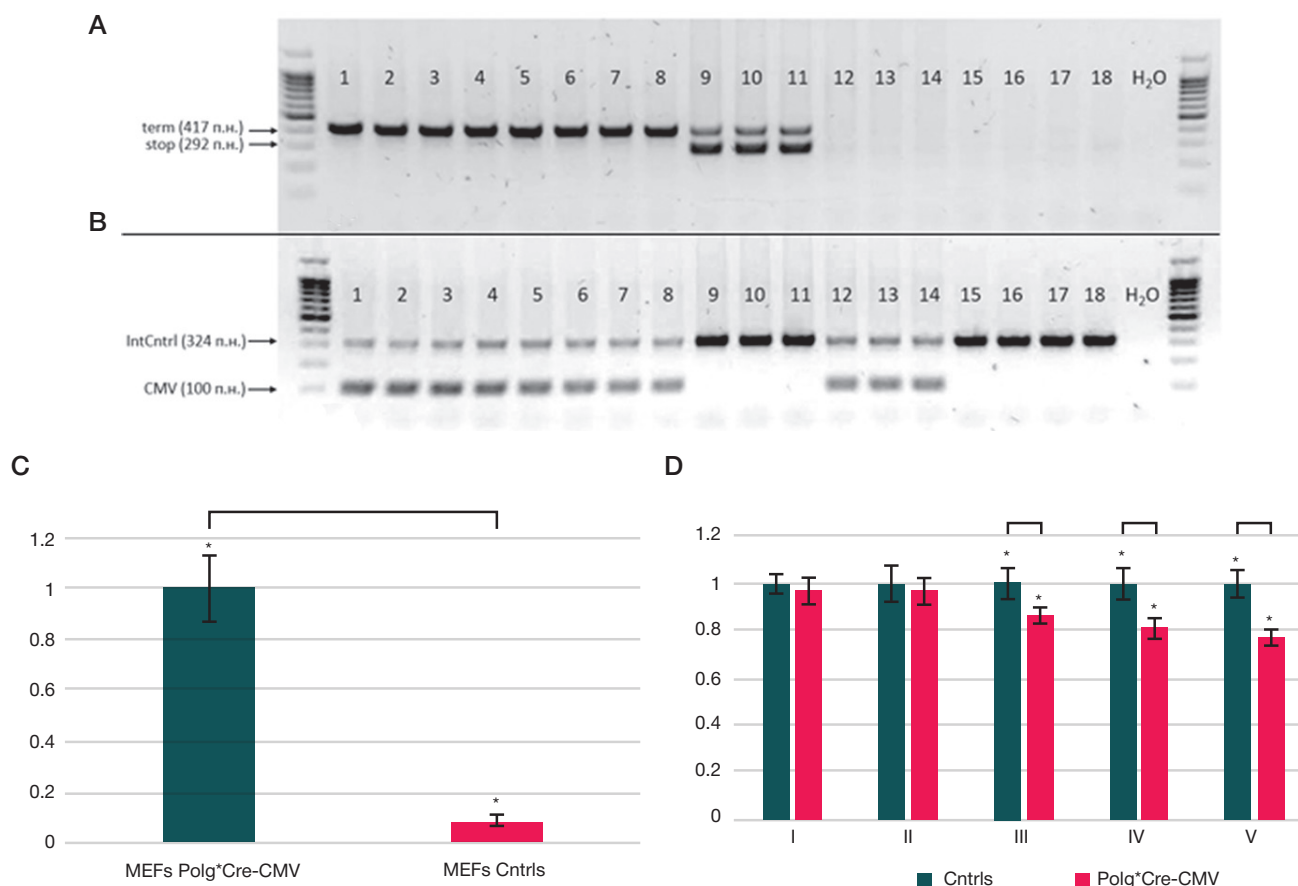


Fig. 1. Genotyping bands and group-wise histograms of *Polg* mutant variant expression and mitochondrial membrane potential in MEF cultures. **A.** Genotyping for STOP-cassette (292 bp) and terminator (417 bp). **B.** Genotyping for CMV (100 bp) and internal control (324 bp). **C.** Expression of the mutant variant in Polg*Cre-CMV, Polg, CMV-Cre, and wild-type (WT) MEF cultures. Expression of the mutant variant in Polg*Cre-CMV cultures was used as a basis (=1.0) to calculate expression levels for other genotypes, and the Polg, CMV-Cre, and WT levels were averaged. **D.** Serial measurements of the mitochondrial membrane potential in MEF cultures over 5 weeks of culturing. The measurements for Polg, CMV-Cre, and WT control cultures were averaged and used as a basis (=1.0) to calculate the mitochondrial membrane potential for Polg*Cre-CMV cultures. * — significant differences

the mitophagy-related genes of interest: *Map1lc3a* (P15/P16), *Lamp2* (P17/P18), *Pink1* (P19/P20), *Parkin* (P21/P22), and *Nix* (P23/P24) (see Table for the structures). All manipulations with cell lysates, RNA, and cDNA were carried out in accordance with manufacturer's protocols (Evrogen; Russia). Relative gene expression levels for mitophagy markers at different time points were determined by $2^{-\Delta Ct}$ method, with Ct (cycle threshold) corresponding to the reaction cycle number when the fluorescence crossed the threshold level; $\Delta Ct = Ct(\text{reference gene}, Hprt) - Ct(\text{gene of interest})$. Expression of a given gene of interest in control cells at a given time point was taken as a basis (= 1.0) for calculating relative expression levels in the Polg*Cre-CMV cultures [11].

We also evaluated the effects of systemic expression of the mutant *Polg* transgene on muscular functionalities. The experiments involved Polg*Cre-CMV transgenic line of (CBA X C57BL/6) hybrid mice developed by us previously [8] and wild-type (CBA X C57BL/6) hybrid mice purchased from the "Stolbovaya" breeding facilities. Only female mice, aged 3 months, were used in the experiments. The animals, weighting 19.9 ± 2.2 g (Polg*Cre-CMV) and 22.7 ± 2.5 g (wild-type), were housed at the Institute of Gene Biology animal facilities with *ad libitum* access to food and water, 12/12 light cycle, 23 ± 1 °C air temperature, and $42 \pm 5\%$ humidity. Each group of the study (5 animals) was subject to "grip strength" and "wire hang" tests. The wire hang test was carried out as described in [12] with modifications (the total time for 10 attempts was limited to 300 s). The grip strength test was carried out as described in [13] with modifications (a grid was used instead of a bar). All animals

were sacrificed by cervical dislocation; the spleens and the thymuses were dissected for subsequent examination.

Functional state of the immune system was assessed indirectly by measuring gene expression levels for T cell receptor (TCR) subunit α and CD3 coreceptor complex subunits δ and ϵ in total splenocytes of Polg*Cre-CMV mice and matched wild-type controls. We also analyzed representation of CD4/CD8 double-negative, double-positive, and single-positive cell populations of the thymus along with its absolute cellularity. The mice were sacrificed by cervical dislocation; the abdominal wall was cut open with scissors; the spleen and the thymus were carefully dissected and thoroughly homogenized. The splenic cells were lysed for RNA extraction and reverse transcription PCR assay using the reagents and protocols listed in the previous paragraphs. The real-time PCR assay used gene-specific primers to the reference gene *Hprt* (P13/P14) and lymphocyte markers *Cd3d* (P26), *Cd3e* (P27/P28), and *Tcr- α* (P29/P30) (see Table for the structures). Relative expression levels were calculated by $2^{-\Delta Ct}$ method described in the previous paragraphs. Single-cell suspensions of thymus cells were analyzed by flow cytometry as described elsewhere [14]. The thymus cells were counted in a Goryaev chamber.

Statistical processing of the data was carried out in Excel (Microsoft; USA) and Statistica (Statsoft; Russia) program packages. The normality of distributions was tested with Shapiro–Wilk test. The samples were characterized using nonparametric one-way two-sample analysis and Mann–Whitney U-test for between-the group comparisons. The differences were considered significant at $p \leq 0.05$.

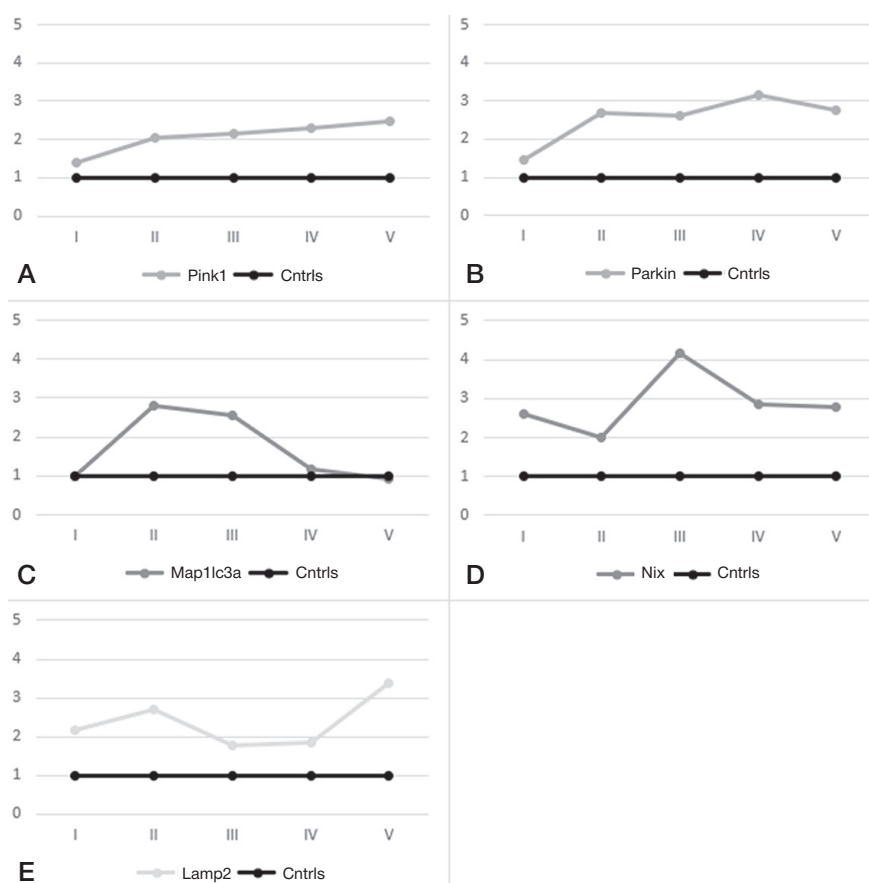


Fig. 2. Expression of mitophagy markers *Pink1* (A), *Parkin* (B), *Map1lc3a* (C), *Nix* (D), and *Lamp2* (E) in MEFs over 5 weeks of culturing

RESULTS

All obtained MEF cultures were genotyped; the results are shown in Figs. 1A, B. In Polg*Cre-CMV double transgenes, the STOP cassette is excised due to systemic activation of Cre recombinase, leaving the embryos STOP cassette-negative and internal control-, terminator-, and CMV-positive. The individual MEF cultures derived from different embryos were distributed into groups based on genotype: eight Polg*Cre-CMV cultures constituted the main group; the rest (three Polg, three Cre-CMV, and four wild-type) were assigned to the control group.

Expression levels of the *Polg* mutant variant were measured in all cultures (Fig. 1C). The mutant variant was strongly expressed in cultures genotyped as Polg*Cre-CMV (main group) and none of the controls. The observed differences were significant ($p \leq 0.05$).

Dynamics of the mitochondrial membrane potential in MEF cultures are shown in Fig. 1D. The mitochondrial membrane potential of Polg*Cre-CMV MEFs was significantly reduced starting from week 3 of culturing compared with the controls ($p \leq 0.05$).

Comparison of expression profiles for the panel of mitophagy markers revealed significant between-the-group differences (Figs. 2A–E):

1. Expression of *Pink1/Parkin* genes, the well-known markers of mitophagy, gradually increased over time (Figs. 2A, B), consistently with the presumed increase in the number of dysfunctional mitochondria [15].

2. Accumulation of random mutations in the mitochondrial genome promotes a decrease in oxidative phosphorylation, which mimics hypoxia, with a concomitant increase in *Nix* expression [16]. The sharp increase in *Nix* expression recorded during week 3 of culturing was probably induced by critically

accumulated intermediates of the disrupted energy-dependent processes (Fig. 2C). In mitophagy, the *Map1lc3a* gene expression product binds Nix protein anchored in the outer mitochondrial membrane, thus tethering it to autophagosome. This protein is also known to initiate the autophagy [17], which explains the sharp positive dynamics of *Map1lc3a* expression during week 2 and its subsequent correlation with *Nix* expression levels (Fig. 2D). This does not explain, however, the observed decrease of *Nix* and *Map1lc3a* expression in transgenic MEFs during weeks 4 and 5 of culturing. Apparently, the decrease reflects the stalled elimination of the mitochondrial ballast (progressively dysfunctional) due to physiological stress and the loss of viability.

3. *Lamp2* protein is a structural component of the lysosomal membrane [18]. Expression of the corresponding *Lamp2* gene in Polg*Cre-CMV cultures exceeded its expression in control cultures 2-fold on the first week of culturing and stayed elevated, apparently reflecting the increased number of lysosomes required for efficient autophagy (Fig. 2E).

To study the impact of mitochondrial dysfunction on muscular functionalities in Polg*Cre-CMV transgenic animals, we tested muscular endurance and grip strength in Polg*Cre-CMV transgenic mice compared with wild-type controls. The results of wire hang test are shown in Fig. 3A. Wild-type mice held on the wire throughout the experiment with a maximum loss of 4 points, while Polg*Cre-CMV mice performed significantly worse: the animals quitted the task in 199 s on average. In grip strength tests, Polg*Cre-CMV mice also performed significantly worse than wild-type controls ($p \leq 0.05$) (Fig. 3B).

To assess the influence of activated transgene on peripheral pools of T cells, we studied expression of genes encoding ϵ and δ subunits of CD3 complex and α chain of TCR in total

splenocytes of Polg*Cre-CMV animals compared with wild-type controls. The levels of *Cd3ε*, *Cd3δ*, and *Tcr-α* expression in lymphocytes of Polg*Cre-CMV mice were significantly reduced compared with wild-type controls ($p \leq 0.05$) (Fig. 4). The fluorescence flow cytometry of single-cell suspensions of viable thymus cells revealed no shifts in CD4/CD8 double-negative, double-positive, and single-positive subpopulation ratio (Figs. 5A, B); however, the absolute cellularity of the thymus in Polg*Cre-CMV mice was significantly lower ($p \leq 0.05$) (Fig. 5C).

DISCUSSION

Development of mitochondrial dysfunction through accumulation of mutations in the mitochondrial genome affects almost all organs and tissues. The alterations caused by mitochondrial mutations begin in embryogenesis. Our experiments indicate that primary cultures of embryonic fibroblasts with Polg*Cre-CMV genotype develop mitochondrial dysfunction in the course of 3 weeks. This effect entirely results from expression of the pathogenic mutant variant, given its absence in control cultures. Thus, embryonic fibroblast cultures derived from Polg*Cre-CMV transgenic mice represent a convenient *in vitro* model for studying mitochondrial dysfunction caused by accumulation of harmful mutations in the mitochondrial genome.

High mitochondrial efficiency is essential for normal functioning of tissues and organ systems, notably the immune system and the muscles [19, 20]. Our experiments demonstrate a considerable negative impact of pathogenic mutations in Polg on the functional state of muscular apparatus, revealed by decreased muscle endurance and grip strength in animals with systemic expression of the Polg*Cre-CMV transgene compared with wild-type controls. The transgene also had a negative effect on the immune system: decreased expression levels of δ and ϵ subunits of CD3 complex and α chain of T cell receptor in splenocytes indirectly indicate reduced functionality of peripheral T cells in Polg*Cre-CMV transgenic animals. Examination of the thymus in transgene-positive animals revealed accelerated involution of this organ with preservation of its main function. These findings are consistent with the reported association of mitochondrial mutagenesis with progeroid phenotypes [4]. Overall, the results justify the use of Polg*Cre-CMV transgenic animals with inducible expression of mutated *Polg* as a relevant model for studying mitochondrial dysfunction and its consequences.

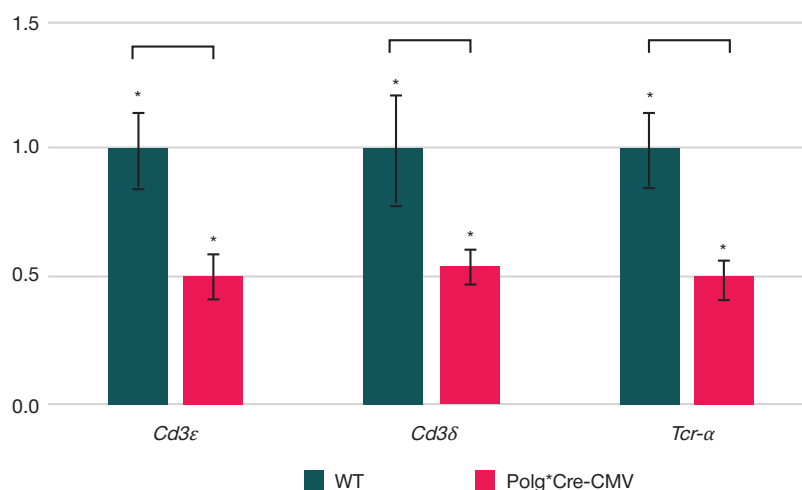


Fig. 4. Decreased expression of *Cd3ε*, *Cd3δ*, and *Tcr-α* in mixed splenocytes of Polg*Cre-CMV mice compared with wild-type controls. * — significant differences

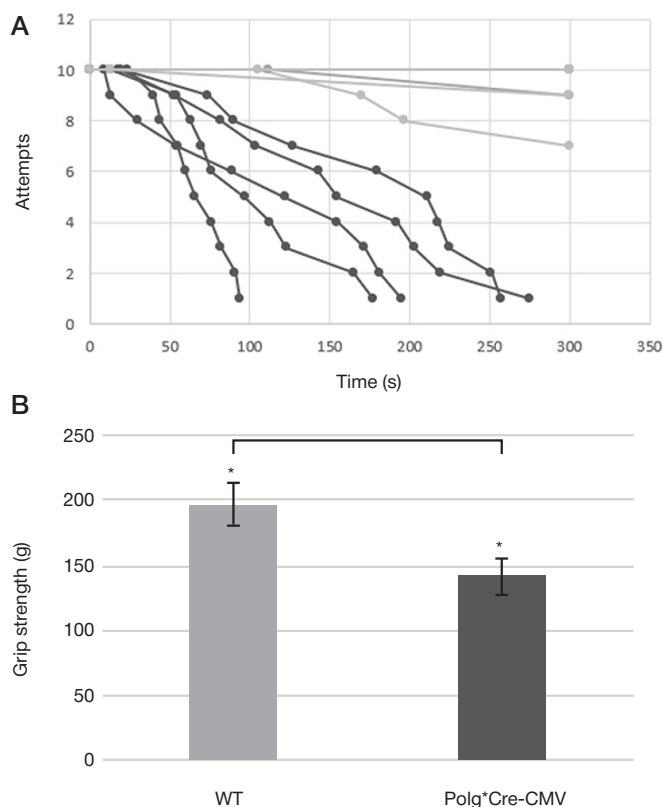


Fig. 3. Results of muscular endurance tests for Polg*Cre-CMV mice (dark-gray) and wild-type controls (light-gray). A. Wire hang test. B. Grip strength test. * — significant differences

CONCLUSIONS

Expression of the mutated Polg gene promotes an increase in mitophagy and a concomitant decrease in the mitochondrial membrane potential in cultured mouse embryonic fibroblasts, as revealed by a series of experiments involving Polg*Cre-CMV transgenic animals. The wire hang and grip strength functional tests revealed significantly reduced muscular endurance in Polg*Cre-CMV mice compared with wild-type controls. Expression of the mutant *Polg* gene also affects immune functionalities, as indicated by reduced TCR/CD3 gene expression in peripheral lymphocytes of Polg*Cre-CMV mice. Systemic expression of the transgene affects cellularity of the thymus, albeit not its CD4/CD8 subpopulation ratio. The obtained results are convincing; however, it would be interesting

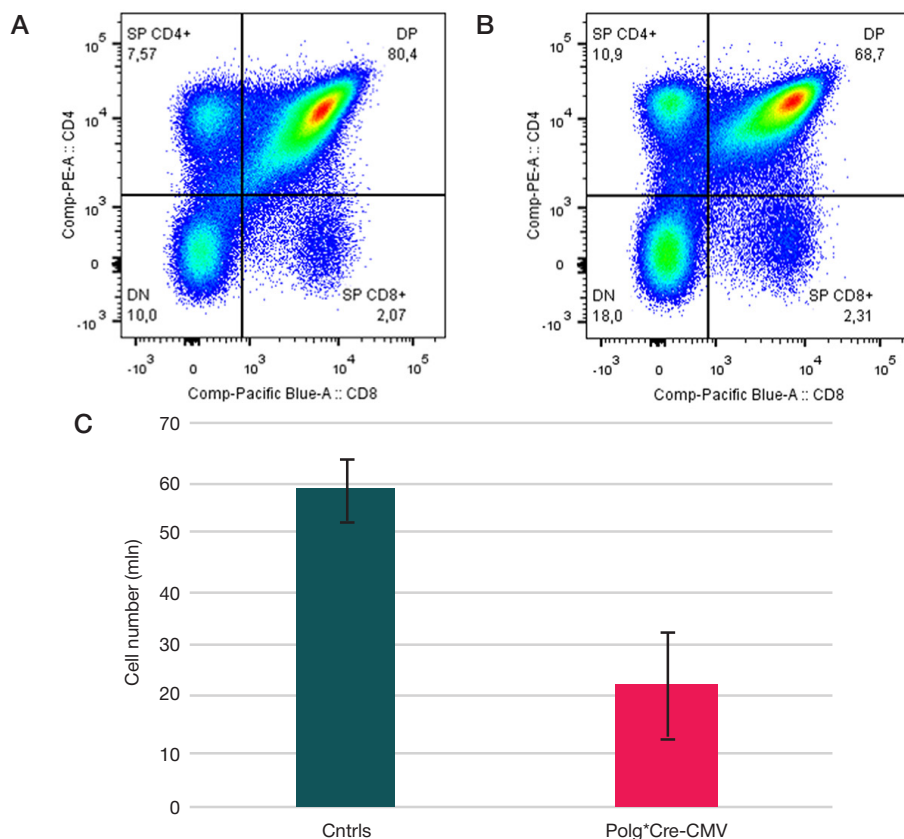


Fig. 5. CD4/CD8 dot plots for the single-cell suspensions of thymus cells from *Polg*Cre-CMV* transgenic animals (**B**) compared to wild-type controls (**A**) and a histogram of thymus cell counts (**C**). * — significant differences

to study effects of the mutant *Polg* gene in other organs and systems. The dedicated *in vitro* and *in vivo* models are needed

to improve our understanding of mitochondrial dysfunctions and their therapy.

References

- Davis RL, Liang C, Sue CM. Mitochondrial diseases. *Handb Clin Neurol*. 2018; 147: 125–41. doi: 10.1016/B978-0-444-63233-3.00010-5.
- Alston CL, Rocha MC, Lax NZ, Turnbull DM, Taylor RW. The genetics and pathology of mitochondrial disease. *J Pathol*. 2017 Jan; 241 (2): 236–50. DOI: 10.1002/path.4809.
- Trifunovic A, Wredenberg A, Falkenberg M, Spelbrink JN, Rovio AT, Bruder CE, et al. Premature ageing in mice expressing defective mitochondrial DNA polymerase. *Nature*. 2004 May 27; 429 (6990): 417–23. DOI: 10.1038/nature02517.
- Kukat A, Trifunovic A. Somatic mtDNA mutations and aging—facts and fancies. *Exp Gerontol*. 2009; 44 (1–2): 101–5. DOI: 10.1016/j.exger.2008.05.006.
- McCormick EM, Muresanu CC, Falk MJ. Mitochondrial Genomics: A complex field now coming of age. *Curr Genet Med Rep*. 2018 Jun; 6 (2): 52–61. DOI: 10.1007/s40142-018-0137-x.
- Dombi E, Mortiboys H, Poulton J. Modulating Mitophagy in Mitochondrial Disease. *Curr Med Chem*. 2018; 25 (40): 5597–612. DOI: 10.2174/0929867324666170616101741.
- Diot A, Morten K, Poulton J. Mitophagy plays a central role in mitochondrial ageing. *Mamm Genome*. 2016 Aug; 27 (7–8): 381–95. DOI: 10.1007/s00335-016-9651-x.
- Kubekina MV, Silaeva YYu, Bruter AV, Korshunova DS, Ilchuk LA, Okulova YD, et al. Transgenic mice Cre-dependently expressing mutant polymerase-gamma: novel test-system for pharmacological study of mitoprotective drugs. *Research Results in Pharmacology*. 2021; 7 (3): 33–39. DOI: 10.3897/rpharmacology.7.72784.
- Tan YS, Lei YL. Generation and Culture of Mouse Embryonic Fibroblasts. *Methods Mol Biol*. 2019; 1960: 85–91. DOI: 10.1007/978-1-4939-9167-9_7.
- Giorgi C, Bouhamida E, Danese A, Previati M, Pinton P, Patergnani S. Relevance of Autophagy and Mitophagy Dynamics and Markers in Neurodegenerative Diseases. *Biomedicines*. 2021 Feb 4; 9 (2): 149. DOI: 10.3390/biomedicines9020149.
- Rao X, Huang X, Zhou Z, Lin X. An improvement of the 2^{-ΔΔCT} method for quantitative real-time polymerase chain reaction data analysis. *Biostat Bioinforma Biomath*. 2013 Aug; 3 (3): 71–85.
- The use of hanging wire tests to monitor muscle strength and condition over time: Treat-nmd neuromuscular network. Available from: https://treat-nmd.org/wp-content/uploads/2016/08/dmd-DMD_M.2.1.004.pdf.
- Use of grip strength meter to assess the limb strength of mdx mice: Treat-nmd neuromuscular network. Available from: https://treat-nmd.org/wp-content/uploads/2016/08/MDX-DMD_M.2.2.001-42.pdf.
- Kalinina AA, Khromykh LM, Kazansky DB, Dejkin AV, Silaeva YuYu. Adoptivnyj perenos singennyx splenocitov podavlyaet immunnyj otvet subletal'no obluchennyx myshej. *Acta Naturae*. 2021; 13 (1): 116–26. Russian.
- Vives-Bauza C, Zhou C, Huang Y, Cui M, de Vries RL, Kim J, et al. PINK1-dependent recruitment of Parkin to mitochondria in mitophagy. *Proc Natl Acad Sci USA*. 2010; 107 (1): 378–83. DOI: 10.1073/pnas.0911187107.
- Tracy K, Dibling BC, Spike BT, Knabb JR, Schumacker P, Macleod KF. BNIP3 is an RB/E2F target gene required for hypoxia-induced autophagy. *Mol Cell Biol*. 2007; 27 (17): 6229–42. DOI: 10.1128/MCB.02246-06.
- Killackey SA, Philpott DJ, Girardin SE. Mitophagy pathways in

health and disease. *J Cell Biol.* 2020; 219 (11): e202004029. DOI: 10.1083/jcb.202004029.

18. Eskelinen EL, Illert AL, Tanaka Y, Schwarzmann G, Blanz J, Von Figura K, et al. Role of LAMP-2 in lysosome biogenesis and autophagy. *Mol Biol Cell.* 2002; 13 (9): 3355–68. DOI: 10.1091/mbc.e02-02-0114.

Литература

1. Davis RL, Liang C, Sue CM. Mitochondrial diseases. *Handb Clin Neurol.* 2018; 147: 125–41. doi: 10.1016/B978-0-444-63233-3.00010-5.
2. Alston CL, Rocha MC, Lax NZ, Turnbull DM, Taylor RW. The genetics and pathology of mitochondrial disease. *J Pathol.* 2017 Jan; 241 (2): 236–50. DOI: 10.1002/path.4809.
3. Trifunovic A, Wredenberg A, Falkenberg M, Spelbrink JN, Rovio AT, Bruder CE, et al. Premature ageing in mice expressing defective mitochondrial DNA polymerase. *Nature.* 2004 May 27; 429 (6990): 417–23. DOI: 10.1038/nature02517.
4. Kukat A, Trifunovic A. Somatic mtDNA mutations and aging--facts and fancies. *Exp Gerontol.* 2009; 44 (1–2): 101–5. DOI: 10.1016/j.exger.2008.05.006.
5. McCormick EM, Muraresku CC, Falk MJ. Mitochondrial Genomics: A complex field now coming of age. *Curr Genet Med Rep.* 2018 Jun; 6 (2): 52–61. DOI: 10.1007/s40142-018-0137-x.
6. Dombi E, Mortiboys H, Poulton J. Modulating Mitophagy in Mitochondrial Disease. *Curr Med Chem.* 2018; 25 (40): 5597–612. DOI: 10.2174/0929867324666170616101741.
7. Diot A, Morten K, Poulton J. Mitophagy plays a central role in mitochondrial ageing. *Mamm Genome.* 2016 Aug; 27 (7–8): 381–95. DOI: 10.1007/s00335-016-9651-x.
8. Kubekina MV, Silaeva YYu, Bruter AV, Korshunova DS, Ilchuk LA, Okulova YD, et al. Transgenic mice Cre-dependently expressing mutant polymerase-gamma: novel test-system for pharmacological study of mitoprotective drugs. *Research Results in Pharmacology.* 2021; 7 (3): 33–39. DOI: 10.3897/rpharmacology.7.72784.
9. Tan YS, Lei YL. Generation and Culture of Mouse Embryonic Fibroblasts. *Methods Mol Biol.* 2019; 1960: 85–91. DOI: 10.1007/978-1-4939-9167-9_7.
10. Giorgi C, Bouhamida E, Danese A, Preati M, Pinton P, Patergnani S. Relevance of Autophagy and Mitophagy Dynamics and Markers in Neurodegenerative Diseases. *Biomedicines.* 2021 Feb 4; 9 (2): 149. DOI: 10.3390/biomedicines9020149.
11. Rao X, Huang X, Zhou Z, Lin X. An improvement of the 2^Δ(delta CT) method for quantitative real-time polymerase chain reaction data analysis. *Biostat Bioinforma Biomath.* 2013 Aug; 3 (3): 71–85.
12. The use of hanging wire tests to monitor muscle strength and condition over time: Treat-nmd neuromuscular network. Available from: https://treat-nmd.org/wp-content/uploads/2016/08/dmd-DMD_M.2.1.004.pdf.
13. Use of grip strength meter to assess the limb strength of mdx mice: Treat-nmd neuromuscular network. Available from: https://treat-nmd.org/wp-content/uploads/2016/08/MDX-DMD_M.2.2.001-42.pdf.
14. Калинина А. А., Хромых Л. М., Казанский Д. Б., Дейкин А. В., Силаева Ю. Ю. Адоптивный перенос сингенных спленоцитов подавляет иммунный ответ сублетально облученных мышей. *Acta Naturae.* 2021; 13 (1): 116–26.
15. Vives-Bauza C, Zhou C, Huang Y, Cui M, de Vries RL, Kim J, et al. PINK1-dependent recruitment of Parkin to mitochondria in mitophagy. *Proc Natl Acad Sci USA.* 2010; 107 (1): 378–83. DOI: 10.1073/pnas.0911187107.
16. Tracy K, Dibling BC, Spike BT, Knabb JR, Schumacker P, Macleod KF. BNIP3 is an RB/E2F target gene required for hypoxia-induced autophagy. *Mol Cell Biol.* 2007; 27 (17): 6229–42. DOI: 10.1128/MCB.02246-06.
17. Killackey SA, Philpott DJ, Girardin SE. Mitophagy pathways in health and disease. *J Cell Biol.* 2020; 219 (11): e202004029. DOI: 10.1083/jcb.202004029.
18. Eskelinen EL, Illert AL, Tanaka Y, Schwarzmann G, Blanz J, Von Figura K, et al. Role of LAMP-2 in lysosome biogenesis and autophagy. *Mol Biol Cell.* 2002; 13 (9): 3355–68. DOI: 10.1091/mbc.e02-02-0114.
19. López-Lluch G. Essential role of mitochondrial dynamics in muscle physiology. *Acta Physiol (Oxf).* 2017; 219 (1): 20–21. DOI: 10.1111/apha.12750.
20. Weinberg SE, Sena LA, Chandel NS. Mitochondria in the regulation of innate and adaptive immunity. *Immunity.* 2015; 42 (3): 406–17. DOI: 10.1016/j.immuni.2015.02.002.

FOOTPRINTS OF INTERACTION AMONG FINNIC-SPEAKING, SLAVIC, AND TURKIC-SPEAKING POPULATIONS IN MODERN GENE POOL AND THEIR REFLECTION IN PHARMACOGENETICS

Balanovska EV^{1,2,3}✉, Gorin IO¹, Ponomarev GY², Pylev VY^{1,3}, Petrushenko VS¹, Markina NV², Mamaeva AD², Larin AK⁴, Agdzhoyan AT²

¹ Bochkov Research Centre of Medical Genetics, Moscow, Russia

² Vavilov Institute of General Genetics, Moscow, Russia

³ Biobank of North Eurasia, Moscow, Russia

⁴ Federal Research and Clinical Center of Physical-Chemical Medicine, Moscow, Russia

Genetic contribution of pre-Slavic populations to gene pools of modern Russia is increasingly relevant, along with genetic footprints of the Golden Horde invasion. The novel genome-wide approaches enable advanced solutions in this field. The study aimed at searching for the footprints of genetic interaction among Finnic-speaking, Slavic and Turkic-speaking populations of Central Russia and Volga Region and their reflection in pharmacogenetic landscape. Modeling ancestral components by ADMIXTURE software and their mapping involved genome-wide genotyping data for 248 individual genomes representing 47 populations of 9 ethnic groups. Of specific ancestral components identified in each of the Finnic-speaking peoples, only Mordovian ancestral components are common for all populations within the studied geographic area, regardless of their linguistic affiliation. Gene pools of Russian populations include 80% of intrinsic component, 19% contribution from Finnic-speaking peoples, and 1% of Central Asian influence. The Tatar gene pool combines all identified ancestral components, including 81% contribution from Finnic-speaking peoples and only 12% of Central Asian influence, which prevents using it as a reference for the assessment of Golden Horde footprints in Russian gene pools. A map of genetic distances from Ryazan Russians based on a panel of 42 pharmacogenetic markers reveals a landscape strikingly independent from the selectively neutral ancestral genomic patterns. For instance, populations of Mordovia, Kaluga, Smolensk, and Kostroma regions are the closest to Ryazan Russians in pharmacogenetic status, whereas populations of Ryazan and Nizhny Novgorod regions have strikingly divergent pharmacogenetic status despite the similarity of the selectively neutral ancestral genomic patterns. These findings confirm the relevance of targeted pharmacogenetic characterization for gene pools of Russia.

Keywords: gene pool, gene geography, ancestral component, ADMIXTURE, genome-wide panel, pharmacogenetics, European part of Russia

Funding: the study was supported by RFBR grant 20-29-01017 Ancient DNA (bioinformatics analysis), RSF grant 21-14-00363 (analysis of pharmacogenetics markers), and State Assignment of the Ministry of Science and Higher Education of the Russian Federation to Vavilov Institute of General Genetics (cartographic analysis) and Bochkov Research Centre of Medical Genetics (data interpretation).

Acknowledgements: the authors thank all sample donors who participated in this study and the Biobank of North Eurasia for the access to DNA collections.

✉ **Correspondence should be addressed:** Elena V. Balanovska
Moskvorechie, 1, 115522, Moscow, Russia; balanovska@mail.ru

Received: 01.04.2022 **Accepted:** 16.04.2022 **Published online:** 26.04.2022

DOI: 10.24075/brsmu.2022.019

СЛЕДЫ ВЗАИМОДЕЙСТВИЯ ФИННОЯЗЫЧНОГО, СЛАВЯНСКОГО И ТЮРКОЯЗЫЧНОГО НАСЕЛЕНИЯ В СОВРЕМЕННОМ ГЕНОФОНДЕ И ИХ ОТРАЖЕНИЕ В ФАРМАКОГЕНЕТИКЕ

Е. В. Балановская^{1,2,3}✉, И. О. Горин¹, Г. Ю. Пономарев², В. Ю. Пылёв^{1,3}, В. С. Петрушенко¹, Н. В. Маркина², А. Д. Мамаева², А. К. Ларин⁴, А. Т. Агджоян²

¹ Медико-генетический научный центр имени Н. П. Бочкова, Москва, Россия

² Институт общей генетики имени Н. И. Вавилова, Москва, Россия

³ Биобанк Северной Евразии, Москва, Россия

⁴ Федеральный научно-клинический центр физико-химической медицины Федерального медико-биологического агентства, Москва, Россия

Актуальность проблемы генетического вклада дославянского населения в генофонд русских популяций и генетического следа вторжения Золотой орды со временем лишь возрастает. Включение в арсенал полногеномных данных о широком круге популяций позволяет искать наиболее корректные решения этой проблемы. Целью работы был поиск следов взаимодействия генофондов финноязычных, славянских и тюркоязычных народов Центральной России и Поволжья и их отражения в фармакогенетическом ландшафте по данным о 248 геномах представителей 47 популяций 9 этносов с помощью моделирования и картографирования предковых компонент ADMIXTURE. Выявлены специфические компоненты для каждого из финноязычных народов, но лишь предковые компоненты мордвы распространены во всех популяциях региона независимо от их языковой принадлежности. Генофонды русских популяций включают 80% собственной компоненты, 19% вклада финноязычных народов, 1% центральноазиатского влияния. Генофонд татар является комбинацией всех выявленных предковых компонент, включая 81% вклада финноязычных народов и лишь 12% центральноазиатского вклада, что затрудняет оценку их влияния на русский генофонд. Карта генетических расстояний от русских Рязанской области по панели 42 фармакогенетических маркеров выявила ландшафт, резко отличный от селективно-нейтрального ландшафта предковых компонент. Наиболее близки по фармакогенетическому статусу к рязанским русским популяции Мордовии, Калужской, Смоленской и Костромской областей. Схожие по селективно-нейтральным геномам рязанские и нижегородские популяции резко различаются по фармакогенетическому статусу. Это подтверждает необходимость прицельно исследовать фармакогенетические особенности популяций России.

Ключевые слова: генофонд, геногеография, предковые компоненты, ADMIXTURE, полногеномные панели, фармакогенетика, европейская часть России

Финансирование: исследование выполнено при поддержке грантов РФФИ №20-29-01017 Древняя ДНК (биоинформационный анализ), РНФ №21-14-00363 (анализ фармакогенетических маркеров), а также Государственного задания Министерства науки и высшего образования РФ для Института общей генетики им. Н. И. Вавилова РАН (картографический анализ) и Медико-генетического научного центра им. академика Н. П. Бочкова (интерпретация результатов).

Благодарности: авторы благодарят всех доноров образцов, которые принимали участие в данном исследовании, АНО «Биобанк Северной Евразии» за предоставление коллекций ДНК.

✉ **Для корреспонденции:** Елена Владимировна Балановская,
ул. Москорецье, д. 1, 115522, г. Москва, Россия; balanovska@mail.ru

Статья получена: 01.04.2022 **Статья принята к печати:** 16.04.2022 **Опубликована онлайн:** 26.04.2022

DOI: 10.24075/vrgmu.2022.019

Genetic history of the Russian people involves contributions from pre-Slavic populations and genetic footprints of the Golden Horde invasion. Gene pools of modern Russians are thought to result from interactions of three ethnic layers: pre-Slavic (Finnic-speaking), Slavic, and Golden Horde (Turkic-speaking). In the perspective of population genetics, these interactions have diverse projections including Y-chromosome phylogeography, selectively neutral ancestral components of autosomal genomes, and selectively relevant pharmacogenetic landscapes of DNA markers that determine drug sensitivity. However, the degree of interaction significantly varies within the indigenous geographical range of Russians [1]. For informative analysis, it is reasonable to focus on a nodal territory with the highest possible degree of interpenetration of the three genetic influences [2]. An excellent candidate territory for this role is the Volga-Oka interfluvium in general and Ryazan region in particular.

In the second half of the 1st millennium AD, Slavic tribes started to penetrate into these lands, inhabited by Finnic-speaking and partly Baltic tribes, and the vectors of their migration were diverse. According to existing evidence, Slavic tribes initially arriving from southwestern territories were subsequently joined by Slavs from the northwest of Eastern Europe at the beginning of the 2nd millennium [1, 3–6]. In the early 11th century, the Murom principality was established, incorporating Ryazan lands [4, 7]. In the mid 12th century, the Murom principality splits into two, with capitals in Murom and Staraya Ryazan. In 1237, the Ryazan principality becomes the first casualty of the Mongol invasion led by Batu; since then, raids and devastation of Ryazan lands continue for over 350 years. In 1521, the Ryazan principality experiencing critical loss of its territories ultimately comes under control of Moscow sovereigns, but, even with subordination to Moscow, the ruin of Ryazan lands by Tatar raids continues until 1594. Taking into account the early military encounters of Ryazan people with the neighboring Volga Bulgaria (Ryazan campaigns against them in 1172 and 1183 are documented), the interaction of Ryazan people with the Turkic world, located at its borders, can be dated to the 12th century or earlier. In addition, the Ryazan region was, in a sense, an outpost that bordered on the Wild Field (rus. Дикое Поле; the vast steppes sparsely populated by nomadic groups). It is reasonable therefore to view the Ryazan region as the major hub of interpenetration between gene pools of Slavic and Turkic-speaking populations, with corresponding genetic footprints in its modern Russian populations. The interaction between Slavic and Finnic-speaking tribes has an even longer history. Overall, the “nodal” territory of the Volga-Oka interfluvium and Ryazan lands provides arguably the best model for studying genetic footprints of Finnic-speaking, Slavic, and Turkic-speaking tribes and peoples.

The modern methods of DNA analysis allow reconstruction of ancient genomes from excavated human remains [8–14]. However, the number of ancient genomes suitable for analysis is limited, especially for populations that practiced, like the Slavs, cremation of the dead. An alternative important source of information on population history is provided by modern genomes subject to genome-wide genotyping or sequencing [15–19]. The most appropriate bioinformatics handling for such data is provided by the autosomal genome ancestral component modeling tool ADMIXTURE [20].

Genetic interactions among peoples of Indo-European, Uralic, and Altaic language families have been considered in a number of studies applying genome-wide analysis to the modern gene pool of Northern Eurasia [21–26]. For instance, a genome-wide panel-assisted reconstruction of gene pools for Balto-Slavic populations [21] reveals the genetic proximity

of the Balts (Lithuanians, Latvians) to the Volga group of Finno-Ugric peoples and especially to Mordovians. The Slavs, both Eastern and Western, absorbed the local pre-Slavic Eastern European genetic substratum. A genome-wide study of modern ethnic groups populating the East European Plain [22] reveals the “East Asian” ancestral component contributing 20% to gene pool of Bashkirs and 5% to gene pools of Chuvashs and Volga Tatars. Another genome-wide study identifies a specific ancestral component shared by peoples of the Uralic language family, including Finnic-speaking Karelians, Mordovians, Mari, and Udmurts, and defining the degree of their genetic relationship [23]. A genome-wide genetic study of North Eurasian populations reveals three clines stretching from west to east [24]. Subsequent analysis shows that gene pools of Turkic-speaking and Uralic-speaking populations in Povolzhye are highly similar, although the Uralic-speaking populations genetically gravitate towards Trans-Ural Ugrians. Comparison of autosomal genome data between Novgorod region and a wide range of populations in the European part of Russia and the Urals produced a hypothesis on considerable preservation of the local pre-Slavic population legacy in gene pools of the Novgorod region, which turned out to be closer to the eastern Finnic-speaking groups (Volga and Perm) than to the western (Baltic) [25]. Another important line of evidence is provided by pharmacogenetic studies, which enable creation of cartographic atlases of subcontinents, but consider local variants as well. For instance, Besermians and Udmurts are pharmacogenetically close to indigenous populations of Volga Region, Urals, and Southern Urals, but distant from inhabitants of more remote regions [26].

This study aimed at modeling of ancestral components in order to reveal genetic footprints of interactions among Finnic-speaking, Slavic and Turkic-speaking ethnic groups in the autosomal gene pool of modern Russian populations inhabiting the nodal region of the Volga-Oka interfluvium. The second, more applied, goal of this study was to create maps of pharmacogenetic DNA markers and contemplate pharmacogenetic landscape of the studied geographic area.

METHODS

Methodological and bioinformatics aspects of the analysis of autosomal gene pools using genome-wide panels have been described in detail previously [27]. The genotyping for a genome-wide panel of 4.5 million SNP markers was performed using Infinium OmniExome BeadChip Kit (Illumina; USA) with an iScan system (Illumina; USA). Primary analysis and quality assessment of the data was carried out in the GenomeStudio v2011.1 software at a CallRate of at least 0.99.

The population genetic analysis for small panels of autosomal markers requires samples of at least 50 individuals. By contrast, genome-wide panels comprising millions of DNA markers afford a reliable output on much smaller samples of 5–10 individuals. Since the reduced sample size implies ultimate tightening of the sampling criteria, we emphasize that all genomes included in this study were selected in accordance with internationally recognized criteria [28]. In particular, genealogies of all participants, traced at least three generations backward, proved their origin from a given population and identification with a given ethnic group.

The “nodal” Ryazan region was represented by 20 genomes from 4 ethnic Russian populations (Mikhailovsky, Spassky, Sapozhkovsky, and Saraevsky districts), with Russian populations in Tver, Kostroma, Smolensk, Kaluga, Oryol, Tambov, and Nizhny Novgorod regions included for comparison.

Table. Estimated contribution of each of the ten ancestral components identified by ADMIXTURE at $k = 3$ and $k = 7$ to genomes in each of the studied populations

Ethnic groups Populations		Population number	Genome number	ANCESTRAL COMPONENT CONTRIBUTION, AVERAGE (%)											Total contribution of Finnic- speaking ethnic groups (%)	
				k = 3			k = 7									
				"Western"	"Ural"	"Eastern"	"Karelian"	"Slavic"	"Mordovian-1"	"Mordovian-2"	"Mari"	"Udmurt"	"Kalmyk"	except "Karelian"		
Karelians	South	1	9	75	24	2	94	0	6	0	0	0	0	6	100	
Russians	Tver region	2	16	95	5	0	6	70	19	3	1	1	0	24	30	
	Kostroma region	1	20	87	10	3	11	73	3	3	4	4	3	14	25	
	Smolensk and Kaluga regions	6	20	97	2	0	2	82	12	2	1	1	0	16	18	
	Oryol and Tambov regions	3	19	97	3	1	1	87	7	2	1	1	1	11	12	
	Ryazan region, Mikhailovsky district	1	5	98	0	2	2	86	5	5	0	1	1	11	13	
	Ryazan region, Spassky district	1	5	95	3	3	1	86	3	5	2	1	2	11	12	
	Ryazan region, Sapozhkovsky district	1	5	93	6	1	1	87	3	5	1	0	2	9	10	
	Ryazan region, Saraevsky district	1	5	96	1	3	4	81	6	4	3	2	1	15	19	
	Ryazan region totally	4	20	95	2	2	2	85	4	5	1	1	2	11	13	
	Nizhny Novgorod region	4	9	90	8	3	3	81	4	4	3	3	3	14	17	
Mordovians	Moksha, Erzya, Shoksha	3	41	78	19	3	5	3	53	37	1	1	0	92	97	
Tatars	Kazan	5	19	52	34	14	13	6	36	7	15	10	12	68	81	
Chuvashes	Chuvashian	4	13	23	67	9	7	0	20	2	62	3	5	87	94	
Mari	Meadow	1	15	4	92	5	2	0	1	1	96	0	0	98	100	
Udmurts	Udmurtian	7	16	0	99	1	0	0	0	0	0	100	0	100	100	
Nogais	Astrakhan, Stavropol	2	15	25	13	62	2	0	33	1	1	2	61	37	39	
Kalmyks	Six tribal groups	6	16	0	0	100	0	0	0	0	0	0	100	0	0	
	TOTALLY	49	248													

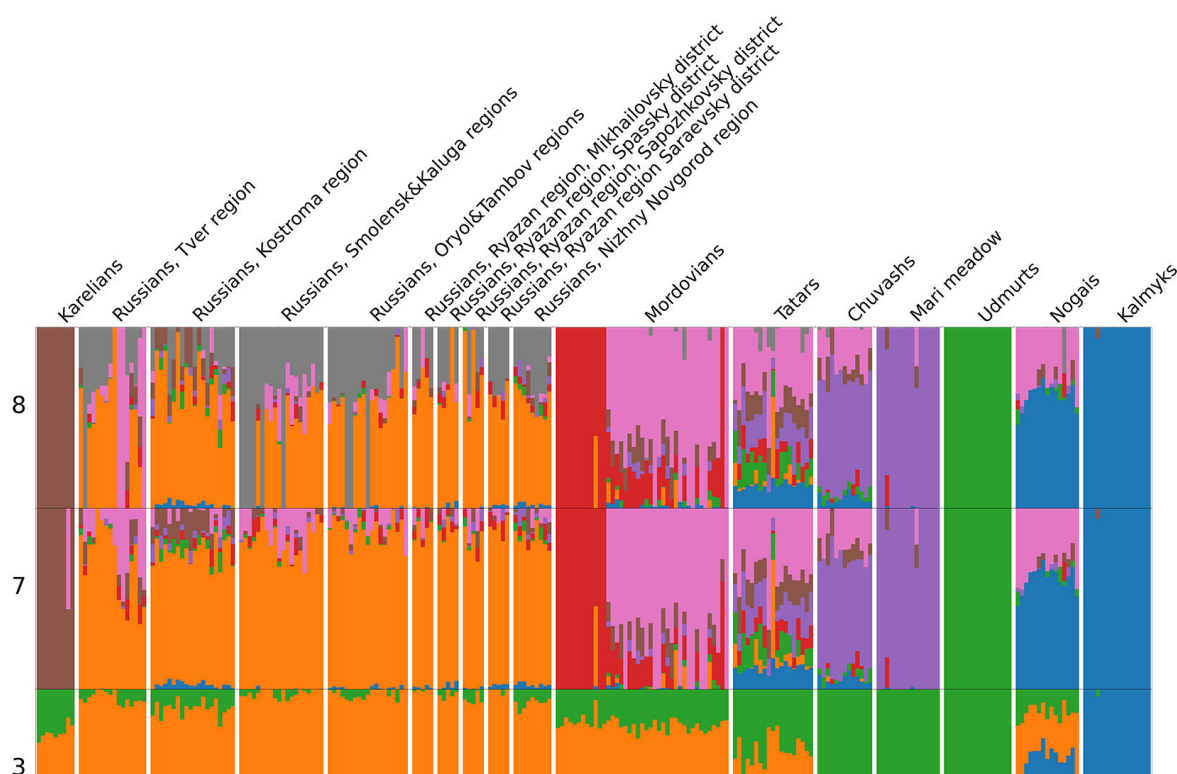


Fig. 1. Contributions of the ancestral components identified by ADMIXTURE at $k = 3$, $k = 7$, and $k = 8$ to individual genomes in the studied populations. Each ancestral component is indicated by specific color; each vertical line represents individual genome with a palette of ancestral component contributions; the populations are demarcated by white lines; the raw data are given in the table

The Finnic-speaking populations of the Volga-Ural region were represented by Mordovians (Erzya, Moksha, Shoksha), Mari, and Udmurts, whereas southern Karelians were included as the most geographically close representative of the western branch of the Finnic-speaking peoples. The Turkic-speaking populations of Volga Region and Ural were represented by Kazan Tatars and Chuvashs, with Astrakhan and Stavropol Nogais included for comparison. Identification of genetic footprints of Mongolic-speaking peoples involved genome-wide data for six tribal groups of Kalmyks.

The analysis of ancestral components was carried out using the ADMIXTURE bioinformatics tool for 248 individual genomes representing 47 populations of 9 ethnic groups (Table), including 104 genomes from Russian populations, 81 genomes from four Finnic-speaking peoples, 47 genomes from three Turkic-speaking peoples, and 16 genomes of Mongolic-speaking Kalmyks. The ADMIXTURE tool affords quantitative assessment for the contributions of different ancestral components to each individual genome [20, 29]. The ancestral components are modeled for the same uploaded set of genomes, with each level of modeling carried out independently. The number of ancestral components k is the only parameter specified by the user. At $k = 2$, contributions of two ancestral components are modeled for each genome; at $k = 3$, the tool presents the same genomes with three ancestral components; at $k = 20$, the tool reconstructs contributions of twenty ancestral components for the same set of genomes, etc.; as the k increases, the patterns become increasingly elaborated. The contribution of particular ancestral component to a gene pool is estimated by averaging its contributions to individual genomes.

A series of pharmacogenetic maps were built to assess the interactions among Finnic-speaking, Slavic, and Turkic-speaking ethnic groups in pharmacogenetic perspective and estimate their impact on the modern pharmacogenetic landscape.

The mapping employed data on 42 key pharmacogenetic markers (the absorption, distribution, metabolism, and excretion (ADME) genes; pharmacological target-encoding genes; and hemostasis system genes) derived from the same genome-wide genotyping datasets previously used in the ADMIXTURE processing [26]. The incidence matrix for the studied 42 pharmacogenetic DNA markers comprised data for 16 pooled populations (to increase sample size). Calculation of Nei's genetic distances (d) based on this matrix produced 42 partial maps showing the extent of pharmacogenetic similarity between Ryazan and other regions for each of the studied markers. The averaging of partial maps produced the map of average pharmacogenetic distances from Ryazan, reflecting its pharmacogenetic status with regard to other subjects within the studied geographic area.

All maps of pharmacogenetic landscapes and ancestral components were built using the original GeneGeo mapping package [30] using the weighted average interpolation method with an influence radius of 400 km and a weight function value of 3. The genogeographic technology has been described in detail elsewhere [2, 31].

RESULTS

Modeling of ancestral components for the studied scope of 47 populations was carried out at 13 levels of k , obtained by sequentially incrementing k by 1, from 2 to 14 inclusive. Two models turned out to be the most informative for solving the main problem: at $k = 3$ and $k = 7$ (Table). The level of $k = 3$ reveals three ancestral components conventionally defined as "Western", "Ural" and "Eastern". At the level of $k = 7$, the ancestral components of the western and eastern Finnic-speaking peoples become separated for the first time, which allows differentiating their contributions. The estimated contributions to individual genomes for each of the identified

ancestral components are given in Table. Contributions to individual genomes for each ancestral component at $k = 3$, $k = 7$, and $k = 8$ are presented in Fig. 1. The level of $k = 8$ preserves the contributions of all components identified at the previous steps of analysis, while the new eighth component further elaborates the structure of Russian populations.

To validate the observed trends, modeling at each level from $k = 2$ to $k = 14$ was run in 10 repeats (yielding a total of 130 models). At $k = 3$, all models were virtually identical; at $k = 7$, six of ten runs revealed stable ancestral components (these are described in the text of the article). In the remaining four runs, one of the ancestral components was replaced by an alternative, and each of these runs presented with a higher simulation error value.

DISCUSSION

Modeling of three ancestral components

The analysis at $k = 3$ revealed three ancestral components conventionally designated “Western”, “Ural”, and “Eastern”. Most notably, the identified ancestral components poorly fit into the framework of three language families (Slavic, Finnic, and Turkic) (Fig. 1, Table).

“Western” ancestral component

This component prevails in all Russian populations (95%), but also in Finnic-speaking populations of Karelians (75%) and Mordovians (78%) (Fig. 2A, Table). Moreover, it constitutes a significant portion of gene pools in Turkic-speaking peoples: more than a half in Kazan Tatars (52%) and about a quarter in both Nogais (25%) and Chuvashs (23%).

“Ural” ancestral component

This component dominates in gene pools of Udmurts (99%) and Mari (91%) (Fig. 2B, Table). It is also prominent in Turkic-speaking peoples, accounting for two-thirds of Chuvash (67%) and a third of Tatar (34%) gene pools. A smaller but still substantive contribution of the “Ural” ancestral component is found in Karelians (24%) and Mordovians (19%). The average contribution of this component to Russian populations is small (4%) with the maxima in Kostroma and Nizhny Novgorod regions.

“Eastern” ancestral component

This component totally prevails (100%) in all six Kalmyk tribal groups included in this study, so it provides a suitable measure of the Central Asian influence on European gene pools (Fig. 2C, Table). This component is also prominent in Nogais (62%), which confirms its “Central Asian” status. Among Volga Region peoples, the highest Central Asian influence is observed in Kazan Tatars (14%) and Chuvashs (9%). In other studied gene pools, the “Eastern” influence is small, 5% (in Mari) or lower. Its average contribution to Russian gene pools is 1% (up to 3% in eastern districts of the Nizhny Novgorod and Ryazan regions).

Kazan Tatars

The “composite” nature of gene pool in Kazan Tatars, represented by five populations, should be discussed in detail. The subtle interpopulation divergence is due to variable “Western” (48–60%) and “Ural” (26–38%) contributions

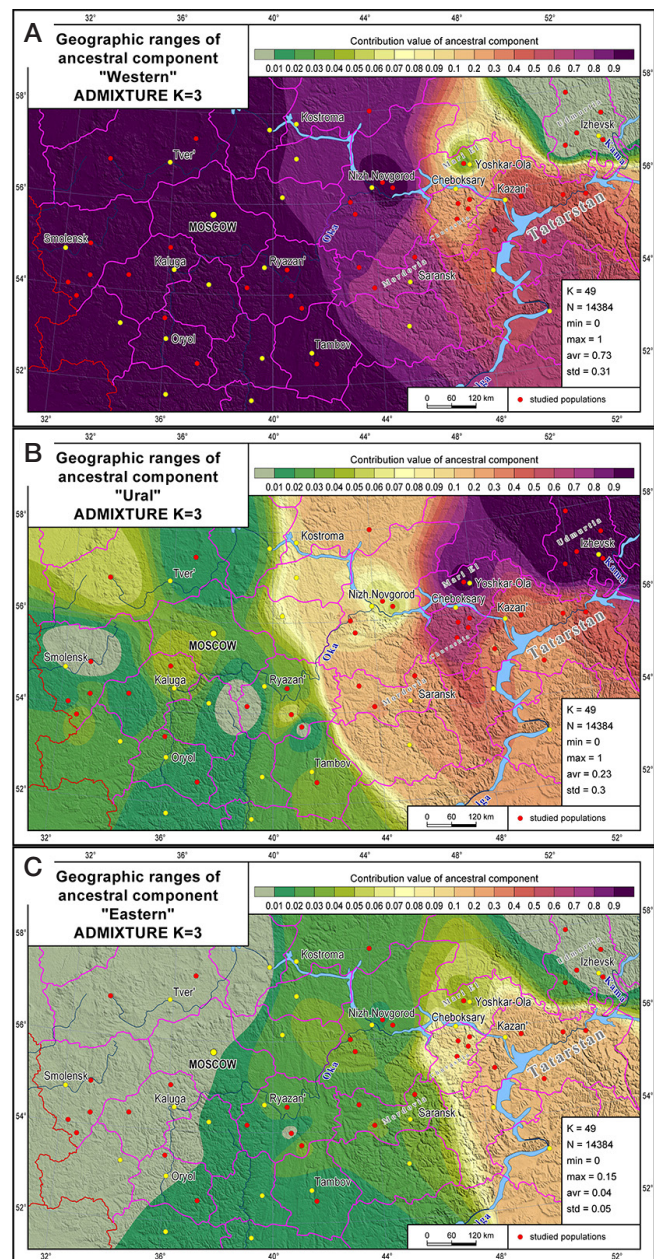


Fig. 2. Geographic ranges of three ancestral components identified by ADMIXTURE at $k = 3$: “Western” (A), “Ural” (B), and “Eastern” (C). High prevalence rates are colored red-to-purple, low values are green, the scale of transitions is given in the map; studied populations are indicated by red circles

accompanied by similar “Eastern” contributions (14–15%). The dominant “Western” component (a half or more) was followed by “Ural” (roughly one third) and “Eastern” (14%) components in all studied populations. Increasing the resolution of analysis by incrementing k revealed some minor ancestral components, but these were shared with other ethnic groups. The analysis identified no singular ancestral component for Kazan Tatars; the “composite” structure preserved at higher levels of k prevents using their gene pool for evaluation of the “tatar” influence on the neighboring Russian populations.

Modeling of seven ancestral components

Analysis at $k = 7$ yielded four new ancestral components, though not as a result of sheer branching of those identified at previous steps of the analysis. The picture is much more complex: the new components mosaically absorb the elements

of “Western” and “Ural” components revealed at $k = 3$. It should be emphasized that the components were attributed with “ethnic” trivial names only for the sake of brevity.

“Karelian” ancestral component

This component, which marks the contribution of Western Finnic-speaking ethnic groups, accounts for 94% of Karelian gene pools and is minor in other populations (Table), with secondary maxima in gene pools of Kazan Tatars and Kostroma Russians (11%).

“Slavic” ancestral component

This component dominates in all ethnic Russian populations (81% on average, within the total range of 70–87%) (Fig. 3A, Table) and is virtually absent in other gene pools with the exception of Kazan Tatars (6%). The accentuated presence of the “Slavic” component in the Tatar gene pool cannot be explained genealogically, given its 80% prevalence in individual genomes. Although this component is also detectable in Mordovian gene pools (3%), it is present in only 17% of genomes in the northwest of Mordovia.

“Mordovian-1” ancestral component

This component shares the second largest geographic range with “Mordovian-2” (Fig. 3B, Table). Reaching maximum (53%) in gene pools of Mordovia, it is also ubiquitously found in other populations. Its prominent contributions are characteristic of Turkic-speaking peoples: 36%, 35%, and 20% in gene pools of Kazan Tatars, Astrakhan Nogais, and Chuvashs. Importantly, the “Mordovian-1” component shows almost total prevalence in these ethnic groups, contributing to almost all individual genomes (Table 2), which indicates its historical significance in gene pools of the Turkic-speaking peoples of Volga Region.

Contribution of the “Mordovian-1” ancestral component to gene pools of ethnic Russians is modest (7%) despite rather high prevalence (60% of individual genomes). The maxima are encountered in Tver (19%) and Kaluga (16%) regions, with a very high prevalence (80–90% of individual genomes; Fig. 4); in other regions, the prevalence is lower (45–65% of genomes). Overall, the “Mordovian-1” ancestral component is ubiquitously found in gene pools of almost all Slavic-speaking, Turkic-speaking and Finnic-speaking populations within the studied geographic area.

“Mordovian-2” ancestral component

The component shown in Fig. 3C and Table 1, has a more distinguished authenticity: it is already identifiable at $k = 4$, whereas the “Mordovian-1” component arrives at $k = 7$. Genomes of Mordovia show distinct clusterization (Fig. 1): one-fifth of them are 100% “Mordovian-1” and another one-fifth are 100% “Mordovian-2”. This component is found in gene pools of all studied populations (except Udmurts). In none of them, however, its contribution exceeds 5%, apart from, again, Kazan Tatars: with the average contribution of 6%, the “Mordovian-2” component is 90% prevalent in Tatars (in Chuvashs, it is found in 40% of genomes only).

In gene pools of ethnic Russians, the “Mordovian-2” component is relatively weak (3% on average) but ubiquitous. Moreover, it is encountered in 60% of individual Russian genomes, most commonly in eastern regions (Kostroma, Nizhny Novgorod, and Ryazan) (Figs. 3C and 4).

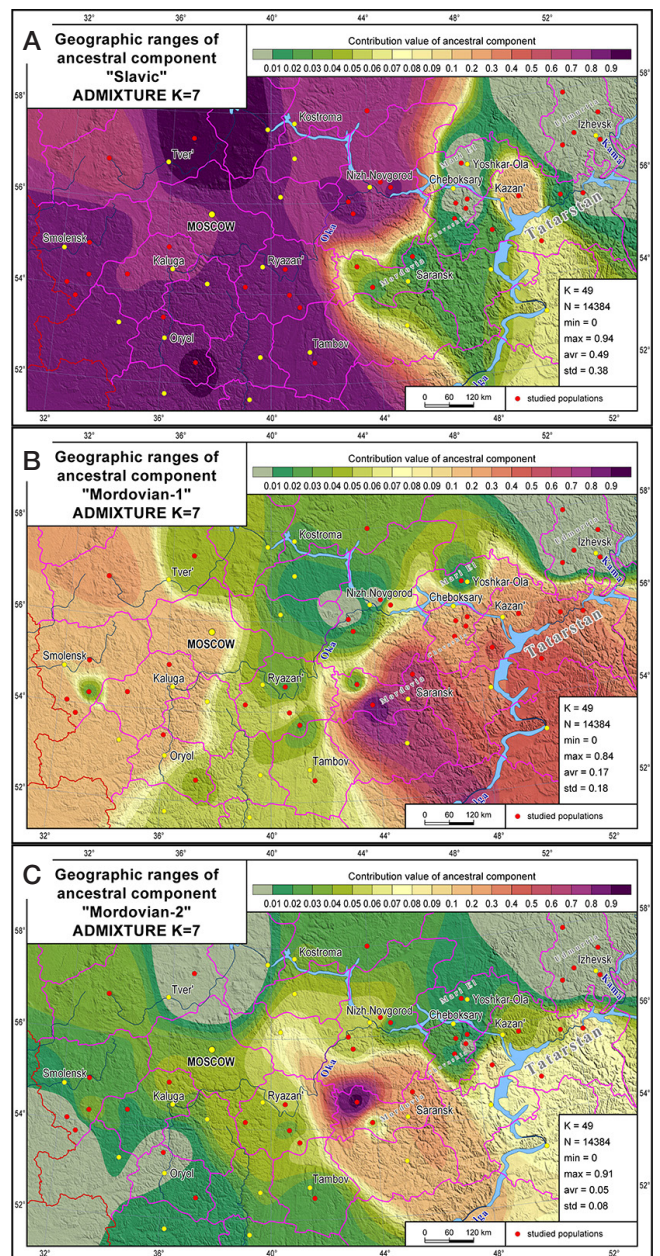


Fig. 3. Geographic ranges of three ancestral components identified by ADMIXTURE at $k = 7$: “Slavic” (A), “Mordovian-1” (B), and “Mordovian-2” (C). High prevalence rates are colored red-to-purple, low values are green, the scale of transitions is given in the map; studied populations are indicated by red circles

“Mari” ancestral component

This component firstly arrives at the level of five ancestral components ($k = 5$) and almost totally prevails in the meadow Mari gene pool (96%). It also accounts for two-thirds of the Chuvash gene pool (62%), with similarly high levels in all Chuvash populations (57–65%) (Table). Of other ethnic groups, the most significant contribution of the “Mari” component is encountered in Kazan Tatars (15% on average, with 100% prevalence in individual genomes). In other studied populations, contributions of the “Mari” component never exceeds 4% (Table).

“Udmurt” ancestral component

This component firstly arrives at $k = 3$ and has been already described by us as “Ural” (Table, Fig. 2B). At all higher levels it

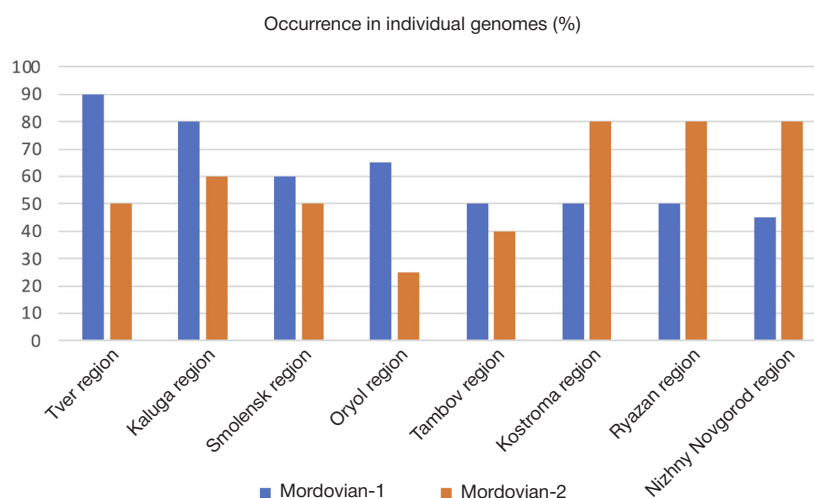


Fig. 4. Fractions of individual genomes (%) harboring “Mordovian-1” and “Mordovian-2” ancestral components in ethnic Russian populations

accounts for 100% of the Udmurt gene pool, while being minor (within 4%) in gene pools of other peoples. The only exception is, again, Kazan Tatars: the “Udmurt” component accounts for 10% of the gene pool and is present in almost all individual Tatar genomes with a maximal contribution of 21%.

“Kalmyk” ancestral component

This component fixes the “breath” of Central Asia; it firstly arrives at $k = 2$ and has been already described by us as “Eastern” (Fig. 2C). Among the studied populations, it is only prominent in gene pools of Kalmyks (100%) and Nogais (61%). Of other ethnic groups, it is present at highest in Kazan Tatars (12%). Noteworthy, the “Kalmyk” component was found in all individual genomes of Tatars, constituting 7–17%. In other studied gene pools, contributions of the “Kalmyk” component never exceeded 5% (Table).

Ryazan gene pool

Four modern populations of ethnic Russians (Figs. 1–3, Table) provided a relevant model for the assessment of the mutual

genetic influence of pre-Slavic, Slavic, and Turkic-speaking populations in the “nodal” Ryazan region. We picked one district (Mikhailovsky) at the very west of Ryazan region and three districts (Spassky, Sapozhkovsky, and Saraevsky) located on the same transect from north to south, with Saraevsky being borderline. The analysis indicates similar genetic constitution of the four gene pools, with certain differences in contributions of Finnic-speaking peoples: 19% in the borderline Saraevsky district and as low as 10–13% in the other three districts (Table). Given the equally small Central Asian influence in all four populations (1–2%), this difference could not be directly related to the Golden Horde invasion, nor attributed to the influence of any known pre-Slavic tribe. The only suggestion to explain the authenticity of gene pools in the southeastern Ryazan lands is the higher influence of the Wild Field in this borderline area.

Pharmacogenetic status of Ryazan Russians

Analysis of genetic markers associated with pharmacologic phenotypes is a prerequisite in the transition to personalized medicine in terms of optimal drug choice and medication regimen adjustment. However, the majority of studies in this

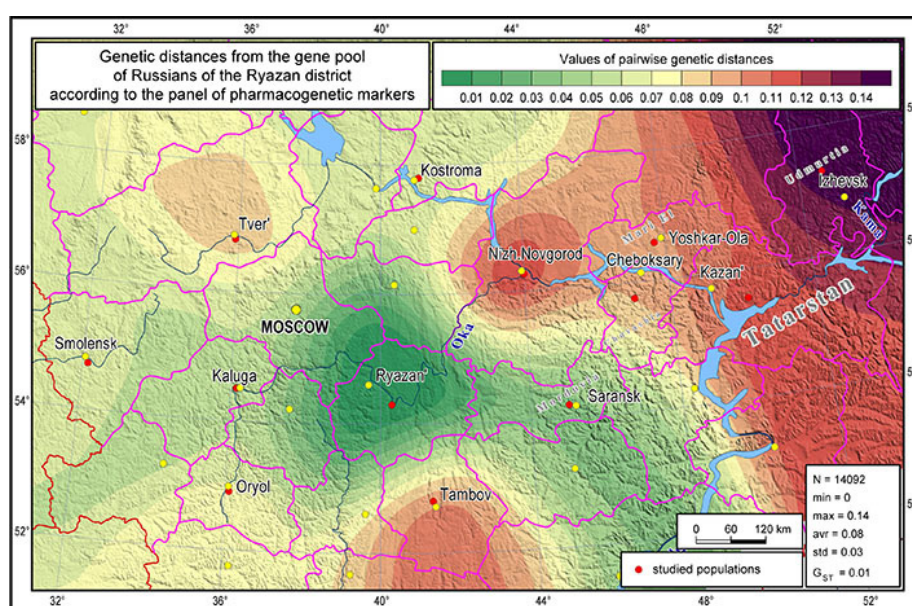


Fig. 5. Pharmacogenetic landscape of the studied geographic area, representing genetic distances from Ryazan Russians according to pharmacogenetic markers. Small genetic distances (indicating pharmacogenetic proximity to Ryazan Russians) are shown in green; large genetic distances (indicating pharmacogenetic divergence from Ryazan Russians) are shown in red-to-purple; the scale of transitions is given in the map

field have been focused on Western Europe and the results have little application to populations of Russia with their huge genetic diversity [31].

To assess the uniqueness of pharmacogenetic landscape within the studied geographic area, a map of genetic distances (d) from Ryazan Russians was created using an extensive panel of pharmacogenetic markers (Fig. 5). In contrast with the ancestral component maps based on selectively neutral DNA markers (Figs. 2 and 3), pharmacogenetic mapping revealed the highest proximity of Ryazan Russians to their Finnic-speaking neighbor — Mordovian populations ($0.03 < d < 0.04$). One step more distant from Ryazan Russians in terms of pharmacogenetic status were Russian populations of Kaluga, Smolensk, and Kostroma regions ($0.05 < d < 0.07$), followed by Russians in Oryol and Tver regions ($0.08 < d < 0.09$). The third most similar to Ryazan Russians were Tambov Russians and their eastern neighbors — the Finnic-speaking Mari and the Turkic-speaking Chuvash peoples ($0.09 < d < 0.10$). Pharmacogenetic portraits of Tatar and Udmurt peoples were expectedly divergent from those of Ryazan Russians ($0.11 < d < 0.15$). The highest pharmacogenetics divergency from Ryazan Russians was most unexpectedly revealed by Russians of the adjacent Nizhny Novgorod region ($0.11 < d < 0.12$) despite the substantive similarity of selectively neutral genomic patterns between the two regions (Figs. 1–4).

Overall, comparing pharmacogenetic landscape and selectively neutral genomic pattern maps demonstrates that optimization of healthcare programs at the regional level should not be based on averaged genetic status of the target populations, but requires specific assessment of local pharmacogenetic landscapes.

CONCLUSIONS

Modeling of ancestral components for the autosomal gene pool of modern populations in the nodal region of interaction between Finnic-speaking, Slavic, and Turkic-speaking peoples revealed that (1) the Finnic-speaking ethnic groups of

Volga Region (Udmurts, Mari, and Mordovians) lack common ancestral components; instead, each of these groups has its own characteristic ancestral components. Remarkably, two ancestral components identified in the Mordovian gene pool can be traced in almost all populations within the studied geographic area, regardless of their linguistic affiliation, which allows us to suggest that genetic portrait of pre-Slavic population of the studied geographic area included two main “colors” preserved in the modern gene pool of Mordovia. (2) The contribution of Finnic-speaking ethnicities to gene pools of modern Turkic-speaking peoples in Volga Region is enormous: ancestral components associated with Finnic-speaking ethnic groups constitute 81% and 94% in gene pools of Kazan Tatars and Chuvashs, respectively. (3) Gene pool of Kazan Tatars is the most “composite” of all gene pools in this study, most organically incorporating all ancestral components observed in other gene pools within the studied geographic area. Although the Central Asian influence is most pronounced among the Kazan Tatars, its contribution is low (12%), seven times lower than the total contribution of the Finnish-speaking peoples (81%), which makes it a poor basis for evaluation of the “Tatar” influence. (4) Gene pools of the studied Russian populations represent a single cluster, which can be basically (80%) described by characteristic ancestral component. At the same time, gene pools of modern ethnic Russians incorporate all other ancestral components found in genetic landscapes of other ethnic groups within the studied geographic area. The “nodal” Ryazan region is fully archetypal in terms of common features of the Slavic cluster with a somewhat increased total contribution of Finnish-speaking groups towards its southeastern border. (5) The picture of diversity based on selectively neutral ancestral components is complemented by unique pharmacogenetic landscapes revealed with a custom panel within the same genome-wide genotyping platform. The knowledge of pharmacogenetic parameters for a given population is essential for the future of personalized medicine and proper logistics of pharmaceuticals at the regional level with regard to genetic diversity of modern Russian populations.

References

1. Sedov VV. Osvoenie slavyanami Vostochnoevropejskoj ravniny. V knige: Vostochnye slavyane. Antropologiya i etnicheskaya istoriya. M.: Nauchnyj mir, 1999; s. 153–160. Russian.
2. Balanovskaya EV, Balanovskij OP. Russkij genofond na Russkoj ravnine. M.: Luch, 2007. Russian.
3. Leontev AE, Ryabinin EA. Ehtapy i formy assimilyacii letopisnoj meri (postanovka voprosa). Sovetskaya arxeologiya. 1980; (2): 67–79. Russian.
4. Bejlekchi VV. Drevnosti letopisnoj muromy (pogrebal'nyj obryad i poseleniya). M.: Murom, 2005; 278 s. Russian.
5. Alekseeva TI. Ehtnogenez vostochnyx slavyan po dannym antropologii. M.: Nauka, 1973; 329 s. Russian.
6. Sedov VV. Drevnerusskaya narodnost': Istoriko-arxeologicheskoe issledovanie. M.: Yazyki russkoj kul'tury, 1999; 316 s. Russian.
7. Goryunova EI. Etnicheskaya istoriya Volgo-Okskogo mezhdurech'ya. M.: Izd-vo AN SSSR, 1961; 264 s. Russian.
8. Rizzi E, Lari M, Gigli E, De Bellis G, Caramelli D. Ancient DNA studies: new perspectives on old samples. Genet Sel Evol. 2012 Jul 6; 44 (1): 21. DOI: 10.1186/1297-9686-44-21.
9. Lazaridis I, Patterson N, Mitnik A, Renaud G, Mallick S, Kirsanow K et al. Ancient human genomes suggest three ancestral populations for present-day Europeans. Nature. 2014; 513: 409–413. DOI: 10.1038/nature13673.
10. Haak W, Lazaridis I, Patterson N, Rohland N, Mallick S, Llamas B et al. Massive migration from the steppe was a source for Indo-European languages in Europe. Nature. 2015 Jun 11; 522 (7555): 207–11. DOI: 10.1038/nature14317.
11. Allentoft ME, Sikora M, Sjögren KG, Rasmussen S, Rasmussen M, Stenderup J et al. Population genomics of Bronze Age Eurasia. Nature. 2015 Jun 11; 522 (7555): 167–72. DOI: 10.1038/nature14507.
12. Jones ER, Zarina G, Moiseyev V, et al. The Neolithic Transition in the Baltic Was Not Driven by Admixture with Early European Farmers. Curr Biol. 2017 Feb 20; 27 (4): 576–82. DOI: 10.1016/j.cub.2016.12.060.
13. Mitnik A, Wang CC, Pfrengle S, Daubaras M, Zarina G, Hallgren F et al. The genetic prehistory of the Baltic Sea region. Nat Commun. 2018 Jan 30; 9 (1): 442. DOI: 10.1038/s41467-018-02825-9.
14. Lamnidis TC, Majander K, Jeong C, Salmela E, Wessman A, Moiseyev V et al. Ancient Fennoscandian genomes reveal origin and spread of Siberian ancestry in Europe. Nat Commun. 2018 Nov 27; 9 (5018). DOI: 10.1038/s41467-018-07483-5.
15. Li JZ, Absher DM, Tang H, et al. Worldwide human relationships inferred from genome-wide patterns of variation. Science. 2008; 319 (5866): 1100–4. DOI: 10.1126/science.1153717.
16. Novembre J, Johnson T, Bryc K, Kutalik Z, Boyko A, Auton A, et

- al. Genes mirror geography within Europe. *Nature*. 2008 Aug 31; 456: 98–101. DOI: 10.1038/nature07331.
17. Pagani L, Lawson D, Jagoda E, Morseburg A, Eriksson A, Mitt M, et al. Genomic analyses inform on migration events during the peopling of Eurasia. *Nature*. 2016 Oct 13; 538 (7624): 238–42. DOI: 10.1038/nature19792.
 18. Mallick S, Li H, Lipson M, Mathieson I, Gymrek M, Racimo F, et al. The Simons Genome Diversity Project: 300 genomes from 142 diverse populations. *Nature*. 2016 Oct 13; 538 (7624): 201–6. DOI: 10.1038/nature18964.
 19. Malaspina AS, Westaway M, Muller C, Sousa V, Lao O, Alves I et al. A genomic history of Aboriginal Australia. *Nature*. 2016 Oct 13; 538 (7624): 207–14. DOI: 10.1038/nature18299.
 20. Alexander DH, Lange K. Enhancements to the ADMIXTURE algorithm for individual ancestry estimation. *BMC Bioinformatics*. 2011; 12 (1): 246. DOI: 10.1186/1471-2105-12-246.
 21. Kushniarevich A, Utevska O, Chuhryaeva M, Agdzhoyan A, Dibirova K, Uktverite I et al. Genetic heritage of the Balto-Slavic speaking populations: a synthesis of autosomal, mitochondrial and Y-chromosomal data. *PLoS ONE*. 2015 Sep 2; 10 (9). PubMed PMID: 26332464. DOI: 10.1371/journal.pone.0135820.
 22. Triska P, Chekanov N, Stepanov V, Khusnutdinova E, Arun Kumar GP, Akhmetova V. Between Lake Baikal and the Baltic Sea: genomic history of the gateway to Europe. *BMC Genetics*. 2017 Dec 28; 18 (1): 5–20. PubMed PMID: 29297395. DOI: 10.1186/s12863-017-0578-3.
 23. Tambets K, Yunusbayev B, Hudjashov G, Ilumäe A-M, Rootsi S, Honkola T. Genes reveal traces of common recent demographic history for most of the Uralic-speaking populations. *BMC Genome Biology*. 2018 Sep 21; 19 (1): 1–20. DOI: 10.1186/s13059-018-1522-1.
 24. Jeong C, Balanovsky O, Lukianova E, Kahbatkyz N, Flegontov P, Zaporozhchenko V, et al. The genetic history of admixture across inner Eurasia. *Nature ecology & evolution*. 2019 Jun; 3 (6): 966–76. PubMed PMID: 31036896. DOI: 10.1038/s41559-019-0878-2.
 25. Balanovska EV, Chernovsky DK, Balanovsky OP. Svoeobrazie Novgorodskogo genofonda v kontekste narodonaseleniya evropejskoj chasti Rossii. *Vestnik Novgorodskogo gosudarstvennogo universiteta. Ser.: Medicinskie nauki*. 2021; 124 (3): 51–57. DOI: 10.34680/2076-8052.2021. Russian.
 26. Balanovska EV, Petruschenko VS, Koshel SM, Pocheshhova EA, Chernovsky DK, Mirzaev KB, et al. Cartographic atlas of frequency variation for 45 pharmacogenetic markers in populations of Russia and its neighbor states. *Vestnik RGMU*. 2020; (6): 38–50. DOI: 10.24075/brsmu.2020.080.
 27. Balanovsky OP, Gorin IO, Zapisetskaya YS, Golubeva AA, Kostryukova ES, Balanovska EV. Interactions between gene pools of Russian and Finnish-speaking populations from Tver region: analysis of 4 million SNP markers. *Vestnik RGMU*. 2020; (6): 15–22. DOI: 10.24075/brsmu.2020.072.
 28. Balanovska EV, Zhabagin MK, Agdjoyan AT, Chuhryaeva MI, Markina NV, Balaganskaya OA, et al. Populyacionnye biobanki: principy organizatsii i perspektivy primeneniya v genogeografii i personalizirovannoj medicine. *Genetika*. 2016; 52 (12): 1371–87. DOI: 10.7868/S001667581612002X. Russian.
 29. Alexander DH, Novembre J, Lange K. Fast model-based estimation of ancestry in unrelated individuals. *Genome Res*. 2009 Sep; 19 (9): 1655–64. DOI: 10.1101/gr.094052.109.
 30. Koshel SM. Geoinformacionnye tekhnologii v genogeografii. V knige: *Sovremennaya geograficheskaya kartografiya*. M.: Data+, 2012; s. 158–166. Russian.
 31. Balanovsky OP. *Genofond Evropy. M.: Tovarishhestvo nauchnykh izdanij KMK*, 2015. Russian.

Литература

1. Седов В. В. Освоение славянами Восточноевропейской равнины. В книге: *Восточные славяне. Антропология и этническая история*. М.: Научный мир, 1999; с. 153–160.
2. Балановская Е. В., Балановский О. П. Русский генофонд на Русской равнине. М.: Луч, 2007.
3. Леонтьев А. Е., Рябинин Е. А. Этапы и формы ассимиляции летописной мери (постановка вопроса). *Советская археология*. 1980; (2): 67–79.
4. Бейлекчи В. В. Древности летописной муромы (погребальный обряд и поселения). М.: Муром, 2005; 278 с.
5. Алексеева Т. И. Этногенез восточных славян по данным антропологии. М.: Наука, 1973; 329 с.
6. Седов В. В. Древнерусская народность: Историко-археологическое исследование. М.: Языки русской культуры, 1999; 316 с.
7. Горюнова Е. И. Этническая история Волго-Окского междуречья. М.: Изд-во АН СССР, 1961; 264 с.
8. Rizzi E, Lari M, Gigli E, De Bellis G, Caramelli D. Ancient DNA studies: new perspectives on old samples. *Genet Sel Evol*. 2012 Jul 6; 44 (1): 21. DOI: 10.1186/1297-9686-44-21.
9. Lazaridis I, Patterson N, Mitnik A, Renaud G, Mallick S, Kirsanov K et al. Ancient human genomes suggest three ancestral populations for present-day Europeans. *Nature*. 2014; 513: 409–413. DOI: 10.1038/nature13673.
10. Haak W, Lazaridis I, Patterson N, Rohland N, Mallick S, Llamas B et al. Massive migration from the steppe was a source for Indo-European languages in Europe. *Nature*. 2015 Jun 11; 522 (7555): 207–11. DOI: 10.1038/nature14317.
11. Allentoft ME, Sikora M, Sjögren KG, Rasmussen S, Rasmussen M, Stenderup J et al. Population genomics of Bronze Age Eurasia. *Nature*. 2015 Jun 11; 522 (7555): 167–72. DOI: 10.1038/nature14507.
12. Jones ER, Zarina G, Moiseyev V, et al. The Neolithic Transition in the Baltic Was Not Driven by Admixture with Early European Farmers. *Curr Biol*. 2017 Feb 20; 27 (4): 576–82. DOI: 10.1016/j.cub.2016.12.060.
13. Mitnik A, Wang CC, Pfrengle S, Daubaras M, Zarina G, Hallgren F et al. The genetic prehistory of the Baltic Sea region. *Nat Commun*. 2018 Jan 30; 9 (1): 442. DOI: 10.1038/s41467-018-02825-9.
14. Lamnidis TC, Majander K, Jeong C, Salmela E, Wessman A, Moiseyev V et al. Ancient Fennoscandian genomes reveal origin and spread of Siberian ancestry in Europe. *Nat Commun*. 2018 Nov 27; 9 (5018). DOI: 10.1038/s41467-018-07483-5.
15. Li JZ, Absher DM, Tang H, et al. Worldwide human relationships inferred from genome-wide patterns of variation. *Science*. 2008; 319 (5866): 1100–4. DOI: 10.1126/science.1153717.
16. Novembre J, Johnson T, Bryc K, Kutalik Z, Boyko A, Auton A, et al. Genes mirror geography within Europe. *Nature*. 2008 Aug 31; 456: 98–101. DOI: 10.1038/nature07331.
17. Pagani L, Lawson D, Jagoda E, Morseburg A, Eriksson A, Mitt M, et al. Genomic analyses inform on migration events during the peopling of Eurasia. *Nature*. 2016 Oct 13; 538 (7624): 238–42. DOI: 10.1038/nature19792.
18. Mallick S, Li H, Lipson M, Mathieson I, Gymrek M, Racimo F, et al. The Simons Genome Diversity Project: 300 genomes from 142 diverse populations. *Nature*. 2016 Oct 13; 538 (7624): 201–6. DOI: 10.1038/nature18964.
19. Malaspina AS, Westaway M, Muller C, Sousa V, Lao O, Alves I et al. A genomic history of Aboriginal Australia. *Nature*. 2016 Oct 13; 538 (7624): 207–14. DOI: 10.1038/nature18299.
20. Alexander DH, Lange K. Enhancements to the ADMIXTURE algorithm for individual ancestry estimation. *BMC Bioinformatics*. 2011; 12 (1): 246. DOI: 10.1186/1471-2105-12-246.
21. Kushniarevich A, Utevska O, Chuhryaeva M, Agdzhoyan A, Dibirova K, Uktverite I et al. Genetic heritage of the Balto-Slavic speaking populations: a synthesis of autosomal, mitochondrial and Y-chromosomal data. *PLoS ONE*. 2015 Sep 2; 10 (9). PubMed PMID: 26332464. DOI: 10.1371/journal.pone.0135820.
22. Triska P, Chekanov N, Stepanov V, Khusnutdinova E, Arun Kumar GP, Akhmetova V. Between Lake Baikal and the Baltic Sea: genomic history of the gateway to Europe. *BMC Genetics*. 2017 Dec 28; 18 (1): 5–20. PubMed PMID: 29297395. DOI: 10.1186/s12863-017-0578-3.
23. Tambets K, Yunusbayev B, Hudjashov G, Ilumäe A-M, Rootsi S,

- Honkola T. Genes reveal traces of common recent demographic history for most of the Uralic-speaking populations. *BMC Genome Biology*. 2018 Sep 21; 19 (1): 1–20. DOI: 10.1186/s13059-018-1522-1.
24. Jeong C, Balanovsky O, Lukianova E, Kahbatkyzy N, Flegontov P, Zaporozhchenko V, et al. The genetic history of admixture across inner Eurasia. *Nature ecology & evolution*. 2019 Jun; 3 (6): 966–76. PubMed PMID: 31036896. DOI: 10.1038/s41559-019-0878-2.
 25. Балановская Е. В., Черневский Д. К., Балановский О. П. Своеобразие Новгородского генофонда в контексте народонаселения европейской части России. *Вестник Новгородского государственного университета. Сер.: Медицинские науки*. 2021; 124 (3): 51–57. DOI: 10.34680/2076-8052.2021.
 26. Балановская Е. В., Петрушенко В. С., Кошель С. М., Почешхова Э. А., Черневский Д. К., Мирзаев К. Б. и др. Картографический атлас распространения 45 фармакогенетических маркеров в народонаселении России и сопредельных стран. *Вестник РГМУ*. 2020; (6): 39–52. DOI: 10.24075/vrgmu.2020.080.
 27. Балановский О. П., Горин И. О., Записецкая Ю. С., Голубева А. А., Кострюкова Е. С., Балановская Е. В. Взаимодействие генофондов русского и финноязычного населения Тверской области: анализ 4 млн SNP-маркеров. *Вестник РГМУ*. 2020; (6): 15–22. DOI: 10.24075/vrgmu.2020.072.
 28. Балановская Е. В., Жабагин М. К., Агджоян А. Т., Чухряева М. И., Маркина Н. В., Балаганская О. А. и др. Популяционные биобанки: принципы организации и перспективы применения в геногеографии и персонализированной медицине. *Генетика*. 2016; 52 (12): 1371–87. DOI: 10.7868/S001667581612002X.
 29. Alexander DH, Novembre J, Lange K. Fast model-based estimation of ancestry in unrelated individuals. *Genome Res*. 2009 Sep; 19 (9): 1655–64. DOI: 10.1101/gr.094052.109.
 30. Кошель С. М. Геоинформационные технологии в геногеографии. В книге: *Современная географическая картография*. М: Дата+, 2012; с. 158–166.
 31. Балановский О. П. Генофонд Европы. М.: Товарищество научных изданий КМК, 2015.

ACTIVITY OF NUCLEAR FACTOR κ B IN LYMPHOCYTE POPULATIONS OF CHILDREN WITH PSORIASISKuptsova DG¹✉, Petrichuk SV¹, Murashkin NN^{1,2,3}, Kurbatova OV¹, Radygina TV¹, Khotko AA², Ivanov RA¹¹ National Medical Research Center for Children's Health, Moscow, Russia² Central State Medical Academy of the Administrative Department of the President of the Russian Federation, Moscow, Russia³ I.M. Sechenov First Moscow State Medical University, Moscow, Russia

Alterations in intracellular signaling pathways affecting immune cell activation, proliferation and differentiation of keratinocytes in psoriasis could explain the complex pathogenesis of the disease. NF- κ B is one of the intracellular signaling pathways, which is involved in regulation of numerous pro-inflammatory genes, and affects the synthesis of pro-inflammatory cytokines directly involved in the development of psoriasis. The study was aimed to assess the number of cells with NF- κ B translocation in lymphocyte populations of children with psoriasis depending in the disease severity and therapy. A total of 130 children with psoriasis vulgaris were examined. The comparison group included 30 healthy children. The study was conducted using the imaging flow cytometry Amnis ImageStreamX system. It was found that there were significant differences in the number of cells with NF- κ B translocation in the lymphocyte populations of both children with psoriasis and comparison group. Children with psoriasis had a higher number of cells with NF- κ B translocation in the populations of T helper cells, T_{act}⁺ T_{reg}⁺, and Th17 compared to healthy children ($p < 0.05$). The number of cells with NF- κ B translocation in children with psoriasis correlated with the disease severity PASI ($R_{\text{mul}} = 0.32$) and BSA ($R_{\text{mul}} = 0.31$) scores, as well as with the disease duration ($p < 0.05$). NF- κ B determination could be considered an additional criterion for the disease severity assessment in children with psoriasis. The differences in the degree of reduction of the number of cells with NF- κ B translocation 24 h after administration of biologics (adalimumab, etanercept, ustekinumab) have been shown. Studying NF- κ B in cell populations offers the prospect of understanding pathogenetic mechanisms of inflammation and developing new therapeutic methods for psoriasis.

Keywords: children, psoriasis vulgaris, PASI, BSA, lymphocyte, NF- κ B, biologics**Finding:** the study was part of the state assignment for the Ministry of Health of the Russian Federation, № AAAA-A19-119013090093-2.**Acknowledgements:** the authors wish to thank all the patients for active cooperation and express their thanks to the researchers of the Laboratory of Immunology and Virology, as well as to dermatologists and nurses at the Dermatology Department, National Medical Research Center for Children's Health, Moscow, Russia, who contributed to the study.**Author contribution:** Kuptsova DG, Petrichuk SV — study concept and design, experimental data acquisition and analysis, statistical analysis, manuscript writing and editing; Kurbatova OV, Radygina TV — experimental data acquisition, manuscript editing; Murashkin NN, Khotko AA, Ivanov RA — data analysis, manuscript editing.**Compliance with ethical standards:** the study was approved by the Ethics Committee of the National Medical Research Center for Children's Health (protocol № 2 dated February 14, 2020), conducted in accordance with the principles of the Declaration of Helsinki, and registered with ClinicalTrials.gov ID: NCT04989296. Parents of all children and adolescents enrolled submitted the informed consent to medical intervention in hospital settings, personal data processing and the use of data for scientific purposes.✉ **Correspondence should be addressed:** Darya G. Kuptsova
Lomonosovsky prospect, 2, str. 1, Moscow, 119296; dg.kuptsova@gmail.com**Received:** 11.02.2022 **Accepted:** 03.03.2022 **Published online:** 20.03.2022**DOI:** 10.24075/brsmu.2022.012АКТИВНОСТЬ ЯДЕРНОГО ФАКТОРА ТРАНСКРИПЦИИ κ B В ПОПУЛЯЦИЯХ ЛИМФОЦИТОВ У ДЕТЕЙ С ПСОРИАЗОМД. Г. Купцова¹✉, С. В. Петричук¹, Н. Н. Мурашкин^{1,2,3}, О. В. Курбатова¹, Т. В. Радыхина¹, А. А. Хотко², Р. А. Иванов¹¹ Национальный медицинский исследовательский центр здоровья детей, Москва, Россия² Центральная государственная медицинская академия Управления делами Президента РФ, Москва, Россия³ Первый Московский государственный медицинский университет имени И. М. Сеченова, Москва, Россия

Изменения в путях передачи внутриклеточных сигналов, влияющих на активацию иммунных клеток, пролиферацию и дифференцировку кератиноцитов при псориазе, могут объяснить сложный патогенез заболевания. Одним из путей передачи внутриклеточных сигналов является NF- κ B, участвующий в регуляции большого количества провоспалительных генов и влияющий на продукцию провоспалительных цитокинов, непосредственно участвующих в развитии псориаза. Целью исследования было оценить число клеток с транслокацией NF- κ B в популяциях лимфоцитов у детей с псориазом в зависимости от тяжести заболевания и проводимой терапии. Обследовано 130 детей с вульгарным псориазом. В группу сравнения вошли 30 здоровых детей. Исследование проводили методом проточной цитометрии с визуализацией Amnis ImageStreamX. Показано, что число клеток с транслокацией NF- κ B достоверно различалось в популяциях лимфоцитов как у детей с псориазом, так и в группе сравнения. У детей с псориазом выявлено повышение числа клеток с транслокацией NF- κ B в популяциях Т-хелперов, T_{act}⁺ T_{reg}⁺ и Th17 по сравнению со здоровыми детьми ($p < 0,05$). Число клеток с транслокацией NF- κ B у детей с псориазом соотносится с тяжестью состояния по PASI ($R_{\text{mul}} = 0,32$), BSA ($R_{\text{mul}} = 0,31$) и длительностью заболевания ($p < 0,05$). Определение NF- κ B может быть рассмотрено как дополнительный критерий оценки тяжести состояния у детей с псориазом. Показаны различия в степени снижения числа клеток с транслокацией NF- κ B через сутки после введения биологической терапии (адалимумаб, этанерцепт, устекинумаб). Исследование активации NF- κ B в популяциях клеток открывает перспективы понимания патогенетических механизмов воспаления и разработки новых методов лечения псориаза.

Ключевые слова: дети, вульгарный псориаз, PASI, BSA, лимфоциты, NF- κ B, биологические препараты**Финансирование:** исследование выполнено в рамках государственного задания Минздрава России, № темы AAAA-A19-119013090093-2.**Благодарности:** авторы выражают благодарность за активное сотрудничество всем участвовавшим пациентам и выражают признательность научным сотрудникам лаборатории иммунологии и вирусологии, а также врачам-дерматологам и медицинским сестрам отделения дерматологии ФГБУ «Национального медицинского исследовательского центра здоровья детей» г. Москва, Россия, принимавших участие в этом исследовании.**Вклад авторов:** Д. Г. Купцова, С. В. Петричук — концепция и дизайн исследования, набор экспериментальных данных и анализ результатов, статистическая обработка данных, написание и редактирование рукописи; О. В. Курбатова, Т. В. Радыхина — набор экспериментальных данных, редактирование рукописи; Н. Н. Мурашкин, А. А. Хотко, Р. А. Иванов — анализ результатов, редактирование рукописи.**Соблюдение этических стандартов:** исследование одобрено этическим комитетом ФГАУ «НМИЦ здоровья детей» (протокол № 2 от 14 февраля 2020 г.), проведено в соответствии с этическими принципами Хельсинкской декларации, зарегистрировано в ClinicalTrials.gov ID: NCT04989296. Родители всех детей и подростков, участвовавших в исследовании, подписали добровольное информированное согласие на медицинское вмешательство в стационаре, обработку персональных данных и использование данных в научных целях.✉ **Для корреспонденции:** Дарья Геннадьевна Купцова
Ломоносовский проспект, д. 2, стр. 1, г. Москва, 119296, Россия; dg.kuptsova@gmail.com**Статья получена:** 11.02.2022 **Статья принята к печати:** 03.03.2022 **Опубликована онлайн:** 20.03.2022**DOI:** 10.24075/vrgmu.2022.012

Psoriasis is a multifactorial immune-mediated inflammatory skin disorder with a complex pathogenesis [1–3], caused by interactions of immune system, psoriasis susceptibility loci, psoriasis autoantigens, and numerous environmental factors [4]. Psoriasis has various cutaneous clinical manifestations, based on which a number of disease forms is distinguished. Psoriasis vulgaris, being the most common form, is diagnosed in 90% cases [5, 6]. Psoriasis is characterized by hyperproliferation of keratinocytes, blood vessel dilation and leukocyte cell infiltration in skin dermis, and skin plaques [7].

It is believed that synthesis of pro-inflammatory cytokines, being the pathogenic cascade triggers, by activated T cells plays a key role in the skin inflammation associated with psoriasis [8]. Disease begins with T cell activation by unknown antigen or gene product. After the T cell activation, a number of pro-inflammatory cytokines and chemokines are secreted [9]. Cytokine action contributes to proliferation of keratinocytes, epidermal hyperplasia, neutrophil migration, enhanced T helper type 1 (Th1) cell response [10]. The increase in the number of T helper 17 cells (Th17) in blood and skin of patients with psoriasis with the progression of skin lesions was reported [11–13]. It was also found that elevated blood counts of regulatory T cells (Treg) in patients with psoriasis did not suppress inflammatory response due to the cells' functional failure [14, 15].

Complex pathogenesis of psoriasis could be explained by alterations in the intracellular signaling pathways. Impaired regulation of the signal transduction pathways affects activation, proliferation and differentiation of keratinocytes, associated with psoriasis [16, 17]. The nuclear factor κ B (NF- κ B) pathway, which has been first discovered in mature B cells by R. Sen and D. Baltimore, is one of the intracellular signaling pathways [18]. NF- κ B is capable of binding with the gene promoter encoding the immunoglobulin — light chain. NF- κ B is a family of structurally similar transcription factors, such as RelA (p65), NF- κ B1 (p50/p105), NF- κ B2 (p52/p100), c-Rel, and RelB. The NF- κ B family members function as various hetero- and homodimers (p50-p65; RelB-p100), except for RelB. The main active form of NF- κ B is a complex formed by subunit p65 and subunit p50 or p52 bound to the I- κ B inhibitor protein [19]. The advanced Amnis ImageStreamX imaging flow cytometry system makes it possible to assess the percentage of cells with NF- κ B translocation (% of activated cells with nuclear localization of NF- κ B) in various populations [20, 21].

Under physiological conditions, the NF- κ B/I- κ B complex is a self-regulating system [22]. NF- κ B activation occurs in response to the wide range of stimuli [23]. Stimulus activates the NF- κ B signaling pathway, which leads to the NF- κ B release from the inhibitor complex and NF- κ B translocation from cytoplasm into cell nucleus. NF- κ B is involved in regulation of numerous pro-inflammatory genes and affects synthesis of pro-inflammatory cytokines, such as IL1 β , IL6, IL8, TNF α , directly involved in the development of psoriasis [24–26].

Multiple studies confirmed impaired regulation of the NF- κ B signaling pathways associated with psoriasis in *in vitro* models, animal models, and skin biopsy samples, obtained from patients with psoriasis [10, 25, 26]. Furthermore, anti-TNF therapy and glucocorticoid therapy reduce the levels of active NF- κ B and related elements of the signaling pathway [27, 30]. Currently, the effects of other targeted biologics on the variation in the number of cells with NF- κ B translocation are under study, however, chronic NF- κ B pathway inhibition may reduce therapeutic efficacy in patients with immune-mediated diseases [28]. Thus, quantification of cells with NF- κ B translocation could be a promising tool for evaluation of the disease severity and therapeutic efficacy in patients with

immune-mediated diseases. The study was aimed to quantify cells with NF- κ B translocation in the lymphocyte populations of children with psoriasis depending on the disease severity and therapy.

METHODS

Clinical characteristics of patients

A total of 130 children and adolescents with psoriasis vulgaris were enrolled in the study, of them 42 patients were followed-up. The comparison group included 30 healthy children. The surveyed children's age was 1–18 years: psoriasis — Me 12.5 [8.3; 15.5], comparison group — Me 12.4 [7.4; 16.1]. There were 62 girls and 68 boys in the group with psoriasis, and 18 girls and 12 boys in the comparison group. All children were of European origin. Inclusion criteria: proven case of psoriasis vulgaris. Exclusion criteria: other forms of psoriasis, 18 years of age or more, inability to obtain blood sample.

Severity of psoriasis was assessed in all patients using the PASI (Psoriasis Area and Severity Index) and BSA (Body Surface Area, %) indices. Children with psoriasis received different pathogenetic therapy in accordance with the guidelines and psoriasis severity. Children were prescribed topical corticosteroids and emollients with keratolytic effects ($n = 41$), systemic methotrexate therapy ($n = 28$), genetically-engineered biological drugs (GEBD; $n = 61$). The effects of GEBD were assessed in 42 patients with psoriasis before and 24 hours after administration of the following drugs: adalimumab ($n = 24$), etanercept ($n = 8$), ustekinumab ($n = 10$).

Isolation of peripheral blood mononuclear cells

To isolate the peripheral blood mononuclear cells (PBMCs), the 5 mL fasting whole blood samples were used, collected in the morning into EDTA tubes. Blood samples were processed on the same day. Whole blood was diluted with warm glutamine-free RPMI 1640 medium (PanEco; Russia) in a ratio of 1 : 3, gently layered over 2 mL of the Histopaque-1.077 g/cm³ medium (Sigma-Aldrich; USA), then centrifuged at 2000 RPM for 20 min at room temperature. Buffy coat was collected into 15 mm Falcon tubes (BD; USA) and washed with RPMI medium for 8 min under the same conditions. After that supernatant was drained, and the cells were diluted with the RPMI-1640 medium to the desired volume.

Lymphocyte immunophenotyping and evaluation of NF- κ B translocation from cytoplasm into nucleus

Cell populations were isolated by step-wise gating using monoclonal antibodies (mAbs) labeled with fluorochromes (Beckman Coulter; USA): CD19-PE, CD4-PE, CD8-PE, CD (16/56)-PE, CD127-PE, CD161-PE, CD3-ECD, CD4-PB, CD25 PE-Cy7. Cells with NF- κ B translocation were quantified in lymphocyte populations with the imaging flow cytometry Amnis ImageStreamX Mk II platform (Luminex; USA) using the Amnis NF- κ B Translocation Kit (Luminex; USA), which included antibody Anti-Hu NF- κ B (p50) conjugated to Alexa Fluor 488 for detection of NF- κ B and the 7-AAD nuclear dye. The tubes, containing 100 μ L of PBMCs, were added 10 μ L of mAb and incubated for 20 min in a dark place, then NF- κ B translocation was assessed in accordance with the manufacturer's instructions. The following cell populations were assessed: CD3⁺ (T cells); CD3⁺CD4⁺ (T helper cells); CD3⁺CD8⁺ (cytotoxic T cells); CD3⁺CD19⁺ (B cells); CD3⁺CD16⁺/CD56⁺ (natural killer

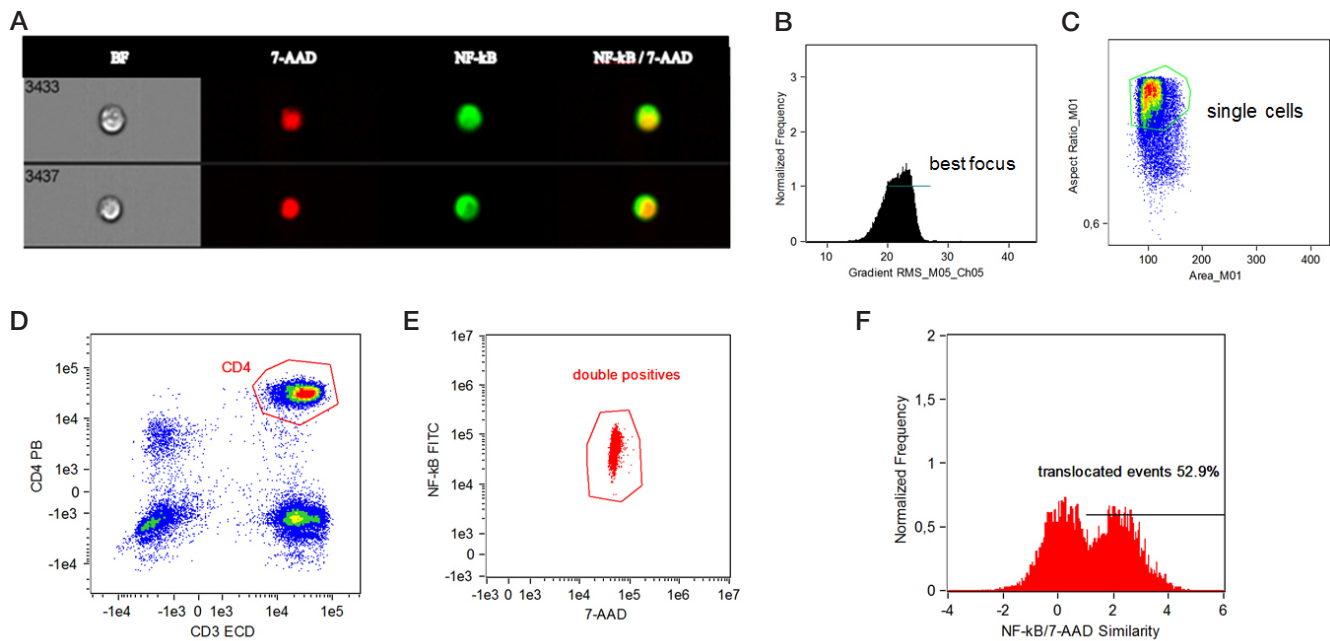


Fig. 1. Stages of analysis when quantifying cells with NF- κ B translocation. **A.** Gallery of recorded cell images. **B.** Isolation of cells in good focus based on Gradient RMS. **C.** Isolation of single events. **D.** Isolation of the studied lymphocyte population, particularly CD3⁺CD4⁺ (CD3_ECD — channel 4; CD4_PB — channel 3). **E.** Isolation of double-positive cells: NF- κ B+/7-AAD+ (NF- κ B_FITC — channel 2; 7-AAD — channel 5). **F.** Isolation of the proportion of cells with NF- κ B translocation based on Similarity > 1

cells); CD3⁺CD16⁺/CD56⁺ (natural killer T cells); CD3⁺CD4⁺CD8⁺ (immature T cells); CD4⁺CD25⁺CD127^{high} (activated T helper cells, T_{act}); CD4⁺CD25⁺CD127^{low} (T_{reg}); CD4⁺CD161⁺CD3⁺ (Th17).

Data recording and analysis with the ImageStream Mk II Imaging Flow Cytometer

Cell imaging and recording were performed with the ImageStream Mk II Imaging Flow Cytometer using the INSPIRE™ software (Luminex; USA) at 40x magnification and low flow rate. Image recording involved collecting at least 20,000 events per sample in the lymphoid region for the major lymphocyte populations, and at least 40,000 events for the T_{reg}, T_{act} and Th17 populations.

The images acquired were analyzed using the IDEAS® ImageStreamX software (Luminex; USA) in accordance with the algorithm provided in Fig. 1. Data analysis started with digital pixel-based spectral compensation applied to each cell image. After compensation, single cells were analyzed with good focus, and single events were isolated (Fig. 1B, C). The percentage of the NF- κ B+/7-AAD+ double-positive cells was defined based on fluorescence intensity (Fig. 1D, E). At the next stage, Similarity was assessed, which reflected the degree of the NF- κ B and 7-AAD colocalization in the studied population

regardless of morphology (Fig. 1F). Similarity was calculated based on the Pearson correlation coefficient as described earlier [20, 21].

Statistical analysis

Statistical processing of the research data was performed using the Statistica 10.0 software package (StatSoft; USA). Descriptive statistics of quantitative indicators was presented as median (lower and upper quartiles), Me (Q_{0.25}; Q_{0.75}). The nonparametric Mann-Whitney U test was used to assess the significance of differences between groups. The stepwise multiple regression method with exceptions was used to obtain regression equations. The differences were considered significant at $p < 0.05$.

RESULTS

Assessment of lymphocyte populations with NF- κ B translocation in children with psoriasis and comparison group

There was a significant increase in the percentage of cells with NF- κ B translocation in the populations of T helper cells ($p = 0.001$),

Table 1. Number of cells with NF- κ B translocation in children with psoriasis and comparison group

Population	Patients with psoriasis ($n = 130$)	Healthy children ($n = 30$)	p
B cells	48.3 [38;64]	58.4 [40;72]	0.322
T cells	19.9 [17;26]	18.0 [16;21]	0.113
T helper cells	20.1 [17;26]	18.4 [14;20]	0.001
Cytotoxic T cells	18.0 [15;24]	17.2 [15;23]	0.402
Immature T cells	24.4 [18;36]	23.7 [19;33]	0.473
NK cells	28.0 [19;39]	29.9 [18;42]	0.829
NKT cells	22.3 [16;34]	20.1 [17;25]	0.315
Activated T helper cells	18.7 [15;24]	15.2 [14;18]	0.012
Regulatory T cells	23.0 [19;32]	20.3 [16;26]	0.032
T helper 17 cells	20.7 [17;27]	19.6 [17;23]	0.034

Note: p — significance of differences between groups, Mann-Whitney U test.

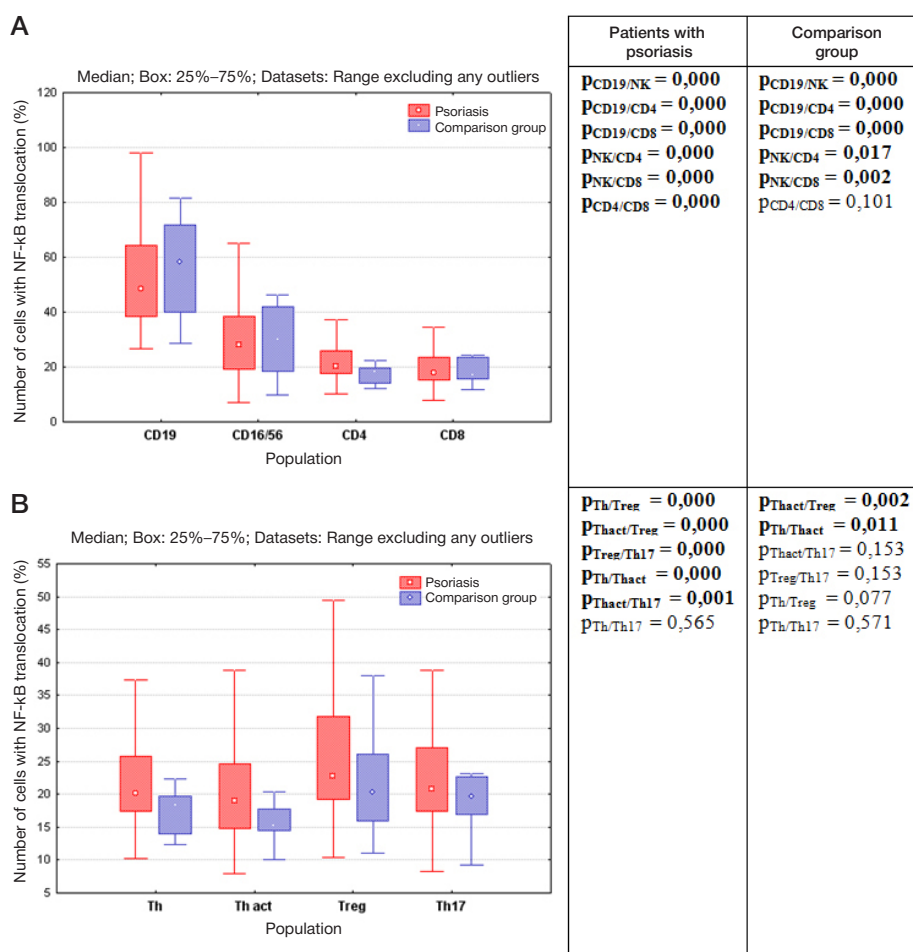


Fig. 2. Number of major (A) and minor (B) populations of lymphocytes and NK cells with NF-κB translocation in children with psoriasis and comparison group. p — significance of differences between populations, Wilcoxon signed rank test for dependent variables

T_{act} ($p = 0.012$), T_{reg} ($p = 0.032$), and $Th17$ ($p = 0.034$) in children with psoriasis compared to healthy children (Table 1). In children with psoriasis, an upward trend was observed in the percentage of cells with NF-κB translocation in the populations of T cells, cytotoxic T cells, and natural killer T (NKT) cells, however, in the populations of B cells and natural killer (NK) cells there was a downward trend. The largest proportion of cells with NF-κB translocation was revealed in B cell populations of both children with psoriasis and comparison group (Table 1).

Analysis revealed differences in the percentage of cells with NF-κB translocation in the studied cell populations of surveyed children. The number of cells with NF-κB translocation was significantly ($p = 0.000$) higher in B cell population compared to NK cells, T helper cells, cytotoxic T cells, and in the NK cell population it was significantly ($p = 0.000$) higher compared to the populations of T helper cells and cytotoxic T cells in both children with psoriasis and comparison group; moreover, it was 2.5 times higher compared to other cell populations (Table 1; Fig. 2A). In the group

Table 2. Correlations of the number of cells with NF-κB translocation in lymphocyte populations with the patients' age and the duration of psoriasis

Population	Psoriasis ($n = 130$)				Comparison group ($n = 30$)	
	Age		Disease duration		Age	
	r	p	r	p	r	p
B cells	0.09	0.299	-0.02	0.796	0.25	0.182
T cells	0.21	0.016	0.21	0.22	0.28	0.142
T helper cells	0.22	0.011	0.21	0.022	0.25	0.194
Cytotoxic T cells	0.19	0.031	0.19	0.003	0.32	0.09
Immature T cells	0.2	0.028	0.21	0.021	0.24	0.214
NK cells	0.24	0.006	0.27	0.002	0.11	0.577
NKT cells	0.16	0.071	0.15	0.083	0.41	0.052
Activated T helper cells	0.21	0.023	0.16	0.109	0.16	0.433
Regulatory T cells	0.2	0.031	0.15	0.116	0.18	0.383
T helper 17 cells	0.23	0.015	0.21	0.021	0.46	0.015

Note: r — Pearson correlation coefficient, p — probability of non-zero regression coefficients.

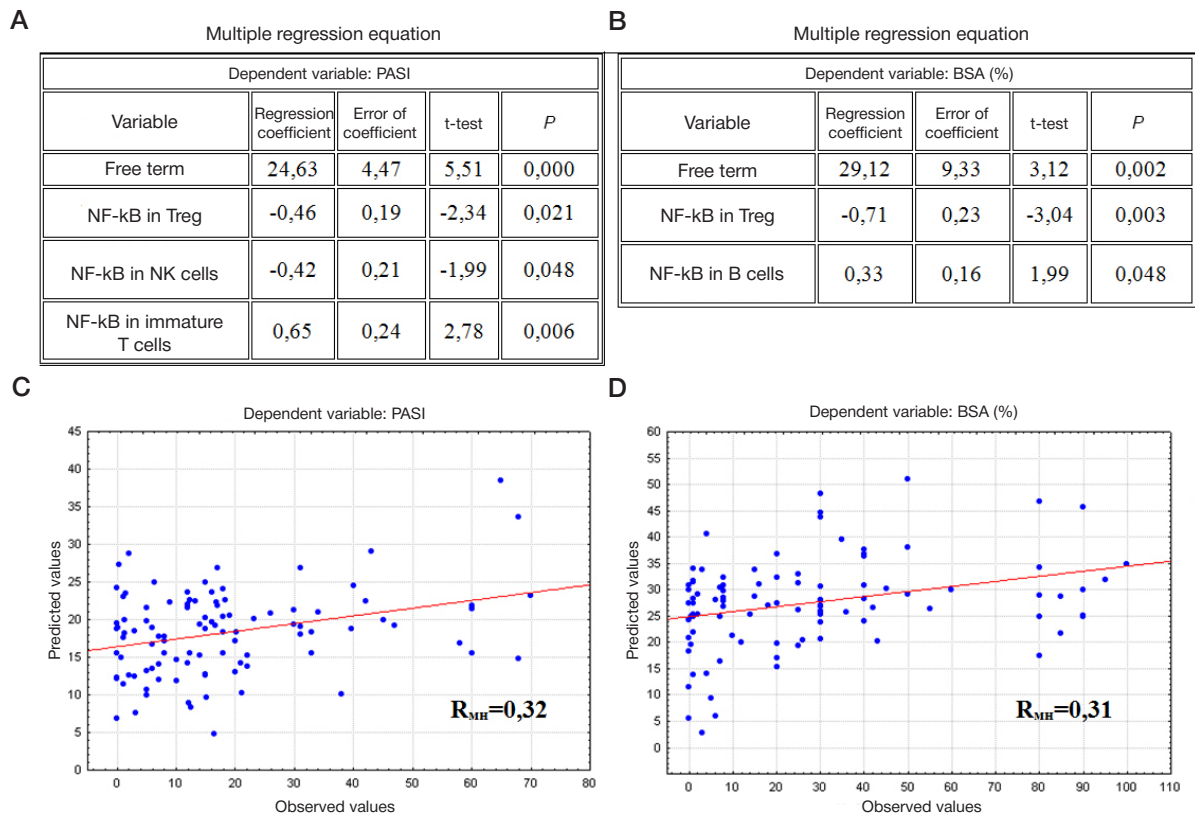


Fig. 3. Multiple regression equation for the relationship between PASI (A) and BSA (B) scores and the number of cells with NF-κB translocation in children with psoriasis, and the relationship between the observed and predicted values calculated using the regression equation for PASI (C) and BSA (D) indices. Regression equations were constructed using the stepwise multiple regression method with exceptions. R_{mul} — coefficient of multiple correlation, R ; p — significance of non-zero regression coefficients

of healthy children, the number of cells with NF-κB translocation in the populations of T helper cells and cytotoxic T cells was the same ($p = 0.101$). In contrast to healthy children, the increased percentage of cells with NF-κB translocation in the population of T helper cells compared to cytotoxic T cells was revealed in patients with psoriasis ($p = 0.000$; Fig. 2A).

In the group of healthy children, it was found that the average number of cells with NF-κB translocation in T cell populations, including T_{reg} , $Th17$, and T_{act} , was 15κ20%. The largest proportion of cells with NF-κB translocation was found in the T_{reg} population (20% of cells), and the lowest proportion was observed in the T_{act} population (15% of cells; $p = 0.011$), the difference was considered significant ($p = 0.002$; Fig. 2B).

In children with psoriasis, the number of cells with NF-κB translocation in the T_{reg} , $Th17$, and T_{act} populations was significantly higher compared to the comparison group (Table 1). In healthy children, the highest percentage of cells with NF-κB translocation was also found in the T_{reg} population (23% of cells), and was significantly higher than in the populations of T helper cells, $Th17$, and T_{act} ($p = 0.000$; Fig. 2B). The number of T_{act} with NF-κB translocation was significantly lower compared to the T helper cell population, just like in the group of healthy children ($p = 0.000$; Fig. 2B). In contrast to healthy children, the number of $Th17$ with NF-κB translocation was significantly higher compared to the T_{act} population ($p = 0.001$).

Table 3. Number of cells with NF-κB translocation in children with psoriasis before and 24 h after administration of GEBD

Population	Number of cells with NF-κB translocation								
	Adalimumab (<i>n</i> = 24)			Etanercept (<i>n</i> = 8)			Ustekinumab (<i>n</i> = 10)		
	before	after	<i>p</i>	before	after	<i>p</i>	before	after	<i>p</i>
B cells	46.0 [39; 65]	38.2 [33; 45]	0.002	36.7 [33; 42]	28.0 [27; 31]	0.004	51.7 [35; 71]	44.8 [32; 51]	0.217
T cells	20.2 [17; 25]	19.5 [15; 21]	0.12	17.0 [16; 20]	17.6 [15; 19]	0.721	24.9 [18; 36]	18.2 [16; 25]	0.105
T helper cells	20.2 [18; 24]	18.3 [16; 21]	0.025	19.0 [18; 21]	17.5 [16; 19]	0.049	24.8 [19; 32]	19.6 [16; 25]	0.191
Cytotoxic T cells	19.2 [16; 24]	17.2 [15; 18]	0.021	16.30 [16; 18]	16.6 [15; 18]	0.99	23.9 [19; 35]	16.6 [14; 25]	0.052
Immature T cells	22.5 [16; 31]	21.2 [20; 38]	0.814	21.2 [19; 24]	19.2 [17; 23]	0.161	36.2 [30; 48]	21.4 [14; 30]	0.009
NK cells	27.7 [18; 32]	26.2 [19; 29]	0.574	30.6 [29; 36]	30.7 [27; 33]	0.721	37.9 [35; 42]	25.3 [17; 29]	0.018
NKT cells	21.6 [15; 27]	19.7 [15; 24]	0.418	20.9 [18; 23]	18.4 [17; 21]	0.131	30.0 [26; 44]	24.7 [13; 31]	0.052
Activated T helper cells	19.1 [16; 21]	17.1 [14; 20]	0.165	19.7 [16; 24]	14.3 [14; 16]	0.007	24.4 [17; 34]	16.4 [13; 24]	0.042
Regulatory T cells	19.1 [16; 21]	20.5 [19; 23]	0.005	23.2 [19; 28]	19.4 [19; 21]	0.105	34.9 [22; 48]	21.5 [15; 29]	0.018
T helper 17 cells	22.4 [18; 23]	18.5 [16; 21]	0.032	18.6 [18; 20]	17.2 [15; 18]	0.021	27.3 [27; 39]	19.1 [14; 25]	0.011

Note: p — significance of differences in the numbers of cells with NF-κB translocation obtained before and 24 h after administration of GEBD, Mann–Whitney U test.

Correlations of the number of cells with NF- κ B translocation with the patients' age and the duration of psoriasis

Analysis of the relationship between the number of cells with NF- κ B translocation and the healthy children's age revealed no correlations in all cell populations, except for T helper 17 cells, the number of which increased with age (Table 2). In children with psoriasis, the proportion of cells with NF- κ B translocation increased with age in all populations, except for B cells and NKT cells. With increased disease duration, the number of cells with NF- κ B translocation significantly increased in the populations of T helper cells, cytotoxic T cells, immature T cells, NK cells and Th17 (Table 2). In children with psoriasis, correlation between the patient's age and the disease duration was revealed ($p = 0.000$): the older the child, the longer he was ill.

Relationship between the content of cells with NF- κ B translocation and psoriasis severity in children

PASI and BSA indices were evaluated in the surveyed children with psoriasis. The psoriasis severity PASI scores in children varied between 0–70% (Me 13.3 [5; 22]), and BSA scores varied between 0–100% (Me 20 [4; 40]).

Multiple correlation analysis of the relationship between the psoriasis severity and the number of cells with NF- κ B translocation showed the increase in the PASI score with the decrease in the number of T_{reg} and NK cells with NF- κ B translocation and the increase in the proportion of immature T cells with translocation ($R_{mul} = 0.32$; Fig. 3A). The increased BSA scores are associated with the decreased number of cells with NF- κ B translocation in the T_{reg} population and increased number in B cell population ($R_{mul} = 0.31$; Fig. 3B).

Assessing the number of cells with NF- κ B translocation in children with psoriasis receiving various types of therapy

Comparison of the proportion of cells with NF- κ B translocation in lymphocyte populations of children with psoriasis receiving various types of therapy revealed no significant differences between groups of children receiving different therapy. However, maximum deviation from healthy children was observed in the group of children, who received biological therapy. The number of cells with NF- κ B translocation in the T helper cell populations of children, who received topical therapy, increased by 6%, in the group of children, who received methotrexate, it increased by 10%, and in the group of children, who received biologics, by 11.5% compared to healthy children. The number of cells with NF- κ B translocation in B cell population decreased by 17% in patients, who received topical therapy, by 4% in patients, who received methotrexate, and by 29% in children, who received biologics, compared to healthy children.

To assess the effects of GEBC on the number of cells with NF- κ B translocation, we examined 42 children with psoriasis before and 24 h after administration of adalimumab, etanercept, ustekinumab. A significantly decreased number of cells with NF- κ B translocation in the populations of B cells, T helper cells, cytotoxic T cells, T_{reg} , and Th17 was observed 24 h after administration of adalimumab (Table 3).

The significantly decreased number of cells with NF- κ B translocation was revealed in the populations of B cells, T helper cells, T_{act} , and Th17 after administration of etanercept. The significantly decreased number of NF- κ B cells was observed in the populations of NK cells, immature T cells, T_{act} , T_{reg} , and Th17 after administration of ustekinumab (Table 3).

It is interesting to note that biologics, adalimumab and etanercept, significantly decreased the number of B cells with NF- κ B translocation after 24 h: by 20.4 and 31%, respectively. However, administration of ustekinumab resulted in the insignificantly decreased number (Table 3). The same downward trend was observed in the T helper cell population after administration of adalimumab (by 10.4%) and etanercept (by 8.6%). Significant alterations in the number of cytotoxic lymphocytes with NF- κ B translocation were observed after administration of adalimumab (Table 3).

The number of Tact with NF- κ B translocation significantly decreased 24 h after administration of etanercept (by 37.8%) and ustekinumab (by 48.7%) (Table 3). Only the administration of ustekinumab resulted in the decrease in the number of T_{reg} with NF- κ B translocation by 62%, however, administration of adalimumab resulted in the significant decrease in their number by 6%. Administration of all biologics resulted in the decreased number of Th17 with NF- κ B translocation: the maximum decrease was observed after administration of ustekinumab (by 42.9%), and administration of adalimumab and etanercept resulted in the decrease by 21.1 and 8%, respectively (Table 3).

Furthermore, only administration of ustekinumab decreased the number of cells with NF- κ B translocation in the population of NK cells by 49.8% and in the population of immature T cells by 69%.

DISCUSSION

Alterations in signaling pathways, such as NF- κ B, JAK-STAT, Janus kinase (JAK)/signal transducer pathway, Akt and Wnt signaling pathways, are observed in individuals with psoriasis [16, 17]. The number of cells with NF- κ B translocation in children with psoriasis was assessed using the ImageStreamX advanced technique. Our findings about the number of cells with NF- κ B translocation are in line with the data reported by other researchers: the maximum number of cells with NF- κ B translocation has been revealed in B cell population [18].

Our study has shown that in children with psoriasis, the number of cells with NF- κ B translocation in the populations of T helper cells, T_{reg} , T_{act} , and Th17 is increased compared to healthy children. That could explain the effects of the NF- κ B signaling pathway activation in these cells, which are responsible for production of pro-inflammatory cytokines directly involved in pathogenesis of psoriasis [24–26].

There was a direct correlation between the number of cells with NF- κ B translocation and the children's age in children with psoriasis; the proportion of such cells in healthy children did not change with age. Probably, our findings about the relationship between the number of cells with NF- κ B translocation and age in children with psoriasis are attributable to the correlation between the duration of psoriasis and the surveyed children's age.

The number of T_{reg} with NF- κ B translocation decrease with the increase in the psoriasis severity in children according to PASI and BSA, which is in line with the other researchers' report of the decreased T_{reg} functional activity in psoriasis [27]. This fact confirms the importance of assessing both T_{reg} number and functional activity [14, 15]. As one of the factors involved in the cell functional activity regulation, NF- κ B determination could be considered an additional criterion for the disease severity evaluation in patients with psoriasis.

Our findings are in line with the data on the NF- κ B activation reduction by anti-TNF therapy (adalimumab) in adults with psoriasis [28–30]. The maximum decrease in the number of cells with NF- κ B translocation in the populations of NK cells, immature T cells, T_{act} , T_{reg} , and Th17 of children with

psoriasis was detected when using ustekinumab. The use of TNF α and IL12/23 blockers reduces the number of cells with NF- κ B translocation to varying degrees, depending on the cell population and therapy applied. Taking into account the findings and the minimally invasive method of assessing the number of cells with NF- κ B translocation in the whole blood of children with psoriasis, we consider this line of research to be perspective for diagnosis of the disease severity and predicting therapeutic efficacy.

CONCLUSIONS

Significant differences between lymphocyte populations by the number of cells with NF- κ B translocation were revealed

in both children with psoriasis and comparison group. The increased number of cells with NF- κ B translocation in the populations of T helper cells, T_{act}⁺ T_{reg}⁺, and Th17 in children with psoriasis compared to healthy children was observed. The number of cells with NF- κ B translocation correlates with the disease severity and duration. NF- κ B determination could be considered an additional criterion for evaluation of the disease severity in children with psoriasis. The number of cells with NF- κ B translocation in lymphocyte populations decreases 24 h after administration of GEBD and depends on the antipsoriatic therapy targets. Studying NF- κ B activation in cell populations offers the prospect of understanding pathogenetic mechanisms of inflammation and developing new treatment methods for psoriasis.

References

- Gisondi P, Bellinato F, Girolomoni G, Albanesi C. Pathogenesis of Chronic Plaque Psoriasis and Its Intersection With Cardio-Metabolic Comorbidities. *Front Pharmacol*. 2020; 11: 117. DOI: 10.3389/fphar.2020.00117.
- Hugh JM, Weinberg JM. Update on the pathophysiology of psoriasis. *Cutis*. 2018; 102 (5S): 6–12.
- Smirnova SV, Smolnikova MV. Immune Pathogenesis of Psoriasis and Psoriatic Arthritis. *Medical Immunology (Russia)*. 2014; 16 (2): 127–138. (In Russ.) <https://doi.org/10.15789/1563-0625-2014-2-127-138>.
- Hawkes JE, Chan TC, Krueger JG. Psoriasis pathogenesis and the development of novel targeted immune therapies. *J Allergy Clin Immunol*. 2017; 140 (3): 645–53. DOI: 10.1016/j.jaci.2017.07.004.
- Relvas M, Torres T. Pediatric Psoriasis. *Am J Clin Dermatol*. 2017; 18 (6): 797–811. DOI: 10.1007/s40257-017-0294-9.
- Tangatco JAA, Lara-Corrales I. Update in the management of pediatric psoriasis. *Curr Opin Pediatr*. 2017; 29 (4): 434–42. DOI: 10.1097/MOP.0000000000000517.
- Deng Y, Chang C, Lu Q. The Inflammatory Response in Psoriasis: a Comprehensive Review. *Clin Rev Allergy Immunol*. 2016; 50 (3): 377–89. DOI: 10.1007/s12016-016-8535-x.
- Georgescu SR, Tampa M, Caruntu C, Sarbu MI, Mitran CI, Mitran MI, et al. Advances in Understanding the Immunological Pathways in Psoriasis. *Int J Mol Sci*. 2019; 20 (3): 739. DOI: 10.3390/ijms20030739.
- Chiricozzi A, Romanelli P, Volpe E, Borsellino G, Romanelli M. Scanning the Immunopathogenesis of Psoriasis. *Int J Mol Sci*. 2018; 19 (1): 179. DOI: 10.3390/ijms19010179.
- Frischknecht L, Vecellio M, Selmi C. The role of epigenetics and immunological imbalance in the etiopathogenesis of psoriasis and psoriatic arthritis. *Ther Adv Musculoskelet Dis*. 2019; 11: 1759720X19886505. DOI: 10.1177/1759720X19886505.
- Diani M, Altomare G, Reali E. T Helper Cell Subsets in Clinical Manifestations of Psoriasis. *J Immunol Res*. 2016; 2016: 7692024. DOI: 10.1155/2016/7692024.
- Solberg SM, Aarebrot AK, Sarkar I, Petrovic A, Sandvik LF, Bergum B, et al. Mass cytometry analysis of blood immune cells from psoriasis patients on biological therapy. *Eur J Immunol*. 2020. DOI: 10.1002/eji.202048857.
- Kuptsova D, Radygina T, Murashkin N, Petrichuk SV. Indicators of cellular immunity and suppressor cells of myeloid origin in children with psoriasis. *J Immunopathology, allergology, infectology*. 2020; 3: 55–65. doi: 10.14427/jipai.2020.3.55.
- Uttarkar S, Brembilla NC, Boehncke WH. Regulatory cells in the skin: Pathophysiologic role and potential targets for anti-inflammatory therapies. *J Allergy Clin Immunol*. 2019; 143 (4): 1302–10. DOI: 10.1016/j.jaci.2018.12.1011.
- Zhang L, Li Y, Yang X, Wei J, Zhou S, Zhao Z, et al. Characterization of Th17 and FoxP3(+) Treg Cells in Paediatric Psoriasis Patients. *Scand J Immunol*. 2016; 83 (3): 174–80. DOI: 10.1111/sji.12404.
- Lizzul PF, Aphale A, Malaviya R, Sun Y, Masud S, Dombrovskiy V, et al. Differential expression of phosphorylated NF-kappaB/RelA in normal and psoriatic epidermis and downregulation of NF-kappaB in response to treatment with etanercept. *J Invest Dermatol*. 2005; 124 (6): 1275–83. DOI: 10.1111/j.0022-202X.2005.23735.x.
- Woo YR, Cho DH, Park HJ. Molecular Mechanisms and Management of a Cutaneous Inflammatory Disorder: Psoriasis. *Int J Mol Sci*. 2017; 18 (12): 2684. DOI: 10.3390/ijms18122684.
- Lawrence T. The nuclear factor NF-kappaB pathway in inflammation. *Cold Spring Harb Perspect Biol*. 2009; 1 (6): a001651. DOI: 10.1101/cshperspect.a001651.
- Sun SC, Chang JH, Jin J. Regulation of nuclear factor- κ B in autoimmunity. *Trends Immunol*. 2013; 34 (6): 282–9. DOI: 10.1016/j.it.2013.01.004.
- George TC, Fanning SL, Fitzgerald-Bocarsly P, Medeiros RB, Highfill S, Shimizu Y, et al. Quantitative measurement of nuclear translocation events using similarity analysis of multispectral cellular images obtained in flow. *J Immunol Methods*. 2006; 311 (1–2): 117–29. DOI: 10.1016/j.jim.2006.01.018.
- Barteneva NS, Vorobjev IA. Imaging Flow Cytometry Methods and protocols. *Methods Mol Biol*. 2017; 178–88.
- Karin M, Ben-Neriah Y. Phosphorylation meets ubiquitination: the control of NF-[kappa]B activity. *Annu Rev Immunol*. 2000; 18: 621–63. DOI: 10.1146/annurev.immunol.18.1.621.
- Liao G, Zhang M, Harhaj EW, Sun SC. Regulation of the NF-kappaB-inducing kinase by tumor necrosis factor receptor-associated factor 3-induced degradation. *J Biol Chem*. 2004; 279 (25): 26243–50. DOI: 10.1074/jbc.M403286200.
- Bhatt D, Ghosh S. Regulation of the NF- κ B-Mediated Transcription of Inflammatory Genes. *Front Immunol*. 2014; 5: 71. DOI: 10.3389/fimmu.2014.00071.
- Moorchun N, Kulaar JS, Chatterjee M, Vasudevan B, Tripathi T, Dutta V. Role of NF- κ B in the pathogenesis of psoriasis elucidated by its staining in skin biopsy specimens. *Int J Dermatol*. 2014; 53 (5): 570–4. DOI: 10.1111/ijd.12050.
- Goldminz AM, Au SC, Kim N, Gottlieb AB, Lizzul PF. NF- κ B: an essential transcription factor in psoriasis. *J Dermatol Sci*. 2013; 69 (2): 89–94. DOI: 10.1016/j.jdermsci.2012.11.002.
- Nussbaum L, Chen YL, Ogg GS. Role of regulatory T cells in psoriasis pathogenesis and treatment. *Br J Dermatol*. 2021; 184 (1): 14–24. DOI: 10.1111/bjd.19380.
- Luan L, Han S, Wang H, Liu X. Down-regulation of the Th1, Th17, and Th22 pathways due to anti-TNF- α treatment in psoriasis. *Int Immunopharmacol*. 2015; 29 (2): 278–84. DOI: 10.1016/j.intimp.2015.11.005.
- Johansen C, Riis JL, Gedebjerg A, Kragballe K, Iversen L. Tumor necrosis factor α -mediated induction of interleukin 17C in human keratinocytes is controlled by nuclear factor κ B. *J Biol Chem*. 2011; 286 (29): 25487–94. DOI: 10.1074/jbc.M111.240671.
- Andres-Ejarque R, Ale HB, Grys K, et al. Enhanced NF- κ B signaling in type-2 dendritic cells at baseline predicts non-response to adalimumab in psoriasis. *Nat Commun*. 2021; 1: 4741. Available from: <https://doi.org/10.1038/s41467-021-25066-9>.

Литература

- Gisondi P, Bellinato F, Girolomoni G, Albanesi C. Pathogenesis of Chronic Plaque Psoriasis and Its Intersection With Cardio-Metabolic Comorbidities. *Front Pharmacol*. 2020; 11: 117. DOI: 10.3389/fphar.2020.00117.
- Hugh JM, Weinberg JM. Update on the pathophysiology of psoriasis. *Cutis*. 2018; 102 (5S): 6–12.
- Смирнова С. В., Смольникова М. В. Иммунопатогенез псориаза и псориатического артрита. *Медицинская иммунология*. 2014; 16 (2): 127–38. <https://doi.org/10.15789/1563-0625-2014-2-127-138>.
- Hawkes JE, Chan TC, Krueger JG. Psoriasis pathogenesis and the development of novel targeted immune therapies. *J Allergy Clin Immunol*. 2017; 140 (3): 645–53. DOI: 10.1016/j.jaci.2017.07.004.
- Relvas M, Torres T. Pediatric Psoriasis. *Am J Clin Dermatol*. 2017; 18 (6): 797–811. DOI: 10.1007/s40257-017-0294-9.
- Tangtaco JAA, Lara-Corrales I. Update in the management of pediatric psoriasis. *Curr Opin Pediatr*. 2017; 29 (4): 434–42. DOI: 10.1097/MOP.0000000000000517.
- Deng Y, Chang C, Lu Q. The Inflammatory Response in Psoriasis: a Comprehensive Review. *Clin Rev Allergy Immunol*. 2016; 50 (3): 377–89. DOI: 10.1007/s12016-016-8535-x.
- Georgescu SR, Tampa M, Caruntu C, Sarbu MI, Mitran CI, Mitran MI, et al. Advances in Understanding the Immunological Pathways in Psoriasis. *Int J Mol Sci*. 2019; 20 (3): 739. DOI: 10.3390/ijms20030739.
- Chiricozzi A, Romanelli P, Volpe E, Borsellino G, Romanelli M. Scanning the Immunopathogenesis of Psoriasis. *Int J Mol Sci*. 2018; 19 (1): 179. DOI: 10.3390/ijms19010179.
- Frischknecht L, Vecellio M, Selmi C. The role of epigenetics and immunological imbalance in the etiopathogenesis of psoriasis and psoriatic arthritis. *Ther Adv Musculoskelet Dis*. 2019; 11: 1759720X19886505. DOI: 10.1177/1759720X19886505.
- Diani M, Altomare G, Reali E. T Helper Cell Subsets in Clinical Manifestations of Psoriasis. *J Immunol Res*. 2016; 2016: 7692024. DOI: 10.1155/2016/7692024.
- Solberg SM, Aarebrot AK, Sarkar I, Petrovic A, Sandvik LF, Bergum B, et al. Mass cytometry analysis of blood immune cells from psoriasis patients on biological therapy. *Eur J Immunol*. 2020. DOI: 10.1002/eji.202048857.
- Купцова Д. Г., Радыгина Т. В., Мурашкин Н. Н., Петричук С. В. Показатели клеточного иммунитета и клетки-супрессоры миелоидного происхождения у детей с псориазом. *Иммунопатология, аллергология, инфектология*. 2020; (3): 55–65. DOI: 10.14427/jpai.2020.3.55.
- Uttarkar S, Brembilla NC, Boehncke WH. Regulatory cells in the skin: Pathophysiologic role and potential targets for anti-inflammatory therapies. *J Allergy Clin Immunol*. 2019; 143 (4): 1302–10. DOI: 10.1016/j.jaci.2018.12.1011.
- Zhang L, Li Y, Yang X, Wei J, Zhou S, Zhao Z, et al. Characterization of Th17 and FoxP3(+) Treg Cells in Paediatric Psoriasis Patients. *Scand J Immunol*. 2016; 83 (3): 174–80. DOI: 10.1111/sji.12404.
- Lizzul PF, Aphale A, Malaviya R, Sun Y, Masud S, Dombrovskiy V, et al. Differential expression of phosphorylated NF-kappaB/RelA in normal and psoriatic epidermis and downregulation of NF-kappaB in response to treatment with etanercept. *J Invest Dermatol*. 2005; 124 (6): 1275–83. DOI: 10.1111/j.0022-202X.2005.23735.x.
- Woo YR, Cho DH, Park HJ. Molecular Mechanisms and Management of a Cutaneous Inflammatory Disorder: Psoriasis. *Int J Mol Sci*. 2017; 18 (12): 2684. DOI: 10.3390/ijms18122684.
- Lawrence T. The nuclear factor NF-kappaB pathway in inflammation. *Cold Spring Harb Perspect Biol*. 2009; 1 (6): a001651. DOI: 10.1101/cshperspect.a001651.
- Sun SC, Chang JH, Jin J. Regulation of nuclear factor-κB in autoimmunity. *Trends Immunol*. 2013; 34 (6): 282–9. DOI: 10.1016/j.it.2013.01.004.
- George TC, Fanning SL, Fitzgerald-Bocarsly P, Medeiros RB, Highfill S, Shimizu Y, et al. Quantitative measurement of nuclear translocation events using similarity analysis of multispectral cellular images obtained in flow. *J Immunol Methods*. 2006; 311 (1–2): 117–29. DOI: 10.1016/j.jim.2006.01.018.
- Barteneva NS, Vorobjev IA. Imaging Flow Cytometry Methods and protocols. *Methods Mol Biol*. 2017; 178–88.
- Karin M, Ben-Neriah Y. Phosphorylation meets ubiquitination: the control of NF-[kappa]B activity. *Annu Rev Immunol*. 2000; 18: 621–63. DOI: 10.1146/annurev.immunol.18.1.621.
- Liao G, Zhang M, Harhaj EW, Sun SC. Regulation of the NF-kappaB-inducing kinase by tumor necrosis factor receptor-associated factor 3-induced degradation. *J Biol Chem*. 2004; 279 (25): 26243–50. DOI: 10.1074/jbc.M403286200.
- Bhatt D, Ghosh S. Regulation of the NF-κB-Mediated Transcription of Inflammatory Genes. *Front Immunol*. 2014; 5: 71. DOI: 10.3389/fimmu.2014.00071.
- Moorchung N, Kulaar JS, Chatterjee M, Vasudevan B, Tripathi T, Dutta V. Role of NF-κB in the pathogenesis of psoriasis elucidated by its staining in skin biopsy specimens. *Int J Dermatol*. 2014; 53 (5): 570–4. DOI: 10.1111/ijd.12050.
- Goldminz AM, Au SC, Kim N, Gottlieb AB, Lizzul PF. NF-κB: an essential transcription factor in psoriasis. *J Dermatol Sci*. 2013; 69 (2): 89–94. DOI: 10.1016/j.jdermsci.2012.11.002.
- Nussbaum L, Chen YL, Ogg GS. Role of regulatory T cells in psoriasis pathogenesis and treatment. *Br J Dermatol*. 2021; 184 (1): 14–24. DOI: 10.1111/bjd.19380.
- Luan L, Han S, Wang H, Liu X. Down-regulation of the Th1, Th17, and Th22 pathways due to anti-TNF-α treatment in psoriasis. *Int Immunopharmacol*. 2015; 29 (2): 278–84. DOI: 10.1016/j.intimp.2015.11.005.
- Johansen C, Riis JL, Gedebjerg A, Kragballe K, Iversen L. Tumor necrosis factor α-mediated induction of interleukin 17C in human keratinocytes is controlled by nuclear factor κB. *J Biol Chem*. 2011; 286 (29): 25487–94. DOI: 10.1074/jbc.M111.240671.
- Andres-Ejarque R, Ale HB, Grys K, et al. Enhanced NF-κB signaling in type-2 dendritic cells at baseline predicts non-response to adalimumab in psoriasis. *Nat Commun*. 2021; 1: 4741. Available from: <https://doi.org/10.1038/s41467-021-25066-9>.

EFFECTS OF COVID-19 VECTOR VACCINE ON AUTOANTIBODY PROFILE IN REPRODUCTIVE AGE WOMEN

Dovgan AA , Drapkina YuS, Dolgushina NV, Menzhinskaya IV, Krechetova LV, Sukhikh GT

Kulakov National Medical Research Center for Obstetrics, Gynecology and Perinatology, Moscow, Russia


Autoimmune mechanisms have been implicated in the negative effects of vaccines on female reproductive health. This study evaluates the endogenous levels of self-reactive antibodies and ovarian reserve-associated hormones before and after immunization with the domestically developed Gam-COVID-Vac combined vector vaccine to check for possible reproductive sequelae. The prospective study enrolled 120 women aged 18–49, subject to vaccination with Gam-COVID-Vac. Ovarian reserve was assessed prior to vaccination and 90 days after the first component injection. Profiles of specific antibodies to self-antigens, including phospholipids, nuclear antigens, FSH, progesterone, and also thyroid, ovarian, trophoblast, and zona pellucida antigens, were assessed at the same time points by enzyme immunoassay. Overall, the vaccination had no effect on the levels of ovarian reserve-associated hormones and autoantibodies, apart from a transient increase in positivity for anti-phosphatidylethanolamine IgM and anti-dsDNA IgG. Seroprevalence of elevated serum autoantibodies constituted 70.8% before and 75% after vaccination. According to the results, immunization with Gam-COVID-Vac does not affect ovarian reserve or autoimmune status, thus being safe for the female reproductive potential.

Keywords: COVID-19, SARS-CoV-2, Gam-COVID-Vac (Sputnik V) vaccine, reproduction, autoantibody profile

Funding: the study was supported by the “Investment to the Future” Sberbank Charitable Foundation within the framework of “Stop the Coronavirus Together” initiative.

Author contributions: Dovgan AA, Drapkina YuS — patient management, manuscript writing; Dolgushina NV — literature research, manuscript editing, statistical analysis; Menzhinskaya IV, Krechetova LV — laboratory research, manuscript editing; Sukhikh GT — conclusive editing and approval of the manuscript.

Compliance with ethical standards: the study was approved by Ethical Review Board at Kulakov National Medical Research Center for Obstetrics, Gynecology and Perinatology (Protocol No. 12 of November 26, 2020). All participants provided informed consent for the study.

 **Correspondence should be addressed:** Alina A. Dovgan
Oparina, 4, Moscow, 117198, Russia; lina.dovgan@gmail.com

Received: 30.03.2022 **Accepted:** 14.04.2022 **Published online:** 21.04.2022

DOI: 10.24075/brsmu.2022.016

ВЛИЯНИЕ ВЕКТОРНОЙ ВАКЦИНЫ ОТ COVID-19 НА ПРОФИЛЬ АУТОАНТИТЕЛ У ЖЕНЩИН РЕПРОДУКТИВНОГО ВОЗРАСТА

А. А. Довгань , Ю. С. Драпкина, Н. В. Долгушина, И. В. Менжинская, Л. В. Кречетова, Г. Т. Сухих

Национальный медицинский исследовательский центр акушерства, гинекологии и перинатологии имени В. И. Кулакова, Москва, Россия


Один из механизмов негативного влияния вакцин на репродуктивное здоровье женщин носит аутоиммунный характер. Целью работы было оценить влияние иммунизации отечественной комбинированной векторной вакциной для профилактики коронавирусной инфекции, вызываемой вирусом SARS-CoV-2, на уровень аутоантител и гормонов, отражающих овариальный резерв, и связь между ними у женщин репродуктивного возраста. В проспективное исследование было включено 120 женщин в возрасте 18–49 лет, вакцинированных Гам-КОВИД-Вак. Овариальный резерв определяли перед вакцинацией и через 90 дней после введения первого компонента. С помощью ИФА изучали профиль антифосфолипидных антител, антител к ядерным антигенам, антигенам щитовидной железы, антиовариальных, антитрофобластических антител, к зоне пеллюцида, ФСГ, прогестерону. После вакцинации не обнаружено повышения уровня аутоантител, за исключением анти-ФЭ IgM и анти-дсДНК IgG-антител, которое носило транзитный характер. Доля позитивных женщин до вакцинации составляла 70,8%, после вакцинации — 75%. Не выявлено корреляционной связи между уровнем аутоантител и гормонов, отражающих овариальный резерв. Согласно результатам, вакцинация Гам-КОВИД-Вак не оказывает негативного влияния на овариальный резерв, не вызывает развития аутоиммунных реакций и ассоциированного с ними снижения репродуктивного потенциала у женщин.

Ключевые слова: COVID-19, SARS-CoV-2, вакцина Гам-КОВИД-Вак (Спутник V), репродукция, профиль аутоантител

Финансирование: работа выполнена при поддержке благотворительного фонда «Вклад в будущее» в рамках программы-акции «Остановим корона-вирус вместе».

Вклад авторов: А. А. Довгань, Ю. С. Драпкина — ведение пациенток, принимающих участие в исследовании, написание статьи; Н. В. Долгушина — сбор и анализ литературных данных, редактирование рукописи, статистический анализ данных; И. В. Менжинская, Л. В. Кречетова — выполнение лабораторной части исследования, редактирование рукописи; Г. Т. Сухих — редактирование и утверждение рукописи.

Соблюдение этических стандартов: исследование одобрено этическим комитетом НМИЦ АГП им. В. И. Кулакова (протокол № 12 от 26 ноября 2020 г.); все пациентки подписали информированное добровольное согласие на участие в исследовании.

 **Для корреспонденции:** Алина Анатольевна Довгань
ул. Академика Опарина, д. 4, г. Москва, 117198, Россия; lina.dovgan@gmail.com

Статья получена: 30.03.2022 **Статья принята к печати:** 14.04.2022 **Опубликована онлайн:** 21.04.2022

DOI: 10.24075/vrgmu.2022.016

Registered COVID-19 vaccines, mostly based on spike glycoprotein (S-protein) of SARS-CoV-2 [1], include whole inactivated vaccines, combined vector vaccines containing recombinant adenoviral particles with SARS-CoV-2 S protein gene, mRNA vaccines, and recombinant protein vaccines. The combined vector Gam-COVID-Vac (Sputnik V™) was the world's first registered COVID-19 vaccine, approved by the Ministry of Health of Russia. The vaccine contains adenoviral vector cargoed with a coding sequence of S-protein intended for

delivery to human cells in order to educate the immune system in a disease-specific manner [2]. The advent and ubiquitous propagation of COVID-19 vaccines has raised concerns on long-range safety of these medications, particularly on their possible influence on human reproductive health [3–7].

Early (pre-pandemic) studies emphasized the potentially negative impact of adjuvant vaccines developed for other infectious diseases. The vaccines allegedly affected reproductive function by triggering autoimmune responses in

animals and humans [8]. For many immunological adjuvants, mechanisms of action remain understudied. The adjuvants are believed to amplify the innate immunity reactions by mimicking certain evolutionary conserved epitopes (e.g. those of bacterial lipopolysaccharides). These molecules act through binding Toll-like receptors (TLR) on dendritic cells and macrophages; the binding triggers cytoplasmic inflammasome signaling, production of pro-inflammatory cytokines, and expression of antigen-presenting proteins [9].

The normal immune response is sometimes accompanied by ancillary autoimmune reactions. Their diverse mechanisms involve (1) participation of cryptic antigens with subsequent activation of autoreactive Th1 cells; (2) exposure of intracellular epitopes upon tissue damage; (3) amassing of inflammation-specific autoantigens leading to systemic propagation of immune response with the incrementing role of autoantigens; (4) molecular mimicry based on structural similarities between foreign and host epitopes, resulting in activation of cross-reactive T cells and non-specific activation of self-reactive Th1 cells mediated by various TCR dependent and independent mechanisms [9]. Such reactions are collectively known as “autoimmune/inflammatory syndrome induced by adjuvants (ASIA)”; the term was introduced in 2011 [10]. Meta-analysis reveals about 500 cases of ASIA recorded in 2016–2019, most of them associated with vaccines against hepatitis B, influenza, and HPV [11].

Another meta-analysis assessed for correlations between vaccination and the risks of systemic lupus erythematosus (SLE) or rheumatoid arthritis to show significant correlation with the risk of SLE [12]. In women, SLE has been associated with autoimmune oophoritis leading to premature ovarian failure, which proves that rheumatoid conditions may result in infertility. Moreover, about one third of female patients with SLE develop the antiphospholipid syndrome accompanied by recurrent pregnancy losses and thromboembolic complications in connection with thrombocytopenia and antiphospholipid antibody (aPL) persistence. The antiphospholipid syndrome etiology clearly involves molecular mimicry based on the homology between certain exogenous agents and self-antigens, and the resulting cross-reactivity of corresponding antibodies. For instance, IgM antibodies produced in response to immunization with tetanus toxoid also react with cardiolipin and β 2-glycoprotein I (β 2GPI) self-antigens [13].

It should be noted that Gam-COVID-Vac is a combined vector vaccine and does not contain adjuvants. Preliminary data on the influence of Gam-COVID-Vac on the levels of aPL to cardiolipin (anti-CL), β 2GPI (anti- β 2GPI), annexin V (anti-AnV), and phosphatidylserine (anti-PS) have been published. According to the results of examination for 51 vaccinated female participants, immunization with Gam-COVID-Vac (Sputnik V) caused no elevation in circulating aPL levels [6]. The lack of correlation between circulating levels of aPL, follicle-stimulating hormone (FSH), and anti-müllerian hormone (AMH) indirectly confirmed the lack of negative impact on female reproductive potential.

A more dedicated assessment of the vaccination safety in terms of reproductive health requires studying a wide range of autoantibodies involved in the development of systemic autoimmune diseases before and after vaccination on more representative samples of reproductive age women.

This study evaluates endogenous levels of self-reactive antibodies and hormones, associated with ovarian reserve, before and after immunization with the domestically developed Gam-COVID-Vac combined vector vaccine against SARS-CoV-2, to check for possible reproductive sequelae of the vaccination.

METHODS

This prospective study was carried out at the Kulakov National Medical Research Center for Obstetrics, Gynecology and Perinatology, Moscow, Russia. The participants ($n = 120$) were enrolled within the period from December, 2020 to December, 2021; all participants received immunization with the Gam-COVID-Vac combined vector vaccine for the prophylaxis of SARS-CoV-2-induced new coronavirus infection. The inclusion criteria were as follows: age 18–49 years; preserved menstrual function; negative PCR test for SARS-CoV-2 RNA and negative tests for IgM and IgG antibodies to SARS-CoV-2 (before vaccination); no clinical history of COVID-19; and no contact with COVID-19 cases for at least 14 days prior to the start of the study. The non-inclusion criteria were as follows: listed contraindications for Gam-COVID-Vac use; pregnancy and lactation; acute inflammatory and infectious diseases; rheumatic diseases; oncological diseases of any localization; hormone therapy affecting the menstrual cycle; immunomodulatory therapy; or vaccination within three months preceding the enrollment. Patients with decreased ovarian reserve (FSH >12 mIU/mL and antral follicle count (AFC) below six in both ovaries) or morbid obesity (BMI ≥ 40.0 kg/m²) were not included in the study. The exclusion criteria were COVID-19 during the vaccination period, pronounced side effects of immunization requiring the abolition of the second component, and vaccination refusal.

The participants were examined twice: (1) before vaccination and (2) 90–100 days after injection of the first component. Patients with autoantibody levels above reference range (RR) were subject to additional round of tests performed at 6 months after the first component injection. Serum levels of FSH and AMH were determined by electrochemiluminescence assay on day 2–5 of the menstrual cycle.

Autoantibody levels were measured by enzyme immunoassay before and after vaccination. The scope included antiphospholipid IgM and IgG antibodies (Ab), both “criterial” (anti-CL and anti- β 2GPI) and “non-criterial” (anti-AnV, anti-PS) (reagents by ORGENTEC Diagnostika GmbH; Germany); phosphatidylethanolamine (anti-PE) and phosphatidylserine/prothrombin complexes (anti-PS/PT) (reagents by AESKU Diagnostics; Germany); antinuclear IgG Ab (ANA) and Ab to double stranded DNA (anti-dsDNA), ribonucleoprotein 70 (anti-RNP70), and cytoplasmic antigens SS-A(Ro) and SS-B(La) (respectively, anti-SS-A and anti-SS-B) (reagents by ORGENTEC Diagnostika; GmbH); IgG Ab to thyroid antigens: thyroglobulin (anti-TG) and thyroid peroxidase (anti-TPO) (reagents by ORGENTEC Diagnostika GmbH; Германия), and thyroid-stimulating hormone receptor (anti-TSH receptor) (reagents by Medipan GmbH; Germany). Immunoassay targets also included anti-trophoblast and anti-zona pellucida IgG (reagents by QAYEE-BIO for Life Science; China), anti-ovary Ab (reagents by DRG; Germany); and Ab to FSH and progesterone (respectively, anti-FSH and anti-PRG) (reagents by Xema-Medica; Russia).

The patients were vaccinated in accordance with the current recommendations issued by the Ministry of Health of Russia [14]. Handling of the vaccine strictly followed the official instructions for this medication.

Statistical processing of the data was performed using Microsoft Excel spreadsheet and Statistica V10 packages (TIBCO; USA). The categorical data were converted into percentages (%). McNemar's test was applied to analyze the paired binary data for the patients before and after vaccination. The distributions were assessed with Kolmogorov–Smirnov test

Table 1. Serum levels of antiphospholipid antibodies (aPL) in women before and after vaccination

Parameter	Reference range	Before vaccination	90 days after vaccination	<i>p</i> -value
anti-CL IgM, U/mL	< 7 U/mL	2.2 (1.4–3.5)	2.3 (1.7–3.1)	0.575
anti-CL IgG, U/mL	< 10 U/mL	2.9 (2.0–4.1)	2.4 (1.8–3.3)	< 0.001
anti-β2GPI IgM, U/mL	< 5 U/mL	2.6 (1.7–3.5)	2.3 (1.7–3.2)	0.022
anti-β2GPI IgG, U/mL	< 5 U/mL	1.8 (1.3–2.9)	1.7 (1.3–2.3)	0.003
anti-AnV IgM, U/mL	< 5 U/mL	2.9 (2.2–4.1)	3.4 (2.6–4.4)	< 0.001
anti-AnV IgG, U/mL	< 5 U/mL	2.3 (1.7–3.0)	4.0 (2.2–4.8)	< 0.001
anti-PS IgM, U/mL	< 10 U/mL	2.5 (1.8–3.4)	2.5 (1.9–3.2)	0.630
anti-PS IgG, U/mL	< 10 U/mL	2.6 (2.0–3.4)	3.5 (2.8–4.6)	< 0.001
anti-PE IgM, U/mL	< 12 U/mL	5.2 (2.6–10.4)	6.1 (3.4–13.4)	< 0.001
anti-PE IgG, U/mL	< 12 U/mL	1.0 (1.0–1.3)	1.5 (1.2–2.1)	< 0.001
anti-PS/PT IgM, U/mL	< 12 U/mL	1.9 (1.3–2.8)	1.9 (1.3–3.2)	0.949
anti-PS/PT IgG, U/mL	< 12 U/mL	2.3 (1.7–3.3)	2.8 (1.9–3.7)	0.002

Note: Me (X–Y), *p*-values by the sign test.

using graphical data representation. Given non-normality of the distributions, the data were analyzed non-parametrically, with the variables described by medians and interquartile ranges, Me (Q25–Q75), and the non-parametric sign test applied for paired samples. The differences were considered statistically significant at $p < 0.05$.

RESULTS

Median age of the participants was 33 years; median BMI constituted 22.4 kg/m². All participants complied with the inclusion criteria; prevalence of gynecological diseases did not exceed 10%; non-gynecological diagnoses were dominated by allergic conditions (encountered in 30% of participants). Ovarian reserves were assessed before and after vaccination using FSH and AMH tests combined to AFC. No significant alterations in hormone levels and AFC were encountered. The medians/interquartile ranges fell within RR for all studied hormones, and similar numbers of patients presented with FSH levels above RR and AMH levels below RR before and after vaccination.

The study of serum antiphospholipid antibodies (aPL) revealed reciprocal dynamics for the levels of criterial and non-criterial aPL, respectively (Table 1).

In 30 pts (25%) aPL levels exceeded RR initially (Table 2). After vaccination, elevated aPL levels were observed in 28 pts (23.3%), most frequently for anti-PE IgM (20 pts, 16.7%). In 7 pts

(5.8%) elevated aPL levels were encountered after vaccination only, whereas in 9 pts (7.5%) the initially elevated aPL levels decreased to normal after vaccination. Two pts (1.7%) with histories of autoimmune thyroiditis and allergic reactions revealed aPL persistence after vaccination. It should be noted that both of them had ovarian reserve parameters within the normal range, showing no decrease after vaccination.

Possible correlations in the dynamics of aPL and hormone levels we assessed by setting Δ values for the parameters (e. g. $\Delta\text{AMH} = \text{AMH1} - \text{AMH2}$, $\Delta\text{FSH} = \text{FSH2} - \text{FSH1}$, etc.); a positive Δ always indicated an adverse trend (Fig. 1). The only identified correlation (a weak negative one of negligible clinical relevance) reflected an increase in AMH levels accompanied by an increase in anti-PS/PT IgM.

All 7 pts with elevated aPL as measured 90 days after vaccination showed normal aPL in the repeated tests performed 6 months after vaccination.

Thus, all median values and interquartile ranges for serum aPL levels fell within RR. The analysis revealed no significant increase in the prevalence of elevated aPL levels after vaccination, except for anti-PE IgM. In patients revealing elevated serum aPL at the second reference time point of the study (90 days after the first component injection), the values returned to normal range within a 3 months follow-up. The analysis revealed no clinically relevant dynamic associations for the ovarian reserve-related hormones and aPL.

Table 2. Prevalence of elevated serum aPL in women before and after vaccination

Parameter	Before vaccination	90 days after vaccination	<i>p</i> -value
anti-CL IgM, U/mL	4 (3.3%)	4 (3.3%)	0.683
anti-CL IgG, U/mL	4 (3.3%)	1 (0.8%)	0.248
anti-β2GPI IgM, U/mL	0	1 (0.8%)	–
anti-β2GPI IgG, U/mL	4 (3.3%)	2 (1.7%)	0.479
anti-AnV IgM, U/mL	3 (2.5)	5 (4.2%)	0.723
anti-AnV IgG, U/mL	3 (2.5)	3 (2.5)	0.617
anti-PS IgM, U/mL	1 (0.8%)	1 (0.8%)	1.00
anti-PS IgG, U/mL	0	1 (0.8%)	–
anti-PE IgM, U/mL	15 (12.5%)	20 (16.7%)	0.043
anti-PE IgG, U/mL	0	2 (1.7%)	–
anti-PS/PT IgM, U/mL	1 (0.8%)	0	–
anti-PS/PT IgG, U/mL	0	1 (0.8%)	–
At least one type of aPL above RR	30 (25%)	28 (23.3%)	0.802

Note: *p*-values by McNemar's test, RR — reference range.

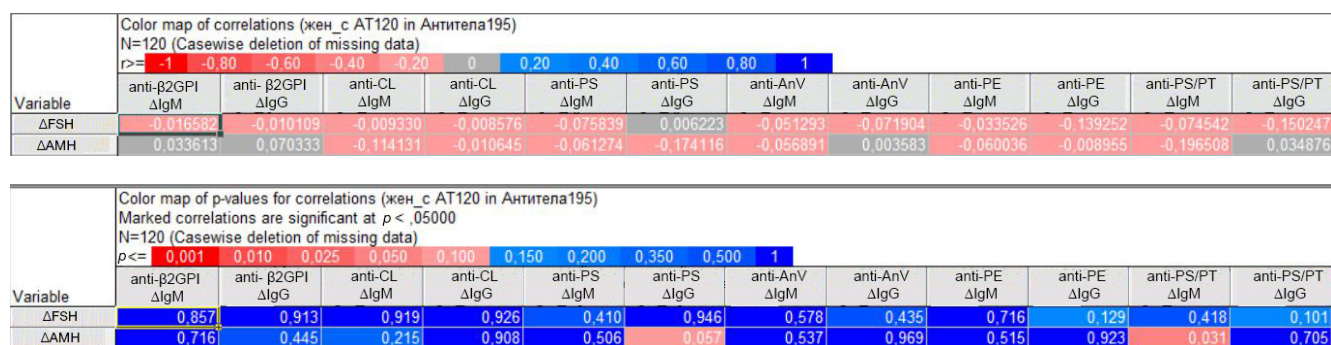


Fig. 1. Correlation analysis for possible dynamic associations between serum levels of hormones (ΔFSH, ΔAMH) and antiphospholipid antibodies (ΔaPL) in women before and after vaccination

Apart from aPL, we analyzed a scope of other self-reactive antibodies with diverse specificities (organ-specific, antinuclear, and anti-hormone) before and after vaccination (Table 3). Significantly decreased serum levels were observed for anti-FSH IgM, anti-TSH receptor IgG, ANA IgG, anti-SS-A IgG, and-RNP70 IgG, along with significantly increased serum levels of anti-trophoblast IgG, anti-ovary IgG, anti-PRG IgG, anti-SS-B IgG, and anti-dsDNA IgG.

However, these trends are hardly relevant: despite the statistically significant dynamics, Ab levels stayed within RR in the majority of patients. Comparing seroprevalence of elevated autoantibodies is more indicative (Table 4). Patients with at least one type of elevated serum autoantibodies constituted 70.8% before vaccination and 75% after vaccination. Patients with at least two autoAb above RR constituted 38.3% and 45.8%, respectively. It should be noted that different classes of anti-PRG and anti-FSH Ig showed reciprocal dynamics: the prevalence of elevated serum IgM decreased, whereas the prevalence of elevated serum IgG increased. Anti-dsDNA IgG were the only autoantibodies with the elevated serum levels more prevalent after vaccination than before, although in most of the cases their levels only slightly exceeded RR.

Correlation analysis revealed no dynamic associations between serum levels of ovarian reserve-related hormones (FSH, AMH) and self-reactive antibodies to nuclear antigens, thyroid-, ovarian-, and trophoblast-specific antigens, or hormones (Fig. 2).

The results indicate high incidence of serum autoantibody persistence in reproductive age women. The only antibodies showing increased seroprevalence after vaccination were anti-dsDNA IgG. In patients showing elevated serum Ab at the second reference time point of the study, these levels returned to normal within 6 months after the first component injection. Correlation analysis revealed no dynamic associations between serum levels of ovarian reserve-related hormones and autoantibodies.

DISCUSSION

According to *in vivo* studies and pilot clinical research, vaccination may cause reproductive failure by promoting ASIA and certain autoimmune disorders including antiphospholipid syndrome and SLE [12, 13, 15]. It is known that aPL can destroy the annexin V protective layer formed over the negatively charged surface of syncytiotrophoblast and endothelium, thus promoting coagulation and development of a hypercoagulable state. In addition, aPL can initiate apoptosis in trophoblast cells, interfere with cell proliferation, expression of cell adhesion molecules, and chorionic gonadotropin secretion, while supporting pro-inflammatory reactions [16].

Autoantibody persistence is rather prevalent in women. This asymptomatic condition may favor development of autoimmune diseases in genetically predisposed individuals. In connection with this concern, the present study analyzed a wide range of

Table 3. Serum levels of autoantibodies in women before and after vaccination

Parameter	Reference range	Before vaccination	90 days after vaccination	p-value
anti-zona pellucida IgG, ng/mL	< 250 ng/mL	156.0 (126.5–183.5)	157.0 (133.7–218.2)	0.114
anti-trophoblast IgG, ng/mL	< 150 ng/mL	101.7 (84.0–117.0)	127.2 (106.0–137.2)	< 0.001
anti-ovary IgG, U/mL	< 10 U/mL	4.0 (3.3–5.1)	4.8 (4.0–5.7)	< 0.001
anti-PRG IgM, OD u	< 0.4 OD u	0.28 (0.22–0.40)	0.29 (0.23–0.35)	0.302
anti-PRG IgG, OD u	< 0.4 OD u	0.28 (0.21–0.37)	0.33 (0.25–0.44)	0.002
anti-FSH IgM, OD u	< 0.4 OD u	0.29 (0.22–0.38)	0.25 (0.19–0.30)	< 0.001
anti-FSH IgG, OD u	< 0.4 OD u	0.27 (0.20–0.34)	0.29 (0.23–0.35)	0.575
anti-TPO IgG, IU/mL	< 50 IU/mL	12.2 (8.7–18.7)	12.4 (9.5–18.9)	1.00
anti-TSH receptor IgG, IU/L	≤ 1 IU/L	0.5 (0.3–0.6)	0.3 (0.2–0.5)	< 0.001
anti-TG IgG, IU/mL	< 100 IU/mL	19.4 (15.0–28.5)	20.7 (14.8–31.5)	0.227
ANA IgG, PI	< 1 PI	0.5 (0.4–0.7)	0.45 (0.4–0.65)	< 0.001
анти-SS-A IgG, IU/mL	< 15 IU/mL	3.3 (2.6–5.3)	3.0 (2.6–4.3)	0.032
анти-SS-B IgG, IU/mL	< 15 IU/mL	3.2 (2.1–4.8)	3.3 (2.3–5.1)	0.038
anti-dsDNA IgG, IU/mL	< 20 IU/mL	11.8 (9.3–14.7)	15.3 (12.8–18.1)	< 0.001
anti-RNP70 IgG, U/mL	< 25 U/mL	4.1 (2.8–5.6)	2.3 (1.7–3.1)	< 0.001

Note: Me (X–Y), p-values by the sign test.

Table 4. Prevalence of elevated serum autoantibodies in women before and after vaccination

Parameter	Reference range	Before vaccination	90 days after vaccination	p-value
anti-zona pellucida IgG, ng/mL	< 250 ng/mL	17 (14.2%)	19 (15.8%)	0.844
anti-trophoblast IgG, ng/mL	< 150 ng/mL	7 (5.8%)	13 (10.8%)	0.211
anti-ovary IgG, U/mL	< 10 U/mL	1 (0.8%)	2 (1.6%)	1.00
anti-PRG IgM, OD u	< 0,4 OD u	32 (26.7%)	19 (15.8%)	0.012
anti-PRG IgG OD u	< 0,4 OD u	21 (17.5%)	41 (34.2%)	< 0.001
anti-FSH IgM, OD u	< 0,4 OD u	23 (19.2%)	11 (9.2%)	0.006
anti-FSH IgG, OD u	< 0,4 OD u	14 (11.7%)	21 (17.5%)	0.190
anti-TPO IgG, IU/mL	< 50 IU/mL	12 (10%)	13 (10.8%)	1.00
anti-TSH receptor IgG, IU/L	≤ 1 IU/L	2 (1.6%)	1 (0.8%)	1.00
anti-TG IgG, IU/mL	< 100 IU/mL	6 (5%)	7 (5.8%)	1.00
ANA IgG, PI	< 1 PI	11 (9.2%)	12 (10%)	1.00
anti-SS-A IgG, IU/mL	< 15 IU/mL	4 (3.3%)	7 (5.8%)	0.248
anti-SS-B IgG, IU/mL	< 15 IU/mL	1 (0.8%)	1 (0.8%)	–
anti-dsDNA IgG, IU/mL	< 20 IU/mL	4 (3.3%)	18 (15%)	0.003
anti-RNP70 IgG, U/mL	< 25 U/mL	4 (3.3%)	0	–
At least one type of autoAb above RR		85 (70.8%)	90 (75%)	0.423
Two or more types of autoAb above RR		46 (38.3%)	55 (45.8%)	0.176

Note: p-values by McNemar's test, RR — reference range.

autoantibodies to organ-specific and systemic self-antigens in reproductive age women before and after COVID-19 vaccination. The tests for criterial and non-criterial aPL were performed to assess the risks of antiphospholipid syndrome with possible complications including infertility, thrombosis, thrombocytopenia, and habitual miscarriage [17].

The study also included the antinuclear antibody (ANA) tests conventionally used in diagnostics of connective tissue autoimmune disorders (SLE, Sjögren syndrome, the mixed connective tissue disease (Sharp syndrome), polymyositis/dermatomyositis, and progressive systemic sclerosis) [18]. ANA are widely employed as biomarkers of particular connective tissue disorders. Apart from ANA, the women were tested for autoantibodies to double-stranded DNA (dsDNA) and extractable nuclear antigens SS-A/Ro, SS-B/La, and RNP70. Rheumatoid autoimmune diseases are often associated with the presence of autoantibodies to extractable nuclear and cytoplasmic antigens. The anti-SS-B and anti-SS-A autoantibodies are usually detectable in Sjögren syndrome [19]. The study also included serum and plasma tests for anti-RNP70 IgG conventionally used in diagnostics of the mixed connective tissue disease (Sharp syndrome) and related autoimmune disorders [20].

In addition, the participants were tested for autoantibodies to organ-specific antigens, including anti-ovary, anti-trophoblast, and anti-zona pellucida species, associated with the

risks of reduced fertility, infertility, or premature ovarian failure. In particular, anti-oocyte autoantibodies have been associated with poor ovarian response upon ovarian stimulation in IVF cycles [21].

Other serological targets included autoantibodies to thyroid antigens including thyroglobulin (TG), thyroid peroxidase (TPO), and thyroid-stimulating hormone receptor (TSH receptor). These tests are used in differential diagnostics of autoimmune thyroid diseases including Hashimoto thyroiditis and Graves' disease [22].

We also used novel modifications of enzyme immunoassay enabling detection of antibodies to the most important female reproductive hormones, particularly FSH and progesterone. Such antibodies can interfere with the effects of exogenous and endogenous hormones and affect follicular growth, endometrial readiness, and the course of early pregnancy.

The results indicate significant decrease in blood levels of criterial aPL (anti-CL and anti-β2GPI) accompanied by significant increase in non-criterial aPL (anti-AnV, anti-PS, anti-PE, and anti-PS/PT) after vaccination. However, these findings have low clinical relevance: in the majority of patients, aPL levels stayed within the normal range despite the observed negative and positive dynamics.

The analysis of prevalence of elevated aPL levels with regard to vaccination is certainly more informative. We observed a significant increase in the prevalence of elevated anti-PE IgM in response to vaccination, which was transient.

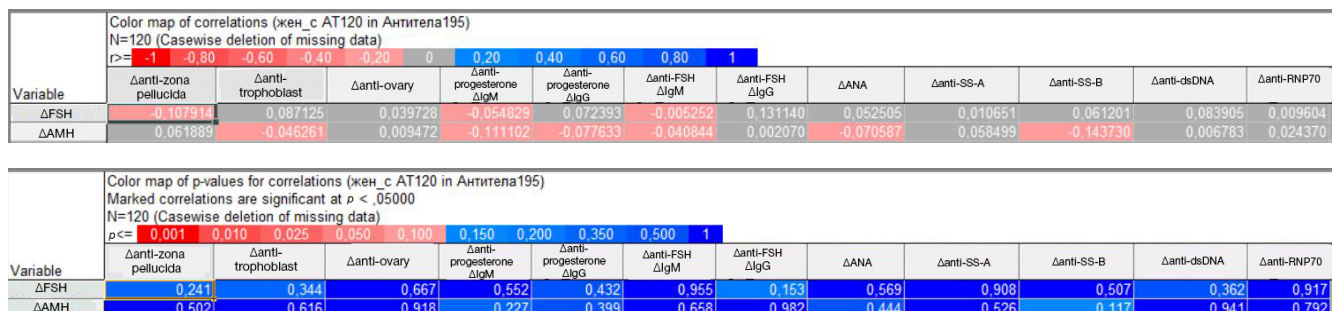


Fig. 2. Correlation analysis for possible dynamic associations between serum levels of hormones (ΔFSH, ΔAMH) and autoantibodies (ΔautoAB) in women before and after vaccination

It should be noted that anti-PE aPL typically arise during infectious processes induced by viral or bacterial pathogens and persist for a considerable period [23–24]. PE, a major lipid component of microbial membranes, is also found in human cell membranes. Immunologically compelling circumstances (immunization, activation of chronic infection foci, etc.) accompanied by release of pro-inflammatory mediators and tissue damage may facilitate exposure of PE in cell membranes, triggering the production of corresponding self-reactive autoantibodies capable of transient or long-term persistence. Infectious agents are capable of triggering autoimmune reactions, whereas anti-PE antibody persistence may indicate chronic infections possibly prone to the vaccination-mediated enhancement.

Overall, the observed trends were clinically irrelevant, except, perhaps, the transiently increased prevalence of elevated serum levels for anti-dsDNA IgG after vaccination. Elevated levels of anti-dsDNA antibodies may result from a variety of events (both physiological and pathological) where DNA fragments are released from cells along with other nuclear antigens. For instance, such release of nuclear antigens occurs in apoptosis or necrosis. Production of anti-dsDNA antibodies at systemic level can be induced by exogenous factors, e.g. bacterial lipopolysaccharide stimulation [25]. These findings explain the boosted synthesis of anti-dsDNA antibodies during Gram-negative bacterial infections [26].

One study focusing on the autoimmune effects of different types of vaccines demonstrates that production of autoantibodies occurs in healthy people in response to immunization against hepatitis B, influenza, or hepatitis A (including a transient increase observed for antinuclear antibodies). At the same time, none of the patients presented

with autoimmune disease at follow-up. The authors suggest that a transient increase in serum titers observed for certain autoantibodies may reflect the non-specific activation of T and B cells in response to vaccination [27].

Importantly, in the current study, we found no dynamic associations between serum levels of ovarian reserve-related hormones and corresponding levels of aPL and other autoantibodies. This ultimately confirms the reproductive safety of vaccination with Gam-COVID-Vac by excluding adverse autoimmune reactions.

Moreover, anti-SARS-CoV-2 vaccination in women is increasingly justified by recent studies emphasizing the negative impact of COVID-19 on female reproductive function, reflected by reduced AMH levels [28]. The mechanism may involve direct infection of ovarian tissues, oocytes, and endometrial cells with SARS-CoV-2 leading to impaired ovulatory function, production of infected or aneuploid oocytes, reduced fertilization potential, and impaired embryo implantation [29].

CONCLUSIONS

The results indicate that immunization with Gam-COVID-Vac combined vector vaccine for the prophylaxis of SARS-CoV-2-induced new coronavirus infection has no adverse effects on serum levels of ovarian reserve-related hormones and self-reactive antibodies in reproductive age women. Immunization with Gam-COVID-Vac entails neither conspicuous autoimmune reactions, nor associated decrease in female reproductive potential. Further research will be required to elucidate the mechanisms of immune response to vaccination and dynamic immune status with an emphasis on the cellular wing of immunity.

References

- Enjuanes L, Zúñiga S, Castaño-Rodríguez C, Gutierrez-Alvarez J, Canton J, Sola I. Molecular Basis of Coronavirus Virulence and Vaccine Development. *Adv Virus res.* 2016; 96: 245–86.
- Logunov DY, Dolzhikova IV, Shcheblyakov DV, Tukhvatulin AI, Zubkova OV, Dzharullaeva AS, et al. Safety and efficacy of an rAd26 and rAd5 vector-based heterologous prime-boost COVID-19 vaccine: an interim analysis of a randomised controlled phase 3 trial in Russia. *Lancet.* 2021; 397 (10275): 671–81.
- Orvieto R, Noach-Hirsh M, Segev-Zahav A, Haas J, Nahum R, Aizer A. Does mRNA SARS-CoV-2 vaccine influence patients' performance during IVF-ET cycle? *Reprod Biol Endocrinol.* 2021; 19 (1): 69.
- Bentov Y, Beharier O, Moav-Zafir A, Kabessa M, Godin M., Greenfield CS, et al. Ovarian follicular function is not altered by SARS-CoV-2 infection or BNT162b2 mRNA COVID-19 vaccination. *Hum Reprod.* 2021; 36 (9): 2506–13.
- Drapkina YS, Dolgushina NV, Shatylko TV, Nikolaeva MA, Menzhinskaya IV, Ivanets TY, et al. Gam-COVID-Vac (Sputnik V) vaccine has no adverse effect on spermatogenesis in men. *Akusherstvo i Ginekol.* 2021; 7: 88–94.
- Dolgushina NV, Drapkina YS, Krechetova LV, Ivanets TY, Menzhinskaya IV, Gus GAI, et al. Gam-COVID-Vac (Sputnik V) vaccine has no adverse effect on ovarian reserve in reproductive-age women. *Akusherstvo i Ginekol.* 2021; 7: 81–6.
- Gonzalez DC, Nassau DE, Khodamoradi K, Ibrahim E, Blachman-Braun R, Ory J, et al. Sperm Parameters Before and After COVID-19 mRNA Vaccination. *JAMA.* 2021; 326 (3): 273–4.
- World Health Organization (WHO). Module 2: types of vaccine and adverse reactions. *WHO Vaccine Saf Basics.* 2013: 38–60.
- Pellegrino P, Clementi E, Radice S. On vaccine's adjuvants and autoimmunity: Current evidence and future perspectives. *Autoimmun Rev.* 2015; 14 (10): 880–8.
- Guimarães LE, Baker B, Perricone C, Shoenfeld Y. Vaccines, adjuvants and autoimmunity. *Pharmacol Res.* 2015; 100 (January): 190–209.
- Wataad A, Bragazzi NL, McGonagle D, Adawi M, Bridgwood C, Damiani G, et al. Autoimmune/inflammatory syndrome induced by adjuvants (ASIA) demonstrates distinct autoimmune and autoinflammatory disease associations according to the adjuvant subtype: Insights from an analysis of 500 cases. *Clin Immunol.* 2019; 203 (March): 1–8.
- Wang B, Shao X, Wang D, Xu D, Zhang J. Vaccinations and risk of systemic lupus erythematosus and rheumatoid arthritis: A systematic review and meta-analysis. *Autoimmun Rev.* 2017; 16 (7): 756–65.
- Cruz-Tapias P, Blank M, Anaya JM, Shoenfeld Y. Infections and vaccines in the etiology of antiphospholipid syndrome. *Curr Opin Rheumatol.* 2012; 24 (4): 389–93.
- Pis'mo Ministerstva zdravooxraneniya RF ot 30 oktyabrya 2021 g. N 30-4/1/2-17927 O napravlenii aktualizirovannykh vremennykh metodicheskikh rekomendatsiy «Poryadok provedeniya vaktsinatsii vzroslogo naseleniya protiv COVID-19». Available from: https://base.garant.ru/403013668/#block_. Russian.
- Shoenfeld Y, Agmon-Levin N. "ASIA" — autoimmune/inflammatory syndrome induced by adjuvants. *J Autoimmun.* 2011; 36 (1): 4–8.
- Kraeva EE, Dolgushina NV, Menzhinskaya IV, Shpiluyuk MA, Beznoshchenko OS, Krechetova LV. Outcomes of assisted reproductive technologies in patients with persistence of antiphospholipid antibodies. *Akush Ginekol (Sofia).* 2020; 4: 97–103.
- Shoenfeld Y, Carp HJA, Molina V, Blank M, Cervera R, Balasch J, et al. Autoantibodies and Prediction of Reproductive Failure. *Am J Reprod Immunol.* 2006; 56 (5–6): 337–44.
- Aleksandrova EN, Novikov AA, Nasonov EL. *Sovremennyye*

- podxody k laboratornoj diagnostike revmaticheskix zabolevanij: rol' molekulyarnyx i kletochnyx biomarkerov. Nauchno-prakticheskaya revmatologiya. 2016; 3: 324–38. Russian.
19. Pisetsky DS. Antinuclear Antibodies in Rheumatic Disease: A Proposal for a Function-Based Classification. *Scand J Immunol*. 2012; 76 (3): 223–8.
 20. Alves MR, Isenberg DA. “Mixed connective tissue disease”: a condition in search of an identity. *Clin Exp Med*. 2020; 20 (2): 159–66.
 21. Pires ES, Parikh FR, Mande PV, Uttamchandani SA, Savkar S, Khole VV. Can anti-ovarian antibody testing be useful in an IVF-ET clinic? *J Assist Reprod Genet*. 2011; 28 (1): 55–64.
 22. Trimboli P, Rossi F, Condorelli E, Laurenti O, Ventura C, Nigri G, et al. Does Normal Thyroid Gland by Ultrasonography match with Normal Serum Thyroid Hormones and Negative Thyroid Antibodies? *Exp Clin Endocrinol Diabetes*. 2009; 118 (09): 630–2.
 23. Bessis S, Bertin D, Million M, Meddeb L, Drancourt M, Lagier J-C, et al. Thromboses in tuberculosis are linked to antiphosphatidylethanolamine antibodies levels: A cross-sectional study. *J Clin Tuberc Other Mycobact Dis*. 2019; 15: 100092.
 24. Goodridge A, Zhang T, Miyata T, Lu S, Riley LW. Antiphospholipid IgM antibody response in acute and chronic *Mycobacterium tuberculosis* mouse infection model. *Clin Respir J*. 2014; 8 (2): 137–44.
 25. Grayzel A, Solomon A, Aranow C, Diamond B. Antibodies elicited by pneumococcal antigens bear an anti-DNA--associated idiotype. *J Clin Invest*. 1991; 87 (3): 842–6.
 26. Fournié GJ, Lambert PH, Miescher PA. Release of DNA in circulating blood and induction of anti-DNA antibodies after injection of bacterial lipopolysaccharides. *J Exp Med*. 1974; 140 (5): 1189–206.
 27. Toplak N, Avčin T. Autoantibodies Induced by Vaccine. In: *Vaccines and Autoimmunity*. Hoboken, NJ, USA: John Wiley & Sons, Inc, 2015; p. 93–102.
 28. Ding T, Wang T, Zhang J, Cui P, Chen Z, Zhou S, et al. Analysis of Ovarian Injury Associated With COVID-19 Disease in Reproductive-Aged Women in Wuhan, China: An Observational Study. *Front Med*. 2021; 8.
 29. Dolgushin GO, Romanov AY. Effects of SARS-CoV-2 on human reproduction. *Akush Ginekolog (Sofia)*. 2020; 11: 6–12.
- Литература**
1. Enjuanes L, Zúñiga S, Castaño-Rodríguez C, Gutiérrez-Alvarez J, Canton J, Sola I. Molecular Basis of Coronavirus Virulence and Vaccine Development. *Adv Virus res*. 2016; 96: 245–86.
 2. Logunov DY, Dolzhikova IV, Shcheblyakov DV, Tukhvatulin AI, Zubkova OV, Dzharullaeva AS, et al. Safety and efficacy of an rAd26 and rAd5 vector-based heterologous prime-boost COVID-19 vaccine: an interim analysis of a randomised controlled phase 3 trial in Russia. *Lancet*. 2021; 397 (10275): 671–81.
 3. Orvieto R, Noach-Hirsh M, Segev-Zahav A, Haas J, Nahum R, Aizer A. Does mRNA SARS-CoV-2 vaccine influence patients' performance during IVF-ET cycle? *Reprod Biol Endocrinol*. 2021; 19 (1): 69.
 4. Bentov Y, Beharier O, Moav-Zafir A, Kabessa M, Godin M., Greenfield CS, et al. Ovarian follicular function is not altered by SARS-CoV-2 infection or BNT162b2 mRNA COVID-19 vaccination. *Hum Reprod*. 2021; 36 (9): 2506–13.
 5. Drapkina YS, Dolgushina NV, Shatylo TV, Nikolaeva MA, Menzhinskaya IV, Ivanets TY, et al. Gam-COVID-Vac (Sputnik V) vaccine has no adverse effect on spermatogenesis in men. *Akusherstvo i Ginekolog*. 2021; 7: 88–94.
 6. Dolgushina NV, Drapkina YS, Krechetova LV, Ivanets TY, Menzhinskaya IV, Gus GAI, et al. Gam-COVID-Vac (Sputnik V) vaccine has no adverse effect on ovarian reserve in reproductive-age women. *Akusherstvo i Ginekolog*. 2021; 7: 81–6.
 7. Gonzalez DC, Nassau DE, Khodamoradi K, Ibrahim E, Blachman-Braun R, Ory J, et al. Sperm Parameters Before and After COVID-19 mRNA Vaccination. *JAMA*. 2021; 326 (3): 273–4.
 8. World Health Organization (WHO). Module 2: types of vaccine and adverse reactions. *WHO Vaccine Saf Basics*. 2013: 38–60.
 9. Pellegrino P, Clementi E, Radice S. On vaccine's adjuvants and autoimmunity: Current evidence and future perspectives. *Autoimmun Rev*. 2015; 14 (10): 880–8.
 10. Guimarães LE, Baker B, Perricone C, Shoenfeld Y. Vaccines, adjuvants and autoimmunity. *Pharmacol Res*. 2015; 100 (January): 190–209.
 11. Watad A, Bragazzi NL, McGonagle D, Adawi M, Bridgewood C, Damiani G, et al. Autoimmune/inflammatory syndrome induced by adjuvants (ASIA) demonstrates distinct autoimmune and autoinflammatory disease associations according to the adjuvant subtype: Insights from an analysis of 500 cases. *Clin Immunol*. 2019; 203 (March): 1–8.
 12. Wang B, Shao X, Wang D, Xu D, Zhang J. Vaccinations and risk of systemic lupus erythematosus and rheumatoid arthritis: A systematic review and meta-analysis. *Autoimmun Rev*. 2017; 16 (7): 756–65.
 13. Cruz-Tapias P, Blank M, Anaya JM, Shoenfeld Y. Infections and vaccines in the etiology of antiphospholipid syndrome. *Curr Opin Rheumatol*. 2012; 24 (4): 389–93.
 14. Письмо Министерства здравоохранения РФ от 30 октября 2021 г. N 30-4/И/2-17927 О направлении актуализированных временных методических рекомендаций «Порядок проведения вакцинации взрослого населения против COVID-19». Доступно по ссылке: https://base.garant.ru/403013668/#block_.
 15. Shoenfeld Y, Agmon-Levin N. “ASIA” — autoimmune/inflammatory syndrome induced by adjuvants. *J Autoimmun*. 2011; 36 (1): 4–8.
 16. Kraevaya EE, Dolgushina NV, Menzhinskaya IV, Shpiluyuk MA, Beznoshchenko OS, Krechetova LV. Outcomes of assisted reproductive technologies in patients with persistence of antiphospholipid antibodies. *Akush Ginekolog (Sofia)*. 2020; 4: 97–103.
 17. Shoenfeld Y, Carp HJA, Molina V, Blank M, Cervera R, Balasch J, et al. Autoantibodies and Prediction of Reproductive Failure. *Am J Reprod Immunol*. 2006; 56 (5–6): 337–44.
 18. Александрова Е. Н., Новиков А. А., Насонов Е. Л. Современные подходы к лабораторной диагностике ревматических заболеваний: роль молекулярных и клеточных биомаркеров. *Научно-практическая ревматология*. 2016; 3: 324–38.
 19. Pisetsky DS. Antinuclear Antibodies in Rheumatic Disease: A Proposal for a Function-Based Classification. *Scand J Immunol*. 2012; 76 (3): 223–8.
 20. Alves MR, Isenberg DA. “Mixed connective tissue disease”: a condition in search of an identity. *Clin Exp Med*. 2020; 20 (2): 159–66.
 21. Pires ES, Parikh FR, Mande PV, Uttamchandani SA, Savkar S, Khole VV. Can anti-ovarian antibody testing be useful in an IVF-ET clinic? *J Assist Reprod Genet*. 2011; 28 (1): 55–64.
 22. Trimboli P, Rossi F, Condorelli E, Laurenti O, Ventura C, Nigri G, et al. Does Normal Thyroid Gland by Ultrasonography match with Normal Serum Thyroid Hormones and Negative Thyroid Antibodies? *Exp Clin Endocrinol Diabetes*. 2009; 118 (09): 630–2.
 23. Bessis S, Bertin D, Million M, Meddeb L, Drancourt M, Lagier J-C, et al. Thromboses in tuberculosis are linked to antiphosphatidylethanolamine antibodies levels: A cross-sectional study. *J Clin Tuberc Other Mycobact Dis*. 2019; 15: 100092.
 24. Goodridge A, Zhang T, Miyata T, Lu S, Riley LW. Antiphospholipid IgM antibody response in acute and chronic *Mycobacterium tuberculosis* mouse infection model. *Clin Respir J*. 2014; 8 (2): 137–44.
 25. Grayzel A, Solomon A, Aranow C, Diamond B. Antibodies elicited by pneumococcal antigens bear an anti-DNA--associated idiotype. *J Clin Invest*. 1991; 87 (3): 842–6.
 26. Fournié GJ, Lambert PH, Miescher PA. Release of DNA in circulating blood and induction of anti-DNA antibodies after injection of bacterial lipopolysaccharides. *J Exp Med*. 1974; 140 (5): 1189–206.
 27. Toplak N, Avčin T. Autoantibodies Induced by Vaccine. In: *Vaccines and Autoimmunity*. Hoboken, NJ, USA: John Wiley & Sons, Inc, 2015; p. 93–102.
 28. Ding T, Wang T, Zhang J, Cui P, Chen Z, Zhou S, et al. Analysis of Ovarian Injury Associated With COVID-19 Disease in Reproductive-Aged Women in Wuhan, China: An Observational Study. *Front Med*. 2021; 8.
 29. Dolgushin GO, Romanov AY. Effects of SARS-CoV-2 on human reproduction. *Akush Ginekolog (Sofia)*. 2020; 11: 6–12.

EXPERIENCE OF TOCILIZUMAB IN HOSPITAL PATIENTS WITH MODERATE COVID-19

Burgasova OA^{1,2}, Dolinniy SV³, Tetova VB¹, Ogarkova DA², Odnorolov MA¹, Bacalin VV¹, Smetanina SV³, Antipyat NA³, Taranova MV⁴¹ Peoples Friendship University of Russia, Moscow, Russia² Gamaleya National Research Center for Epidemiology and Microbiology, Moscow, Russia³ Clinical Hospital for Infectious Diseases №1, Moscow, Russia⁴ Sechenov First Moscow State Medical University (Sechenov University), Moscow, Russia

Severe form of COVID 19 has been linked to the phenomenon of dysregulated inflammation with excessive cytokine release and elevated interleukin 6 (IL6) levels. Suppressive agents enabling specific inhibition of cytokines, notably monoclonal antibodies to IL6 and its receptors, have been applied as a rescue therapy in COVID 19 despite the underexplored clinical scope for these biologic medications. This study aimed to evaluate the clinical utility of IL6 receptor antagonist tocilizumab in moderate symptomatic COVID 19 prone to aggravation. The retrospective cohort study enrolled two groups of hospitalized patients (a total of $n = 72$) diagnosed with moderate COVID-19. The main group received a single 400 mg dose of tocilizumab (TCZ) on top of standard therapy. The comparative analysis included statistical evaluation for a number of clinical and laboratory parameters at reference time points and disease outcomes with regard to treatment strategy. Overall, TCZ administration provided no advantages in terms of oxygen supplementation status, disease progression, or survival. Lethal cases constituted 19.2% (10 pts) and 5% (1 pt) in TCZ and comparison groups, respectively. The results indicate that administration of monoclonal antibody drugs in hospital patients with COVID-19 must follow differential schemes with regard to the disease severity and comorbidities, as well as proper commencement schedules.

Keywords: COVID-19, SARS-CoV-2, acute respiratory distress syndrome (ARDS), interleukin 6 (IL6) inhibitors, tocilizumab, dexamethasone

Author contribution: OA Burgasova — initiative and design, supervision of the clinical part of the study, writing of the manuscript; SV Dolinniy — literature review, clinical observations, data processing; VB Tetova — literature review, editing of the manuscript; DA Ogarkova — statistical analysis; MA Odnorolov, VV Bacalin — clinical observations, processing of clinical and laboratory data; SV Smetanina — concept; NA Antipyat — supervision of the clinical part of the study; MV Taranova — literature review, data processing.

Compliance with ethical standards: the study was approved by the ethics committee at the Clinical Hospital for Infectious Diseases №1 (Protocol 1 of January 11, 2021); all participants provided informed consent for the study.

✉ **Correspondence should be addressed:** Olga A. Burgasova
Volokolamskoe sh., 47, str. 8, korp. 5, Moscow, 125310, Russia; olgaburgasova@mail.ru

Received: 10.03.2022 **Accepted:** 03.04.2022 **Published online:** 15.04.2022

DOI: 10.24075/brsmu.2022.015

ОПЫТ ПРИМЕНЕНИЯ ТОЦИЛИЗУМАБА У СТАЦИОНАРНЫХ ПАЦИЕНТОВ СО СРЕДНЕТЕЖЕЛЫМ ТЕЧЕНИЕМ COVID-19

О. А. Бургасова^{1,2}, С. В. Долинный³, В. Б. Тетова¹, Д. А. Огаркова², М. А. Одноралов¹, В. В. Бакалин¹, С. В. Сметанина³, Н. А. Антипят³, М. В. Таранова⁴¹ Российский университет дружбы народов, Москва, Россия² Национальный исследовательский центр эпидемиологии и микробиологии имени Н. Ф. Гамалеи, Москва, Россия³ Инфекционная клиническая больница № 1, Москва, Россия⁴ Первый Московский государственный медицинский университет имени И. М. Сеченова (Сеченовский университет), Москва, Россия

Осложненное течение COVID-19 ассоциировано с феноменом нерегулируемого воспаления, синдромом избыточного выброса цитокинов, в том числе повышением уровня интерлейкина-6 (IL6). Для лечения пациентов с COVID-19 стали активно применять супрессивные средства с векторным блокированием цитокинов — моноклональные антитела к IL6 и его рецепторам. Терапевтическая эффективность различных биологических средств при COVID-19 пока недостаточно изучена. Целью исследования было оценить влияние антагониста рецептора IL6 тоцилизумаба на клиническое течение COVID-19 в сравнении с поддерживающей кортикостероидной терапией. В ретроспективном когортном исследовании наблюдали две группы пациентов ($n = 72$) со среднетяжелым течением COVID-19 и риском прогрессирования заболевания. Пациентам основной группы к стандартной терапии однократно вводили тоцилизумаб в дозе 400 мг. Проведен сравнительный анализ основных параметров клинико-лабораторного профиля и исходов заболевания в контрольных временных точках при использовании различных лечебных стратегий. Результаты применения тоцилизумаба у пациентов со среднетяжелым течением COVID-19 не продемонстрировали преимуществ его использования для снижения потребности в дополнительной кислородной поддержке и риска прогрессирования заболевания до тяжелой формы, а также числа летальных исходов по сравнению с поддерживающей терапией. Число летальных случаев составило 10 (19,2%) и 1 (5%) в группах с применением тоцилизумаба и поддерживающей терапии соответственно. Использование препаратов моноклональных антител у пациентов с COVID-19, возможно, требует избирательного подхода с учетом не только степени тяжести заболевания, коморбидности, но и сроков начала введения биологических супрессивных средств.

Ключевые слова: COVID-19, SARS-CoV-2, острый респираторный дистресс-синдром (ОРДС), ингибитор IL6, тоцилизумаб, дексаметазон

Вклад авторов: О. А. Бургасова — инициатор исследования, дизайн, руководство клинической частью, подготовка рукописи; С. В. Долинный — анализ литературных источников, клинические наблюдения, обработка результатов; В. Б. Тетова — анализ литературных источников, редактирование статьи; Д. А. Огаркова — статистический анализ; М. А. Одноралов, В. В. Бакалин — клинические наблюдения, обработка клинических и лабораторных данных; С. В. Сметанина — концепция исследования; Н. А. Антипят — руководство клинической частью исследования; М. В. Таранова — анализ литературных источников, обработка результатов.

Соблюдение этических стандартов: исследование одобрено этическим комитетом Инфекционной клинической больницы № 1 г. Москвы (протокол № 1 от 11 января 2021 г.). Все пациенты подписали добровольное информированное согласие.

✉ **Для корреспонденции:** Ольга Александровна Бургасова
ул. Волоколамское шоссе, д. 47, стр. 8, кorp. 5, г. Москва, 125310, Россия; olgaburgasova@mail.ru

Статья получена: 10.03.2022 **Статья принята к печати:** 03.04.2022 **Опубликована онлайн:** 15.04.2022

DOI: 10.24075/vrgmu.2022.015

The coronavirus pandemic remains a major challenge to global healthcare, responsible for over 4 million deaths as of October 2021 [1]. Despite the enormous vaccination efforts, the problem will persist due to the high mutation capacity of the SARS-CoV-2 virus.

Immune response plays a pivotal role in individual susceptibility to infectious diseases. Dysfunctional immune reactions are responsible for severe respiratory distress syndrome in viral pathologies, including the acute viral respiratory infections. The excessive release of pro-inflammatory cytokines, termed “cytokine storm”, is the critical immunological event leading to severe clinical syndrome, a grave complication of infectious and inflammatory diseases. The cytokine storm and acute respiratory distress syndrome (ARDS) are directly related to adverse prognosis in COVID-19 [2–10].

The availability of safe and effective therapeutics for the treatment of hospitalized patients with COVID-19 remains a major clinical issue, which is far from being solved decidedly. The progress will depend on clinical trials for antiviral and anti-inflammatory drugs including monoclonal antibodies.

As demonstrated in a number of cohort and clinical studies, properly scheduled administration of immunomodulatory agents to patients with COVID-19 can substantively improve the clinical status, reduce the hospital stay, and ultimately alleviate the risk of lethal outcome [11]. Several studies on the therapeutic efficacy of neutralizing monoclonal antibodies in patients with COVID-19 have shown significant reduction of SARS-CoV-2 viral loads and prevention of the disease progression [12–15]. One of such molecules, tocilizumab (TCZ), specifically targets the receptor of interleukin 6 (IL6). Systematic reviews suggest that rational use of TCZ may prevent the irreversible lung damage in severely and critically ill patients with COVID-19 [16].

Meta-analysis of available evidence on the efficacy of TCZ in hospitalized patients with COVID-19, encompassing eight randomized clinical studies ($n = 5,340$) and 28 observational cohort studies ($n = 15,484$), revealed a negative association between TCZ therapy and the demand for mechanical ventilation at a high level of significance. In addition, TCZ therapy has been associated with reduced probability of adverse outcome and reduced risks of secondary infections in patients with COVID-19, albeit at a medium level of significance [17]. On the other hand, a systematic review on the use of TCZ for the treatment of COVID-19, based on the results of three indirect preclinical studies and 28 clinical studies enrolling 5,776 patients with COVID-19 and viral pneumonia/sepsis treated with TCZ before June 20, 2020, failed to confirm the rationale due to the scarcity and controversy of the clinical evidence [18]. Yet another three clinical studies on IL6 antagonists, RCT-TCZ-COVID, CORIMUNO, and STOP-COVID, unanimously conclude that the most promising member of this pharmacological group, TCZ, has negligible efficacy in mild or moderate COVID-19 [19–21]. The benefits of TCZ in severe COVID-19 are conditional, and their dedicated scrutiny will require extra randomized trials enrolling large clinical samples at different stages of pathogenesis.

This study aimed to evaluate the therapeutic efficacy of TCZ as a part of combination therapy in hospitalized patients with moderate COVID-19.

METHODS

This retrospective cohort study was carried out in a city clinical hospital for infectious diseases between January 11, 2021 and December 31, 2021. The initial demographic, clinical, and epidemiological data were retrieved from printed and electronic

medical records. The diagnosis of COVID-19 was conclusively confirmed by positive results of real-time polymerase chain reaction (RT-PCR) test for SARS-CoV-2 in nasopharyngeal swabs.

The observations encompassed 72 inpatients diagnosed with moderate symptomatic COVID-19 in accordance with the 2021 WHO guidelines. The patients presented with certain risk factors for aggravation of the disease and were hospitalized on day 8 ± 3.5 since the initial symptoms. The patients were assigned into two groups: the main group ($n = 52$) received tocilizumab (TCZ) on top of standard therapy and the comparison group ($n = 20$) received standard therapy with dexamethasone (DMX).

The inclusion criteria were as follows: moderate symptomatic COVID-19 with developed pneumonia and various comorbidities, risk factors for disease aggravation (age ≥ 60 , diabetes, chronic respiratory and/or cardiovascular conditions, arterial hypertension, and/or presentation with X-ray signs of pneumonia). The exclusion criteria were the absence of characteristic symptoms of COVID-19, the absence of pneumonia, and the use of alternative biologic medications.

The clinical status was assessed on the following basis: clinical blood tests including leukocyte differential and erythrocyte sedimentation rate; biochemical blood tests including C-reactive protein (CRP) levels; chest X-ray scan for the signs of pneumonia; and pulse oximeter readings (SpO_2). Importantly, the positive RT-PCR test for SARS-CoV-2 in a nasopharyngeal swab collected at admission was a prerequisite for the final diagnosis of COVID-19. The data analysis involved between-the-group comparisons of survival rates, as well as clinical and laboratory profiling before (baseline data) and after the treatment (clinical and laboratory indicators collected at reference time points after the medications had been administered).

Patients of the main group (TCZ group, $n = 52$) were admitted to inpatient care units at different time points with regard to initial symptoms: 9 pts (17.3%) were hospitalized on day 1–5, the majority (32 pts, 61.5%) on day 6–10, 8 pts (15.4%) on day 11–15, and 3 pts (5.8%) on > 15 day of the illness. Age of patients in the main group constituted 30–50 years (7 pts, 13.5%), 51–70 years (24 pts, 46.2%), and > 71 years (21 pt, 40.3%). The main group included 19 (36.5%) men and 33 (63.5%) women.

Patients of the main group received TCZ at a single 400 mg dose administered by intravenous drip on day 10 ± 3.7 of the illness on top of standard scheme in compliance with the current regulatory guidelines. The dynamic observation encompassed clinical and laboratory-instrumental indicators.

Patients of the comparison group ($n = 20$), who received the standard scheme with DMX, were also admitted at different time points with regard to the disease onset: 4 pts (20%) were hospitalized on day 1–5, the majority (13 pts, 65%) on day 6–10, 2 pts (10%) on day 11–15, and 1 pt was hospitalized on > 15 day of the illness. Age of patients in the comparison group constituted 51–70 years (9 pts, 45%) and > 71 years (11 pts, 55%). The comparison group included 10 (50%) men and 10 (50%) women. According to the guidelines of the Ministry of Health of the Russian Federation, all patients of the comparison group received DMX infusions on day 8 ± 3.7 , 4 mg 2 times a day. Structure of clinical symptoms for the two groups is given in Table 1; baseline data, dynamics of clinical and laboratory parameters, and outcomes are given in Table 2. The groups were similar in age structure (68 [59–80.5] vs. 72.5 [64.5–82] years; $p = 0.308$), hospitalization time point (day 8 [6–10] vs. 8 [6.5–8.5] of the illness; $p = 0.505$), and initial laboratory parameters.

Table 1. Structure of clinical symptoms in patients receiving tocilizumab vs. standard therapy (+dexamethasone)

Symptoms	Tocilizumab		Maintenance therapy/dexamethasone	
	(n = 52)		(n = 20)	
Fatigue	n = 52	100%	n = 20	100%
Headache	n = 3	5.8%	n = 0	0%
Myalgia	n = 2	3.8%	n = 3	15%
Chills	n = 46	88.5%	n = 14	70%
Rash	n = 2	3.8%	n = 1	5%
Oropharyngeal hyperemia	n = 3	5.8%	n = 1	5%
Sore throat	n = 5	9.6%	n = 1	5%
Nasal congestion	n = 0	0%	n = 0	0%
Dry cough	n = 33	63.5%	n = 12	60%
Wet cough	n = 4	7.7%	n = 0	0%
Abdominal pain	n = 3	5.8%	n = 1	5%
Nausea/vomiting	n = 9	17.3%	n = 0	0%
Diarrhea	n = 11	21.2%	n = 2	10%
Fainting	n = 1	1.9%	n = 2	10%
Vertigo	n = 7	13.5%	n = 1	5%
Meningeal signs	n = 0	0%	n = 0	0%
Dysosmia	n = 4	7.7%	n = 1	5%
Dysgeusia	n = 1	1.9%	n = 0	0%

The main group received the biologic medication on day 10 [8–12] of the illness, whereas the comparison group received standard therapy plus DMX starting from day 8 [5.5–10] of the illness. Equivalent proportions of patients in both groups received steroids (100%). None of the patients in both groups received other immunosuppressive drugs (e.g. levilimab, baricitinib).

Statistical analysis of the data was carried out using IBM SPSS Statistics 26 (IBM; USA). Distributions of most quantitative variables differed from normal ($p > 0.05$; Shapiro–Wilk test); these were described nonparametrically as median [interquartile range]. The comparisons were carried out using Mann–Whitney test for independent samples (groups), Wilcoxon rank test for dependent samples, and Pearson's χ^2 test or Fisher's exact test for categorical data.

RESULTS

The analysis of clinical and laboratory parameters revealed significant 10-fold decrease in serum CRP to 7 mg/L (3.5–41.5 mg/L) at 24 h after TCZ infusion ($p < 0.001$). In addition, the use of TCZ was associated with significant increase in platelet counts at 24 h after the infusion ($p < 0.001$). At the same time, the main group showed adverse dynamics for LDH, progressively increased to 341 U/L (280–522 U/L, $p < 0.05$), and no dynamics for oxygen saturation levels. Dynamics of clinical and laboratory parameters for the main group are given in Table 3.

The comparison group, treated with DMX only, showed identical positive dynamics for CRP (11-fold reduction compared with baseline measurements, $p = 0.001$) and platelet counts (to 274.5, 222–357, $p = 0.002$) during the same reference period, and no dynamics for oxygen saturation. Dynamics of clinical and laboratory parameters for the comparison group are given in Table 4.

The lethality constituted 19.2% for the main group (10 pts died in the inpatient care unit, including 1 pt (1.9%) aged < 60 years and 9 pts (17.3%) aged > 60 years), and 5% for the comparison group (1 pt aged > 60 years).

DISCUSSION

Therapeutic use of monoclonal antibody drugs in patients with COVID-19 has multiple shortcomings including the understudied safety profiles, high costs, and unproved efficacy. According to WHO recommendations, the use of TCZ is only justified in critically ill patients with COVID-19. By contrast, clinical guidelines adopted in Russia suggest using this medication for a broader clinical spectrum including moderate COVID-19 in hospitalized patients with risk burden [22]. To date, many specialized inpatient care units practise the use of TCZ as first line treatment for COVID-19 despite the in many ways unconvincing results of clinical trials and rather controversial clinical experience.

In this study on clinical efficacy of TCZ, encompassing individuals with moderate COVID-19 and risks for aggravation, we monitored known indicators of disease progression, including of CRP and SpO₂ levels. Positive dynamics of certain clinically validated parameters (CRP, platelets) after TCZ administration should be noted.

However, we observed no significant reduction in the rate of disease progression to severe form in response to TCZ. In particular, respiratory support was required in 71.2% (37 pts) of the main group and 45% (9 pts) of the comparison group. Aggravation of the respiratory failure syndrome was encountered in 9.6% (5 pts) of the main group and 5% (1 pt) of the comparison group. The lethality constituted 19.2% (10 pts) in the main group and 5% (1 pt) in the comparison group.

The increase in IL6 levels and sharp decrease in CRP levels observed in TCZ-treated patients of our cohort

Table 2. Baseline data, dynamics of clinical and laboratory parameters, and clinical outcomes in patients receiving tocilizumab vs. standard therapy (+dexamethasone)

Parameter	Tocilizumab (n = 52)	Maintenance therapy/ dexamethasone (n = 20)	p
Demographic data			
Age	68 [59–80.5]	72.5 [64.5–82]	0.308 (Mann–Whitney test)
Sex	M: 19 (36.5%)	M: 10 (50%)	
	F: 33 (63.5%)	F: 10 (50%)	
Hospitalized, day of illness	8 [6–10]	8 [6.5–8.5]	0.505 (Mann–Whitney test)
Medication administered, day of illness	10 [8–12]	8 [5.5–10]	0.022* (Mann–Whitney test)
Comorbidities			
Arterial hypertension	39 75%	16 80%	0.764 (Pearson's χ^2 test)
Cardiovascular disorders	25 48%	14 70%	0.118 (Pearson's χ^2 test)
Diabetes mellitus	12 23%	6 30%	0.762 (Pearson's χ^2 test)
Chronic respiratory disorders	11 21%	3 15%	0.744 (Fisher's exact test)
Obesity	(known for 46)	(known for 16)	0.020* (Pearson's χ^2 test)
	28 61%	4	
		25%	
Clinical indicators			
Temperature, initially	36.8 [36.6–37.4]	36.8 [36.6–37.35]	0.845 (Mann–Whitney test)
Temperature, 4 days after treatment	36.6 [36.45–36.8]	36.65 [36.5–36.8]	0.978 (Mann–Whitney test)
Saturation, initially	95.5 [93–96.5]	95.5 [94.5–97]	0.318 (Mann–Whitney test)
Saturation, 4 days after treatment	96 [94–97]	96 [95–98]	0.247 (Mann–Whitney test)
Laboratory test results			
Leukocytes, total, initially	7 [5.2–9]	7.05 [6.20–10.05]	0.427 (Mann–Whitney test)
Leukocytes, total, 4 days after treatment	5.7 [4.2–11]	8.35 [5.8–10.5]	0.075 (Mann–Whitney test)
Lymphocytes, total, initially	1.23 [0.84–1.57]	1.24 [0.85–1.64]	0.832 (Mann–Whitney test)
Lymphocytes, total, 4 days after treatment	1.09 [0.70–1.75]	1.62 [1.14–1.84]	0.107 (Mann–Whitney test)
CRP, initially	72 [28.5–130.5]	74 [39.5–105.5]	0.977 (Mann–Whitney test)
CRP, 24 h after treatment	7 [3.5–41.5]	6 [5–12.5]	0.945 (Mann–Whitney test)
Ferritin, initially	499.5 [251–1033]	319 [295–399]	0.872 (Mann–Whitney test)
Ferritin, 24 h after treatment	708 [375–904]	1252 [783–1500]	0.127 (Mann–Whitney test)
Interleukin, initially	37 [19–182]	12 [7–439]	0.479 (Mann–Whitney test)
Interleukin, 24 h after treatment	319 [167–807.5]	16 [8–37]	0.017* (Mann–Whitney test)
Procalcitonin, initially	0.14 [0.08–0.22]	0.23 [0.10–0.6.10]	0.497 (Mann–Whitney test)
Procalcitonin, 24 h after treatment	0.145 [0.06–0.16]	0.14 [0.08–0.18]	0.859 (Mann–Whitney test)
D-dimer, initially	359 [189–937]	391.5 [163–1193]	0.903 (Mann–Whitney test)
D-dimer, 24 h after treatment	385 [297–1130]	332 [252–1009]	0.618 (Mann–Whitney test)
LDH, initially	312 [275–422]	385 [265–443]	0.737 (Mann–Whitney test)
LDH, 24 h after treatment	341 [280–522]	245 [197–324]	0.005* (Mann–Whitney test)
Platelets, initially	156 [135.5–193.5]	172 [143–185]	0.499 (Mann–Whitney test)
Platelets, 24 h after treatment	231 [175–300]	274.5 [222–357]	0.099 (Mann–Whitney test)
Lethality	10 (19.2%)	1 (5%)	0.275 (Fisher's exact test)

indicates an improvement in hyperinflammatory status, consistently with a systematic review on clinical utility of this biologic medication in COVID-19 at the level of individual patient data including baseline records, laboratory tests, and outcomes [23].

In this study, we had no means to identify the entire complex of causal factors that determined the course of the disease for each patient individually. Apparently, one of the key adverse factors was delayed hospitalization,

when the time had already been lost and the aggravation was inevitable. This point is consistent with the reported association between higher demand for oxygen support and delayed commencement of TCZ therapy. It can be speculated that earlier administration of TCZ may effectively prevent or alleviate the generalized inflammation syndrome [21, 23]. The low anti-covid efficacy of TCZ in certain settings may also involve miscellaneous understudied factors. For example, in this study we disregarded the possible impacts of viral

Table 3. Dynamics of clinical and laboratory parameters in patients treated with tocilizumab

Parameter	Initially	After treatment	<i>p</i>
Body temperature	36.8 [36.6–37.4]	36.6 [36.45–36.8]	< 0.001* (Wilcoxon test for dependent samples)
Oxygen saturation	95.5 [93–96.5]	96 [94–97]	0.161 (Wilcoxon test for dependent samples)
Leukocytes	7 [5.2–9]	5.7 [4.2–11]	0.945 (Wilcoxon test for dependent samples)
Lymphocytes	1.23 [0.84–1.57]	1.09 [0.70–1.75]	0.637 (Wilcoxon test for dependent samples)
CRP	72 [28.5–130.5]	7 [3.5–41.5]	< 0.001* (Wilcoxon test for dependent samples)
Ferritin	499.5 [251–1033]	708 [375–904]	0.859 (Wilcoxon test for dependent samples)
Interleukin	37 [19–182]	319 [167–807.5]	0.144 (Wilcoxon test for dependent samples)
Procalcitonin	0.14 [0.08–0.22]	0.145 [0.06–0.16]	0.498 (Wilcoxon test for dependent samples)
D-dimer	359 [189–937]	385 [297–1130]	0.878 (Wilcoxon test for dependent samples)
LDH	312 [275–422]	341 [280–522]	0.020* (Wilcoxon test for dependent samples)
Platelets	156 [135.5–193.5]	231 [175–300]	< 0.001* (Wilcoxon test for dependent samples)

Table 4. Dynamics of clinical and laboratory parameters in patients treated with standard therapy (+dexamethasone)

Parameter	Initially	After treatment	<i>p</i>
Body temperature	36.8 [36.6–37.35]	36.65 [36.5–36.8]	0.005 (Wilcoxon test for dependent samples)
Oxygen saturation	95.5 [94.5–97]	96 [95–98]	0.810 (Wilcoxon test for dependent samples)
Leukocytes	7.05 [6.20–10.05]	8.35 [5.8–10.5]	0.140 (Wilcoxon test for dependent samples)
Lymphocytes	1.24 [0.85–1.64]	1.62 [1.14–1.84]	0.121 (Wilcoxon test for dependent samples)
CRP	74 [39.5–105.5]	6 [5–12.5]	0.001* (Wilcoxon test for dependent samples)
Ferritin	319 [295–399]	1252 [783–1500]	1.000 (Wilcoxon test for dependent samples)
Interleukin	12 [7–439]	16 [8–37]	paired values available for one patient only
Procalcitonin	0.23 [0.10–6.10]	0.14 [0.08–0.18]	paired values available for one patient only
D-dimer	391.5 [163–1193]	332 [252–1009]	0.500 (Wilcoxon test for dependent samples)
LDH	385 [265–443]	245 [197–324]	0.893 (Wilcoxon test for dependent samples)
Platelets	172 [143–185]	274.5 [222–357]	0.002* (Wilcoxon test for dependent samples)

mutagenesis and viral loads due to technical limitations and small size of the cohort. Identification of other factors interfering with TCZ therapy should rely on larger trials that account for viral mutations.

The analysis accounted for key baseline factors including age, sex, and comorbidities. During the observation period, the protocols for management of moderate COVID-19 underwent no significant alterations; however, there was a spread of new SARS-CoV-2 variants in many countries including Russia. A number of limitations of our study include, first of all, smaller size of the comparison group compared with the main group. Secondly, the research was confined to a single hospital and the long-term results after redirection to outpatient facilities were disregarded. In addition, despite the mandatory confirmation of

the diagnosis by RT-PCR test, the analysis disregarded SARS-CoV-2 mutations and viral loads.

CONCLUSIONS

This retrospective cohort study demonstrated negligible advantages of tocilizumab in hospitalized patients with moderate symptomatic COVID-19 with regard to disease aggravation risks and lethality. The lack of efficacy may reflect the delayed commencement of the therapy. The data contributes to the cumulative clinical evidence on the use of monoclonal antibody drugs as the basis for clinical guidelines. Advanced specification of antiviral strategies (biologic, generic, etc.) in various groups of patients with COVID-19 will require further efforts.

References

1. WHO Coronavirus (COVID-19) Dashboard (2021). Available from: <https://covid19.who.int/> (Accessed 19 October, 2021).
2. Song P, Li W, Xie J, et al. Cytokine storm induced by SARS-CoV-2. Clin Chim Acta. 2020; 509: 280–7. DOI: 10.1016/j.cca.2020.06.017.
3. Zhao Z, Wei Y, Tao C. An enlightening role for cytokine storm in coronavirus infection. Clin Immunol. 2021; 222: DOI: 10.1016/j.clim.2020.108615.
4. Moradian N, Gouravani M, Salehi MA, et al. Cytokine release syndrome: inhibition of pro-inflammatory cytokines as a solution for reducing COVID-19 mortality. Eur Cytokine Netw. 2020; 31 (3): 81–93. DOI: 10.1684/ecn.2020.0451.
5. Pum A, Ennemoser M, Adage T, Kungl AJ. Cytokines and Chemokines in SARS-CoV-2 Infections—Therapeutic Strategies Targeting Cytokine Storm. Biomolecules. 2021; 11 (1): DOI: 10.3390/biom11010091.
6. Nasonov E, Samsonov M. The role of Interleukin 6 inhibitors in therapy of severe COVID-19. Biomed Pharmacother. 2020; 131: DOI: 10.1016/j.biopha.2020.110698.
7. Zhou Z, Price C. Overview on the use of IL6 agents in the treatment of patients with cytokine release syndrome (CRS) and pneumonitis related to COVID-19 disease. Expert Opin Investig Drugs. 2020; 29 (12): 1407–12. DOI: 10.1080/13543784.2020.1840549.
8. Chen J, Zhang L, Hou H, et al. Interleukin 6 signaling blockade treatment for cytokine release syndrome in COVID 19 (Review). Exp Ther Med. 2021; 21 (1): 24. DOI: 10.3892/etm.2020.9456.
9. Moore JB, June CH. Cytokine release syndrome in severe COVID-19. Science. 2020; 368 (6490): 473–4. DOI: 1126/

- science. *Abb* 8925.
10. Kumar A, Sharma A, Tirpude NV, Sharma S, Padwad YS, Kumar S. Pharmac-immunomodulatory interventions for averting cytokine storm-linked disease severity in SARS-CoV-2 infection. *Inflammopharmacology*. 2022 Jan 20; 1–27. DOI: 10.1007/s10787-021-00903-x. Online ahead of print. PMID: 35048262.
 11. Jiang Y, Rubin L, Peng T, Liu L, Xing X, Lazarovici P, Zheng W. Cytokine storm in COVID-19: from viral infection to immune responses, diagnosis and therapy. *Int J Biol Sci*. 2022 Jan 1; 18 (2): 459–72. DOI: 10.7150/ijbs.59272. eCollection 2022. PMID: 35002503.
 12. Group A-TL-CS. A Neutralizing Monoclonal Antibody for Hospitalized Patients With Covid-19. *N Engl J Med*. 2020; 384 (10): 905–14. DOI: 10.1056/NEJMoa2033130.
 13. Weinreich DM, Sivapalasingam S, Norton T, Ali S, Gao H, Bhore R, et al. REGN-COV2, a Neutralizing Antibody Cocktail, in Outpatients With Covid-19. *N Engl J Med*. 2020; 384 (3): 238–51. DOI: 10.1056/NEJMoa2035002.
 14. Verderese JP, Stepanova M, Lam B, Racila A, Kolacevski A, Allen D, et al. Neutralizing Monoclonal Antibody Treatment Reduces Hospitalization for Mild and Moderate COVID-19: A Real-World Experience. *Clin Infect Dis*. 2021; DOI: 10.1093/cid/ciab579.
 15. Chen P, Nirula A, Heller B, Gottlieb RL, Boscia J, Morris J, et al. SARS-CoV-2 Neutralizing Antibody LY-CoV555 in Outpatients With Covid-19. *N Engl J Med*. 2021; 384 (3): 229–37. DOI: 10.1056/NEJMoa2029849.
 16. Kulanthaivel S, Kaliberdenko VB, Balasundaram K, Shterenshis MV, Scarpellini E, Abenavoli L. Tocilizumab in SARS-CoV-2 Patients with the Syndrome of Cytokine Storm: A Narrative Review. *Rev Recent Clin Trials*. 2021; 16 (2): 138–45. DOI: 10.2174/1574887115666200917110954. PMID: 32940187 Review.
 17. Tleyjeh IM, Kashour Z, Riaz M, Hassett L, Veiga VC, Kashour T. Efficacy and safety of tocilizumab in COVID-19 patients: a living systematic review and meta-analysis, first update. *Clin Microbiol Infect*. 2021 Aug; 27 (8): 1076–82. DOI: 10.1016/j.cmi.2021.04.019. Epub 2021 Apr 27.
 18. Cortegiani A, Ippolito M, Greco M, Granone V, Protti A, Gregoretti C, et al. Rationale and evidence on the use of tocilizumab in COVID-19: a systematic review. *Pulmonology*. 2021 Jan-Feb; 27 (1): 52–66. DOI: 10.1016/j.pulmoe.2020.07.003. Epub 2020 Jul 20. PMID: 32713784.
 19. Salvarani C, Dolci G, Massari M, et al. Effect of tocilizumab vs standard care on clinical worsening in patients hospitalized with COVID-19 pneumonia: A Randomized Clinical Trial. *JAMA Intern Med*. 2021; 181 (1): 24–31. DOI: 10.1001/jamainternmed.2020.6615.
 20. Stone JH, Frigault MJ, Serling-Boyd NJ, et al. Efficacy of Tocilizumab in Patients Hospitalized with Covid-19. *N Engl J Med*. 2020; 383 (24): 2333–44. DOI: 10.1056/NEJMoa2028836.
 21. Verderese JP, Stepanova M, Lam B, Racila A, Kolacevski A, Allen D, et al. Neutralizing Monoclonal Antibody Treatment Reduces Hospitalization for Mild and Moderate COVID-19: A Real-World Experience. *Clin Infect Dis*. 2021; DOI: 10.1093/cid/ciab579.
 22. Vremennye metodicheskie rekomendacii # 14 ot 27.12.2021 «Profilaktika, diagnostika i lechenie novoj koronavirusnoj infekcii (COVID-19)». Russian.
 23. Antwi-Amoabeng D, Kanji Z, Ford B, Beutler BD, Riddle MS, Siddiqui F. Clinical outcomes in COVID-19 patients treated with tocilizumab: An individual patient data systematic review. *J Med Virol*. 2020 Nov; 92 (11): 2516–22. DOI: 10.1002/jmv.26038. Epub 2020 Jun 9.

Литература

1. WHO Coronavirus (COVID-19) Dashboard (2021). Available from: <https://covid19.who.int/> (Accessed 19 October, 2021).
2. Song P, Li W, Xie J, et al. Cytokine storm induced by SARS-CoV-2. *Clin Chim Acta*. 2020; 509: 280–7. DOI: 10.1016/j.cca.2020.06.017.
3. Zhao Z, Wei Y, Tao C. An enlightening role for cytokine storm in coronavirus infection. *Clin Immunol*. 2021; 222: DOI: 10.1016/j.clim.2020.108615.
4. Moradian N, Gouravani M, Salehi MA, et al. Cytokine release syndrome: inhibition of pro-inflammatory cytokines as a solution for reducing COVID-19 mortality. *Eur Cytokine Netw*. 2020; 31 (3): 81–93. DOI: 10.1684/ecn.2020.0451.
5. Pum A, Ennemoser M, Adage T, Kungl AJ. Cytokines and Chemokines in SARS-CoV-2 Infections—Therapeutic Strategies Targeting Cytokine Storm. *Biomolecules*. 2021; 11 (1): DOI: 10.3390/biom11010091.
6. Nasonov E, Samsonov M. The role of Interleukin 6 inhibitors in therapy of severe COVID-19. *Biomed Pharmacother*. 2020; 131: DOI: 10.1016/j.biopha.2020.110698.
7. Zhou Z, Price C. Overview on the use of IL6 agents in the treatment of patients with cytokine release syndrome (CRS) and pneumonitis related to COVID-19 disease. *Expert Opin Investig Drugs*. 2020; 29 (12): 1407–12. DOI: 10.1080/13543784.2020.1840549.
8. Chen J, Zhang L, Hou H, et al. Interleukin 6 signaling blockade treatment for cytokine release syndrome in COVID 19 (Review). *Exp Ther Med*. 2021; 21 (1): 24. DOI: 10.3892/etm.2020.9456.
9. Moore JB, June CH. Cytokine release syndrome in severe COVID-19. *Science*. 2020; 368 (6490): 473–4. DOI: 1126/science. Abb 8925.
10. Kumar A, Sharma A, Tirpude NV, Sharma S, Padwad YS, Kumar S. Pharmac-immunomodulatory interventions for averting cytokine storm-linked disease severity in SARS-CoV-2 infection. *Inflammopharmacology*. 2022 Jan 20; 1–27. DOI: 10.1007/s10787-021-00903-x. Online ahead of print. PMID: 35048262.
11. Jiang Y, Rubin L, Peng T, Liu L, Xing X, Lazarovici P, Zheng W. Cytokine storm in COVID-19: from viral infection to immune responses, diagnosis and therapy. *Int J Biol Sci*. 2022 Jan 1; 18 (2): 459–72. DOI: 10.7150/ijbs.59272. eCollection 2022. PMID: 35002503.
12. Group A-TL-CS. A Neutralizing Monoclonal Antibody for Hospitalized Patients With Covid-19. *N Engl J Med*. 2020; 384 (10): 905–14. DOI: 10.1056/NEJMoa2033130.
13. Weinreich DM, Sivapalasingam S, Norton T, Ali S, Gao H, Bhore R, et al. REGN-COV2, a Neutralizing Antibody Cocktail, in Outpatients With Covid-19. *N Engl J Med*. 2020; 384 (3): 238–51. DOI: 10.1056/NEJMoa2035002.
14. Verderese JP, Stepanova M, Lam B, Racila A, Kolacevski A, Allen D, et al. Neutralizing Monoclonal Antibody Treatment Reduces Hospitalization for Mild and Moderate COVID-19: A Real-World Experience. *Clin Infect Dis*. 2021; DOI: 10.1093/cid/ciab579.
15. Chen P, Nirula A, Heller B, Gottlieb RL, Boscia J, Morris J, et al. SARS-CoV-2 Neutralizing Antibody LY-CoV555 in Outpatients With Covid-19. *N Engl J Med*. 2021; 384 (3): 229–37. DOI: 10.1056/NEJMoa2029849.
16. Kulanthaivel S, Kaliberdenko VB, Balasundaram K, Shterenshis MV, Scarpellini E, Abenavoli L. Tocilizumab in SARS-CoV-2 Patients with the Syndrome of Cytokine Storm: A Narrative Review. *Rev Recent Clin Trials*. 2021; 16 (2): 138–45. DOI: 10.2174/1574887115666200917110954. PMID: 32940187 Review.
17. Tleyjeh IM, Kashour Z, Riaz M, Hassett L, Veiga VC, Kashour T. Efficacy and safety of tocilizumab in COVID-19 patients: a living systematic review and meta-analysis, first update. *Clin Microbiol Infect*. 2021 Aug; 27 (8): 1076–82. DOI: 10.1016/j.cmi.2021.04.019. Epub 2021 Apr 27.
18. Cortegiani A, Ippolito M, Greco M, Granone V, Protti A, Gregoretti C, et al. Rationale and evidence on the use of tocilizumab in COVID-19: a systematic review. *Pulmonology*. 2021 Jan-Feb; 27 (1): 52–66. DOI: 10.1016/j.pulmoe.2020.07.003. Epub 2020 Jul 20. PMID: 32713784.
19. Salvarani C, Dolci G, Massari M, et al. Effect of tocilizumab vs standard care on clinical worsening in patients hospitalized with COVID-19 pneumonia: A Randomized Clinical Trial. *JAMA Intern Med*. 2021; 181 (1): 24–31. DOI: 10.1001/jamainternmed.2020.6615.
20. Stone JH, Frigault MJ, Serling-Boyd NJ, et al. Efficacy of Tocilizumab in Patients Hospitalized with Covid-19. *N Engl J Med*. 2020; 383 (24): 2333–44. DOI: 10.1056/NEJMoa2028836.
21. Verderese JP, Stepanova M, Lam B, Racila A, Kolacevski A, Allen D, et al. Neutralizing Monoclonal Antibody Treatment Reduces

- Hospitalization for Mild and Moderate COVID-19: A Real-World Experience. *Clin Infect Dis*. 2021; DOI: 10.1093/cid/ciab579.
22. Временные методические рекомендации № 14 от 27.12.2021 «Профилактика, диагностика и лечение новой коронавирусной инфекции (COVID-19)».
23. Antwi-Amoabeng D, Kanji Z, Ford B, Beutler BD, Riddle MS, Siddiqui F. Clinical outcomes in COVID-19 patients treated with tocilizumab: An individual patient data systematic review. *J Med Virol*. 2020 Nov; 92 (11): 2516–22. DOI: 10.1002/jmv.26038. Epub 2020 Jun 9.

MICROGLIA AND PUTATIVE MACROPHAGES OF THE SUBFORNICAL ORGAN: STRUCTURAL AND FUNCTIONAL FEATURES

Guselnikova VV^{1,2} ✉, Razenkova VA¹, Sufieva DA¹, Korzhevskii DE¹

¹ Institute of Experimental Medicine, St Petersburg, Russia

² St Petersburg State University, St Petersburg, Russia

The subfornical organ is an important regulator of water-salt metabolism and energy balance of the body, involved in the control of the cardiovascular system and immune regulation. The organ comprises several cell populations, among which microglia and macrophages remain uncharacterized. The study aimed at structural, cytochemical, and functional characterization of microglia and macrophages of the subfornical organ in rats. Brain specimens were collected from mature male Wistar rats ($n = 8$). Microglia and macrophages were revealed by immunostaining with poly- and monoclonal antibodies against calcium-binding protein Iba1 and lysosomal protein CD68; the slides were examined by light and confocal laser microscopy. The study provides a complex morphological characterization of microglial cells and macrophages of the subfornical organ. We demonstrate that the majority of Iba1-expressing cells in this area of the brain are microglial cells, not macrophages. Microglia of the subfornical organ reveals preactivated state, which may reflect structural and functional features of this organ and specific functions of local microglia. Subependymal microglial cells, the processes of which penetrate into the cavity of the third ventricle of the brain, constitute a distinct subpopulation among the Iba1-expressing cells of the subfornical organ. Apart from microglial elements, the subfornical organ contains sparse tissue macrophages with characteristic strong expression of CD68 accompanied by undetectable or weak expression of Iba1.

Keywords: subfornical organ, microglia, macrophages, circumventricular organs

Funding: the study was supported by Russian Science Foundation, RSF Project № 22-25-00105, <https://rscf.ru/project/22-25-00105/>

Author contribution: Guselnikova VV — literature analysis, interpretation of the results, manuscript preparation; Razenkova VA — fluorescence immunoassay protocols development, confocal laser microscopy; Sufieva DA — histological processing, immunochemical staining, light microscopy; Korzhevskii DE — concept and planning of the study, editing of the manuscript.

Compliance with ethical standards: the study was approved by Ethical Review Board at the Institute of Experimental Medicine (Protocol № 1/22 of 18 February 2022) and carried out in full compliance with the 2013 Declaration of Helsinki.

✉ **Correspondence should be addressed:** Valeria V. Guselnikova
Akad. Pavlova, 12, St Petersburg, 197376, Russia; guselnikova.valeriia@yandex.ru

Received: 27.03.2022 **Accepted:** 18.04.2022 **Published online:** 28.04.2022

DOI: 10.24075/brsmu.2022.020

МИКРОГЛИЯ И ПРЕДПОЛАГАЕМЫЕ МАКРОФАГИ СУБФОРНИКАЛЬНОГО ОРГАНА: СТРУКТУРНО-ФУНКЦИОНАЛЬНЫЕ ОСОБЕННОСТИ

В. В. Гусельникова^{1,2} ✉, В. А. Разенкова¹, Д. А. Суфиева¹, Д. Э. Коржевский¹

¹ Институт экспериментальной медицины, Санкт-Петербург, Россия

² Санкт-Петербургский государственный университет, Санкт-Петербург, Россия

Субфорникальный орган является важным регулятором водно-солевого обмена и энергетического баланса организма, участвует в контроле работы сердечно-сосудистой системы и иммунной регуляции. В состав субфорникального органа входят разные клеточные популяции, среди которых неохарактеризованными остаются микроглия и макрофаги. Целью работы было изучить структурные, цитохимические и функциональные характеристики микроглии и макрофагов субфорникального органа головного мозга крысы. Исследовали образцы головного мозга половозрелых крыс-самцов породы Вистар ($n = 8$). Для выявления микроглии и макрофагов применяли поли- и моноклональные антитела против кальций-связывающего белка Iba1 и лизосомного белка CD68 и анализировали препараты методами световой и конфокальной лазерной микроскопии. В рамках исследования дана комплексная морфологическая характеристика клеток микроглии и макрофагов субфорникального органа. Показано, что большинство Iba1-содержащих клеток этой области головного мозга являются микроглиями, а не макрофагами. Микроглия субфорникального органа находится в преактивированном состоянии, что может быть обусловлено структурно-функциональными особенностями этого органа и специфическими функциями местной микроглии. Среди Iba1-содержащих клеток в субфорникальном органе выявлена особая популяция субependимных микроглиями, отростки которых проникают в полость третьего желудочка головного мозга. Помимо микроглии в субфорникальном органе обнаружены единичные тканевые макрофаги, для которых характерно высокое содержанием CD68, но незначительное количество или отсутствие Iba1.

Ключевые слова: субфорникальный орган, микроглия, макрофаги, циркумвентрикулярные органы

Финансирование: исследование выполнено при финансовой поддержке Российского Научного Фонда, проект № 22-25-00105, <https://rscf.ru/project/22-25-00105/>

Вклад авторов: В. В. Гусельникова — анализ литературы, интерпретация результатов, подготовка рукописи; В. А. Разенкова — отработка протоколов иммунофлуоресцентных реакций, проведение конфокальной лазерной микроскопии; Д. А. Суфиева — гистологическая проводка биологического материала, постановка иммуногистохимических реакций для световой микроскопии; Д. Э. Коржевский — концепция, планирование исследования, редактирование рукописи.

Соблюдение этических стандартов: исследование одобрено этическим комитетом ФГБНУ «ИЭМ» (протокол № 1/22 от 18 февраля 2022 г.), проведено в полном соответствии с положениями Хельсинкской декларации (2013 г.).

✉ **Для корреспонденции:** Валерия Владимировна Гусельникова
ул. Акад. Павлова, д. 12, г. Санкт-Петербург, 197376, Россия; guselnikova.valeriia@yandex.ru

Статья получена: 27.03.2022 **Статья принята к печати:** 18.04.2022 **Опубликована онлайн:** 28.04.2022

DOI: 10.24075/vrgmu.2022.020

The subfornical organ (*organum subfornicum*) is localized near the arch of the telencephalon (*fornix*) along the anterior wall of the third ventricle, where it occupies the dorsal end of the terminal plate, protruding slightly into the lumen of the third ventricle. An important regulator of water-salt metabolism and energy balance of the body, it is involved in the control of the cardiovascular system and immune regulation [1, 2]; hence the considerable interest in overall anatomy and cellular composition of the subfornical organ, which still remains one of the most mystifying brain structures.

Microglia and macrophages are resident cells of the subfornical organ. These two cell types implement similar functions, but differ structurally (by expression profiles of certain genes and immunophenotype) and ontogenetically (by source of origin). The importance of studying these cell types within the context of subfornical organ functionalities is determined by its being one of the circumventricular organs characterized by the lack of the blood-brain barrier. Accordingly, its local macrophages and microglia, by contrast with their counterparts in other brain regions, are in continuous contact with various agents circulating in the blood [3], which implies that these cells have certain structural and functional features. An extra focus on microglia and macrophages of the subfornical organ is due to their possible involvement in the course of coronavirus infection. The strong neurotropism of SARS-CoV-2 is a well-established fact [4]. The chronic activation status of microglia, which is normal for circumventricular organs, is thought to render it hyper-sensitive and hyper-reactive to pathological stimuli (e.g. SARS-CoV-2 infection) [5] and prone to transition into pro-inflammatory phenotypes accompanied by active synthesis of pro-inflammatory mediators and increased rates of phagocytosis. The SARS-CoV-2-associated neuroinflammatory response, which develops in circumventricular organs, confers significant risks of neurodegeneration. In addition, the enhanced migration capacity of the hyper-activated amoeboid microglial cells facilitates the spread of neuroinflammation to other brain regions [5], which may be one of the underlying causes of neurological symptoms in patients with coronavirus infections.

This study aimed at structural, cytochemical, and functional characterization of microglia and macrophages of the subfornical organ in rats.

METHODS

The study was carried out on brain specimens of mature (3–5 months old) male Wistar rats ($n = 8$). The animals were purchased at the “Rappolovo” breeding facilities (Leningrad region, Russia) and housed at standard conditions with ambient temperature, 12-h light cycle, and *ad libitum* access to pellets and water. The brain specimens were fixed in zinc-ethanol-formaldehyde [6] and embedded in paraffin (Paraffin Type 6, ThermoScientific Richard-Allan Scientific; USA) under standard protocol. The blocks were sectioned on a Microm HM 325 rotary microtome (ThermoScientific; USA); the 5 μ m thick frontal sections comprising the subfornical organ region were mounted on adhesion slides (Menzel; Germany). After standard deparaffinization and rehydration, the sections were demasked by heating in 10% aqueous solution of sodium thiosulfate for 23 min [7].

The light microscopy immunohistochemistry assay of microglia and/or macrophages involved anti-Iba1 rabbit polyclonal antibodies (Biocare Medical; USA) diluted 1:1500 and anti-CD68 mouse monoclonal (ED1) antibody (Abcam; UK) diluted 1:4000, with REVEAL Rabbit Specific HRP-DAB Detection System in manufacturer's dilution (Spring Bioscience;

USA) as secondary antibody and 3,3'-diaminobenzidine (DAB+, Agilent; USA) as chromogen. After the reaction, some of the sections were treated with alum hematoxylin as a nuclear counterstain.

For immunofluorescent detection of Iba1, the sections were covered with the rabbit polyclonal antibodies diluted 1:1000 (Biocare Medical; USA). The antigen-antibody complexes were visualized with REVEAL Rabbit Specific HRP-DAB Detection System in manufacturer's dilution (Spring Bioscience; USA) followed by Cy3-conjugated AffiniPure Goat Anti-Horseradish Peroxidase polyclonal antibodies (Jackson ImmunoResearch; USA). The nuclei were counterstained with SYTOX Green fluorescent dye (Invitrogen; USA).

For double-fluorescent immunostaining of Iba1/CD68 the sections were covered with a 1:1 mixture of rabbit polyclonal antibodies to Iba1 diluted 1:500 (Biocare Medical; USA) and mouse monoclonal antibodies to CD68 diluted 1:1000 (Agilent; USA), followed by a mixture of (anti-)Rabbit IgG Biotinylated Antibody (R&D Systems; USA) and EnVision+/HRP-Anti-Mouse reagent (Agilent; USA) as secondary antibodies. After incubation in the mixture of secondary antibodies, the sections were sequentially treated with solutions of Cy2-Streptavidin (Jackson ImmunoResearch; USA) and Cy3-conjugated AffiniPure Goat Anti-Horseradish Peroxidase polyclonal antibodies (Jackson ImmunoResearch; USA).

Examination of the slides and image acquisition were carried out with Leica DM750 light microscope (Leica; Germany) equipped with Leica ICC₅₀ camera (Leica; Germany) and Zeiss LSM800 confocal laser microscope (Zeiss; Germany). The fluorescence was excited using a 488 nm laser for Cy2 and SYTOX Green and a 561 nm laser for Cy3. The images were analyzed in ZEN2012 and LSM Image Browser software packages (Zeiss; Germany).

RESULTS

Immunohistochemical detection of Iba1 calcium-binding protein

Immunohistochemical staining for calcium-binding protein Iba1 specifically expressed in microglia and macrophages revealed immunopositive cells of the subfornical region in all studied rat brain specimens (Fig. 1). The subfornical organ is clearly visualized at low magnification ($\times 10$) as a compact cellular aggregation protruding into the cavity of the third ventricle (Fig. 1A, SFO). The organ shows high cellularity revealed by counterstaining of the nuclei with hematoxylin (Fig. 1A, SFO, blue), as well as the high intensity of the Iba1 signal (Fig. 1A, SFO, brown). Thus, already at a low magnification of the microscope, the subfornical organ presents with abundant Iba1-immunopositive elements distributed rather evenly within the organ.

Examination of the subfornical organ region and its boundary with adjacent white matter at higher magnifications ($\times 40$, $\times 100$) revealed specific localization of the Iba1 immunostaining in cells with ramified processes, of diverse morphology (Fig. 1B–E, brown). In white matter (Fig. 1B, WM), the Iba1-positive cells are mostly fusiform, with two long non-ramified or poorly ramified processes located at the poles; cell bodies and processes of these cells are oriented along the nerve fibers (Fig. 1B, WM, brown). In subfornical organ (Fig. 1B–E, SFO), the Iba1-positive cells are visually larger compared with the corresponding cells in white matter. These cells have more complex architecture of the processes and show considerable morphological heterogeneity: one morphotype has fusiform shape with small

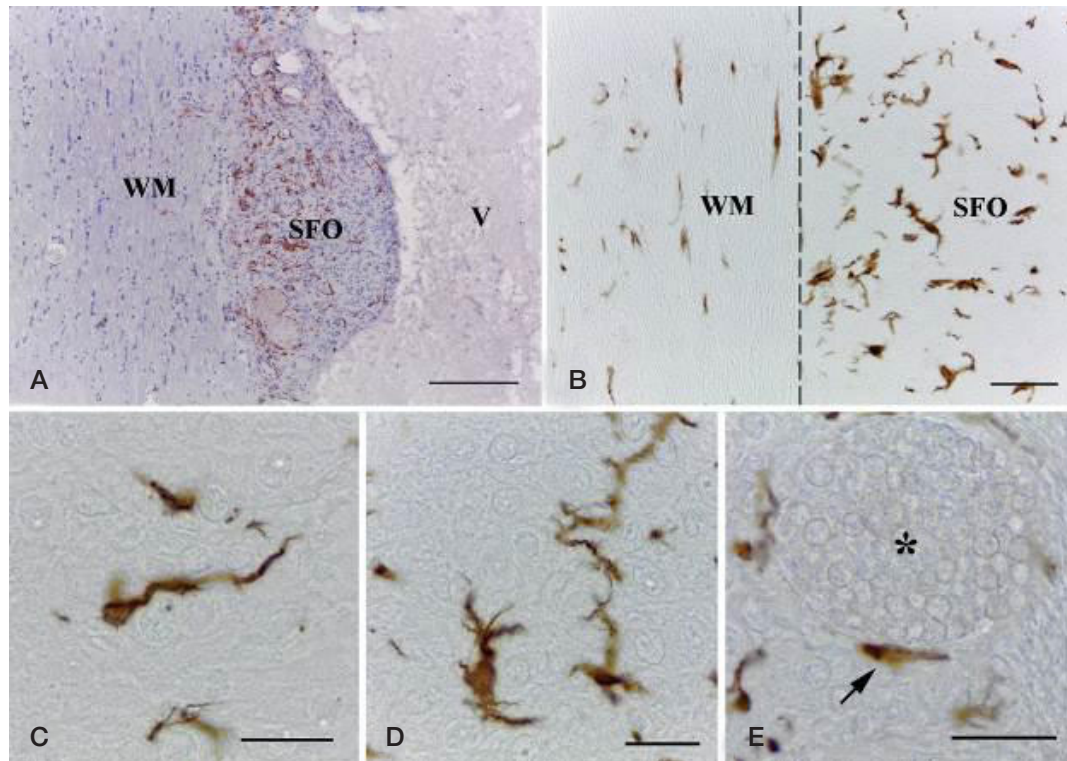


Fig. 1. Iba1-immunopositive cells in rat subfornical organ and adjacent white matter. **A.** Overall view. **B.** The boundary between subfornical organ and the underlying white matter. **C–E.** Different morphotypes of Iba1-immunopositive cells within subfornical organ. SFO — subfornical organ, WM — white matter, V — third ventricle of the brain (cavity); the *dashed line* indicates the boundary between subfornical organ and white matter; the *asterisk* indicates blood vessel (lumen); the *arrow* indicates a small perivascular cell with few processes, containing Iba1. Scale bars, 200 μ m (**A**), 50 μ m (**B**), and 20 μ m (**C–E**)

body and a long non-ramified process (Fig. 1C, *brown*), another morphotype exhibits relatively thick processes moderately branching in multiple directions (Fig. 1D, *brown*), whereas the sparse perivascular Iba1-positive cells with few processes are spread over the surface of dilated thin-walled vessels of the subfornical organ (Fig. 1E, *arrow*).

The fluorescent immunostaining for Iba1 produced similar results (Fig. 2). The subfornical organ region presents with high cellularity revealed by counterstaining of the nuclei with SYTOX Green fluorescent dye (Fig. 2, *green fluorescence*). Consistently with the corresponding light microscopy assay, the fluorescent immunostaining for Iba1 revealed high density

of Iba1-containing cells within subfornical organ (Fig. 2, *red fluorescence*). Examination of these cells at higher magnifications revealed their considerable morphological heterogeneity. The immunofluorescence assay produced a more contrasted visualization of the thin processes of the Iba1-containing cells compared to light microscopy, which allowed us to describe a specific subpopulation of these cells confined to the ependymal lining of the third ventricle at the level of the subfornical organ. The bodies of these Iba1-immunopositive cells were immediately adjacent to the ependymal layer and often spread over it, and their thin processes permeated the ependymal layer and reached the cavity of the third ventricle (Fig. 2, *arrow*).

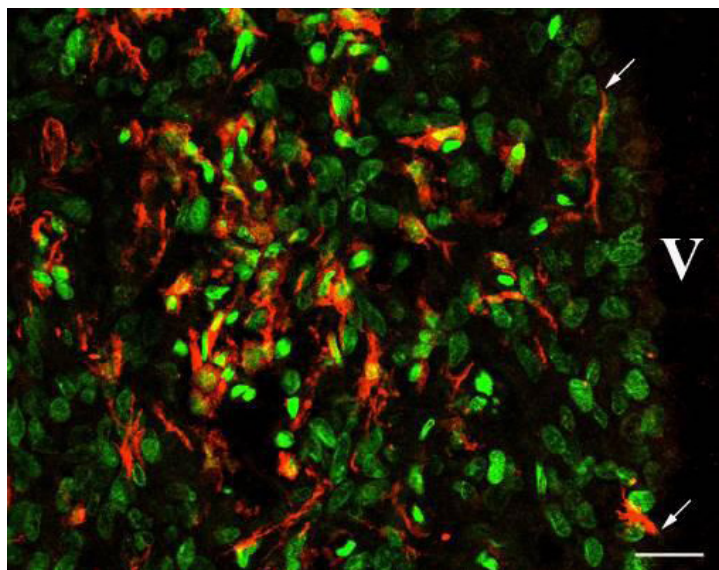


Fig. 2. Immunofluorescent detection of Iba1-positive cells in rat subfornical organ. The Iba1 specific signal is *red* (Cy3 fluorochrome) and the nuclei are *green* (SYTOX Green). V — third ventricle of the brain (cavity); the *arrow* indicates processes of the Iba1-containing cells reaching the ventricular cavity. Scale bar, 20 μ m

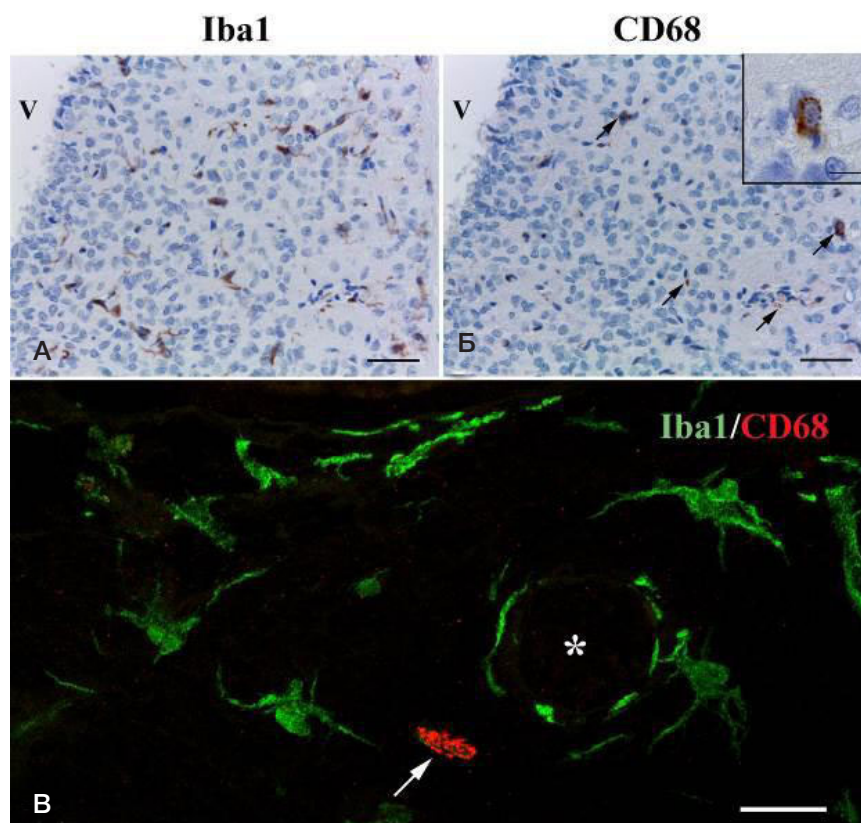


Fig. 3. Characteristic patterns of Iba1 and CD68 immunostaining in rat subfornical organ. **A.** Immunohistochemical reaction for Iba1 with alum hematoxylin nuclear counterstaining. **B.** Immunohistochemical reaction for CD68 with alum hematoxylin nuclear counterstaining; the arrows indicate CD68-immunopositive structures within the subfornical organ; the insert shows a magnified area comprising CD68-immunopositive cell. Images **A** and **B** represent histologically identical serial sections of the same specimen (light microscopy). **C.** Double-fluorescent immunostaining of Iba1/CD68 (confocal laser microscopy). The Iba1 signal is green (Cy2 fluorochrome) and the CD68 signal is red (Cy3 fluorochrome); the arrow indicates a CD68-containing cell; the asterisk indicates blood vessel (lumen). Scale bars, 50 μ m (**A**, **B**) and 10 μ m (**B** insert, **C**)

Immunohistochemical detection of CD68

Comparative examination of light microscopy immunostaining images for Iba1 (Fig. 3A) and CD68 (Fig. 3B), representing two histologically identical serial sections of the same brain tissue specimen, revealed much lower density of CD68-positive elements and higher density of Iba1-positive elements in the subfornical organ. Only sparse CD68-positive elements were visualized in the subfornical organ, found in parenchyma or perivascular spaces. Most of the signal appeared as small CD68-immunopositive granules scattered in the nervous tissue (Fig. 3B, arrow). Only a minority of CD68-immunopositive elements had cellular outlines. These few cells were oval or elongated and showed distinct cytoplasmic granularity (Fig. 3B, insert).

As shown by the double-fluorescent Iba1/CD68 immunostaining, the majority of positively stained cells are Iba1⁺/CD68⁻ (Fig. 3C, green fluorescence). These cells have ramified appearance and heterogeneous morphology, similarly with the Iba1-immunopositive cells revealed by the light microscopy assay. A very minor fraction of cells (solitary cells) in the subfornical organ are Iba1⁻/CD68⁺ (i.e. contain CD68, but no Iba1). These cells are oval or elongated, with characteristic cytoplasmic granularity, and no observable processes (Fig. 3C; arrow, red fluorescence). In certain CD68-immunopositive cells, Iba1 was present in small amounts, but it never colocalized with CD68.

DISCUSSION

The subfornical organ remains one of the least studied brain structures. The main scientific findings on its structure and

function date back to the 1960–80s. The organ receives synaptic inputs from solitary tract nuclei [8], lateral hypothalamus and medial hypothalamic nuclei [9], while sending projections to diverse brain centers including paraventricular nucleus and lateral hypothalamus [10], arcuate nucleus [11], and median preoptic nucleus [9]. Seminal research on the role of this organ in osmoregulation [12] and control of cardiovascular functionalities [13] also dates to the mid-20th century. The findings obviously need verification and refinement with the use of modern immunomorphological methods, along with the available data on cellular composition of the organ. A comprehensive morphological study on structural and functional features of different subpopulations of neurons, astrocytes, and vascular cells in rat subfornical organ was carried out in 2021 [2]; however, it completely disregarded such important cell types as macrophages and microglia.

Microglia and tissue macrophages of the brain make important contribution to immunity by forming the first-line defense of the central nervous system from various infectious agents capable of crossing the endothelial barrier. Despite their similar functions, these cell populations originate from different embryonic sources [14]. The microglial progenitor cells are formed within the embryonic yolk sac wall during the first wave of hemopoiesis and migrate to the developing brain before the onset of the blood-brain barrier. In the brain, these progenitors differentiate into microglial cells which constitute a self-perpetuating population. Other macrophage lineages found in the brain (meningeal macrophages, perivascular macrophages, choroid plexus macrophages) descend from the erythromyeloid progenitor cells and hemopoietic stem cells of the embryonic liver and the bone marrow during the second and

the third waves of hemopoiesis. In connection with their yolk sac origin and by contrast with macrophages, the microglial differon comprises no equivalent of the monocyte stage [15–17]. Apart from the origin, microglial cells differ from the “true” brain macrophages both structurally and phenotypically. For instance, microglial cells express unique molecular markers P2RY12, Sall1, and Tmem119 along with very moderate levels of CD45 transmembrane tyrosine phosphatase. By contrast, brain macrophages express CD45 and the major histocompatibility complex class II molecules at much higher levels than microglia, which reflects the important antigen-presenting role of these cells. Also by contrast with microglia, perivascular and meningeal macrophages abundantly express CD206 protein known as macrophage mannose receptor [18].

It is believed that under normal physiological conditions (in the absence of pathogenic processes) microglial cells have “ramified” morphologies with numerous thin branching processes that constantly monitor the microenvironment for potential hazards (the so-called sentinel or resting microglia). Upon the exposure to pathological stimuli, microglia is converted into active (activated) state with characteristic amoeboid morphologies. The conversion involves substantial enlargement of the cell body (through increase in the perinuclear cytoplasm volume) accompanied by reduction of the processes. These morphological metamorphoses correspond to a functional shift towards increased phagocytic activity and/or cytokine production [19, 20]. In other words, morphological features of microglial cells reflect their functional status.

In this study, we used calcium-binding protein Iba1 (ionized calcium-binding adaptor molecule 1) as a marker to assess the morphological and functional state of microglia in the subfornical organ. It should be noted that, despite its common use as immunohistochemical marker for microglia [21], Iba1 is not uniquely expressed in microglial cells but also detected in typical tissue macrophages, e.g. in Kupffer cells [22]. Immunostaining with anti-Iba1 antibody reveals both resting and activated microglia and all intermediate states as well [20, 23]. The homogeneous distribution of Iba1 protein in the cytoplasm of microglial cells enables the use of anti-Iba1 immunohistochemistry as a valuable tool for detailed morphological characterization of these cells [24]. Our use of anti-Iba1 immunostaining on paraffin sections of rat subfornical organ revealed numerous positive cells with ramified morphology corresponding to microglia. The examination revealed high density of microglial cells in the subfornical organ and their substantial morphological heterogeneity. Although the identified cells had thicker and shorter processes with reduced degree of branching compared with the classical images of resting microglia, we encountered no amoeboid microglial cell morphologies in the studied histological specimens. Apparently, all microglial cells observed by us in the subfornical organ can be assigned with intermediate status loosely defined as “preactivated”.

It is important to emphasize that the subfornical organ is a circumventricular organ which lacks the blood-brain barrier. The signs of microglial activation under normal physiological conditions have been previously described for other circumventricular organs. The physiologically activated microglia in circumventricular organs of mice [3] shows overall reduction in the length and number of microglial cell processes compared with other brain regions, accompanied by elevated expression levels of certain molecular markers. The high degree of microglial activation under normal physiological conditions was also observed in the median eminence area of rat brain [25].

Exact causes of the chronic microglial activation observed in circumventricular organs are disputable. Obviously, the condition reflects specific physiological features of these organs. One of such features is the presence of fenestrated capillaries, resulting in the constant exposure of microglial cells to antigens circulating with the blood (by contrast with microglia in other brain regions protected by the blood-brain barrier). A likely responsibility of microglia under these conditions is phagocytosis of neurotoxic molecules that arrive from circulation in order to ensure the maintenance of tissue homeostasis [3]. Another possible function of the activated microglia is its participation in tissue remodeling. Circumventricular organs have been previously characterized as the sites of intensive physiological angiogenesis accompanied by constant proliferation and apoptosis of endothelial cells of the local microcirculatory bed. The activated microglia has been shown to regulate the proliferative activity of endothelium, as well as scavenge the apoptotic leftovers of the dead endothelial cells [26, 27]. Ultimately, microglia can be involved in neurogenesis with concomitant acquisition of an activated morphotype. The presence of neuronal stem cells has been recently demonstrated for certain circumventricular organs including the subfornical organ [28, 29]. This finding suggests a possible contribution of the activated microglia to formation of neurogenic niches in this organ, similar to the well-described involvement of the subventricular zone as well as the subgranular zone of the dentate gyrus in the hippocampus [30].

Another interesting observation made by us in this study reveals a special population of microglial cells of the subfornical organ, which reside beneath the ependymal lining of the third ventricle and reach its cavity with their processes. Similar cell populations termed “subependymal microglial cells” have been described in the subventricular zone of the lateral ventricles [31]. The close contact of subependymal microglia with cerebrospinal fluid may indicate participation of these cells in the control of cerebrospinal fluid composition.

One of the problems that arise in fundamental research on microglia concerns the morphological and cytochemical similarity of these cells with tissue macrophages of the brain. Microglia and macrophages originate from different sources but share a variety of common marker proteins, Iba1 being one of them [32]. It would be virtually impossible to distinguish microglia from tissue macrophages of the brain on a sole basis of immunostaining for Iba1. To specify the identity of the Iba1-immunopositive cells observed by us in the subfornical organ, we additionally performed immunohistochemical staining for CD68 (a transmembrane glycoprotein with a molecular weight of 110 kDa implicated in lysosomal transport). A prominent marker of phagocytic activity, CD68 is highly expressed in monocyte-macrophage lineages and widely used for immunohistochemical detection of Kupffer cells, alveolar macrophages, osteoclasts, dermal Langerhans cells, etc. [33, 34].

Immunostaining with CD68-specific antibody revealed sparse signal and very few CD68-containing cells morphologically similar to macrophages within the subfornical organ. The vast majority of Iba1-immunopositive cells in the subfornical organ do not express CD68, which identifies them as microglia. The absence of CD68 molecules in these cells reveals their rudimentary lysosomal capacity despite the distinct morphological signs of activation. Apparently, the chronic preactivated state of microglia in the subfornical organ has little to do with active phagocytosis and its biological meaning has yet to be discovered. Unexpectedly, the identified CD68-immunopositive macrophages of the subfornical organ contained negligible amounts of the Iba1 protein. According

to the literature, tissue macrophages of the brain express Iba1 in high amounts, which is consistent with our own data for other brain regions in rodents and also in humans [35, 36]. Its low expression in tissue macrophages of subfornical organ may represent a unique cytochemical feature of this local macrophage population.

CONCLUSIONS

The majority of Iba1-containing cells in the subfornical organ are microglial cells, not macrophages. Microglia of the subfornical organ reveals preactivated state, which may reflect

physiological features of this organ and specific functions of local microglia. The subfornical organ contains specific population of subependymal microglial cells, which project into the third brain ventricle and contact cerebrospinal fluid with their processes. Apart from microglia, the organ contains solitary tissue macrophages with high content of CD68 and low or negligible expression of Iba1. Continued research on microglia and macrophages is important, considering their regulatory role in normal functioning of the nervous system and notably their involvement in neuroinflammatory and neurodegenerative processes, particularly in the context of targeted pharmacotherapy for neurodegenerative diseases.

References

- McKinley MJ, McAllen RM, Davern P, Giles ME, Penschow J, Sunn N, Uschakov A, Oldfield BJ. The sensory circumventricular organs of the mammalian brain. *Adv Anat Embryol Cell Biol.* 2003; 172: III–XII, 1–122. DOI: 10.1007/978-3-642-55532-9.
- Hicks A-I, Kobrinsky S, Zhou S, Yang J, Prager-Khoutorsky M. Anatomical organization of the rat subfornical organ. *Front Cell Neurosci.* 2021; 15: 691711. DOI: 10.3389/fncel.2021.691711.
- Takagi S, Furube E, Nakano Y, Morita M, Miyata S. Microglia are continuously activated in the circumventricular organs of mouse brain. *J Neuroimmunol.* 2019; 331: 74–86. DOI: 10.1016/j.jneuroim.2017.10.008.
- DosSantos MF, Devalle S, Aran V, Capra D, Roque NR, Coelho-Aguiar JdM, et al. Neuromechanisms of SARS-CoV-2: A Review *Front Neuroanat.* 2020; 14: 37. DOI: 10.3389/fnana.2020.00037.
- Tremblay M-E, Madore C, Bordeleau M, Tian L, Verkhratsky A. Neuropathobiology of COVID-19: The Role for Glia. *Front. Cell. Neurosci.* 2020; 14: 592214. DOI: 10.3389/fncel.2020.592214.
- Korzhevskii DE, Sukhorukova EG, Kirik OV, Grigorev IP. Immunohistochemical demonstration of specific antigens in the human brain fixed in zinc-ethanol-formaldehyde. *Eur J Histochem.* 2015; 59 (3): 2530. DOI: 10.4081/ejh.2015.2530.
- Korzhevskiy DEh, Kirik OV, Alekseeva OS. Sposob demaskirovaniya antigenov pri provedenii immunocitoximicheskix reakcij. Patent RF #2719163. 17.04.2020. Russian.
- Tanaka J, Hayashi Y, Shimamune S, Nomura M. Ascending pathways from the nucleus of the solitary tract to the subfornical organ in the rat. *Brain Res.* 1997; 777: 237–41. DOI: 10.1016/S0006-8993(97)01211-0.
- Lind RW, Swanson LW, Ganten D. Angiotensin II immunoreactivity in the neural afferents and efferents of the subfornical organ of the rat. *Brain Res.* 1984; 321: 209–15. DOI: 10.1016/0006-8993(84)90174-4.
- Miselis RR. The subfornical organ's neural connections and their role in water balance. *Peptides.* 1982; 3: 501–2. DOI: 10.1016/0196-9781(82)90115-2.
- Gruber K, McRae-Degueurce A, Wilkin LD, Mitchell LD, Johnson AK. Forebrain and brainstem afferents to the arcuate nucleus in the rat: potential pathways for the modulation of hypophyseal secretions. *Neurosci Lett.* 1987; 75: 1–5. DOI: 10.1016/0304-3940(87)90065-6.
- Felix D. Peptide and acetylcholine action on neurones of the cat subfornical organ. *Naunyn Schmiedeberg's Arch Pharmacol.* 1976; 292: 15–20. DOI: 10.1007/BF00506484.
- Mangiapan ML, Simpson JB. Drinking and pressor responses after acetylcholine injection into subfornical organ. *AJP Regul Integr Comp Physiol.* 1983; 244: R508–13. DOI: 10.1152/ajpregu.1983.244.4.
- Li Q, Barres BA. Microglia and macrophages in brain homeostasis and disease. *Nat Rev Immunol.* 2018; 18 (4): 225–42. DOI: 10.1038/nri.2017.125.
- Gomez Perdiguero E, Klapproth K, Schulz C, et al. Tissue-resident macrophages originate from yolk-sac-derived erythromyeloid progenitors. *Nature.* 2015; 518: 547–51. DOI: <https://doi.org/10.1038/nature13989>
- Hoefel G, Chen J, Lavin Y, et al. C-Myb(+) erythro-myeloid progenitor-derived fetal monocytes give rise to adult tissue-resident macrophages. *Immunity.* 2015; 42 (4): 665–78. DOI: 10.1016/j.immuni.2015.03.011.
- Bennett ML, Bennett FC. The influence of environment and origin on brain resident macrophages and implications for therapy. *Nat Neurosci.* 2020; 23: 157–166. Available from: <https://doi.org/10.1038/s41593-019-0545-6>
- Prinz M, Erny D, Hagemeyer N. Ontogeny and homeostasis of CNS myeloid cells. *Nature Immunology.* 2017; 18 (4): 385–92. DOI: 10.1038/ni.3703
- Hanisch U-K. Functional diversity of microglia — how heterogeneous are they to begin with? *Front Cell Neurosci.* 2013; 7: 65. DOI: 10.3389/fncel.2013.00065.
- Alekseeva OS, Kirik OV, Gilerovich EG, Korzhevskii DE. Microglia of the brain: Origin, structure, functions. *J Evol Biochem Phys.* 2019; 55: 257–68. Available from: <https://doi.org/10.1134/S002209301904001X>.
- Kirik OV, Sukhorukova EG, Korzhevskiy DEh. Kal'cij-svyazyvayushhij belok Iba-1/AIF-1 v kletkax golovnogo mozga krysy. *Morfologiya.* 2010; 137 (2): 5–8. Russian.
- Wijesundera KK, Izawa T, Tennakoon AH, et al. M1- and M2-macrophage polarization in rat liver cirrhosis induced by thioacetamide (TAA), focusing on Iba1 and galectin-3. *Exp Mol Pathol.* 2014; 96 (3): 382–92. DOI: 10.1016/j.yexmp.2014.04.003.
- Kolos E, Korzhevskiy D. Spinal cord microglia in health and disease. *Acta Naturae.* 2020; 12 (1): 4–17. DOI: 10.32607/actanaturae.10934.
- Korzhevskiy DEh, Grigorev IP, Guselnikova VV, Kolos EA, Petrova ES, Kirik OV, i dr. Immunogistoximicheskie markery dlya nejrobiologii. *Med Akad Zhurnal.* 2019; 19 (4): 7–24. DOI: 10.17816/MAJ16548. Russian.
- Sufieva DA, Razenkova VA, Antipova MV, Korzhevskii DE. Microglia and tanycytes of the infundibular recess of the brain in early postnatal development and during aging. *Russ J Dev Biol.* 2020; 51: 189–96. Available from: <https://doi.org/10.1134/S106236042003008X>.
- Morita S, Furube E, Mannari T, Okuda H, Tatsumi K, Wanaka A, et al. Heterogeneous vascular permeability and alternative diffusion barrier in sensory circumventricular organs of adult mouse brain. *Cell Tissue Res.* 2016; 363: 497–511. Available from: <https://doi.org/10.1007/s00441-015-2207-7>.
- Furube E, Mannari T, Morita S, Nishikawa K, Yoshida A, Itoh M, et al. VEGF-dependent and PDGF-dependent dynamic neurovascular reconstruction in the neurohypophysis of adult mice. *J Endocrinol.* 2014; 222: 161–79. Available from: <https://doi.org/10.1038/mp.2017.246>.
- Hourai A, Miyata S. Neurogenesis in the circumventricular organs of adult mouse brains. *J Neurosci Res.* 2013; 91: 757–70. DOI: 10.1002/jnr.23206.
- Furube E, Morita M, Miyata S. Characterization of neural stem cells and their progeny in the sensory circumventricular organs of adult mouse. *Cell Tissue Res.* 2015; 362 (2): 347–65. DOI:


- 10.1007/s00441-015-2201-0.
30. Matarredona ER, Talaverón R, Pastor AM. Interactions between neural progenitor cells and microglia in the subventricular zone: physiological implications in the neurogenic niche and after implantation in the injured brain. *Front Cell Neurosci.* 2018; 12: 268. DOI: 10.3389/fncel.2018.00268.
31. Kirik OV, Suhorukova EG, Alekseeva OS, Korzhevskiy DEh Subependymnye mikrogliocity III zheludochka golovnogo mozga. *Morfologiya.* 2014; 145 (2): 67–9. Russian.
32. Amici SA, Dong J, Guerau-de-Arellano M. Molecular mechanisms modulating the phenotype of macrophages and microglia. *Front Immunol.* 2017; 8: 1520. DOI: 10.3389/fimmu.2017.01520.
33. Chistiakov DA, Killingsworth MC, Myasoedova VA, Orekhov AN, Bobryshev YV. CD68/macrosialin: not just a histochemical marker. *Lab Invest.* 2017; 97 (1): 4–13. DOI: 10.1038/labinvest.2016.116.
34. Jurga AM, Paleczna M, Kuter KZ. Overview of general and discriminating markers of differential microglia phenotypes. *Front Cell Neurosci.* 2020; 14: 198. DOI: 10.3389/fncel.2020.00198.
35. Kirik OV, Tsyba DL, Alekseeva OS, Kolpakova ME, Jakovleva AA, Korzhevskii DE. Alterations in Kolmer cells in SHR line rats after brain ischemia. *Russian Journal of Physiology.* 2021; 107 (2): 177–86. DOI: 10.31857/S0869813921010052.
36. Korzhevskii DE, Kirik OV, Guselnikova VV, Tsyba DL, Fedorova EA, Grigorev IP. Changes in cytoplasmic and extracellular neuromelanin in human substantia nigra with normal aging. *Eur J Histochem.* 2021; 65 (s1): 3283. DOI: 10.4081/ejh.2021.3283.

Литература

1. McKinley MJ, McAllen RM, Davern P, Giles ME, Penschow J, Sunn N, Uschakov A, Oldfield BJ. The sensory circumventricular organs of the mammalian brain. *Adv Anat Embryol Cell Biol.* 2003; 172: III–XII, 1–122. DOI: 10.1007/978-3-642-55532-9.
2. Hicks A-I, Kobrinsky S, Zhou S, Yang J, Prager-Khoutorsky M. Anatomical organization of the rat subfornical organ. *Front Cell Neurosci.* 2021; 15: 691711. DOI: 10.3389/fncel.2021.691711.
3. Takagi S, Furube E, Nakano Y, Morita M, Miyata S. Microglia are continuously activated in the circumventricular organs of mouse brain. *J Neuroimmunol.* 2019; 331: 74–86. DOI: 10.1016/j.jneuroim.2017.10.008.
4. DosSantos MF, Devalle S, Aran V, Capra D, Roque NR, Coelho-Aguiar JdM, et al. Neuromechanisms of SARS-CoV-2: A Review *Front Neuroanat.* 2020; 14: 37. DOI: 10.3389/fnana.2020.00037.
5. Tremblay M-E, Madore C, Bordeleau M, Tian L, Verkhratsky A. Neuropathobiology of COVID-19: The Role for Glia. *Front. Cell. Neurosci.* 2020; 14: 592214. DOI: 10.3389/fncel.2020.592214.
6. Korzhevskii DE, Sukhorukova EG, Kirik OV, Grigorev IP. Immunohistochemical demonstration of specific antigens in the human brain fixed in zinc-ethanol-formaldehyde. *Eur J Histochem.* 2015; 59 (3): 2530. DOI: 10.4081/ejh.2015.2530.
7. Коржевский Д. Э., Кирик О. В., Алексеева О. С. Способ демаскирования антигенов при проведении иммуноцитохимических реакций. Патент РФ №2719163. 17.04.2020.
8. Tanaka J, Hayashi Y, Shimamune S, Nomura M. Ascending pathways from the nucleus of the solitary tract to the subfornical organ in the rat. *Brain Res.* 1997; 777: 237–41. DOI: 10.1016/S0006-8993(97)01211-0.
9. Lind RW, Swanson LW, Ganten D. Angiotensin II immunoreactivity in the neural afferents and efferents of the subfornical organ of the rat. *Brain Res.* 1984; 321: 209–15. DOI: 10.1016/0006-8993(84)90174-4.
10. Miselis RR. The subfornical organ's neural connections and their role in water balance. *Peptides.* 1982; 3: 501–2. DOI: 10.1016/0196-9781(82)90115-2.
11. Gruber K, McRae-Degueurce A, Wilkin LD, Mitchell LD, Johnson AK. Forebrain and brainstem afferents to the arcuate nucleus in the rat: potential pathways for the modulation of hypophyseal secretions. *Neurosci Lett.* 1987; 75: 1–5. DOI: 10.1016/0304-3940(87)90065-6.
12. Felix D. Peptide and acetylcholine action on neurones of the cat subfornical organ. *Naunyn Schmiedeberg's Arch Pharmacol.* 1976; 292: 15–20. DOI: 10.1007/BF00506484.
13. Mangiapane ML, Simpson JB. Drinking and pressor responses after acetylcholine injection into subfornical organ. *AJP Regul Integr Comp Physiol.* 1983; 244: R508–13. DOI: 10.1152/ajpregu.1983.244.4.
14. Li Q, Barres BA. Microglia and macrophages in brain homeostasis and disease. *Nat Rev Immunol.* 2018; 18 (4): 225–42. DOI: 10.1038/nri.2017.125.
15. Gomez Perdiguero E, Klapproth K, Schulz C, et al. Tissue-resident macrophages originate from yolk-sac-derived erythro-myeloid progenitors. *Nature.* 2015; 518: 547–51. DOI: <https://doi.org/10.1038/nature13989>
16. Hoeffel G, Chen J, Lavin Y, et al. C-Myb(+) erythro-myeloid progenitor-derived fetal monocytes give rise to adult tissue-resident macrophages. *Immunity.* 2015; 42 (4): 665–78. DOI: 10.1016/j.immuni.2015.03.011.
17. Bennett ML, Bennett FC. The influence of environment and origin on brain resident macrophages and implications for therapy. *Nat Neurosci.* 2020; 23: 157–166. Available from: <https://doi.org/10.1038/s41593-019-0545-6>
18. Prinz M, Emy D, Hagemeyer N. Ontogeny and homeostasis of CNS myeloid cells. *Nature Immunology.* 2017; 18 (4): 385–92. DOI: 10.1038/ni.3703
19. Hanisch U-K. Functional diversity of microglia — how heterogeneous are they to begin with? *Front Cell Neurosci.* 2013; 7: 65. DOI: 10.3389/fncel.2013.00065.
20. Alekseeva OS, Kirik OV, Gilerovich EG, Korzhevskii DE. Microglia of the brain: Origin, structure, functions. *J Evol Biochem Phys.* 2019; 55: 257–68. Available from: <https://doi.org/10.1134/S002209301904001X>.
21. Кирик О. В., Сухорукова Е. Г., Коржевский Д. Э. Кальций-связывающий белок Iba-1/AIF-1 в клетках головного мозга крысы. *Морфология.* 2010; 137 (2): 5–8.
22. Wijesundera KK, Izawa T, Tennakoon AH, et al. M1- and M2-macrophage polarization in rat liver cirrhosis induced by thioacetamide (TAA), focusing on Iba1 and galectin-3. *Exp Mol Pathol.* 2014; 96 (3): 382–92. DOI: 10.1016/j.yexmp.2014.04.003.
23. Kolos E, Korzhevskiy D. Spinal cord microglia in health and disease. *Acta Naturae.* 2020; 12 (1): 4–17. DOI: 10.32607/actanaturae.10934.
24. Коржевский Д. Э., Григорьев И. П., Гусельникова В. В., Колос Е. А., Петрова Е. С., Кирик О. В., и др. Иммуногистохимические маркеры для нейробиологии. *Мед Акад Журнал.* 2019; 19 (4): 7–24. DOI: 10.17816/MAJ16548.
25. Sufieva DA, Razenkova VA, Antipova MV, Korzhevskii DE. Microglia and tanycytes of the infundibular recess of the brain in early postnatal development and during aging. *Russ J Dev Biol.* 2020; 51: 189–96. Available from: <https://doi.org/10.1134/S106236042003008X>.
26. Morita S, Furube E, Mannari T, Okuda H, Tatsumi K, Wanaka A, et al. Heterogeneous vascular permeability and alternative diffusion barrier in sensory circumventricular organs of adult mouse brain. *Cell Tissue Res.* 2016; 363: 497–511. Available from: <https://doi.org/10.1007/s00441-015-2207-7>.
27. Furube E, Mannari T, Morita S, Nishikawa K, Yoshida A, Itoh M, et al. VEGF-dependent and PDGF-dependent dynamic neurovascular reconstruction in the neurohypophysis of adult mice. *J Endocrinol.* 2014; 222: 161–79. Available from: <https://doi.org/10.1038/mp.2017.246>.
28. Hourai A, Miyata S. Neurogenesis in the circumventricular organs of adult mouse brains. *J Neurosci Res.* 2013; 91: 757–70. DOI: 10.1002/jnr.23206.
29. Furube E, Morita M, Miyata S. Characterization of neural stem cells and their progeny in the sensory circumventricular organs of adult mouse. *Cell Tissue Res.* 2015; 362 (2): 347–65. DOI: 10.1007/s00441-015-2201-0.
30. Matarredona ER, Talaverón R, Pastor AM. Interactions between

- neural progenitor cells and microglia in the subventricular zone: physiological implications in the neurogenic niche and after implantation in the injured brain. *Front Cell Neurosci.* 2018; 12: 268. DOI: 10.3389/fncel.2018.00268.
31. Кирик О. В., Сухорукова Е. Г., Алексеева О. С., Коржевский Д. Э. Субэпендимные микроглиоциты III желудочка головного мозга. *Морфология.* 2014; 145 (2): 67–9.
 32. Amici SA, Dong J, Guerau-de-Arellano M. Molecular mechanisms modulating the phenotype of macrophages and microglia. *Front Immunol.* 2017; 8: 1520. DOI: 10.3389/fimmu.2017.01520.
 33. Chistiakov DA, Killingsworth MC, Myasoedova VA, Orekhov AN, Bobryshev YV. CD68/macrosialin: not just a histochemical marker. *Lab Invest.* 2017; 97 (1): 4–13. DOI: 10.1038/labinvest.2016.116.
 34. Jurga AM, Paleczna M, Kuter KZ. Overview of general and discriminating markers of differential microglia phenotypes. *Front Cell Neurosci.* 2020; 14: 198. DOI: 10.3389/fncel.2020.00198.
 35. Kirik OV, Tsyba DL, Alekseeva OS, Kolpakova ME, Jakovleva AA, Korzhevskii DE. Alterations in Kolmer cells in SHR line rats after brain ischemia. *Russian Journal of Physiology.* 2021; 107 (2): 177–86. DOI: 10.31857/S0869813921010052.
 36. Korzhevskii DE, Kirik OV, Guselnikova VV, Tsyba DL, Fedorova EA, Grigorev IP. Changes in cytoplasmic and extracellular neuromelanin in human substantia nigra with normal aging. *Eur J Histochem.* 2021; 65 (s1): 3283. DOI: 10.4081/ejh.2021.3283.

REGENERATIVE EFFECTS OF GLY-HIS-LYS AND GLY-HIS-LYS-D-ALA PEPTIDES IN INFECTED SKIN WOUNDS

Rakhmetova KK, Mishina ES, Vorvul AO, Bobyntsev II , Dolgintsev ME, Bezhin AI

Kursk State Medical University, Kursk, Russia

Skin wound healing mechanisms and new ways of improving their efficiency represent an important focus in medicine. In this regard, regulatory peptides, which exhibit physiological polyfunctionality and modulate cell growth and differentiation, are of special interest. This study evaluates the effects of Gly-His-Lys (GHK) and Gly-His-Lys-D-Ala (GHK-D-Ala) peptides in the infected skin wound healing. The wounds were modeled in rats ($n=150$) by full-thickness dorsal skin defects. The peptides were administered intracutaneously at daily doses of 0.5 or 1.5 $\mu\text{g/kg}$. The healing was assessed on days 3, 7, and 10 by histomorphometric examination of the wounds with adjacent intact skin. GHK-D-Ala administered at daily doses of 0.5 $\mu\text{g/kg}$ had pronounced positive effect on regeneration processes in the wound, as indicated by significantly reduced numbers of granulocytes and lymphocytes with increased representation of fibroblastic lineages and macrophages, and the resulting higher cellular index ($p < 0.05-0.001$). At higher doses of GHK-D-Ala (1.5 $\mu\text{g/kg}$), the beneficial effects were less pronounced. According to the comparative morphological examination, the highest positive effect was achieved with 0.5 $\mu\text{g/kg}$ of GHK-D-Ala. Thus, local administration of the GHK peptide with extra D-alanine at carboxy-terminus significantly mitigated the inflammatory reaction and facilitated the healing of infected skin wounds in rat model.

Keywords: Gly-His-Lys-D-Ala, GHK-D-Ala, infected wound, regeneration, inflammation

Author contribution: Rakhmetova KK — sample collection, concept and design of the study, data analysis and interpretation, writing of the manuscript; Mishina ES — histological and morphological examination, data analysis and interpretation; Vorvul AO — statistical processing of the data, writing of the manuscript; Bobyntsev II — concept and design of the study, scientific editing of the manuscript; Dolgintsev ME — data analysis and interpretation, writing of the manuscript; Bezhin AI — concept and design of the study.


Compliance with ethical standards: the study was approved by Ethics Committee of the Kursk State Medical University (Protocol № 1 of January 16, 2014). The study was carried out in compliance with the European Convention for the Protection of Vertebrate Animals used for Experimental and other Scientific Purposes and the Guidelines for conducting preclinical drug trials (Moscow, 2012).

✉ **Correspondence should be addressed:** Igor I. Bobyntsev
Karla Marxa, 3, Kursk, 305041, Russia; bobig@mail.ru

Received: 10.02.2022 **Accepted:** 10.03.2022 **Published online:** 13.04.2022

DOI: 10.24075/brsmu.2022.014

РЕГЕНЕРАТИВНЫЕ ЭФФЕКТЫ ПЕПТИДОВ GLY-HIS-LYS И GLY-HIS-LYS -D-ALA ПРИ КОЖНОЙ ИНФИЦИРОВАННОЙ РАНЕ

К. К. Рахметова, Е. С. Мишина, А. О. Ворвуль, И. И. Бобынцев , М. Е. Долгинцев, А. И. Бежин

Курский государственный медицинский университет, Курск

Исследование механизмов регенерации при раневом процессе и поиск новых путей повышения эффективности заживления являются одними из актуальных направлений в медицине. Поэтому представляется целесообразным изучение репаративных эффектов регуляторных пептидов, обладающих физиологической полифункциональностью и оказывающих влияние на процессы роста и дифференцировки клеток. Целью исследования было изучить влияние пептидов Gly-His-Lys (GHK) и Gly-His-Lys-D-Ala (GHK-D-Ala) на процессы регенерации в условиях инфицированной кожной раны у крыс. Рану моделировали на 150 животных путем нанесения на участке спины полнослойной раны, пептиды вводили в дозах 0,5 и 1,5 мг/кг подкожно в области раны раз в день в течение 3, 7 или 10 суток. Для оценки течения раневого процесса изучали гистологические и морфологические препараты участков раны с прилежащей интактной кожей. GHK-D-Ala в дозе 0,5 мг/кг оказывал более выраженное, чем GHK, влияние на регенеративные процессы в ране, что отразилось в значимом снижении числа гранулоцитов и лимфоцитов и повышении числа клеток фибробластического ряда, макрофагов и клеточного индекса по сравнению как с контрольной группой ($p < 0,05-0,001$), так и с животными, которым вводили GHK в эквивалентной дозе ($p < 0,05-0,001$). При увеличении дозы до 1,5 мг/кг эффекты GHK-D-Ala несколько ослабевали. По результатам сравнения исследованных показателей наибольшая активация регенеративных процессов в ране выявлена после введения GHK-D-Ala в дозе 0,5 мг/кг. Таким образом, присоединение D-аланина к С-концу пептида GHK способствовало ослаблению воспалительной реакции и усилению регенеративных процессов при местном введении в условиях инфицированной кожной раны.

Ключевые слова: Gly-His-Lys-D-Ala, GHK-D-Ala, инфицированная рана, регенерация, воспаление

Вклад авторов: К. К. Рахметова — сбор материала, разработка концепции и дизайна исследования, анализ и интерпретация данных, написание рукописи; Е. С. Мишина — проведение гистологического и морфологического исследования, анализ и интерпретация данных; А. О. Ворвуль — статистическая обработка данных, написание рукописи; И. И. Бобынцев — разработка концепции и дизайна исследования, научное редактирование рукописи; М. Е. Долгинцев — анализ и интерпретация данных, написание рукописи; А. И. Бежин — разработка концепции и дизайна исследования.

Соблюдение этических стандартов: исследование одобрено этическим комитетом Курского государственного медицинского университета (протокол № 1 от 16 января 2014 г.), проведено с соблюдением принципов Европейской конвенции по защите позвоночных животных, используемых в экспериментальных исследованиях; «Руководства по проведению доклинических исследований лекарственных средств» (Москва, 2012).

✉ **Для корреспонденции:** Игорь Иванович Бобынцев
ул. К. Маркса, д. 3, г. Курск, 305041, Россия; bobig@mail.ru

Статья получена: 10.02.2022 **Статья принята к печати:** 01.03.2022 **Опубликована онлайн:** 13.04.2022

DOI: 10.24075/vrgmu.2022.014

Regenerative mechanisms of the wound healing and new strategies for its enhancement constitute one of the topical areas in medicine. Skin repair involves all three regulatory systems of the body — nervous, endocrine, and immune [1, 2]. These systems are known to act through regulatory signaling molecules, which exhibit physiological polyfunctionality and modulate cell growth and differentiation [3].

A naturally occurring $\text{NH}_2\text{-Gly-L-His-L-Lys-COOH}$ tripeptide (Gly-His-Lys, GHK) can stimulate tissue regeneration processes [4–6] and confer antioxidant, immunotropic, anti-inflammatory, and neurotrophic effects [7–10]. The curative effect of GHK in skin wounds is significant but moderate [11], probably due to the rapid degradation of the peptide by proteolytic milieu of the wound. To overcome this limitation, we modified the structure of GHK by adding D-alanine (D-Ala) moiety to its carboxy-terminus in order to increase its resistance to proteolysis and thus reinforce its action.

The study aimed at comparative evaluation of the influence of GHK and its structural modification GHK-D-Ala on healing processes in the infected skin wounds in rat model.

METHODS

The experiments were carried out on male Wistar rats, 180–240 g body weight, aged 6–8 months, obtained from the "Stolbovaya" branch of the Scientific Center for Biomedical Technologies of the Federal Medical and Biological Agency of Russia. The animals ($n = 150$) were kept under standard conditions with ad libitum access to chow and water, at 12-h light cycle and $22 \pm 2^\circ\text{C}$. The animals were randomly assigned to 15 groups, 10 animals in each group.

The infected wound was modeled by introducing a 250 mm² full-thickness skin defect to a shaven area of the dorsum in anesthetized animals.

The study used peptides GHK and GHK-D-Ala synthesized in the Institute of Chemistry, Saint Petersburg State University. The peptides were dissolved in saline and administered intracutaneously at two points around the wound, changing the injection sites clockwise by 90° each time. The first injection made at 24 h after wound modeling was followed by repeated injections of the same medication every 24 h for 3, 7 or 10 days. The treatment groups received either 0.5 or 1.5 $\mu\text{g/kg}$ daily doses of either GHK or GHK-D-Ala; the control groups received sham injections of saline pro rata 1 mL per 1 kg body weight.

The animals were withdrawn from the experiment by puncture of the right cardiac ventricle under ether anesthesia. The healing process was assessed by histological examination of wound autopsies on days 3, 7, and 10 post-wounding. The specimens were collected by dissection of the wound area with adjacent intact skin, formalin-fixed, paraffin-embedded, and sectioned using routine techniques. The 7 μm sections were stained with hematoxylin and eosin (H & E) for light microscopy.

Morphological examination of the slides was carried out with a Nikon Eclipse Ci microscope (Nikon; Japan) equipped with a digital camera. The histological assessment accounted for the degree of inflammatory reaction, landmarks of granulation tissue development and marginal epithelization, as well as the structural maturity of the newly formed epithelium.

Morphometric assessment for the course of healing process was carried out by differential cell counts in histological slides. The cells were counted at $\times 400$ magnification of a representative area beneath the leukocyte-fibrinous scab to a total of 100 cells, and the shares of particular cell populations (fibroblastic lineages, macrophages, granulocytes, and lymphocytes) were expressed as percentages.

A quantitative index for the extent of healing and regeneration phase was calculated as follows:

$$\text{CI} = \frac{\text{Fb} + \text{M}}{\text{Gr} + \text{L}} \times 100\%,$$

where CI stands for "cellular index" derived from differential cell counts including Fb — fibroblast lineages (prefibroblasts, fibroblasts, and fibrocytes), M — macrophages, Gr — granulocytes (neutrophils, eosinophils, and basophils), and L — lymphocytes. At $\text{CI} > 100\%$, regeneration processes are considered dominant, whereas at $\text{CI} < 100$ inflammatory processes are considered dominant.

Statistical processing of the data was carried out in R v.4.1.0 [12] using the RStudio Desktop v. 1.4.1717 integrated development environment (RStudio, PBC; USA). The initial processing involved Shapiro–Wilk test for normality (shapiro.test() function of the R base package) and Levene's test for equality of variances (levene.test() function of the lawstat package). Subsequent two-group comparisons used one-way ANOVA (aov() function of the R base package) with a post hoc Dunnett test (DunnettTest() function of the DescTools package); the data are presented as means and standard deviations ($M \pm \text{SD}$) calculated using mean() and sd() functions of the R base package. Multiple comparisons used Kruskal–Wallis test (kruskal.test() function of the R base package) with a post hoc Dunn's test (dunn.test() function of the dunn.test package); the data are presented in the median [lower quartile; upper quartile] format (Me [1Q; 3Q]), calculated using median() and quantile() functions of the R base package. The differences were considered significant at $p < 0.05$.

RESULTS

The results of histological examination of skin defects on day 3 post-wounding were similar in all groups. The defect was filled with polymorphocellular infiltrate showing a predominance of leukocytes beneath the clearly distinguished superficial leukocyte-necrotic layer. The boundary with the intact dermis had signs of edema: sparse "empty" vessels with expanded lumina and thinned walls, and swollen fibers forming a network growing denser towards the leukocyte-necrotic layer.

On day 7 post-wounding, skin defects in the control group had the leukocyte-necrotic layer non-ubiquitously demarcated from the infiltration zone. The deeper layers presented with initial stages of the granulation tissue histogenesis, with cellular composition dominated by neutrophils, histiocytes, and lymphocytes. With the use of 0.5 $\mu\text{g/kg}$ doses of either GHK or GHK-D-Ala, the leukocyte-necrotic layer was preserved, although non-ubiquitously, and was significantly reduced compared with the control. The discontinuities of the leukocyte-necrotic layer showed fibrin deposits clearly demarcated from the infiltration zone. The underlying young connective (granulation) tissue contained the fully perfused dilated rounded capillaries. The signs of edema included the moderately thinned capillary endothelium and prominent interstructural spaces. Cellular composition of the granulation tissue was dominated by macrophages, fibroblasts and lymphocytes. With 1.5 $\mu\text{g/kg}$ doses of either GHK or GHK-D-Ala, the signs of edema were reduced and the leukocyte-necrotic scab was fragmentary. Formation of the granulation tissue and a network of thin collagen fibers were observed in the wound area, accompanied by round-cell infiltration. In addition, the higher-dose groups presented with the onset of wound epithelization at the boundaries with intact skin, in the form of marginal epidermal thickening with preserved stratification.

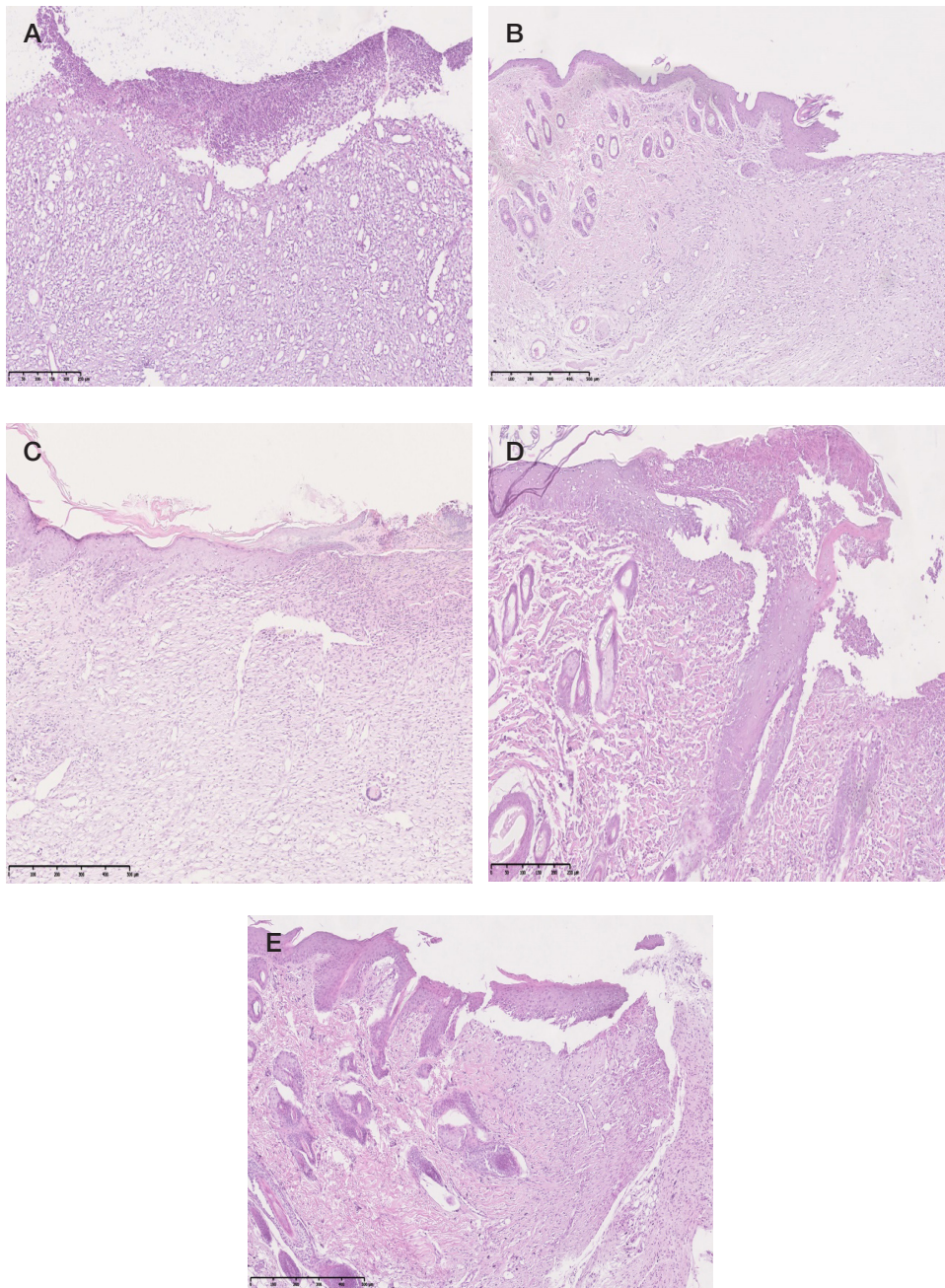


Fig. 1. Microphotographs of the skin wound area on day 10 post-wounding (H & E, magnification $\times 40$). **A.** Control. **B.** GHK peptide, 0.5 $\mu\text{g/kg}$ daily. **C.** GHK-D-Ala peptide, 0.5 $\mu\text{g/kg}$ daily. **D.** GHK peptide, 1.5 $\mu\text{g/kg}$ daily. **E.** GHK-D-Ala peptide, 1.5 $\mu\text{g/kg}$ daily

On day 10 post-wounding, the control group continued to present with inflammatory reactions. In deeper layers of the wound, connective tissue acquired a more mature appearance in terms of cell types and fibrous patterns. Amid the persisting mild lymphocyte infiltration, a fully-formed mature connective tissue appeared above the hypodermis. The boundary of the defect with adjacent intact skin exhibited a thickening of the basal epidermal layer and a major portion of the wound was coated in detritus (Fig. 1A).

In the 0.5 $\mu\text{g/kg}$ GHK group on day 10 post-wounding, the leukocyte-necrotic layer was observed in the central portion of the wound only. The underlying young granulation tissue showed rounded dilated capillaries, as well as less perfused vertical capillaries. The fibers were more mature than in the control. The low degree of edema and mild polymorphous infiltration persisted amid the predominance of fibroblast lineages. The deeper layers presented with fully-formed mature

connective tissue. The adjacent intact skin at the immediate boundary with defect had thickened epidermal layers and showed marginal expansion of the newly formed epithelium with irregular stratification (Fig. 1B).

In the 0.5 $\mu\text{g/kg}$ GHK-D-Ala group on day 10 post-wounding, the leukocyte-necrotic layer was missing. The underlying young connective tissue with underperfused rounded dilated capillaries showed visual predominance of fibroblast lineages and noticeable expansion of the epithelial flap over its surface. The epithelium showed regular structure except in the corneal layer. The scale of epithelial growth matched the size of the defect, with full epithelization observed in certain sections. The dermis of intact skin around the wound retained the signs of edema albeit less prominent than in the control (Fig. 1C).

In the 1.5 $\mu\text{g/kg}$ GHK group on day 10 post-wounding, the leukocyte-necrotic layer was preserved albeit significantly reduced in size and frequently shed off during histological

Table. Dynamics of morphometric indicators upon injections of Gly-His-Lys-D-Ala peptide ($M \pm SD / Me [1Q; 3Q]$, $n = 10$) assessed by histological examination on days 3, 7, and 10 post-wounding

Indicator	Group	Time point		
		Day 3	Day 7	Day 10
Fibroblast lineages, %	Control	15.9 \pm 2.47	15.9 \pm 3.54	20.6 \pm 6.67
	GHK 0,5 μ g/kg	9.5 \pm 3.31***	15.2 \pm 1.55	22.5 \pm 3.50
	GHK-D-Ala 0,5 μ g/kg	17.00 \pm 2.49###	43.20 \pm 4.44***.###	34.80 \pm 1.93***.#
	GHK 1,5 μ g/kg	11.7 \pm 1.77**	22.50 [20.50; 23.00]***	34.8 \pm 1.93***
	GHK-D-Ala 1,5 μ g/kg	12.1 \pm 3.60**	20.5 \pm 1.43**	30.1 \pm 3.38***.\$\$\$
Macrophages, %	Control	13.3 \pm 3.97	17.6 \pm 3.06	16.5 \pm 8.18
	GHK 0,5 μ g/kg	20.7 \pm 4.57**	24.4 \pm 3.12***	19.4 \pm 3.86
	GHK-D-Ala 0,5 μ g/kg	34.60 \pm 3.10***.###	23.30 \pm 4.57**	33.90 \pm 3.14***.##
	GHK 1,5 μ g/kg	27.1 \pm 7.03***	34.3 \pm 3.09***	54.2 \pm 4.52***
	GHK-D-Ala 1,5 μ g/kg	21.4 \pm 5.68***	23.9 \pm 4.20**.\$	26.4 \pm 3.17***.\$\$\$
Granulocytes, %	Control	55 \pm 3.50	36.2 \pm 2.30	20.2 \pm 5.85
	GHK 0,5 μ g/kg	46.5 \pm 2.22***	36.50 [36.00; 37.75]	28.1 \pm 1.20***
	GHK-D-Ala 0,5 μ g/kg	13.00 [12.00; 14.00]***.###	13.50 [11.25; 17.50]***.###	4.00 [3.00; 5.00]***.#
	GHK 1,5 μ g/kg	18.2 \pm 2.53***	23.50 [22.25; 24.75]***	15.5 \pm 5.23*
	GHK-D-Ala 1,5 μ g/kg	44.00 \pm 3.65***.\$\$\$	24.2 \pm 2.30***	18.4 \pm 1.71
Lymphocytes, %	Control	15.8 \pm 4.76	30.3 \pm 4.06	42.7 \pm 8.07
	GHK 0,5 μ g/kg	23.3 \pm 1.25***	24.50 [24.00; 26.00]**	30 \pm 3.94
	GHK-D-Ala 0,5 μ g/kg	35.00 [34.25; 36.75]***.#	18.40 \pm 3.41***.##	27.70 \pm 4.47***
	GHK 1,5 μ g/kg	43.0 \pm 5.10***	21.4 \pm 4.58***	19.9 \pm 4.46***
	GHK-D-Ala 1,5 μ g/kg	22.5 \pm 2.46***.\$\$\$	31.4 \pm 3.10\$\$\$	25.5 [25.00; 26.75]***
Cellular index, %	Control	37.9 [35.6; 44.9]	51.0 \pm 10.35	61.2 \pm 20.92
	GHK 0,5 μ g/kg	43.4 \pm 4.69	63.9 [58.7; 68.8]**	72.9 \pm 12.14
	GHK-D-Ala 0,5 μ g/kg	108.33 [104.08; 112.77]***.###	206.7 \pm 54.09***.###	225.6 \pm 46.76***.###
	GHK 1,5 μ g/kg	65.0 \pm 17.35***	128.31 \pm 20.26***	184.89 \pm 28.27***
	GHK-D-Ala 1,5 μ g/kg	51.1 \pm 10.68*	80.7 \pm 12.88***	130.1 \pm 8.71***.\$

Note: * — $p < 0.05$; ** — $p < 0.01$; *** — $p < 0.001$ compared with the control group; # — $p < 0.05$; ## — $p < 0.01$; ### — $p < 0.001$ compared with the GHK 0.5 μ g/kg group; \$ — $p < 0.05$; \$\$ — $p < 0.01$; \$\$\$ — $p < 0.001$ compared with the GHK 1.5 μ g/kg group

processing; the exposed regions presented with distinct fibrin deposits. The underlying young connective tissue was rich in underperfused rounded dilated capillaries. The epithelial flap outgrowth followed the boundary between the leukocyte-necrotic layer and the young connective tissue. The epithelium showed regular structure except in the corneal layer. The scale of epithelial growth matched the size of the defect, with full epithelization observed in certain sections. Beneath the epithelial outgrowth, the granulation tissue was structurally similar to the typical connective tissue of the dermis (Fig. 1D).

In the 1.5 μ g/kg GHK-D-Ala group on day 10 post-wounding, the leukocyte-necrotic layer was fragmentary. The boundary with adjacent intact skin exhibited a thickening of the basal and granular epidermal layers. The epithelial flap outgrowth followed the boundary between the leukocyte-necrotic layer and the underlying young connective tissue, exceeding the dimensions of outgrowth observed in the control group. The epithelium showed regular structure (except the most distal regions). The dermis retained the signs of edema albeit less prominent than in the control (Fig. 1E).

The observed progression of the inflammatory reactions to regenerative phase was confirmed by morphometric study (Table). Granulocyte counts for 0.5 μ g/kg GHK-D-Ala at all time points were significantly lower compared with both the control (3–5-fold; $p < 0.05$ –0.001) and 0.5 μ g/kg GHK (3.5–7-fold; $p < 0.05$ –0.001), consistently with the milder secondary alterations in the wound area and the enhanced regeneration efficiency achieved with 0.5 μ g/kg GHK-D-Ala. For 1.5 μ g/kg doses, the trends were similar albeit with reduced difference between the peptides. Overall, granulocyte counts in all GHK/GHK-D-Ala groups were significantly lower than in the corresponding control groups at all time points of the experiment.

Macrophage counts for 0.5 μ g/kg GHK-D-Ala were significantly higher compared with the corresponding control groups at all time points ($p < 0.05$ –0.001) and compared with 0.5 μ g/kg GHK groups on days 3 and 10 ($p < 0.05$). The 1.5 μ g/kg doses of both peptides significantly increased the macrophage counts at all time points compared with the control ($p < 0.05$ –0.001) with somewhat more pronounced effects observed for GHK.

Migration of fibroblast lineages to the site of injury, thought to reflect the induction of regeneration processes, was most pronounced for 0.5 µg/kg GHK-D-Ala at all time points of the experiment compared with both the controls and corresponding doses of GHK. The use of 1.5 µg/kg doses of the peptides had similar effects on fibroblast counts ($p < 0.05$ – 0.01) without significant differences between GHK-D-Ala and GHK ($p > 0.05$).

The dynamics of lymphocyte counts in the course of the experiment was generally consistent with the timing of transition from the inflammatory reaction to regenerative phase (for other cell types, the transition was detectable as well). Administration of GHK-D-Ala at 0.5 µg/kg significantly increased the lymphocyte counts compared with both groups of comparison on day 3 ($p < 0.05$ – 0.001), whereas on days 7 and 10 the effect was reverse. On the other hand, administration of GHK at 1.5 µg/kg significantly influenced the lymphocyte counts at all time points ($p < 0.05$ – 0.001 compared with the control), while the effects of GHK-D-Ala were less pronounced.

According to the calculated cellular index, the most pronounced effects at all time points of observation were achieved with daily injections of GHK-D-Ala at 0.5 µg/kg doses ($p < 0.05$ – 0.001). The use of GHK at this dose had no significant impact on regeneration ($p > 0.05$). Of note, daily injections of GHK at 1.5 µg/kg doses afforded a more robust regenerative response on days 7 and 10 post-wounding and a more pronounced overall effect compared with 1.5 µg/kg doses of GHK-D-Ala.

Thus, intracutaneous administration of GHK-D-Ala at daily doses of 0.5 µg/kg provided maximal regeneration benefits, exceeding those achieved with similar doses of GHK. Increased doses of the peptides (1.5 µg/kg) leveled the difference by reducing the positive effects of GHK-D-Ala and enhancing the positive effects of GHK. Overall, the highest morphometric indicators of regeneration processes in this study were obtained with 0.5 µg/kg of GHK-D-Ala.

DISCUSSION

The results indicate enhanced regeneration and decreased inflammatory response in the infected skin wounds treated with GHK peptide reinforced by chemical addition of D-alanine to its carboxy-terminus. The beneficial effects of GHK are well known and multiple hypotheses on their mechanisms can be found in the literature. For instance, GHK has been considered as a transport molecule for Cu^{2+} cations essential for the completion of phagocytosis, which ensures the effective physiological debriding and proper healing of the wound. In particular, it has been demonstrated that Cu^{2+} binds the amino-terminus of GHK through interactions with glycine and histidine [13]. Our study features a structural modification of the GHK tripeptide, which leaves the amino-terminus intact; accordingly, the Cu^{2+} cations can interact with the specified amino acids, rendering GHK capable of its role in cation transfer. Besides, GHK has been implicated as a mediator molecule orchestrating the positioning of cells within extracellular architecture of the dermis, facilitating cell motility and stimulating the production

of signaling and structural molecules including certain growth factors and decorin [4, 14].

The higher degree of healing benefits attributed to the structurally modified tripeptide molecule may be explained by its increased resistance to the degrading action of carboxypeptidases. Our data are consistent with the reported impact of GHK-D-Ala on the phagocytic activity of granulocytes and lipid peroxidation processes in the infected skin wounds in rats [15]. The curative activity of GHK observed by us in this study corresponds to the expectations based on published evidence [11].

Comparative analysis between different studies should take into account the routes of administration. The peptides are administered locally in order to make them available to cells at the site of injury. However, the peptides may enter systemic circulation and influence other organs and systems of the body. In particular, when administered intraperitoneally at comparable doses, GHK exerts an analgesic and anxiolytic effect, which may contribute to the reduction of the stress response and increase the regenerative potential by modulating the cutaneous neuroimmune interactions [2]. However, the chemical addition of D-alanine to the carboxy-terminus of GHK has been shown to neutralize such effects [16, 17]. In this regard, it can be assumed that the enhanced pro-regenerative efficacy of GHK-D-Ala observed by us in this study is not directly related to the neurotrophic effects described for GHK.

The conserved direction of the pro-regenerative and anti-inflammatory effects described for GHK upon administration of GHK-D-Ala are indicative of the common mechanisms. For instance, apart from the aforementioned findings, GHK has been shown to stimulate the expression of vascular endothelial growth factor (VEGF) and fibroblast growth factor 2 (FGF2) [18]. In addition, the unmodified tripeptide improves the rates of skin wound healing and stimulates skin renewal by stimulating the release of growth factors from platelet granules (notably of the transforming growth factor β , TGF β), which promote the recruitment of immune cells to the site of injury [19]. Besides, GHK inhibits the production of pro-inflammatory cytokines, including tumor necrosis factor — (TNF α) and interleukin 6 (IL6), by fibroblasts, which leads to a decrease in cutaneous inflammatory reactions and prevents the formation of hypertrophic scars [20].

CONCLUSIONS

The study shows that modification of GHK peptide through addition of D-alanine at carboxy-terminus may increase its curative effect in infected skin wounds. The modified peptide administered at daily doses of 0.5 or 1.5 µg/kg successfully stimulated tissue repair and alleviated the inflammatory response on days 3, 7, and 10 post-wounding in rat model. The GHK-D-Ala peptide facilitated an increase in fibroblast and macrophage counts accompanied by a decrease in granulocyte and lymphocyte counts. The results highlight the use of structural modifications of GHK peptide to potentiate its efficiency in skin wound healing. Further efforts will be required to elucidate its mechanisms and the role of peptide regulation in regenerative processes.

References

1. Bashkina OA, Samotruyeva MA, Azhikova AK, Paknova LR. Neuroimmunoendocrine regulation of the skin functioning. *Meditinskaya Immunologiya*. 2019; 21 (5): 807–20. DOI: 10.15789/1563-0625-2019-5-807-820. Russian.
2. Makarevich PI, Efimenko AY, Tkachuk VA Biochemical regulation of regenerative processes by growth factors and cytokines: basic mechanisms and relevance for regenerative medicine. *Biochemistry (Moscow)*. 2020; 85 (1): 11–26. DOI: 10.1134/S0006297920010022. PubMed PMID: 32079514.
3. Khavinson VKh. Peptide medicines: past, present, future. *Clinical Medicine (Russian Journal)*. 2020; 98 (3): 165–177. DOI: 10.30629/0023-2149-2020-98-3-165-177. Russian.
4. Siméon A, Wegrowski Y, Bontemps Y, Maquart FX. Expression of glycosaminoglycans and small proteoglycans in wounds: modulation by the tripeptide-copper complex glycyl-L-histidyl-L-lysine-Cu(2+). *J Invest Dermatol*. 2000; 115 (6): 962–8. DOI: 10.1046/j.1523-1747.2000.00166.x. PubMed PMID: 11121126.
5. Pickart L, Margolina A. Regenerative and Protective Actions of the GHK-Cu Peptide in the Light of the New Gene Data. *Int J Mol Sci*. 2018; 19 (7): 1987. DOI: 10.3390/ijms19071987. PubMed PMID: 29986520.
6. Pickart L, Vasquez-Soltero JM, Margolina A. GHK Peptide as a Natural Modulator of Multiple Cellular Pathways in Skin Regeneration. *Biomed Res Int*. 2015; 2015: 648108. DOI: 10.1155/2015/648108. PubMed PMID: 26236730.
7. Ahmed MR, Basha SH, Gopinath D, Muthusamy R, Jayakumar R. Initial upregulation of growth factors and inflammatory mediators during nerve regeneration in the presence of cell adhesive peptide-incorporated collagen tubes. *J Peripher Nerv Syst*. 2005; 10 (1): 17–30. DOI: 10.1111/j.1085-9489.2005.10105.x. PubMed PMID: 15703015.
8. Mazurowska L, Mojski M. Biological activities of selected peptides: skin penetration ability of copper complexes with peptides. *J Cosmet Sci*. 2008; 59 (1): 59–69. PubMed PMID: 18350235.
9. Pickart L, Vasquez-Soltero JM, Margolina A. The human tripeptide GHK-Cu in prevention of oxidative stress and degenerative conditions of aging: implications for cognitive health. *Oxid Med Cell Longev*. 2012; 2012: 324832. DOI: 10.1155/2012/324832. PubMed PMID: 22666519.
10. Siméon A, Emonard H, Hornebeck W, Maquart FX. The tripeptide-copper complex glycyl-L-histidyl-L-lysine-Cu²⁺ stimulates matrix metalloproteinase-2 expression by fibroblast cultures. *Life Sci*. 2000; 67 (18): 2257–65. DOI: 10.1016/S0024-3205(00)00803-1. PubMed PMID: 11045606.
11. Kurtseva AA, Smakhtin MYu, Ivanov AV, Besedin AV, Cherdakov VYu. The effects of Gly-His-Lys peptide on neutrophil functions and its regenerative activity in skin wounds. *Kursk scientific and practical bulletin "Man and his health"*. 2008; (1): 36–40. Russian.
12. R Core Team. R: A language and environment for statistical computing. R Foundation for Statistical Computing, Vienna, Austria. 2020. Available from: <https://www.R-project.org/>.
13. Pickart L, Vasquez-Soltero JM, Margolina A. GHK-Cu may Prevent Oxidative Stress in Skin by Regulating Copper and Modifying Expression of Numerous Antioxidant Genes. *Cosmetics*. 2015; 2 (3): 236–47. DOI: 10.3390/cosmetics2030236.
14. McCormack MC, Nowak KC, Koch RJ. The effect of copper peptide and tretinoin on growth factor production in a serum-free fibroblast model. *Arch Facial Plast Surg*. 2001; 3 (1): 28–32. PubMed PMID: 11176716.
15. Rakhmetova KK, Dolgintsev ME, Bobyntsev II, Bezgin AI, Vorul AO, Belykh AE. Effect of GHK-D-Ala peptide on innate immunity mechanisms and lipid peroxidation processes in infected wounds. *Humans and their Health*. 2021; 24 (1): 54–61. DOI: 10.21626/vestnik/2021-1/07. Russian.
16. Bobyntsev II, Chernysheva OI, Dolgintsev ME, Smakhtin MY, Belykh AE. Anxiolytic effects of Gly-His-Lys peptide and its analogs. *Bull Exp Biol Med*. 2015; 158 (6): 726–8. DOI: 10.1007/s10517-015-2847-3. PubMed PMID: 25900608.
17. Bobyntsev II, Chernysheva OI, Dolgintsev ME, Smakhtin MY, Belykh AE. Effect of Gly-His-Lys peptide and its analogs on pain sensitivity in mice. *Eksper. i klin. farmakol*. 2015; 78 (1): 13–15. DOI: 10.30906/0869-2092-2015-78-1-13-15. Russian.
18. Wang X, Liu B, Xu Q, Sun H, Shi M, Wang D et al. GHK-Cu-liposomes accelerate scald wound healing in mice by promoting cell proliferation and angiogenesis. *Wound Repair Regen*. 2017; 25 (2): 270–8. DOI: 10.1111/wrr.12520. PubMed PMID: 28370978.
19. Gruchlik A, Chodurek E, Dzierzewicz Z. Effect of Gly-His-Lys and its copper complex on TGF- β secretion in normal human dermal fibroblasts. *Acta Pol Pharm*. 2014; 71 (6): 954–8. PubMed PMID: 25745767.
20. Gruchlik A, Jurzak M, Chodurek E, Dzierzewicz Z. Effect of Gly-His-Lys, Gly-His-Lys and their copper complexes on TNF- α -dependent IL-6 secretion in normal human dermal fibroblasts. *Acta Pol Pharm*. 2012; 69 (6): 1303–6. PubMed PMID: 23285694.

Литература

1. Башкина О. А., Самотруева М. А., Ажигова А. К., Пахнова Л. Р. Нейроиммуноэндокринная регуляция физиологических и патофизиологических процессов в коже. *Медицинская иммунология*. 2019; 21 (5): 807–20. DOI: 10.15789/1563-0625-2019-5-807-820.
2. Makarevich PI, Efimenko AY, Tkachuk VA Biochemical regulation of regenerative processes by growth factors and cytokines: basic mechanisms and relevance for regenerative medicine. *Biochemistry (Moscow)*. 2020; 85 (1): 11–26. DOI: 10.1134/S0006297920010022. PubMed PMID: 32079514.
3. Хавинсон В. Х. Лекарственные пептидные препараты: прошлое, настоящее, будущее. *Клиническая медицина*. 2020; 98 (3): 165–77. DOI: 10.30629/0023-2149-2020-98-3-165-177.
4. Siméon A, Wegrowski Y, Bontemps Y, Maquart FX. Expression of glycosaminoglycans and small proteoglycans in wounds: modulation by the tripeptide-copper complex glycyl-L-histidyl-L-lysine-Cu(2+). *J Invest Dermatol*. 2000; 115 (6): 962–8. DOI: 10.1046/j.1523-1747.2000.00166.x. PubMed PMID: 11121126.
5. Pickart L, Margolina A. Regenerative and Protective Actions of the GHK-Cu Peptide in the Light of the New Gene Data. *Int J Mol Sci*. 2018; 19 (7): 1987. DOI: 10.3390/ijms19071987. PubMed PMID: 29986520.
6. Pickart L, Vasquez-Soltero JM, Margolina A. GHK Peptide as a Natural Modulator of Multiple Cellular Pathways in Skin Regeneration. *Biomed Res Int*. 2015; 2015: 648108. DOI: 10.1155/2015/648108. PubMed PMID: 26236730.
7. Ahmed MR, Basha SH, Gopinath D, Muthusamy R, Jayakumar R. Initial upregulation of growth factors and inflammatory mediators during nerve regeneration in the presence of cell adhesive peptide-incorporated collagen tubes. *J Peripher Nerv Syst*. 2005; 10 (1): 17–30. DOI: 10.1111/j.1085-9489.2005.10105.x. PubMed PMID: 15703015.
8. Mazurowska L, Mojski M. Biological activities of selected peptides: skin penetration ability of copper complexes with peptides. *J Cosmet Sci*. 2008; 59 (1): 59–69. PubMed PMID: 18350235.
9. Pickart L, Vasquez-Soltero JM, Margolina A. The human tripeptide GHK-Cu in prevention of oxidative stress and degenerative conditions of aging: implications for cognitive health. *Oxid Med Cell Longev*. 2012; 2012: 324832. DOI: 10.1155/2012/324832. PubMed PMID: 22666519.
10. Siméon A, Emonard H, Hornebeck W, Maquart FX. The tripeptide-copper complex glycyl-L-histidyl-L-lysine-Cu²⁺ stimulates matrix metalloproteinase-2 expression by fibroblast cultures. *Life Sci*. 2000; 67 (18): 2257–65. DOI: 10.1016/S0024-3205(00)00803-1. PubMed PMID: 11045606.
11. Курцева А. А., Смахтин М. Ю., Иванов А. В., Беседин А. В.,

- Чердаков В. Ю. Репаративная и иммуностропная активность пептида gly-his-lys в условиях кожных ран. Курский научно-практический вестник «Человек и его здоровье». 2008; (1): 36–40.
12. R Core Team. R: A language and environment for statistical computing. R Foundation for Statistical Computing, Vienna, Austria. 2020. Available from: <https://www.R-project.org/>.
 13. Pickart L, Vasquez-Soltero JM, Margolina A. GHK-Cu may Prevent Oxidative Stress in Skin by Regulating Copper and Modifying Expression of Numerous Antioxidant Genes. *Cosmetics*. 2015; 2 (3): 236–47. DOI: 10.3390/cosmetics2030236.
 14. McCormack MC, Nowak KC, Koch RJ. The effect of copper peptide and tretinoin on growth factor production in a serum-free fibroblast model. *Arch Facial Plast Surg*. 2001; 3 (1): 28–32. PubMed PMID: 11176716.
 15. Рахметова К. К., Долгинцев М. Е., Бобынцев И. И., Бежин А. И., Ворвуль А. О., Белых А. Е. Влияние пептида GHK-D-Ala на механизмы врожденного иммунитета и процессы перекисного окисления липидов в условиях инфицированной раны. *Человек и его здоровье*. 2021; 24 (1): 54–61. DOI: 10.21626/vestnik/2021-1/07.
 16. Bobyntsev II, Chernysheva OI, Dolgintsev ME, Smakhtin MY, Belykh AE. Anxiolytic effects of Gly-His-Lys peptide and its analogs. *Bull Exp Biol Med*. 2015; 158 (6): 726–8. DOI: 10.1007/s10517-015-2847-3. PubMed PMID: 25900608.
 17. Бобынцев И. И., Чернышёва О. И., Долгинцев М. Е., Смахтин М. Ю., Белых А.Е. Влияние пептида Gly-His-Lys и его аналогов на болевую чувствительность у мышей. *Экспер. и клин. фармакол*. 2015; 78 (1): 13–15. DOI: 10.30906/0869-2092-2015-78-1-13-15.
 18. Wang X, Liu B, Xu Q, Sun H, Shi M, Wang D et al. GHK-Cu-liposomes accelerate scald wound healing in mice by promoting cell proliferation and angiogenesis. *Wound Repair Regen*. 2017; 25 (2): 270–8. DOI: 10.1111/wrr.12520. PubMed PMID: 28370978.
 19. Gruchlik A, Chodurek E, Dzierzewicz Z. Effect of Gly-His-Lys and its copper complex on TGF- β secretion in normal human dermal fibroblasts. *Acta Pol Pharm*. 2014; 71 (6): 954–8. PubMed PMID: 25745767.
 20. Gruchlik A, Jurzak M, Chodurek E, Dzierzewicz Z. Effect of Gly-Gly-His, Gly-His-Lys and their copper complexes on TNF-alpha-dependent IL-6 secretion in normal human dermal fibroblasts. *Acta Pol Pharm*. 2012; 69 (6): 1303–6. PubMed PMID: 23285694.

SPECIFIC FEATURES OF MEMORY CONSOLIDATION AND RECONSOLIDATION IN OLDER INDIVIDUALS WITH VISION AND HEARING IMPAIRMENTS

Zakharova IA¹, Petrash EA¹✉, Nikishina VB¹, Razuvaeva TN², Shuteeva TV³

¹ Pirogov Russian National Research Medical University, Moscow, Russia

² Belgorod State National Research University, Belgorod, Russia

³ Kursk State Medical University, Kursk, Russia

Sensory impairments (visual and auditory) reduce quantity and quality of the information input. The associated memory loss can be classified as intrinsic decline in memory functionalities or mere physiological effect of sensory deprivation. This study aimed to specify this issue by analyzing memory consolidation and reconsolidation processes in older people with sensory deficits. The study enrolled 65–75 year-old individuals ($n = 61$) distributed into four groups: patients with unilateral sensorineural hearing loss ($n = 17$); patients with bilateral sensorineural hearing loss ($n = 14$); patients with visual impairment ($n = 19$); and patients with combined sensory deficits ($n = 11$). The methods included Luria's auditory-verbal ("10 words") and visual memory tests and Bartlett's experimental procedure. A decrease in memory volume for auditory-verbal and visual-figurative short-term memories was observed in all groups. The results reveal significant adverse dynamics of qualitative and quantitative indicators for memory consolidation and reconsolidation processes, associated with decreased volume of short-term memories, both auditory-verbal and visual-figurative. Based on these findings, we conclude that consolidation and reconsolidation efficiency depends on proper accommodation of the newly incoming information to already memorized modules (previous experience) and requires dosing of the newly incoming information in order to preserve its integrity at the stage of consolidation.

Keywords: visual-figurative memory, semantic memory, memory consolidation, memory reconsolidation, sensory impairments, old age

Author contribution: Zakharova IA, Shuteeva TV — empirical research and collection of primary data; Petrash EA — quantitative and qualitative data processing, interpretation and generalization of the results; Nikishina VB, Razuvaeva TN — research concept development, interpretation and generalization of the results.

Compliance with ethical standards: the study was approved by Ethical Review Board at the Pirogov Russian National Research Medical University (Protocol № 207 of April 19, 2021). All participants provided written informed consent for the study.

✉ **Correspondence should be addressed:** Ekaterina A. Petrash
Ostrovityanova, 1, Moscow, 117997, Russia; petrash@mail.ru

Received: 22.03.2022 **Accepted:** 14.04.2022 **Published online:** 28.04.2022

DOI: 10.24075/brsmu.2022.018

ОСОБЕННОСТИ ПРОЦЕССОВ КОНСОЛИДАЦИИ И РЕКОНСОЛИДАЦИИ ПАМЯТИ ПРИ ЗРИТЕЛЬНЫХ И СЛУХОВЫХ НАРУШЕНИЯХ В ПОЖИЛОМ ВОЗРАСТЕ

И. А. Захарова¹, Е. А. Петраш¹✉, В. Б. Никишина¹, Т. Н. Разуваева², Т. В. Шутеева³

¹ Российский национальный исследовательский медицинский университет имени Н. И. Пирогова, Москва, Россия

² Белгородский государственный национальный исследовательский университет, Белгород, Россия

³ Курский государственный медицинский университет, Курск, Россия

Сенсорные нарушения (зрительные, слуховые) ограничивают количество и качество поступающей информации. При этом существенные затруднения вызывает решения вопроса о том, что выявленное нарушение памяти является собственно нарушением памяти или обусловлено сенсорными дефицитами. В связи с поиском ответа на поставленный вопрос нами была сформулирована цель исследования. Целью исследования было изучить процессы консолидации и реконсолидации памяти у лиц пожилого возраста с сенсорными нарушениями. В исследовании участвовали пациенты в возрасте 65–75 лет ($n = 61$), разбитые на четыре группы: пациенты с односторонней нейросенсорной тугоухостью ($n = 17$); пациенты с двусторонней нейросенсорной тугоухостью ($n = 14$); пациенты с нарушением зрения ($n = 19$); пациенты с сочетанным сенсорным дефицитом ($n = 11$). В качестве методов использовали методики А. Р. Лурия «10 слов» и «Зрительная память», а также экспериментальную процедуру, предложенную Ф. Бартлеттом. Установлено снижение объема кратковременной слухоречевой и зрительно-образной памяти по всем группам испытуемых у пациентов пожилого возраста с сенсорными нарушениями. Достоверно показано изменение качественно-количественных характеристик процессов консолидации и реконсолидации памяти при сенсорных нарушениях. Данное изменение обусловлено снижением объема кратковременной памяти (как слухоречевой, так и зрительно-образной). Сделан вывод, что важными условиями повышения эффективности процессов консолидации и реконсолидации являются необходимость «подстройки» вновь поступающей информации к уже имеющейся в памяти (предшествующем опыту), а также необходимость дозированного снижения объема вновь поступающей информации с целью сохранения ее целостности на этапе консолидации.

Ключевые слова: зрительно-образная память, семантическая память, консолидация памяти, реконсолидация памяти, сенсорные нарушения, пожилой возраст

Вклад авторов: И. А. Захарова, Т. В. Шутеева — проведение исследования, сбор первичного эмпирического материала; Е. А. Петраш — количественная и качественная обработка полученного эмпирического материала, интерпретация и обобщение результатов исследования; В. Б. Никишина, Т. Н. Разуваева — формирование концепции исследования, интерпретация и обобщение полученного эмпирического материала.

Соблюдение этических стандартов: исследование одобрено этическим комитетом РНИМУ им. Н. И. Пирогова (протокол № 207 от 19 апреля 2021 г.); все участники подписали информированное согласие на обследование.

✉ **Для корреспонденции:** Екатерина Анатольевна Петраш
ул. Островитянова, д. 1, г. Москва, 117997, Россия; petrash@mail.ru

Статья получена: 22.03.2022 **Статья принята к печати:** 14.04.2022 **Опубликована онлайн:** 28.04.2022

DOI: 10.24075/vrgmu.2022.018

The integration of subjective content of the mind and our picture of the world is provided by systemic diversity of memory types and processes. The age-related alterations in memory functionalities result from accumulation of neural and non-neural impairments.

A number of studies emphasize the relationship of sensory and cognitive impairments in older individuals [1–8].

In particular, some experts associate characteristic memory loss with age-related hearing impairment in older people [5]. One hypothesis attributes the effect to progressive social isolation in connection with the hearing loss. The Wisconsin Longitudinal Study (WLS) participants reported hearing problems with concomitantly reduced engagement in several types of social activity. The self-perceived hearing impairment was related to substantial decline in memory function. The authors further demonstrate that self-reported hearing loss and social isolation represent independent risk factors for memory loss in older people [5].

Memory, from the perspective of processes and types of its implementation and functioning, provides an important compensatory resource for a number of disorders, regardless of age.

A relationship has been established between subjective age-related hearing loss (SARHL) and the functioning of episodic memory [6]. The data indicate that self-perceived hearing loss may have an indirect effect on episodic memory through its negative impact on weekly social activity. The dysfunctional hearing narrows the scope of social interactions and communication, which may negatively affect cognitive performance.

The age-related hearing loss, which affects the ability to hear high frequencies, eventually leads to major difficulties in perception of sounds and speech comprehension, especially under non-optimal listening conditions [7]. The hearing loss can be partly compensated by the use of executive functions such as working memory. Though auditory and speech impairments have been closely associated with cognitive flexibility, in mild to moderate degree of hearing loss, the neural and behavioral features of working memory are usually preserved.

Four possible causative mechanisms linking hearing loss and cognitive decline have been described: 1) generalized pathological process that simultaneously affects hearing and cognitive functions; 2) a decrease in cognitive reserve due to hearing loss (reduced information sources, loss of cognitive integrity); 3) overexpenditure of cognitive resources in perception of auditory-verbal stimuli; 4) a combination of mechanisms 1 and 3, with certain structures affected by a pathological process and the intact areas and neural networks of the brain redirected to compensate for the lost auditory perception [8].

According to a concept proposed by K. V. Anokhin, memory as a process is carried out through memorization, which involves two stages (phases). The short-term phase is characterized by unabridged fixation of stored information (without losses and distortions of content) within a short time period. This labile phase of memory corresponds to retention of an information trace in the form of reverberation of nerve impulses. The long-term phase of memorization is characterized by a reduction in information volume during its subsequent long-term storage without changes (Fig. 1).

The long-term memory implies preservation of a trace through consolidation and associated structural changes. The new information is installed and preserved through formation and reinforcement of synaptic connections between neurons in particular contours. The concomitant formation of retrieval

system allows extracting the information when appropriate, as well as reconsolidation of memories after “using” them (by reproducing the stored information). Every reactivation of particular memory, during which the information is extracted, must be followed by its active reconstruction, recategorization, and, ultimately, reconsolidation (repeated saving of the content). Each memory retrieval event is accompanied by replacement of the existing memory trace with new content (a modified version of the previous).

Sensory impairments (visual and auditory) significantly reduce the information input in terms of quantity and quality. The associated memory loss can be classified as intrinsic decline in memory functionalities or mere physiological effect of sensory deprivation. This study aimed to specify this issue by analyzing the processes of memory consolidation and reconsolidation in older people with sensory deficits.

METHODS

All interactions with participants were carried out on individual basis. All participants provided written informed consent for the study.

The cohort included 61 patients (28 men and 33 women) aged 65–75 years (mean age — 68.4 ± 2.12 лет) and not involved in labor activity for at least 3 years by the time of the study. The first group included 17 patients with unilateral sensorineural hearing loss (ICD-10 code H90.4: Sensorineural hearing loss, unilateral with unrestricted hearing on the contralateral side). The second group included 14 patients with bilateral sensorineural hearing loss (ICD-10 code H90.3: Sensorineural hearing loss, bilateral). The third group included 19 patients with visual impairment (ICD-10 code H52.1: Myopia — visual acuity reduced to -7 D), the fourth group included 11 patients with combined sensory deficit (unilateral sensorineural hearing loss with decreased visual acuity). All groups had balanced gender representation. Inclusion criteria were the lack of cognitive impairment (at least 23 points on the Mini-Mental State Examination scale, MMSE); higher education status; and continued non-involvement in labor activities.

The study included a preparatory step and three experimental procedures.

Preparatory step

This step involved assessment of somatic and neurological status by qualified physicians. The cognitive status was assessed using MMSE scale.

Experimental procedures

Assessment of short-term auditory-verbal and visual-figurative memory volumes

The short-term auditory-verbal memory volume was studied using “10 words” method introduced by A.R. Luria [9]. The patient was read a list of 10 semantically unrelated words denoting specific objects. After listening to the stimulus words, the patient was asked to reproduce them. The procedure was repeated five times. The following indicators were recorded: the number of correctly reproduced stimulus words; the number of multiply repeated words in a single output; the number of added words. The volume of short-term visual-figurative memory was assessed using the “Visual memory” technique. The patients were presented with a table consisting of 16 cells. Each cell contained one contour image of a particular object (geometric

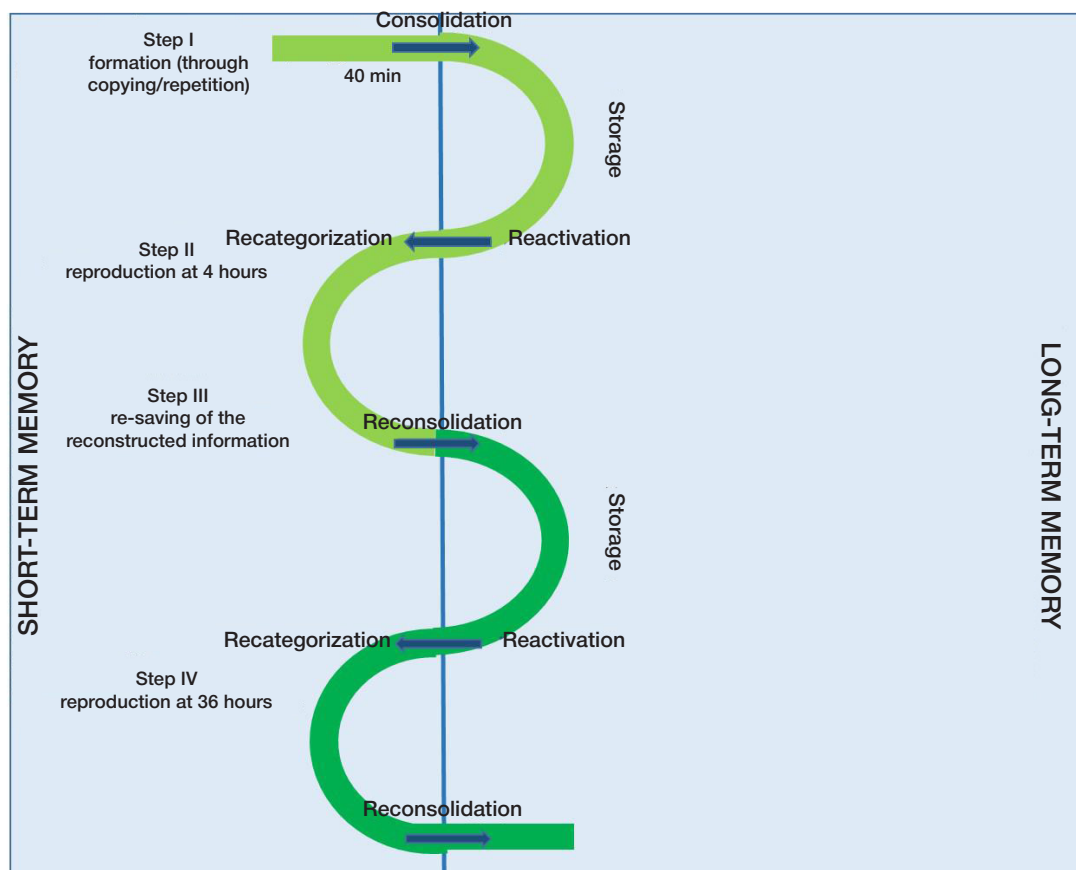


Fig. 1. Conceptual and experimental modeling of research on memory storage and retrieval

figures and schematic representations of objects). After 2 min presentation, the image was withdrawn and the patient was asked to recollect the depicted objects. The presentation was repeated five times and the same set of indicators was recorded after each presentation.

The next two experimental procedures were based on the F. Bartlett's experiments on reconstruction of memories by active retrieval.

Assessment of visual-figurative memory consolidation and reconsolidation processes

The patients were presented with symbolic image — a letter of ancient Greek alphabet resembling an owl (Fig. 2). An important condition of using it as a stimulus material was its absence in the previous experimental procedure.

The symbolic image (symbol) consisted of four parts: "head", "torso with leg", "wing", and "leg". Each of these parts contained distinct elements (for example, the "head" contained

two elements — the outline and the inner "tick"). During presentation the participants were asked to copy the image as close as possible. After specific time periods (40 min, 4 h, and 36 h), the patients were given the following instruction: "Remember, we copied the image together? Draw it now, as you recollect it, as closely to the original as possible." The visual-figurative memory evaluation involved four criteria: the integrity of the produced images, the number of lost elements, the number of distortions, and the number of preserved elements.

Assessment of semantic auditory-verbal memory consolidation and reconsolidation processes

A text from the Indian epic of Canada, presented in Russian, containing 79 semantic units, 33 sentences, 1427 characters, and 295 words, was used as stimulus material. Semantic unit was defined as a grammatic entity bearing semantic content, with a core of a noun combined to other parts of speech (adjectives, verbs, and pronouns). The instruction

Table. Absolute ranges of short-term auditory-verbal and visual-figurative memory volumes in four groups of the study

Groups	Recollected series lengths (min-max)											
	1		2		3		4		5		40 min	
	AV	VF	AV	VF	AV	VF	AV	VF	AV	VF	AV	VF
Unilateral hearing loss	5-7	9-10	5-6	10-12	5-7	11-12	6-7	11-12	6-7	11-12	4-5	8-10
Bilateral hearing loss	5-6	8-9	5-7	8-10	5-6	9-10	5-6	9-11	4-6	9-10	3-6	8-9
Visual impairment	5-7	7-9	6-7	8-9	5-7	8-10	6-7	9-11	6-7	7-9	4-6	6-9
Combined sensory deficits	4-6	5-7	5-6	6-7	5-6	6-8	4-6	7-8	4-5	7-8	3-5	5-7

Note: AV — auditory-verbal memory; VF — visual-figurative memory.

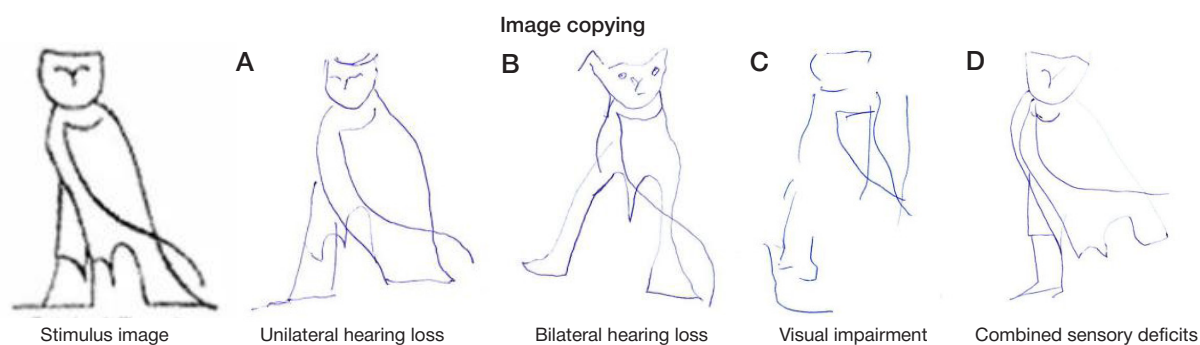


Fig. 2. Stimulus image presented in the redrawing tasks and its immediate copies produced by four groups of the study

ran as follows: "Now I will read you a text. Listen to it and retell the story as close to the text as possible". In 40 min, 4 h, and 36 h, the participants were asked to recollect and retell the text. The evaluation criteria included the number of preserved sentences, the number of preserved semantic units, the number of distorted sentences, the number of distorted semantic units, the number of confabulated sentences, and the number of confabulated semantic units. Categorization of semantic units distinguished object and trait (characterization of an object), object and time (who and when), object and action (who did what), object and place (who and where), as well as causal relationships. A semantic map was developed and used in data recording. Mistakes in the verbal recollection were categorized as substitutions and losses. The substitutions included distorted semantic units and confabulatory semantic units. The losses encompassed incoherent sentences lacking semantic content.

The quantitative data were processed using descriptive statistics (mean values, standard deviations) with nonparametric Mann–Whitney *U*-test and Wilcoxon *T*-test for pairwise comparisons at $p < 0.05$.

RESULTS

The preparatory step produced and verified the enrollment in four groups with distinctive neurological and somatic status.

The primary assessment of short-term memory volume during the first experimental procedure revealed a decrease for both auditory-verbal and visual-figurative modalities in all four groups of the study (Table).

Comparative assessment for the auditory-verbal and visual-figurative stimuli reproduction test performance in four groups of the study revealed no significant between-the group differences. The lowest indicators of short-term auditory

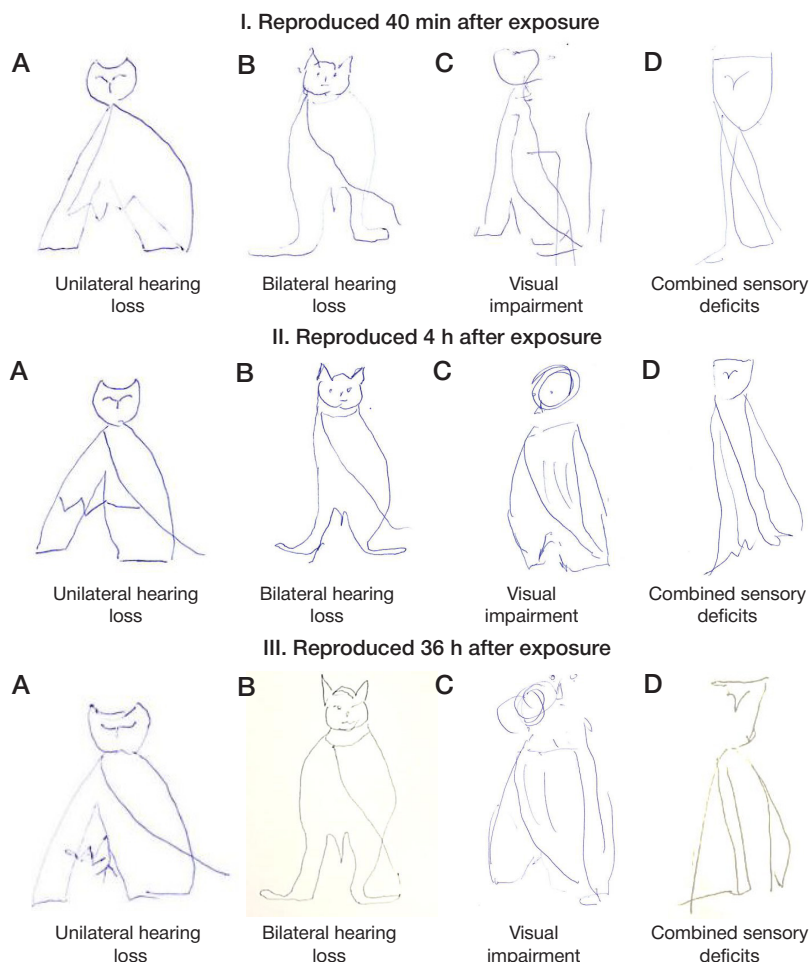


Fig. 3. Representative copies of the stimulus image made at different time points after exposure (40 min, 4 h, and 36 h) in four groups of the study

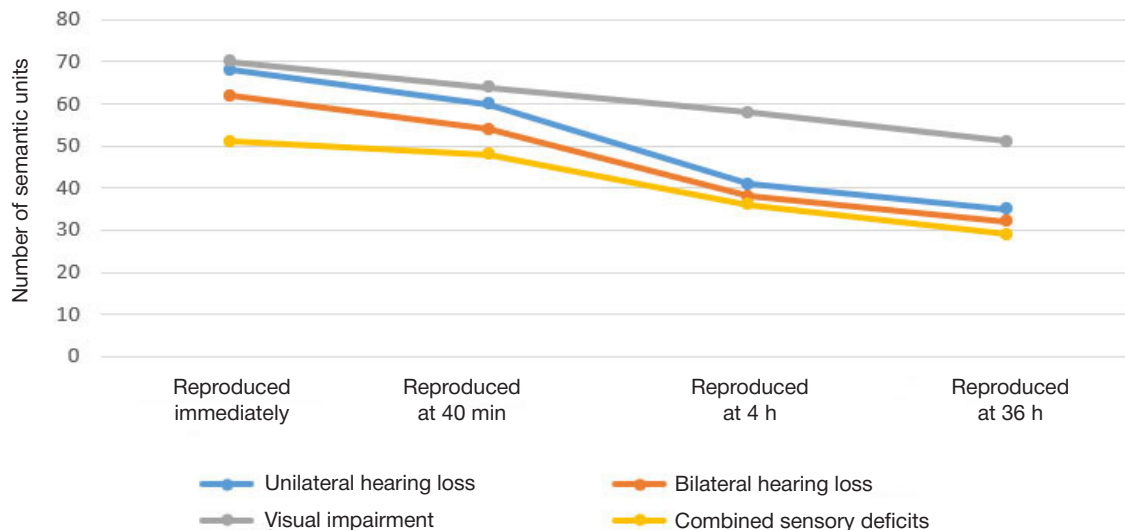


Fig. 4. Averaged profiles of correctly reproduced semantic units during auditory-verbal tasks in four groups of the study

memory volume were revealed in patients with bilaterally impaired hearing ($x \pm \sigma = 5.12 \pm 0.72$) and combined sensory deficits ($x \pm \sigma = 4.12 \pm 0.10$). The loss of original content for these groups was over 50%. The sensory deficiency of the auditory analyzer system leads to substantial loss and distortion of the incoming information already at the stage of perception. Patients with hearing impairments tend to introduce new words while reproducing the word series. For the visual-figurative modality, the lowest indicators of short-term memory volume were revealed in patients with combined sensory deficits ($x \pm \sigma = 7.19 \pm 0.22$) and visual impairments ($x \pm \sigma = 7.42 \pm 0.68$). The loss of original content for these groups was over 50%. The patients presented with characteristic substitutions of the initial visual-image stimuli by similar in size and shape (for example, a bed instead of a sofa; a ball instead of an apple; a dog instead of a goat; etc.). Upon memorization (2 minute exposure of a table with images), the depicted objects were correctly identified and named by all participants.

Experimental study of the auditory-verbal and visual-figurative memory consolidation and reconsolidation in four groups of participants revealed the following features. At the stage of copying (immediate redrawing) of the stimulus image, the maximum degree of similarity with the original, preserving all parts and elements of the symbolic image, was achieved in the group of patients with unilateral hearing loss (Fig. 2A). Corresponding images produced by patients with bilateral hearing impairment preserved the major parts of the stimulus image while distorting their elements; furthermore, the images clearly lent towards the creation of specific image — an owl with eyes and a beak (Fig. 2B). Patients with visual impairment or combined sensory deficits presented with distortion and compromised integrity of the image. In patients with visual impairment, the original image disintegrates into separate, non-interconnected lines (Fig. 2C, D). The observed transformation of symbolic image into figurative one at the stage of immediate copying of stimulus image, which reflects the short-term memory storage for subsequent consolidation, leads to initial fixation of a distorted image.

Upon reconsolidation of the figurative-symbolic information at 40 min, 4 h, or 36 h time points in patients with sensory disorders, the distortion of consolidated visual-figurative content was apparent in all groups of the study, regardless of the degree and modality of sensory deficits (Fig. 3).

Patients with unilateral hearing loss produced images with minimal distortions. Only after 36 h, patients of this group

reduced the number of parts and elements while introducing specific figurative content (bird's paws with clearly drawn fingers) (Fig. 3-III-A).

In patients with bilateral hearing loss, at the stage of initial consolidation (immediate copying of a stimulus symbolic image), the symbolic image is transformed into a figurative replica, with the clearly drawn owl's beak, eyes, and ears). The recollected images produced at 40 min, 4 h and 36 h timepoints preserve the image specificity and detalization as an "owl". At the same time, the number and identity of major parts remains unchanged and corresponds to the original symbolic image. In addition, the reconsolidations performed at 40 min, 4 h, and 36 h time points revealed further simplification of the image by transformation into specific images available in previous experience, with a reduction in the number of elements.

The corresponding images produced by patients with visual impairments (wearing vision correction devices) have more profound distortions with compromised integrity of the image and its portions (Fig. 2C). At 40 min, the decay of the memory trace for initial stimulus is evident. The image becomes specific and totally loses its symbolic character. In the act of reconsolidation, the image acquires a holistic quality; it also contains additional lines and pencil strokes that are superimposed on the image. At 4 h, the patient reproduces a coherent image, which resembles neither the stimulus, nor its copy. During the consolidation process ensuring transition of the image into a long-term memory, the symbol acquires distinctive features of a bird. The patient gives up mechanical copying of the original (especially difficult given a sensory deficit), but recreates it as a new image coherent with the pre-existing experience.

The opposite effect is observed in patients with combined sensory deficits: immediate copy of the stimulus reveals characteristic features of a specific prototype character from the pre-existing experience (Fig. 2D). However, at 40 min, the reproduction shows ultimate disintegrality, with only the "head" preserved, while the "body" is represented by a bunch of disordered lines. This phenomenon can be explained by functioning of certain compensatory mechanisms, which allow the patient to endow the image with integrity based on the experience. Reproductions made at 4 h and 36 h reveal further decay — the loss of individual elements and simplification of the rest to a set of randomly interconnected pencil strokes.

Thus, during retrieval of visual-figurative information in older patients with sensory disorders, specification and detailing of

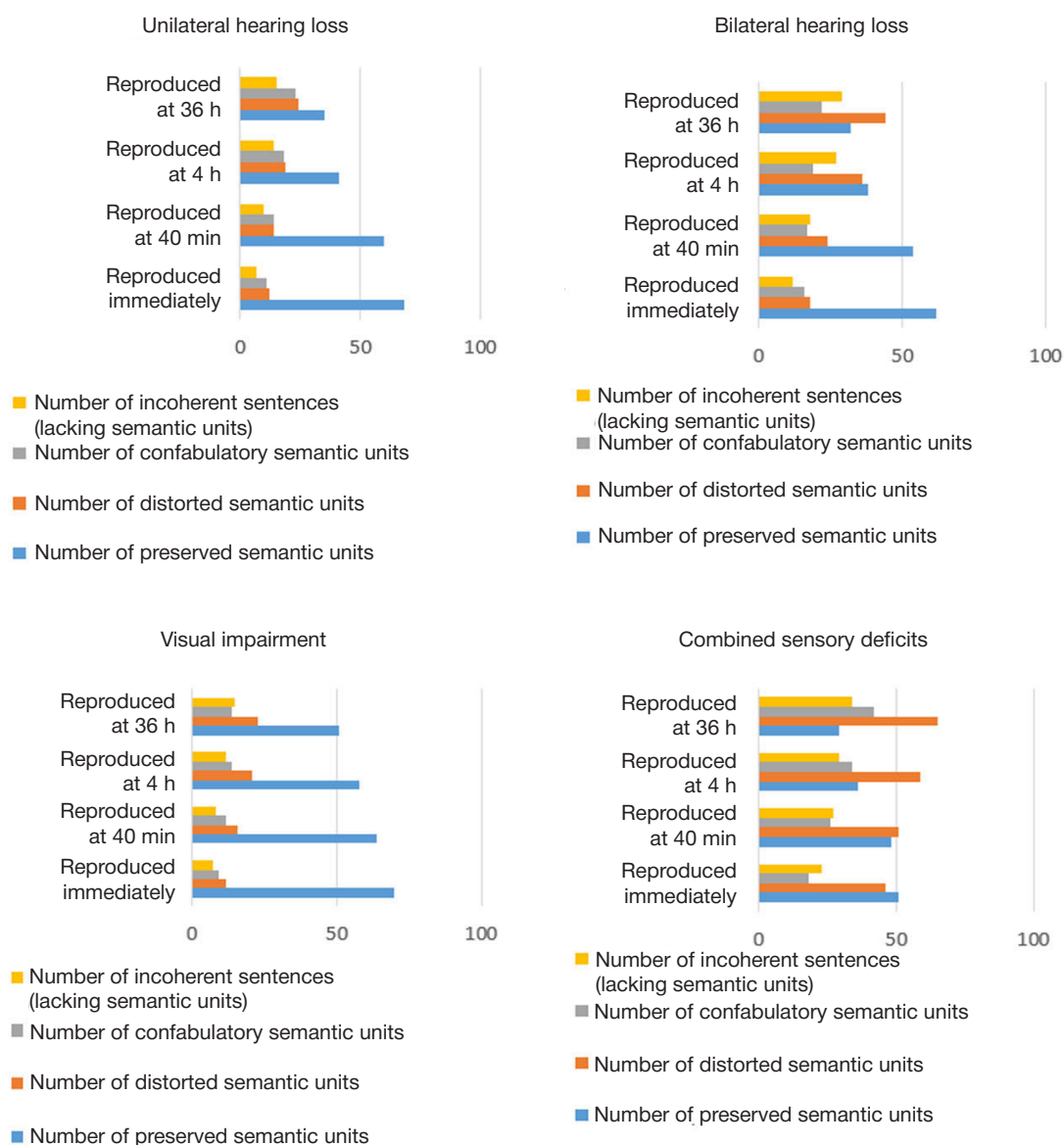


Fig. 5. Histograms of mean values for auditory-verbal memory indicators in four groups of the study

a stimulus image is fixed in accordance with the information available from a previous experience (reducing symbolic image to the image of an owl). Patients with hearing deficit produce integral images; patients with vision deficit produce images with characteristic complete disintegration of the visual-figurative content into two separate unrelated parts — the circumference of head and the “torso” with a set of extra strokes. (Figs. 3-II-C and 3-III-C).

Experimental assessment of the auditory-verbal memory consolidation and reconsolidation profiles of semantic recollection involved profiles of semantic recollection based on averaged counts of correctly reproduced semantic units during verbal recollection tasks (text retelling) in four groups of participants (Fig. 4).

Upon retelling of the text immediately after its auditory perception, the maximum loss of semantic content was observed in patients with combined sensory deficits, whereas the minimal losses of semantic content were observed in patients with visual impairment. Moreover, for patients with visual impairments, numbers of semantic units correctly reproduced at 40 min, 4 h, and 36 h were statistically similar. By contrast, significant decrease in numbers of correctly reproduced semantic units between 40 min and 4 h time points

was revealed in groups of patients with unilateral hearing loss ($p = 0.019$), bilateral hearing loss ($p = 0.021$), and combined sensory deficits ($p = 0.021$). Significant between-the-group differences in the verbal reproduction quality (in terms of semantic content) were observed at 4 h only. At this time point, the number of correctly reproduced semantic units in patients with visual impairment was significantly higher compared with other groups including patients with unilateral hearing loss ($p = 0.022$), patients with bilateral hearing loss ($p = 0.021$), and patients with combined sensory deficits ($p = 0.019$). The analysis revealed no significant between-the-group differences for patients with unilateral hearing loss, bilateral hearing loss, and combined sensory deficits.

The analysis of counts and nature of the errors made during sequential rounds of auditory-verbal recollection at 40 min, 4 h, and 36 h, reveals a decrease in the number of correctly reproduced semantic units accompanied by an increase in the numbers of distorted and confabulatory semantic units, as well as the number of incoherent sentences of no semantic content, in all groups of participants (Fig. 5).

The study of auditory-verbal memory consolidation and reconsolidation processes in older patients with sensory disorders revealed specific patterns, notably a trend towards

schematization and concretization of the text. Another distinct trend was to change the sentence altogether with overall preservation of semantic units. The intrinsic semantic sense of the sentences was preserved better than the structure and specific wording. Overall, the recollections at different time points showed relative stability of the content compared with initial reproduction.

The patients with visual impairment typically revealed a higher degree of syntactic simplification; they also tended to use short sentences or fused several sentences into one if united by a single semantic topic. The patients with hearing loss presented with introduction of multiple details and excessive meticulousness of the stories. The excessive detail and verbosity in retelling was associated with loss of semantic content and often reduced the retelling to a dialogue with oneself regarding the correctness of what was heard: "...One night two young people went hunting from the settlement of Egulac to hunt seals. Seals? I don't think so. Why seals? This is somewhere in the southern latitudes. Weird. OK..."

DISCUSSION

The obtained results are consistent with the data presented by other authors [10–12]. Several studies relate a decrease in memorization volume to the inability of switching attention from actual psychological experiences to cognitive tasks. In such cases, objective impairment of mnemonic functions may be missing or minimal (according to an objective neuropsychological examination). The observed decrease in volume of short-term auditory-verbal and visual-figurative memory in older individuals with sensory impairments manifests as distortion and partial loss of information in copying (redrawing) a symbolic image or immediate retelling of a story. The deficit leads to consolidation of the initially incomplete/distorted information, which is further modified upon subsequent retrieval from long-term memory during reactivation and recategorization with critical losses.

The observed decline in the qualitative and quantitative characteristics of memory consolidation and reconsolidation processes in older people with sensory impairments most probably involves a decrease in short-term memory volume (for both auditory-verbal and visual-figurative modalities). During the short-term phase of the memory process, the information is preserved without loss or content distortion for a short time period. Under conditions of significantly reduced short-term memory volume, experimentally proved in older patients

with auditory and visual deficits, memorization operates with distorted and abridged mnemonic representations. This labile phase of memorization involves complex reverberations of nerve impulses, the capacity which may also decline as a part of natural age-related changes in neurodynamics.

CONCLUSIONS

During reactivation of visual-figurative information in older patients with sensory disorders, specification and detailing of a stimulus image is fixed in accordance with the information available from a previous experience (reducing symbolic image to the image of an owl). Patients with hearing deficit produce integral images; patients with vision deficit produce images with characteristic complete disintegration of the visual-figurative content into two separate unrelated parts — the circumference of head and the "torso" with a set of extra lines. Patients with combined hearing and vision deficits lose individual elements: the image is simplified to several pencil strokes, partially interconnected. Such disintegration reflects the inability to represent the symbol in the internal speech plane through recategorization.

During reactivation of auditory-verbal information in older patients with sensory disorders, the information is critically simplified with compensation for the missing (lost) content by confabulations, semantically "empty" verbose sentences, and repetitions of simplified logical and grammatical constructions that do not correspond in semantic content to the original text.

The results of the study demonstrate the importance of accommodation of the newly incoming information to representations already stored in memory, effectively reducing its distortion upon consolidation and effectively preserving it during subsequent retrieval (extraction) and reconsolidation. At the same time, due to a decrease in the volume of short-term memory, in order to increase the efficiency of memory consolidation and reconsolidation processes, older patients with sensory impairments should be presented with new information in a dosed manner accounting for the reduced short-term memory volume. This mode minimizes the losses of newly incoming information at the stage of consolidation. Subsequent studies on memory consolidation and reconsolidation processes in elderly people with sensory impairments may focus on expanded age groups and nosological specifications of the patients.

References

1. Kuzovkov VE, Sugarova SB, Lilenko AS, Luppov DS. Vliyaniye snizheniya sluxa na kognitivnyuyu funkciyu i ee ocenka. Rossijskaya otorinolaringologiya. 2020; 19 (2-105): 80–84. Russian.
2. Sugarova SB, Kuzovkov VE, Kantemirova RK, Lilenko SV, Luppov DS, Lilenko AS, Kalyapin DD. Vliyaniye snizheniya sluxa na kognitivnyuyu funkciyu u pacientov pozhilogo i starcheskogo vozrasta i ee ocenka posle koxlearnoj implantacii (obzor literatury). Uspexi gerontologii. 2020; 33 (6): 1174–80. Russian.
3. Boboshko MYu, Golovanova LE, Taxtaeva NYu, Efimova MV. Vozrastnye narusheniya sluxa i osobennosti ix korrektsii. Rossijskaya otorinolaringologiya. 2011; 4 (53): 30–33. Russian.
4. Podgornaya NN. Narusheniya zritel'nykh funktsij v pozhilom i starcheskom vozraste: osnovnye prichiny, novye vozmozhnosti lecheniya. Klinicheskaya gerontologiya. 2006; 7: 3–12. Russian.
5. Rosemann S, Thiel CM. Neural Signatures of Working Memory in Age-related Hearing Loss. Neuroscience. 2020; 429: 134–42. DOI: 10.1016/j.neuroscience.2019.12.046.
6. Loughrey DG, Feeney J, Kee F, Lawlor BA, Woodside JV, Setti A, et al. Social factors may mediate the relationship between subjective age-related hearing loss and episodic memory. Aging & Mental Health. 2020; 25 (5): 824–31, DOI: 10.1080/13607863.2020.1727847.
7. Moorman SM, Greenfield EA, Lee CSH. Perceived hearing loss, social disengagement, and declines in memory. Journal of Applied Gerontology. 2020. DOI: 10.1177/0733464820909244.
8. Griffiths TD, Lad M, Kumar S, Holmes E, McMurray B, Eleanor A, et al. How Can Hearing Loss Cause Dementia? Neuron. 2020; 108 (3): 401–2. DOI: 10.1016/j.neuron.2020.08.003.
9. Luriya AR. Poteryannyj i vozvrashchennyj mir. Malen'kaya knizhka o bol'shoj pamyati. SPb.: Piter, 2018; 290 s. Russian.
10. Melokhin AI. Metakognitivnye sposobnosti v pozhilom vozraste: specifika i prediktory. Eksperimental'naya psixologiya. 2019; 12 (3): 47–62. DOI: 10.17759/exppsy.2019120304. Russian.
11. Milokhin AI. Specifika izmenenij v pamyati na lica v pozhilom

i starcheskom vozraste. Kolleksiya gumanitarnyx issledovaniy. 2017; 6 (9): 81–97. Russian.

12. Putilina MV. Narushenie pamyati u pozilyx pacientov. Vozmozhnye terapevticheskie strategii. Poliklinika. 2017; 2: 57–61. Russian.

Литература

1. Кузовков В. Е., Сугарова С. Б., Лиленко А. С., Луппов Д. С. Влияние снижения слуха на когнитивную функцию и ее оценка. Российская оториноларингология. 2020; 19 (2-105): 80–84.
2. Сугарова С. Б., Кузовков В. Е., Кантемирова Р. К., Лиленко С. В., Луппов Д. С., Лиленко А. С., Каляпин Д. Д. Влияние снижения слуха на когнитивную функцию у пациентов пожилого и старческого возраста и ее оценка после кохлеарной имплантации (обзор литературы). Успехи геронтологии. 2020; 33 (6): 1174–80.
3. Бобошко М. Ю., Голованова Л. Е., Тахтаева Н. Ю., Ефимова М. В. Возрастные нарушения слуха и особенности их коррекции. Российская оториноларингология. 2011; 4 (53): 30–33.
4. Подгорная Н. Н. Нарушения зрительных функций в пожилом и старческом возрасте: основные причины, новые возможности лечения. Клиническая геронтология. 2006; 7: 3–12.
5. Rosemann S, Thiel CM. Neural Signatures of Working Memory in Age-related Hearing Loss. Neuroscience. 2020; 429: 134–42. DOI: 10.1016/j.neuroscience.2019.12.046.
6. Loughrey DG, Feeney J, Kee F, Lawlor BA, Woodside JV, Setti A, et al. Social factors may mediate the relationship between subjective age-related hearing loss and episodic memory. Aging & Mental Health. 2020; 25 (5): 824–31, DOI: 10.1080/13607863.2020.1727847.
7. Moorman SM, Greenfield EA, Lee CSH. Perceived hearing loss, social disengagement, and declines in memory. Journal of Applied Gerontology. 2020. DOI: 10.1177/0733464820909244.
8. Griffiths TD, Lad M, Kumar S, Holmes E, McMurray B, Eleanor A, at al. How Can Hearing Loss Cause Dementia? Neuron. 2020; 108 (3): 401–2. DOI: 10.1016/j.neuron.2020.08.003.
9. Лурия А. Р. Потерянный и возвращенный мир. Маленькая книжка о большой памяти. СПб.: Питер, 2018; 290 с.
10. Мелёхин А. И. Метакогнитивные способности в пожилом возрасте: специфика и предикторы. Экспериментальная психология. 2019; 12 (3): 47–62. DOI: 10.17759/exppsy.2019120304.
11. Мелёхин А. И. Специфика изменений в памяти на лица в пожилом и старческом возрасте. Коллекция гуманитарных исследований. 2017; 6 (9): 81–97.
12. Путилина М. В. Нарушение памяти у пожилых пациентов. Возможные терапевтические стратегии. Поликлиника. 2017; 2: 57–61.

HEMOPERFUSION AND FUNCTIONAL STATE OF THE MACULA AFTER SIMULTANEOUS PANCREAS AND KIDNEY TRANSPLANTATION

Vorobyeva IV^{1,2}✉, Bulava EV¹, Moshetova LK¹, Pinchuk AV^{3,4,5}

¹ Russian Medical Academy of Continuous Professional Education, Moscow, Russia

² Peoples' Friendship University of Russia, Moscow, Russia

³ Sklifosovskiy Research Institute for Emergency Medical Aid, Moscow, Russia

⁴ Evdokimov Moscow University of Medicine & Dentistry, Moscow, Russia

⁵ Research Institute of Healthcare Organization and Medical Management, Moscow, Russia

Simultaneous pancreas and kidney transplantation (SPK) provides effective treatment in patients with type 1 diabetes mellitus (T1DM) and end-stage renal failure (ESRF), mitigating the hyperglycemia and uremic syndrome. The study aimed at the assessment of morphofunctional status of the macula and macular hemodynamics in patients with T1DM after SPK. The study enrolled 45 patients subdivided into three groups: Group A — patients with T1DM after SPK; Group B — patients with T1DM and ESRF, maintained on programmed hemodialysis (PH), on waiting list for SPK; and Group C — individuals without ophthalmic or systemic pathologies. All patients were subject to the standard ophthalmological examination complemented by measurements of the central retinal thickness (CRT) and the average perfusion density (PD) in four vascular layers: superficial capillary plexus of the retina (SCP), deep capillary plexus of the retina (DCP), choriocapillaris, and choroid. The patients after SPK had significantly lower CRT ($241 \pm 33 \mu\text{m}$ in Group A, $309 \pm 10 \mu\text{m}$ in Group B; $p < 0.05$) and significantly higher PD of the macular region in both the retina (Group A: SCP — $19.0 \pm 1.6\%$, DCP — $10.7 \pm 1.3\%$; Group B: SCP — $11.7 \pm 0.8\%$, DCP — $4.8 \pm 0.8\%$; $p < 0.05$) and the choroid (Group A: choriocapillaris — $28.1 \pm 1.8\%$, choroid — $31.3 \pm 1.6\%$; Group B: choriocapillaris — $20.4 \pm 1.6\%$, choroid — $21.8 \pm 1.3\%$; $p < 0.05$), as well as significantly higher visual acuity (Group A: 0.7 ± 0.1 ; Group B: 0.5 ± 0.1 ; $p < 0.05$) and macular light threshold (Group A: $25.9 \pm 1.4 \text{ dB}$; Group B: $22.3 \pm 1.1 \text{ dB}$; $p < 0.05$) compared with the patients on PH. Thus, the normalization of carbohydrate metabolism and the mitigation of uremic syndrome in patients with T1DM and ESRF after SPK favorably affect the functional condition of the macular area, as indicated by the improvement in macular blood flow and visual functions.

Keywords: diabetes mellitus, diabetic retinopathy, diabetic nephropathy, simultaneous pancreas and kidney transplantation, optical coherence tomography angiography

Acknowledgements: the authors acknowledge Prof. G.Sh. Arzhimatova of the Botkin Hospital (Moscow) for helpful discussions.

Author contribution: Vorobyeva IV — literature analysis, planning and coordination of the study, data analysis and interpretation; Bulava EV — literature analysis, data collection, analysis and interpretation, preparation of the manuscript; Moshetova LK — study planning and supervision, data analysis and interpretation; Pinchuk AV — study planning and supervision.

Compliance with ethical standards: the study was approved by Ethical Committee at the Russian Medical Academy of Continuous Professional Education (Protocol № 1 of January 18, 2021); the written informed consent for the study was provided by all participants.

✉ **Correspondence should be addressed:** Irina V. Vorobyeva
Botkinsky pr-d, 2, korp. 19, Moscow, 125284 Russia; irina.docent2000@mail.ru

Received: 22.02.2022 **Accepted:** 10.03.2022 **Published online:** 05.04.2022

DOI: 10.24075/brsmu.2022.013

ГЕМОПЕРФУЗИЯ И ФУНКЦИОНАЛЬНОЕ СОСТОЯНИЕ МАКУЛЫ ПОСЛЕ СОЧЕТАННОЙ ТРАНСПЛАНТАЦИИ ПОЧКИ И ПОДЖЕЛУДОЧНОЙ ЖЕЛЕЗЫ

И. В. Воробьева^{1,2}✉, Е. В. Булава¹, Л. К. Мошетова¹, А. В. Пинчук^{3,4,5}

¹ Российская медицинская академия непрерывного профессионального образования, Москва, Россия

² Российский университет дружбы народов, Москва, Россия

³ Научно-исследовательский институт скорой помощи имени Н. В. Склифосовского, Москва, Россия

⁴ Московский государственный медико-стоматологический университет имени А. И. Евдокимова, Москва, Россия

⁵ Научно-исследовательский институт организации здравоохранения и медицинского менеджмента, Москва, Россия

Сочетанная трансплантация почки и поджелудочной железы (СТПиПЖ) — эффективный метод лечения больных с сахарным диабетом 1-го типа (СД1) и терминальной стадией хронической почечной недостаточности (ТХПН), который приводит к купированию гипергликемии и уремического синдрома. Целью работы было изучить морфофункциональное состояние и гемодинамику макулы у пациентов с СД1 после СТПиПЖ. В исследовании участвовали 45 пациентов, разделенных на три группы: в группу А вошли пациенты с СД1 после СТПиПЖ; в группу В — с СД1 и ТХПН, проходящие курсы программного гемодиализа (ПГД) и ожидающие СТПиПЖ; в группу С — лица, не имеющие глазных и системных патологий. Всем пациентам проводили традиционное офтальмологическое обследование, а также измерение центральной толщины сетчатки (ЦТС), среднего значения плотности перфузии в четырех сосудистых слоях: поверхностном (ПКСС) и глубоком (ГКСС) капиллярных сплетениях сетчатки, слое хориокапилляров (ХК) и хориоидеи. После СТПиПЖ, по сравнению с ПГД, выявлено уменьшение ЦТС (в группе А: $241 \pm 33 \text{ мкм}$; в группе В: $309 \pm 10 \text{ мкм}$; $p < 0,05$), увеличение среднего значения плотности перфузии сетчатки (в группе А: ПКСС — $19,0 \pm 1,6\%$, ГКСС — $10,7 \pm 1,3\%$; в группе В: ПКСС — $11,7 \pm 0,8\%$, ГКСС — $4,8 \pm 0,8\%$; $p < 0,05$) и хориоидеи (в группе А: ХК — $28,1 \pm 1,8\%$, хориоидея — $31,3 \pm 1,6\%$; в группе В: ХК — $20,4 \pm 1,6\%$, хориоидея — $21,8 \pm 1,3\%$; $p < 0,05$) в макулярной области, остроты зрения (в группе А: $0,7 \pm 0,1$; в группе В: $0,5 \pm 0,1$; $p < 0,05$) и порога светочувствительности макулы (в группе А: $25,9 \pm 1,4 \text{ дБ}$; в группе В: $22,3 \pm 1,1 \text{ дБ}$; $p < 0,05$). Нормализация углеводного обмена и купирование уремического синдрома у больных с СД1 и ТХПН после СТПиПЖ благоприятно влияют на состояние макулярной области в виде улучшения макулярного кровотока и зрительных функций.

Ключевые слова: сахарный диабет, диабетическая ретинопатия, диабетическая нефропатия, сочетанная трансплантация почки и поджелудочной железы, оптическая когерентная томография-ангиография

Благодарности: МГОЦ ГКБ им. С. П. Боткина в лице Г. Ш. Аржиматовой.

Вклад авторов: И. В. Воробьева — анализ литературы, планирование и руководство исследованием, анализ и интерпретация данных; Е. В. Булава — анализ литературы, сбор, анализ и интерпретация данных, подготовка рукописи; Л. К. Мошетова — планирование и руководство исследованием, анализ и интерпретация данных; А. В. Пинчук — планирование и руководство исследованием.

Соблюдение этических стандартов: исследование одобрено этическим комитетом Российской медицинской академии непрерывного профессионального образования (протокол № 1 от 18 января 2021 г.); все участники подписали добровольное согласие на участие в данном исследовании.

✉ **Для корреспонденции:** Ирина Витальевна Воробьева
2-й Боткинский пр-д, д. 5, корпус 19, г. Москва, 125284, Россия; irina.docent2000@mail.ru

Статья получена: 22.02.2022 **Статья принята к печати:** 10.03.2022 **Опубликована онлайн:** 05.04.2022

DOI: 10.24075/vrgmu.2022.013

About 10% of diabetes cases worldwide are classified as type 1 diabetes mellitus (T1DM). This most severe type of diabetes develops due to autoimmune damage to pancreatic β -cells. Up to 85% of T1DM cases are diagnosed in early adolescence. About 1,100,000 individuals aged under 20 currently live with T1DM, and the global prevalence continues to increase by about 132,600 new cases per annum [1]. In Russia, the prevalence of T1DM at the end of 2020 was 180.9 cases per 100,000 population [2].

Insulin therapy remains the main treatment for T1DM. The proper administration of insulin can mitigate the hyperglycemia and considerably prevent the onset and progression of diabetic complications [3]. However, according to the T1D Exchange registry, as little as 21% of patients with T1DM achieve the recommended levels of glycated hemoglobin (HbA1c) [4]. In this regard, complications of T1DM remain the leading causes of disability and death among the patients [5].

Diabetic nephropathy is the third leading cause of death, surpassed only by cardiovascular disorders and cancers. The patients with T1DM-associated nephropathy, which progresses to the end-stage renal failure (ESRF) over 15–20 years [6], become inevitably faced with the need for the kidney replacement therapy. The dialysis procedures are expensive and require specialized medical facilities, advanced equipment, and dedicated personnel training. Besides, these procedures are debilitating and entail side effects [7]. On the other hand, kidney transplants in T1DM have low efficacy due to the high risks of secondary nephropathy in posttransplantation period [8].

The simultaneous pancreas and kidney transplantation (SPK) is arguably the most advantageous treatment for the patients with T1DM-associated ESRF. The intervention normalizes carbohydrate metabolism and renal excretion, thereby liberating the patients from the constant glucose monitoring, insulin therapy, and debilitating hemodialysis courses [9].

This study aimed at the assessment of morphofunctional status of the macula and macular hemodynamics against the glycemia normalization and the mitigation of uremic syndrome in patients with T1DM after SPK.

METHODS

The study enrolled 45 participants (68 eyes). The inclusion criteria were T1DM-associated ESRF treated with either programmed hemodialysis (PH, group of comparison) or allogeneic pancreas-kidney transplants (main group), or the

absence of ophthalmic and systemic pathologies (control group). The non-inclusion criteria were type 2 diabetes and other systemic pathologies, ESRF of non-diabetic genesis, and the pancreas and/or kidney transplant rejection. Eyes with a history of retinal laser photocoagulation in the macular area, vitrectomy, cataract extraction, or panretinal laser photocoagulation performed less than 6 months before examination, as well as those with proliferative lesions of the macula, comorbid retinal pathologies, glaucoma, pronounced opacities of the optical media, or high-grade refractive errors were excluded from the study.

All patients were divided into three groups: Group A (main group) — patients with T1DM and functional pancreas-kidney transplants (15 individuals, 18 eyes) (Fig. 1); Group B (comparison group) — patients with severe decompensated T1DM and associated ESRF, on waiting list for SPK and currently on PH (15 individuals, 20 eyes); and Group C (control group) — individuals without ophthalmic or systemic pathologies (15 individuals, 30 eyes).

All patients were subject to the standard ophthalmological examination including the maximally corrected visual acuity (MCVA) and intraocular pressure tests, biomicroscopy of the anterior eye segment, indirect slit-lamp biomicroscopy with a 78-diopter aspheric lens, and photorecording funduscopy.

The measurements of central retinal thickness (CRT) and perfusion densities were carried out by optical coherence tomography (OCT) angiography in the RS-3000 Advance 2 system (NIDEK; Japan). The average perfusion density (PD) of the macular region (scan area 3.0–3.0 mm) was measured in four vascular layers: superficial and deep capillary plexuses of the retina (respectively, SCP and DCP), the capillary lamina of choroid (choriocapillaris), and choroid proper (Fig. 2) using AngioScan mode. The macular light threshold (MLT) was determined by Macular Integrity Assessment (MAIA) micropertimetry (CenterVue S.p.A; Italy).

To assess the degree of T1DM compensation and renal functionality, all patients underwent blood tests for HbA1c, creatinine, and urea, providing the estimated glomerular filtration rate, eGFR.

The data were analyzed in StatTech v. 2.6.2 (StatTech; Russia). Quantitative indicators were assessed for compliance with the normal distribution using the Shapiro–Wilk and Kolmogorov–Smirnov criteria. Comparisons of quantitative indicators for three or more groups were carried out using one-way ANOVA and nonparametric Kruskal–Wallis test. Direction

Table. Comparative analysis of perfusion densities in four vascular layers of the macular region

Indicator	Group	M \pm SD	95% CI	n	p	
PD SCP (%)	A	19.0 \pm 1.6	17.0–21.0	18	Group A – Group B	<0.05*
	B	11.7 \pm 0.8	10.7–12.7	20	Group A – Group C	<0.05*
	C	34.3 \pm 1.0	33.6–35.4	30	Group B – Group C	<0.05*
PD DCP (%)	A	10.7 \pm 1.3	9.3–12.2	18	Group A – Group B	<0.05*
	B	4.8 \pm 0.8	3.8–5.8	20	Group A – Group C	<0.05*
	C	14.3 \pm 1.2	13.3–15.6	30	Group B – Group C	<0.05*
PD choriocapillaris (%)	A	28.1 \pm 1.8	25.7–30.5	18	Group A – Group B	<0.05*
	B	20.4 \pm 1.6	18.3–22.4	20	Group A – Group C	<0.05*
	C	45.7 \pm 0.8	45.0–46.4	30	Group B – Group C	<0.05*
PD choroid (%)	A	31.3 \pm 1.6	29.2–33.8	18	Group A – Group B	<0.05*
	B	21.8 \pm 1.3	20.2–23.4	20	Group A – Group C	<0.05*
	C	48.0 \pm 0.8	47.2–48.8	30	Group B – Group C	<0.05*

Note: PD SCP — perfusion density of the superficial capillary plexus of the retina; PD DCP — perfusion density of the deep capillary plexus of the retina; PD choriocapillaris — perfusion density of the choriocapillaris; PD choroid — perfusion density of the choroid; Group A — patients after the simultaneous pancreas and kidney transplantation (SPK); Group B — patients on PH/waiting list for the simultaneous pancreas and kidney transplantation (SPK); Group C — healthy individuals.

and strength of relationships between quantitative variables were described by Pearson's and Spearman's correlation coefficients.

RESULTS

A total of 24 women and 21 men aged 35 ± 7 years on average participated in the study. Groups A, B, and C were statistically similar with regard to gender ($p = 0.784$) and age ($p = 0.839$) of the participants. The average length of time since the diagnosis of T1DM in Groups A and B was 27 ± 8 years, similar between the groups ($p = 0.475$). Patients with pre-proliferative (PPDR) and proliferative (PDR) stages of diabetic retinopathy were encountered in both groups, all of them previously treated with panretinal laser photocoagulation. The incidence of PPDR and PDR between the groups was similar ($p = 0.756$). The average time since transplantation in Group A was 21 ± 11 months. The average time on PH in Group B was 24 ± 8 months.

Comparison of CRT measurements for the three groups revealed statistically significant differences ($p < 0.05$). In patients with decompensated T1DM on PH, the central portion of the retina was thicker (Group B, $309 \pm 10 \mu\text{m}$) than in patients after SPK (Group A, $241 \pm 33 \mu\text{m}$) or healthy individuals (Group C, $260 \pm 6 \mu\text{m}$).

The highest average perfusion density of the retina and choroid was observed in the control group (Group C). The patients with transplants (Group A) had higher perfusion rates of the retina and choroid than the patients on PH/waiting list for SPK (Group B) (Table).

Both MCVA and MLT were significantly higher in the patients with pancreas-kidney transplants (Group A: MCVA — 0.7 ± 0.1 , MLT — 25.9 ± 1.4 dB) than in the patients with decompensated T1DM on PH (Group B: MCVA — 0.5 ± 0.1 , MLT — 22.3 ± 1.1 dB; $p < 0.05$) (Fig. 3).

All three groups revealed pronounced correlations between indicators of the functional state of the macula and perfusion density of the retina and choroid. MCVA positively correlated with the choriocapillaris perfusion density ($p = 0.886$; $p < 0.05$), whereas MLT positively correlated with PD SCP ($p = 0.772$; $p < 0.05$).

HbA1c levels in the patients with transplants were significantly reduced compared with the patients on PH (Group A — $4.8 \pm 0.4\%$; Group B — $7.1 \pm 0.8\%$; $p < 0.05$). Both CRT and PD SCP correlated with the hemoglobin glycation levels: higher levels of HbA1c were accompanied by increased CRT ($p = 0.848$; $p < 0.05$) and decreased SCP perfusion density ($r = -0.723$; $p < 0.05$).

Low perfusion densities for both DCP and choriocapillaris in Group B significantly correlated with the renal functionality indicators (Fig. 4). In particular, creatinine levels negatively correlated with DCP perfusion density ($p = -0.758$; $p < 0.05$), whereas eGFR positively correlated with the choriocapillaris perfusion density ($p = 0.867$; $p < 0.05$).

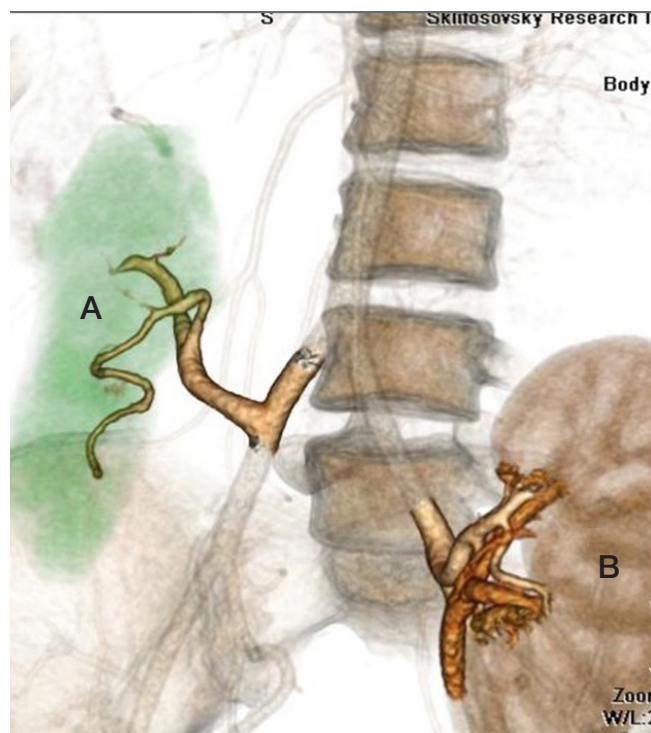


Fig. 1. Computed tomography image with intravenous contrast, 3D reconstruction, showing typical positions of the pancreatic (A) and kidney (B) transplants in the recipient

DISCUSSION

The majority of studies on the condition of the retina after SPK, published in recent decades, assessed the clinical manifestations of diabetic retinopathy (DR) using ophthalmoscopy and fluorescent angiography. These studies demonstrated stabilization and improvement in the condition, manifesting as a reduced need for laser photocoagulation of the retina and vitrectomy in more than 60% of the cases [10–13]. The improvement in the ophthalmoscopic picture, noted in 21.3–41.7% of the patients, was accompanied by a decrease in the grade of hard and soft exudates and intraretinal microvascular abnormalities [14, 15]. An improvement in visual acuity in patients with proliferative DR after SPK was also reported [16].

The advent of modern ophthalmological diagnostic equipment (OCT angiography and microperimetry) enabled detailed investigation of hemodynamics and morphofunctional state of the retina in patients with DR after various treatments [17–21]; however, we failed to find any published evidence on the dynamics of retinal hemoperfusion and light sensitivity in DR after SPK.

Our patients on waiting list for SPK had significantly higher CRT ($309 \pm 10 \mu\text{m}$) and significantly lower average perfusion

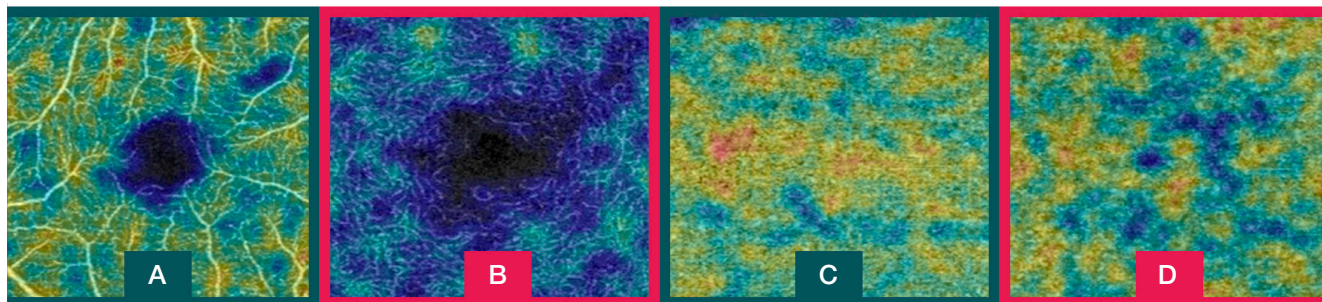


Fig. 2. Perfusion density measured in four vascular layers of the macular region (color-coded OCT angiography, RS-3000 Advance 2 system, NIDEK, Japan). (A) Superficial capillary plexus of the retina. (B) Deep capillary plexus of the retina. (C) Choriocapillaries. (D) Choroid

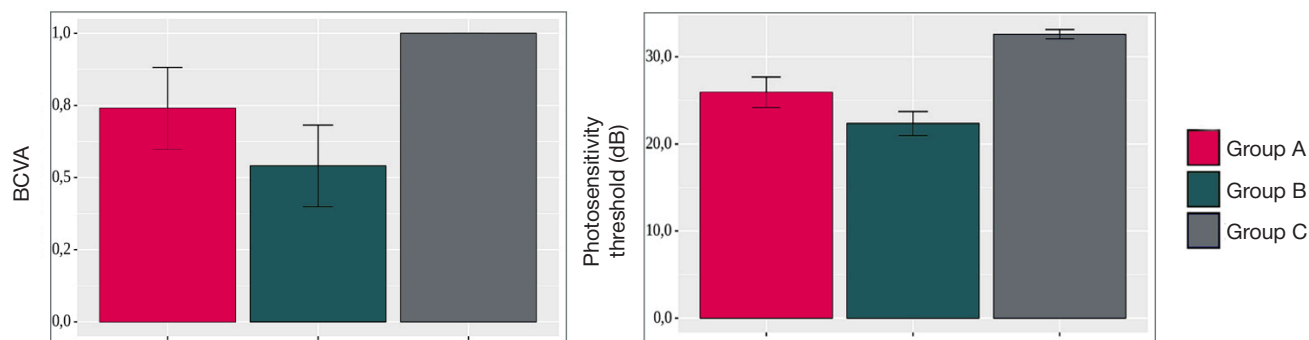


Fig. 3. Analysis of functional indicators for the macular region. BCVA — best corrected visual acuity. Group A — patients after simultaneous kidney and pancreas transplantation. Group B — patients awaiting simultaneous kidney and pancreas transplantation. Group C — healthy patients

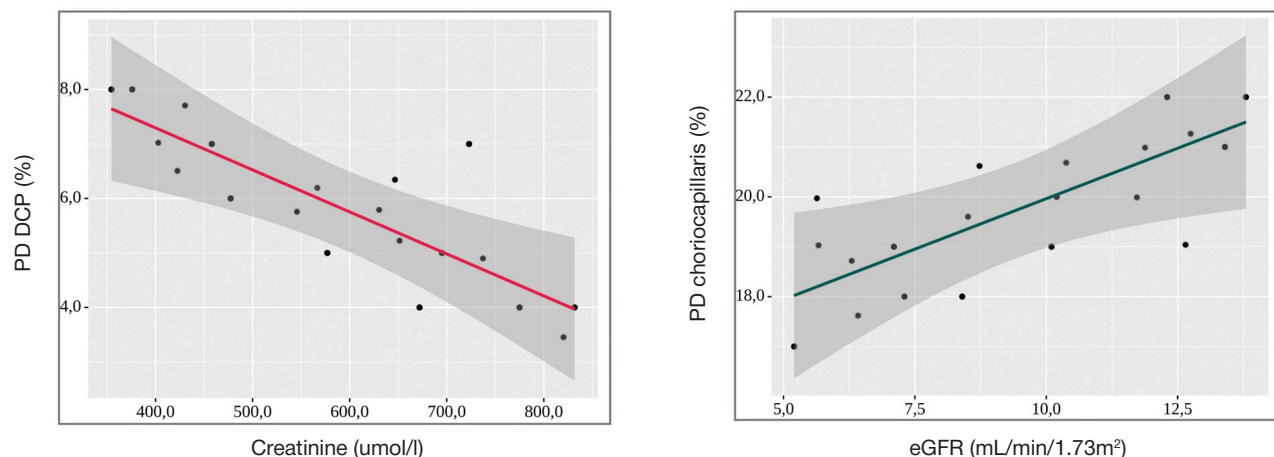


Fig. 4. Regression plots showing correlations of DCP and choriocapillaris perfusion densities with creatinine levels and eGFR, respectively. PD DCP — perfusion density of the deep capillary plexus. PD — perfusion density. EGFR — estimated glomerular filtration rate

density in four macular layers (PD SCP — $11.7 \pm 0.8\%$; PD DCP — $4.8 \pm 0.8\%$; PD choriocapillaris — $20.4 \pm 1.6\%$; PD choroid — $21.8 \pm 1.3\%$) than patients after SPK (Group A: CRT — $241 \pm 33 \mu\text{m}$; PD SCP — $19.0 \pm 1.6\%$; PD DCP — $10.7 \pm 1.3\%$; PD choriocapillaris — $28.1 \pm 1.8\%$; PD choroid — $31.3 \pm 1.6\%$; $p < 0.05$). CRT, macular perfusion density, as well as the laboratory blood test indicators of T1DM decompensation and renal functionality (HbA1c, creatinine, eGFR), revealed significant correlations. Normalization of glucose levels and mitigation of uremia in the aftermath of SPK are beneficial for the peripheral microcirculation. In particular, it results in stronger vascular walls and decreased extravasation of blood plasma and formed elements to the intervascular spaces of ocular tissues, with the resulting reduction in retinal thickness and enhanced hemoperfusion in retina and choroid of the eye. The improved morphometric parameters (reduced CRT)

and macula hemoperfusion indicators (increased perfusion density in four vascular layers) are directly related to the improvement in visual functions (as assessed through MCVA and retinal light sensitivity measurements) in the post-transplantation period.

CONCLUSIONS

The advanced diagnostics involving the non-invasive OCT angiography and fundus-microperimetry enables the accurate functional assessment of the macular region in patients with T1DM before and after SPK. The study demonstrates significant improvement in macular hemoperfusion and morphofunctional status of the macula, as well as improved visual acuity in the post-transplantation period, compared with the patients on waiting list for a similar transplantation.

References

- Diaz-Valencia PA, Bougnères P, Valleron AJ. Global epidemiology of type 1 diabetes in young adults and adults: a systematic review. *BMC Public Health*. 2015; 15: 255. DOI: 10.1186/s12889-015-1591-y.
- Dedov II, Shestakova MV, Vikulova OK, Zheleznyakova AV, Isakov MA. Jepidemiologicheskie karakteristiki saharnogo diabeta v Rossijskoj Federacii: kliniko-statisticheskij analiz po dannym registra saharnogo diabeta na 01.01.2021. *Saharnyj diabet*. 2021; 24 (3): 204–21. Russian.
- Cichocka E, Wietchy A, Nabrdalik K, Gumprecht J. Insulin therapy — new directions of research. *Endokrynol Pol*. 2016; 67 (3): 314–24. DOI: 10.5603/EP.2016.0044.
- Foster NC, Beck RW, Miller KM, Clements MA, Rickels MR, DiMeglio LA, et al. State of Type 1 Diabetes Management and Outcomes from the T1D Exchange in 2016–2018. *Diabetes Technol Ther*. 2019; 21 (2): 66–72. DOI: 10.1089/dia.2018.0384.
- Wong E, Backholer K, Gearon E, Harding J, Freak-Poli R, Stevenson C, et al. Diabetes and risk of physical disability in adults: a systematic review and meta-analysis. *Lancet Diabetes Endocrinol*. 2013; 1 (2): 106–14. DOI: 10.1016/S2213-8587(13)70046-9.
- Baek JH, Lee WJ, Lee BW, Kim SK, Kim G, Jin SM, et al. Age at Diagnosis and the Risk of Diabetic Nephropathy in Young Patients with Type 1 Diabetes Mellitus. *Diabetes Metab J*. 2021; 45 (1): 46–54. DOI: 10.4093/dmj.2019.0134.

7. Schiller B. Leading a Dialysis Organization: Role and Responsibilities of the Chief Medical Officer (Nephrologist Leadership in a Dialysis Provider Organization). *Adv Chronic Kidney Dis.* 2018; 25 (6): 485–9. DOI: 10.1053/j.ackd.2018.08.015.
8. Kaku K, Kitada H, Noguchi H, Kurihara K, Kawanami S, Nakamura U, et al. Living donor kidney transplantation preceding pancreas transplantation reduces mortality in type 1 diabetics with end-stage renal disease. *Transplant Proc.* 2015; 47 (3): 733–7. DOI: 10.1016/j.transproceed.2014.12.048.
9. Barlow AD, Saeb-Parsy K, Watson CJE. An analysis of the survival outcomes of simultaneous pancreas and kidney transplantation compared to live donor kidney transplantation in patients with type 1 diabetes: a UK Transplant Registry study. *Transpl Int.* 2017; 30 (9): 884–92. DOI: 10.1111/tri.12957.
10. Zech JC, Trepsat D, Gain-Gueugnon M, Lefrancois N, Martin X, Dubernard JM. Ophthalmological follow-up of type 1 (insulin-dependent) diabetic patients after kidney and pancreas transplantation. *Diabetologia.* 1991; 34 (1): 89–91. DOI: 10.1007/BF00587628.
11. Chow VC, Pai RP, Chapman JR, O'Connell PJ, Allen RD, Mitchell P, et al. Diabetic retinopathy after combined kidney-pancreas transplantation. *Clinical Transplantation.* 1999; 13 (4): 356–62. DOI: 10.1034/j.1399-0012.1999.130413.x.
12. Pearce IA, Ilango B, Sells RA, Wong D. Stabilisation of diabetic retinopathy following simultaneous pancreas and kidney transplant. *British Journal of Ophthalmology.* 2000; 84 (7): 736–40. DOI: 10.1136/bjo.84.7.736.
13. Glazunova AM, Arutyunova MS, Tarasov EV, Shamhalova MSh, Shestakova MV, Mojsyuk YaG, i dr. Vliyanie sochetannoj transplantacii pochki i podzheludochnoj zhelezy na dinamiku pozdnyh oslozhenenij u bol'nyh saharnym diabetom 1 tipa. *Saharnyj diabet.* 2015; 18 (2): 69–78. Russian.
14. Koznarová R, Saudek F, Sosna T, Adamec M, Jedináková T, Boucek P et al. Beneficial effect of pancreas and kidney transplantation on advanced diabetic retinopathy. *Cell Transplantation.* 2000; 9 (6): 903–8. DOI: 10.1177/096368970000900617.
15. Giannarelli R, Coppelli A, Sartini M, Aragona M, Boggi U, Vistoli F et al. Effects of pancreas-kidney transplantation on diabetic retinopathy. *Transplant International.* 2005; 18 (5): 619–22. DOI: 10.1111/j.1432-2277.2005.00108.x.
16. Shipman KE, Patel CK. The effect of combined renal and pancreatic transplantation on diabetic retinopathy. *Clinical Ophthalmology.* 2009; 3: 531–5. DOI: 10.2147/opth.s7141.
17. Ishibazawa A, Nagaoka T, Takahashi A, Omae T, Tani T, Sogawa K, et al. Optical Coherence Tomography Angiography in Diabetic Retinopathy: A Prospective Pilot Study. *Am J Ophthalmol.* 2015; 160 (1): 35–44. DOI: 10.1016/j.ajo.2015.04.021.
18. Agemy SA, Sripsema NK, Shah CM, Chui T, Garcia PM, Lee JG, et al. Retinal vascular perfusion density mapping using optical coherence tomography angiography in normals and diabetic retinopathy patients. *Retina.* 2015; 35 (11): 2353–63. DOI: 10.1097/IAE.0000000000000862.
19. Nesper PL, Roberts PK, Onishi AC, Chai H, Liu L, Jampol LM, et al. Quantifying Microvascular Abnormalities with Increasing Severity of Diabetic Retinopathy Using Optical Coherence Tomography Angiography. *Invest Ophthalmol Vis Sci.* 2017; 58 (6): 307–15. DOI: 10.1167/iov.17-21787.
20. Vujosevic S, Bottega E, Casciano M, Pilotto E, Convento E, Midena E. Microperimetry and fundus autofluorescence in diabetic macular edema: subthreshold micropulse diode laser versus modified early treatment diabetic retinopathy study laser photocoagulation. *Retina.* 2010; 30 (6): 908–16. DOI: 10.1097/IAE.0b013e3181c96986.
21. Boned-Murillo A, Diaz-Barreda MD, Ferreras A, Bartolomé-Sesé I, Orduna-Hospital E, Montes-Rodríguez P, et al. Structural and functional findings in patients with moderate diabetic retinopathy. *Graefes Arch Clin Exp Ophthalmol.* 2021; 259 (12): 3625–35. DOI: 10.1007/s00417-021-05277-y.

Литература

1. Diaz-Valencia PA, Bougnères P, Valleron AJ. Global epidemiology of type 1 diabetes in young adults and adults: a systematic review. *BMC Public Health.* 2015; 15: 255. DOI: 10.1186/s12889-015-1591-y.
2. Дедов И. И., Шестакова М. В., Викулова О. К., Железнякова А. В., Исаков М. А. Эпидемиологические характеристики сахарного диабета в Российской Федерации: клинико-статистический анализ по данным регистра сахарного диабета на 01.01.2021. *Сахарный диабет.* 2021; 24 (3): 204–21.
3. Cichocka E, Wietchy A, Nabrdalik K, Gumprecht J. Insulin therapy — new directions of research. *Endokrynol Pol.* 2016; 67 (3): 314–24. DOI: 10.5603/EP.2016.0044.
4. Foster NC, Beck RW, Miller KM, Clements MA, Rickels MR, DiMeglio LA, et al. State of Type 1 Diabetes Management and Outcomes from the T1D Exchange in 2016–2018. *Diabetes Technol Ther.* 2019; 21 (2): 66–72. DOI: 10.1089/dia.2018.0384.
5. Wong E, Backholer K, Gearon E, Harding J, Freak-Poli R, Stevenson C, et al. Diabetes and risk of physical disability in adults: a systematic review and meta-analysis. *Lancet Diabetes Endocrinol.* 2013; 1 (2): 106–14. DOI: 10.1016/S2213-8587(13)70046-9.
6. Baek JH, Lee WJ, Kim BW, Kim SK, Kim G, Jin SM, et al. Age at Diagnosis and the Risk of Diabetic Nephropathy in Young Patients with Type 1 Diabetes Mellitus. *Diabetes Metab J.* 2021; 45 (1): 46–54. DOI: 10.4093/dmj.2019.0134.
7. Schiller B. Leading a Dialysis Organization: Role and Responsibilities of the Chief Medical Officer (Nephrologist Leadership in a Dialysis Provider Organization). *Adv Chronic Kidney Dis.* 2018; 25 (6): 485–9. DOI: 10.1053/j.ackd.2018.08.015.
8. Kaku K, Kitada H, Noguchi H, Kurihara K, Kawanami S, Nakamura U, et al. Living donor kidney transplantation preceding pancreas transplantation reduces mortality in type 1 diabetics with end-stage renal disease. *Transplant Proc.* 2015; 47 (3): 733–7. DOI: 10.1016/j.transproceed.2014.12.048.
9. Barlow AD, Saeb-Parsy K, Watson CJE. An analysis of the survival outcomes of simultaneous pancreas and kidney transplantation compared to live donor kidney transplantation in patients with type 1 diabetes: a UK Transplant Registry study. *Transpl Int.* 2017; 30 (9): 884–92. DOI: 10.1111/tri.12957.
10. Zech JC, Trepsat D, Gain-Gueugnon M, Lefrancois N, Martin X, Dubernard JM. Ophthalmological follow-up of type 1 (insulin-dependent) diabetic patients after kidney and pancreas transplantation. *Diabetologia.* 1991; 34 (1): 89–91. DOI: 10.1007/BF00587628.
11. Chow VC, Pai RP, Chapman JR, O'Connell PJ, Allen RD, Mitchell P, et al. Diabetic retinopathy after combined kidney-pancreas transplantation. *Clinical Transplantation.* 1999; 13 (4): 356–62. DOI: 10.1034/j.1399-0012.1999.130413.x.
12. Pearce IA, Ilango B, Sells RA, Wong D. Stabilisation of diabetic retinopathy following simultaneous pancreas and kidney transplant. *British Journal of Ophthalmology.* 2000; 84 (7): 736–40. DOI: 10.1136/bjo.84.7.736.
13. Глазунова А. М., Арутюнова М. С., Тарасов Е. В., Шамхалова М. Ш., Шестакова М. В., Мойсюк Я. Г. и др. Влияние сочетанной трансплантации почки и поджелудочной железы на динамику поздних осложнений у больных сахарным диабетом 1 типа. *Сахарный диабет.* 2015; 18 (2): 69–78.
14. Koznarová R, Saudek F, Sosna T, Adamec M, Jedináková T, Boucek P et al. Beneficial effect of pancreas and kidney transplantation on advanced diabetic retinopathy. *Cell Transplantation.* 2000; 9 (6): 903–8. DOI: 10.1177/096368970000900617.
15. Giannarelli R, Coppelli A, Sartini M, Aragona M, Boggi U, Vistoli F et al. Effects of pancreas-kidney transplantation on diabetic retinopathy. *Transplant International.* 2005; 18 (5): 619–22. DOI: 10.1111/j.1432-2277.2005.00108.x.
16. Shipman KE, Patel CK. The effect of combined renal and pancreatic transplantation on diabetic retinopathy. *Clinical Ophthalmology.* 2009; 3: 531–5. DOI: 10.2147/opth.s7141.
17. Ishibazawa A, Nagaoka T, Takahashi A, Omae T, Tani T, Sogawa K,

- et al. Optical Coherence Tomography Angiography in Diabetic Retinopathy: A Prospective Pilot Study. *Am J Ophthalmol*. 2015; 160 (1): 35–44. DOI: 10.1016/j.ajo.2015.04.021.
18. Agemy SA, Sripsema NK, Shah CM, Chui T, Garcia PM, Lee JG, et al. Retinal vascular perfusion density mapping using optical coherence tomography angiography in normals and diabetic retinopathy patients. *Retina*. 2015; 35 (11): 2353–63. DOI: 10.1097/IAE.0000000000000862.
 19. Nesper PL, Roberts PK, Onishi AC, Chai H, Liu L, Jampol LM, et al. Quantifying Microvascular Abnormalities with Increasing Severity of Diabetic Retinopathy Using Optical Coherence Tomography Angiography. *Invest Ophthalmol Vis Sci*. 2017; 58 (6): 307–15. DOI: 10.1167/iov.17-21787.
 20. Vujosevic S, Bottega E, Casciano M, Pilotto E, Convento E, Midena E. Microperimetry and fundus autofluorescence in diabetic macular edema: subthreshold micropulse diode laser versus modified early treatment diabetic retinopathy study laser photocoagulation. *Retina*. 2010; 30 (6): 908–16. DOI: 10.1097/IAE.0b013e3181c96986.
 21. Boned-Murillo A, Diaz-Barreda MD, Ferreras A, Bartolomé-Sesé I, Orduna-Hospital E, Montes-Rodríguez P, et al. Structural and functional findings in patients with moderate diabetic retinopathy. *Graefes Arch Clin Exp Ophthalmol*. 2021; 259 (12): 3625–35. DOI: 10.1007/s00417-021-05277-y.

THE INFLUENCE OF MIGRATION FACTOR ON THE ESTABLISHMENT OF MENSTRUAL FUNCTION IN GIRLS

Milushkina OYu¹, Popov VI², Skobolina NA¹, Bokareva NA¹, Astashkevich EV¹, Zakharova AA¹, Skobolina EV³ ✉

¹ Pirogov Russian National Research Medical University, Moscow, Russia

² Burdenko Voronezh State Medical University, Voronezh, Russia

³ Institute for Demographic Research of the Federal Research Sociological Center RAS, Moscow, Russia

The problems of migration are becoming increasingly important and have primary impact on women's and children's health. The aim of the study was to evaluate the influence of migration factor on the establishment of menstrual function in girls. The study enrolled 1,222 female undergraduate students of Moscow universities, born in 1995–2000, of diverse ethnicity. The data were collected in 2015–2020 by questionnaire method. The main group included 322 students classified as migrants and the comparison group included 900 students of local origin (Muscovites). Statistical processing of the data was carried out using Statistica 10.0 package (StatSoft; USA). Mean age at menarche constituted 151.35 ± 1.20 months in migrants and 150.88 ± 1.06 months in Muscovites ($p > 0.05$). For all participants, menarcheal age fell within the range of 11–15 years (normal). Other parameters of menstrual function were also similar between the groups and comparable to corresponding data collected in other countries.

Keywords: menstrual function, Muscovites, migrants, reproductive healthcare

Author contribution: all authors made equal contributions to the study and manuscript preparation.

Compliance with ethical standards: The study was approved by Local Ethical Board at Pirogov Russian National Research Medical University (Protocol № 159 of November 21, 2016). All participants provided informed consent for the study.

✉ **Correspondence should be addressed:** Natalia A. Skobolina
Ostrovityanova, 1, Moscow, 117997, Russia; skobolina_dom@mail.ru

Received: 24.03.2022 **Accepted:** 14.04.2022 **Published online:** 24.04.2022

DOI: 10.24075/brsmu.2022.017

ВЛИЯНИЕ ФАКТОРА МИГРАЦИИ НА СТАНОВЛЕНИЕ МЕНСТРУАЛЬНОЙ ФУНКЦИИ У ДЕВОЧЕК

О. Ю. Милушкина¹, В. И. Попов², Н. А. Скоблина¹, Н. А. Бокарева¹, Е. В. Асташкевич¹, А. А. Захарова¹, Е. В. Скоблина³ ✉

¹ Российский национальный исследовательский медицинский университет имени Н. И. Пирогова Минздрава России, Москва, Россия

² Воронежский государственный медицинский университет имени Н. Н. Бурденко, Воронеж, Россия

³ Институт демографических исследований Федерального научно-исследовательского социологического центра Российской академии наук, Москва, Россия

Проблемы миграции приобретают масштабное значение во всем мире оказывают влияние прежде всего на здоровье женщин и детей. Целью исследования было установить влияние фактора миграции на становление менструальной функции у девочек. С помощью анкетирования в период с 2015 по 2020 г. изучали становление менструальной функции и возраст менархе у 1222 студенток 1995–2000 года рождения различной этнической принадлежности, обучающихся на 1–2 курсах университетов г. Москвы. В основную группу вошли 322 студентки-мигрантки, в группу сравнения — 900 москвичек. Средний возраст менархе у мигранток составил $151,35 \pm 1,20$ месяца, у москвичек — $150,88 \pm 1,06$ месяца ($p > 0,05$). У участниц обеих групп возраст наступления менархе составил 11–15 лет, что соответствует норме. В группе мигранток средний возраст менархе не отличался от возраста наступления менархе у москвичек и сопоставим с данными, полученными в разных частях света.

Ключевые слова: менструальная функция, москвички, мигрантки, охрана репродуктивного здоровья

Вклад авторов: все авторы внесли эквивалентный вклад в исследование и подготовку публикации.

Соблюдение этических стандартов: исследование одобрено этическим комитетом РНИМУ им. Н. И. Пирогова (протокол № 159 от 21 ноября 2016 г.), все участницы подписали добровольное информированное согласие.

✉ **Для корреспонденции:** Наталья Александровна Скоблина
ул. Островитянова, д. 1, 117997, г. Москва, Россия; skobolina_dom@mail.ru

Статья получена: 24.03.2022 **Статья принята к печати:** 14.04.2022 **Опубликована онлайн:** 24.04.2022

DOI: 10.24075/vrgmu.2022.017

The national project “Demography” implemented in the Russian Federation since 2019 regards female reproductive health as one of the top priorities.

According to WHO, female reproductive health implies the ability to conceive and bear a child in the absence of sexually transmitted diseases and with access to the means of family planning, ensured safety and security of pregnancy and childbirth, and health maintenance for both the mother and the child. Female reproductive health depends on socio-economic, environmental, hygiene, cultural, and lifestyle factors [1].

Migration processes reflect the economic situation, which is a staple point for the new economic theory of migration. Recent changes in the migration policy of the Russian Federation have been associated with the increase in external and internal migration flows recorded by the Federal State Statistics Service [2].

The global increase in the rates of migration has primary impact on women's and children's health. In this context, protecting the reproductive health of adolescent girls is absolutely essential [3–5].

The age at menarche is considered a sensitive indicator reflecting the impacts of adverse factors (economic, social, etc.) on girls' health [6]. For instance, relocation to another part of the country may affect physical development, physiological rhythms, and ultimately the establishment of menstrual function [7].

A recent study focused on female immigrants in Moscow Region demonstrates that “migration” and “adaptation” are largely interconnected: changing the place of residence requires adaptation to new conditions and integration into new environments [8].

For Moscow Region, protection of the reproductive health of female migrants is especially relevant: according to official statistics, every seventh child in this region is born to a non-permanent female resident, i.e. interregional or international migrant [9].

This study aimed to evaluate the influence of migration factor on the establishment of menstrual function in girls.

METHODS

The study enrolled 1,222 female students of Moscow universities undergraduate year 1–2, born in 1995–2000, of diverse ethnicity. The data were collected in 2015–2020 by questionnaire method. The participants were aged 19.4 ± 0.3 years. The main group consisted of 322 students classified as internal or external migrants; the number of observations was determined as guaranteeing 95% reliability of the results based on the established guidelines by K. A. Otdelnova [10]. In terms of ethnicity, the main group was diverse and encompassed immigrants from North Caucasus and Central Asia (external migrants), as well as Russian citizens — Chechens, Ingushs, Dagestanis, Ossetians, Adygs, and other (internal migrants). In accordance with the UN's International Migration Statistics Practical Guide for the Countries of Eastern Europe and Central Asia, all of them were classified as long-term migrants because their stay in Moscow lasted 1 year or longer [11]. The comparison group consisted of 900 students of local origin (Muscovites). The inclusion criteria were as follows: beginning of menstrual function during stay in Moscow; compliance with sex and age requirements; studying at a university in Moscow; health group I–II; conventional lifestyle with regard to nutrition, physical activity, etc.; correct completion of the questionnaire. The exclusion criteria were as follows: the lack of informed consent for the study; onset of menstrual function before moving to Moscow; non-compliance with sex and age requirements; staying in other regions; studying in other educational institutions; health group III; non-conventional lifestyles including addictions; incorrect completion of the questionnaire. The data were formalized as the "Database for the study of menstrual function in adolescent girls (born in 1995–2000)", registration certificate 2020622018 of October 23, 2020.

Statistical processing was carried out using Statistica 10.0 package (StatSoft; USA). Compliance of variables to the law of normal distribution was verified at the initial stage of the analysis. The descriptive statistics used means (M), standard deviations

(σ), and Student's t -test for between-the-group comparison; the differences were considered significant at $p \leq 0.05$.

RESULTS

Mean age at menarche constituted 151.35 ± 1.20 months (12.5 years) in migrants and 150.88 ± 1.06 months (12.5 years) in Muscovites ($p > 0.05$). The 68% expectance intervals were 11 years 5 months to 13 years 7 months in migrants and 11 years 5 months to 13 years 6 months in Muscovites.

Apart from these characteristics, we analyzed menarcheal age distributions for the two groups of the study (Fig. 1).

Menarche at the age of 11 was reported by 5.3% of migrants and 9.2% of Muscovites. Menarcheal age distributions for the groups differed ($p \leq 0.05$). For Muscovites, the curve had smoother outline and showed a closer fit to the law of normal distribution; 35.8% of this group had menarche at the age of 13. For migrants, the curve had a major peak at 13 years (49.9% of the group) followed by a minor peak at 15 years (20.9% of the group). Equal major proportions of migrants and Muscovites had menarche at the age of 12–14 (73.8% in each group).

Other parameters of menstrual function for the studied cohort are illustrated in Figs. 2 and 3.

Overall, the studied parameters of menstrual function in migrants and Muscovites were similar. Shortened cycles (< 21 day, proimenorrhea) and prolonged cycles (> 35 days, opsomenorrhea) were reported by 2.0% and 7.0% of participants, respectively.

DISCUSSION

Menarcheal age and other parameters of menstrual function were similar between the groups and comparable to corresponding data for other countries.

A Portugal-based study enrolling 11,274 women showed a gradual decrease in menarcheal age in the course of the 20th century, by average 31.1 days every 5 years to the current figure of 12.0 ± 1.25 years [12].

A similar trend towards accelerated onset of puberty was observed in Taiwanese girls, with the average age at menarche constituting 11.35 ± 1.06 years [13].

A Poland-based survey enrolling 11,671 10–16-year-old girls in 1985–1986, 2005–2006, and 2015–2016 assessed the age at menarche with regard to socioeconomic

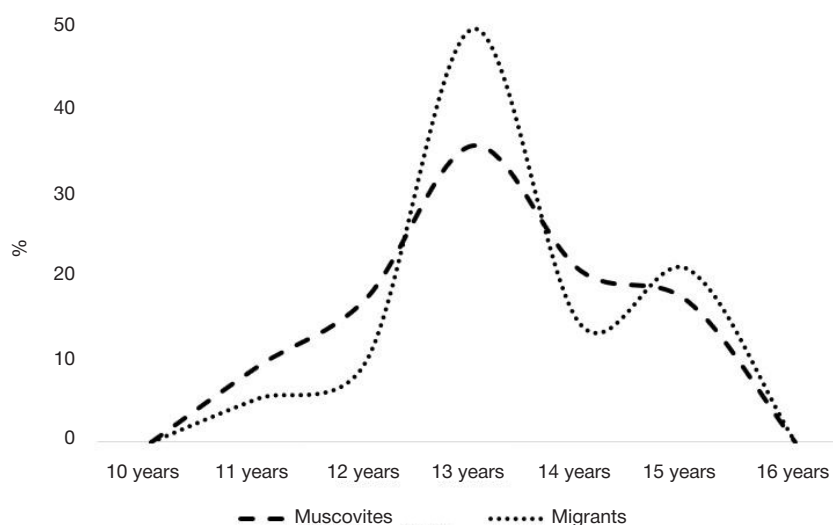


Fig. 1. Menarcheal age distributions for the two groups of the study

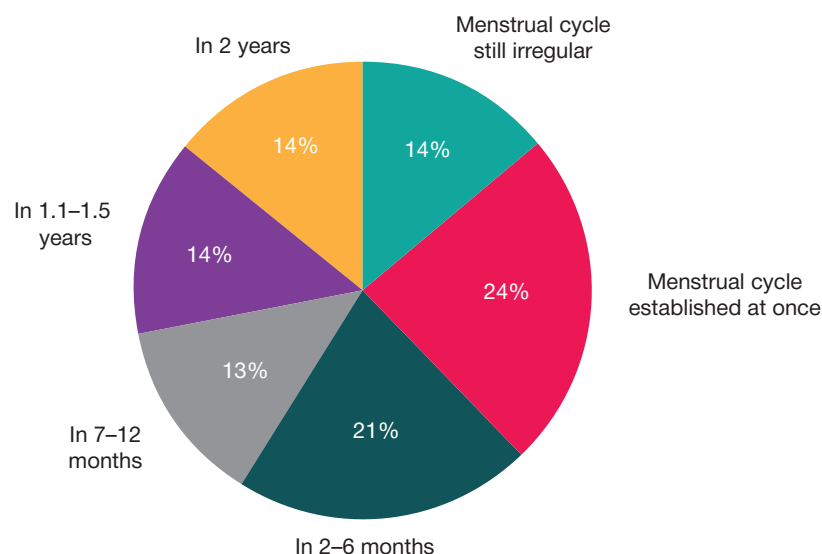


Fig. 2. Pie chart of the time spans from menarche to regular menstrual cycle

background (education level of parents, child number and overall socioeconomic status of the family) to reveal significant acceleration in all groups [14].

Consistently with these findings, the average age at menarche in 24,380 Mexican-born female participants was reduced from 13.3 years among girls born before the 1940s to 12.56 years among girls born in the 1980s and later on. Moreover, in all age cohorts, urban women had menarche significantly earlier than their rural peers. It should be noted that urban non-indigenous women and rural indigenous women were the youngest and the oldest at menarche, respectively [15].

Our findings can also be viewed in the context of other surveys enrolling female migrants.

One study, which encompassed 814 girls adopted internationally, compared menarcheal age between Chinese adoptees in North America and age-matched girls in China. The median menarcheal age in the adoptees constituted 12.37 years (95% CI 11.84–13.00 years), while the estimated prevalence of menarche at an age below 10 years was about 3%. In the non-adopted native residents of China, these parameters were similar [16].

However, a Denmark-based study demonstrated a significant 10–20-fold increase in the risks of precocious puberty for internationally adopted girls. Although the risks of precocious puberty depended on the country of origin, in

children who immigrated with their family these risks were elevated only slightly. Remarkably, older age of adopters significantly increased the risks of precocious puberty in adoptees regardless of their country of origin. The authors believe that psychosocial stressors in infancy and childhood may accelerate the onset of puberty: adoptees typically have a history of traumatic life events which may predispose them to precocious puberty [17].

In our study, none of the participants in both groups reported precocious puberty; on the contrary, a distinct subgroup of migrants (20.9%) reported a somewhat delayed menarche at the age of 15.

Migration, accompanied by a change in climatic and geographic conditions, has been shown to significantly interfere with menstrual function in 3% of girls, in terms of menstrual cycle length and regularity [18].

Other factors that negatively affect female reproductive health in adolescents include poor quality of medical care, unfavorable socio-economic conditions, low family income, and poor healthcare system at the state level [19–21].

According to a number of foreign studies, the negative impact of migration on women's health is reflected by the structure of pregnancy outcomes [22–24], including higher risks of pregnancy and childbirth complications and a 1.3-fold increase in neonatal morbidity among migrants compared with other social groups [3].

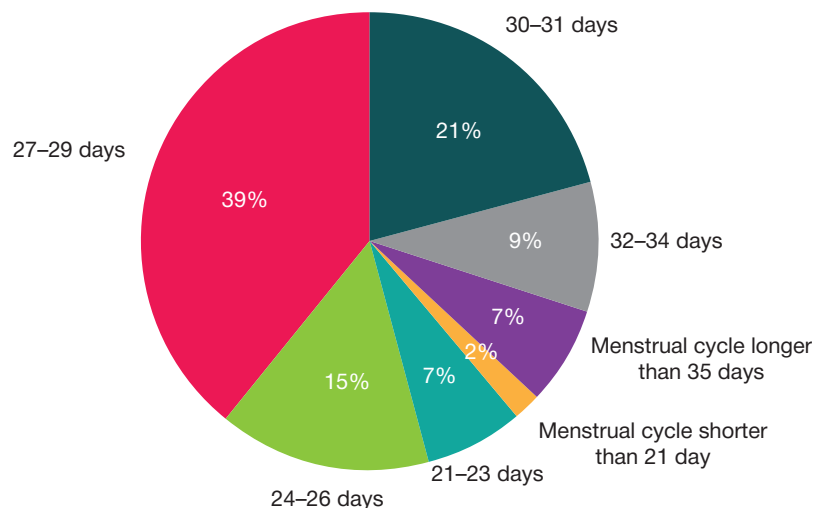


Fig. 3. Pie chart of the menstrual cycle lengths

CONCLUSIONS

In migrants and Muscovites, menarcheal age was similar, within the absolute range of 11–15 years (normal). Other parameters

of menstrual function were also similar between the groups and comparable to corresponding data for other countries. The research can be expanded to long-term migrants from non-CIS countries.

References

1. World Health Organization. Sexual and reproductive health. Доступно по ссылке (дата обращения 14.02.2022): <https://www.who.int/reproductivehealth/en/>.
2. Ioncev VA, Ryazancev SV, Ionceva SV. Novye tendencii i formy ehmiigracii iz Rossi. *Ehkonomika regiona*. 2016; 12 (2): 499–509. Russian.
3. Artyukhov IP, Li-Gi-Ru SYu, Gorbach NA, i dr. Zdorov'e beremennykh migrantok: analiz i vozmozhnosti upravleniya. *Zdravooxranenie Rossijskoj Federacii*. 2016; 60 (1): 27–30. Russian.
4. Fontanelli Sulekova L, Spaziente M, Vita S, et al. The pregnancy outcomes among newly arrived asylum-seekers in Italy: Implications of public health. *J Immigr Minor Health*. 2021; 23 (2): 232–9.
5. Alarcão V, Stefanovska-Petkovska M, Virgolino A, et al. Fertility, migration and acculturation (FEMINA): A research protocol for studying intersectional sexual and reproductive health inequalities. *Reprod Health*. 2019; 16 (1): 140.
6. Sergeyko IV, Lyutsko VV. Ocenka vliyaniya social'no-ehkonomicheskoy situacii na sostoyanie reproduktivnogo zdorov'ya naseleniya. *Sovremennye problemy nauki i obrazovaniya*. 2014; 1: 164. Russian.
7. Bokareva NA, Milushkina OYu, i dr. Vliyaniye migracii na fizicheskoe razvitiye detej. *Zdorov'e naseleniya i sreda obitaniya*. 2017; 8 (293): 40–43. Russian.
8. Izmerov NF, Izmerova NI, Bukhtiyarov IV, i dr. Osobennosti adaptacionnykh reakcij u zhenshhin-migrantok i riski narusheniya zdorov'ya pri razlichnoj dlitel'nosti prebyvaniya na territorii moskovskogo regiona. *Analiz riska zdorov'ya*. 2017; 2: 119–127. Russian.
9. Ryazancev SV, Karimov MM. Vliyaniye trudovoy migracii na reproduktivnoe zdorov'e (na primere tadzhikskix migrantov v Rossii). *Vestnik Tadzhikskogo gosudarstvennogo universiteta prava, biznesa i politiki*. 2013; 2 (54): 40–51. Russian.
10. Otdelnova K. A. Opredeleniye neobxodimogo chisla nablyudenij v social'no-gigienicheskix issledovaniyax. *Sb. trudov 2-go MMI*. 1980; 150 (6): 18–22. Russian.
11. Statistika mezhdunarodnoj migracii. *Prakticheskoe rukovodstvo dlya stran Vostochnoj Evropy i Central'noj Azii*. Zheneva: Organizaciya ob'edinennykh nacij, 2011. Доступно по ссылке (дата обращения 13.04.2022): https://unece.org/fileadmin/DAM/stats/publications/RUS_International_Migration_Statistics_Practical_Guide.pdf. Russian.
12. Queiroga AC, Silva RS, Santos AC, et al. Secular trend in age at menarche in women in Portugal born between 1920 and 1992: Results from three population-based studies. *Am J Human Biol*. 2020; 32 (5).
13. Chow JC, Chou TY, Tung T, et al. Recent pubertal timing trends in northern taiwanese children: Comparison with skeletal maturity. *J Chin Med Assoc*. 2020; 83 (9): 870–5.
14. Sączuk J, Wasiluk A, Pytasz P. Secular trend and social gradients in the menarcheal age of girls from eastern Poland between 1986 and 2016. *Anthropol Rev*. 2020; 83 (3): 279–91.
15. Marván ML, Castillo-López RL, del-Callejo-Canal DD, et al. Secular trends in age at menarche in 20th century Mexico: Differences by ethnicity, area of residency, and socioeconomic status. *Am J Human Biol*. 2020; 32 (6).
16. Hayes P, Tan TX. Timing of menarche in girls adopted from China: a cohort study. *Child Care Health Dev*. 2016; 42 (6): 859–62. DOI: 10.1111/cch.12393.
17. Teilmann G, Pedersen CB, Skakkebaek NE, et al. Increased risk of precocious puberty in internationally adopted children in Denmark. *Pediatrics*. 2006 Aug; 118 (2): e391–9. DOI: 10.1542/peds.2005-2939.
18. Isakova ZhK, Musuraliev MS. Vliyaniye processa migracii na menstrual'nyu funkciyu devushek iz vysokogornyx regionov. *Web of Scholar*. 2018; 2 (4) (22): 26–29.
19. Abramova VM, Chebotareva AA, Krivoshapova II, i dr. Sravnitel'nyy analiz vliyaniya reproduktivnogo zdorov'ya zhenshhiny na posleduyushhee stanovlenie menstrual'noj i reproduktivnoj funkcii u docherej. *Original'nye issledovaniya*. 2014; 2: 46–50. Russian.
20. Uvarova EV, Tarusin DI, Kuchma VR, i dr. Profilaktika narushenij reproduktivnogo zdorov'ya detej i podrostkov. *Voprosy shkol'noj i universitetskoy mediciny i zdorov'ya*. 2018; 2: 45–62. Russian.
21. Castellucci H, Viviani C, Boccardo G, et al. Gender inequality and sexual height dimorphism in Chile. *J Biosoc Sci*. 2021; 53 (1): 38–54.
22. Arcos E, Vollrath A, Sánchez X, et al. Motherhood in migrant women in Chile: A qualitative study. *Midwifery*. 2018; 66: 182–6.
23. Banounin BH, Adekunle AO, Oladokun A, et al. Impact of internal migration on fertility in cotonou, Benin republic. *Etud Popul Afr*. 2018; 32 (2): 4305–18.
24. Rokicki S, Montana L, Fink G. Impact of migration on fertility and abortion: Evidence from the household and welfare study of accra. *Demography*. 2014; 51 (6): 2229–54.

Литература

1. World Health Organization. Sexual and reproductive health. Доступно по ссылке (дата обращения 14.02.2022): <https://www.who.int/reproductivehealth/en/>.
2. Ионцев В. А., Рязанцев С. В., Ионцева С. В. Новые тенденции и формы эмиграции из России. *Экономика региона*. 2016; 12 (2): 499–509.
3. Артюхов И. П., Ли-Ги-Пу С. Ю., Горбач Н. А., и др. Здоровье беременных мигранток: анализ и возможности управления. *Здравоохранение Российской Федерации*. 2016; 60 (1): 27–30.
4. Fontanelli Sulekova L, Spaziente M, Vita S, et al. The pregnancy outcomes among newly arrived asylum-seekers in Italy: Implications of public health. *J Immigr Minor Health*. 2021; 23 (2): 232–9.
5. Alarcão V, Stefanovska-Petkovska M, Virgolino A, et al. Fertility, migration and acculturation (FEMINA): A research protocol for studying intersectional sexual and reproductive health inequalities. *Reprod Health*. 2019; 16 (1): 140.
6. Сергейко И. В., Люцко В. В. Оценка влияния социально-экономической ситуации на состояние репродуктивного здоровья населения. *Современные проблемы науки и образования*. 2014; 1: 164.
7. Бокарева Н. А., Милушкина О. Ю., и др. Влияние миграции на физическое развитие детей. *Здоровье населения и среда обитания*. 2017; 8 (293): 40–43.
8. Измеров Н. Ф., Измерова Н. И., Бухтияров И. В., и др. Особенности адаптационных реакций у женщин-мигранток и риски нарушения здоровья при различной длительности пребывания на территории московского региона. *Анализ риска здоровью*. 2017; 2: 119–127.
9. Рязанцев С. В., Каримов М. М. Влияние трудовой миграции на репродуктивное здоровье (на примере таджикских

- мигрантов в России). Вестник Таджикского государственного университета права, бизнеса и политики. 2013; 2 (54): 40–51.
10. Отдельнова К. А. Определение необходимого числа наблюдений в социально-гигиенических исследованиях. Сб. трудов 2-го ММИ. 1980; 150 (6): 18–22.
 11. Статистика международной миграции. Практическое руководство для стран Восточной Европы и Центральной Азии. Женева: Организация объединенных наций, 2011. Доступно по ссылке (дата обращения 13.04.2022): https://unece.org/fileadmin/DAM/stats/publications/RUS_International_Migration_Statistics_Practical_Guide.pdf.
 12. Queiroga AC, Silva RS, Santos AC, et al. Secular trend in age at menarche in women in portugal born between 1920 and 1992: Results from three population-based studies. *Am J Human Biol.* 2020; 32 (5).
 13. Chow JC, Chou TY, Tung T, et al. Recent pubertal timing trends in northern taiwanese children: Comparison with skeletal maturity. *J Chin Med Assoc.* 2020; 83 (9): 870–5.
 14. Saczuk J, Wasiluk A, Pytasz P. Secular trend and social gradients in the menarcheal age of girls from eastern Poland between 1986 and 2016. *Anthropol Rev.* 2020; 83 (3): 279–91.
 15. Marván ML, Castillo-López RL, del-Callejo-Canal DD, et al. Secular trends in age at menarche in 20th century Mexico: Differences by ethnicity, area of residency, and socioeconomic status. *Am J Human Biol.* 2020; 32 (6).
 16. Hayes P, Tan TX. Timing of menarche in girls adopted from China: a cohort study. *Child Care Health Dev.* 2016; 42 (6): 859–62. DOI: 10.1111/cch.12393.
 17. Teilmann G, Pedersen CB, Skakkebaek NE, et al. Increased risk of precocious puberty in internationally adopted children in Denmark. *Pediatrics.* 2006 Aug; 118 (2): e391–9. DOI: 10.1542/peds.2005-2939.
 18. Исакова Ж. К., Мусуралиев М. С. Влияние процесса миграции на менструальную функцию девушек из высокогорных регионов. *Web of Scholar.* 2018; 2 (4) (22): 26–29.
 19. Абрамова В. М., Чеботарева А. А., Кривошапова И. И., и др. Сравнительный анализ влияния репродуктивного здоровья женщины на последующее становление менструальной и репродуктивной функции у дочерей. Оригинальные исследования. 2014; 2: 46–50.
 20. Уварова Е. В., Тарусин Д. И., Кучма В. Р., и др. Профилактика нарушений репродуктивного здоровья детей и подростков. Вопросы школьной и университетской медицины и здоровья. 2018; 2: 45–62.
 21. Castellucci H, Viviani C, Boccardo G, et al. Gender inequality and sexual height dimorphism in Chile. *J Biosoc Sci.* 2021; 53 (1): 38–54.
 22. Arcos E, Vollrath A, Sánchez X, et al. Motherhood in immigrant women in Chile: A qualitative study. *Midwifery.* 2018; 66: 182–6.
 23. Banounin BH, Adekunle AO, Oladokun A, et al. Impact of internal migration on fertility in cotonou, Benin republic. *Etud Popul Afr.* 2018; 32 (2): 4305–18.
 24. Rokicki S, Montana L, Fink G. Impact of migration on fertility and abortion: Evidence from the household and welfare study of accra. *Demography.* 2014; 51 (6): 2229–54.

CHRONIC NON-TREATED POSTERIOR FRACTURE-DISLOCATION OF THE SHOULDER

Egiazaryan KA, Ershov DS, Badriev DA ✉, Soshnikov DY

Pirogov Russian National Research Medical University, Moscow, Russia

Posterior fracture-dislocations often remain undiagnosed at initial medical attendance. In dislocation, the head of the humerus extends beyond the glenoid to form a zone of impaction, which “fixes” it. The injury is almost unidentifiable in standard frontal X-ray images. Meanwhile, continued fixation of the humerus in the state of posterior dislocation leads to a rapid progression of the traumatic impaction over up to 50% of the articular surface area. The associated damage to the articular lip of the scapula, rupture of the rotator cuff muscles, symptoms of shoulder instability after relocation, and severe pain syndrome require advanced treatments for this type of injury. Here we report a clinical case of anatomical neck fracture of the humerus with displaced consolidation, combined to posterior dislocation. To avoid subacromial impingement, instead of correcting the position of the head, we abandoned the reposition and performed an osteotomy with distal displacement of the greater tubercle of the humerus.

Keywords: posterior dislocation of the shoulder, fracture-dislocation of the shoulder, shoulder joint surgery

Author contribution: all authors made equal contributions to the study and preparation of the article.

Compliance with ethical standards: the study was approved by Ethical Review Board at the Pirogov Russian National Research Medical University (Protocol No. 202 of November 23, 2020) and carried out in compliance with ethical standards established by the Declaration of Helsinki; the patient provided written informed consent for data processing and publication.

✉ **Correspondence should be addressed:** Denis A. Badriev
Ostrovityanova, 1, Moscow, 117997, Russia; ill1dan@mail.ru

Received: 09.04.2022 **Accepted:** 15.04.2022 **Published online:** 29.04.2022

DOI: 10.24075/brsmu.2022.022

ЗАСТАРЕЛЫЙ ЗАДНИЙ ПЕРЕЛОМОВЫВИХ ПЛЕЧА

К. А. Егiazарян, Д. С. Ершов, Д. А. Бадриев ✉, Д. Ю. Сошников

Российский национальный исследовательский медицинский университет имени Н. И. Пирогова, Москва, Россия

Задние переломовывихи нередко являются недиагностированным повреждением при первичном обращении за медицинской помощью. Головка плечевой кости во время вывиха заходит за гленоид, на ней образуется зона импрессии, за счет которой она и «фиксируется». На рентгенограммах в стандартной прямой проекции практически невозможно заподозрить данное повреждение. В случае длительного нахождения плечевой кости в фиксированном заднем вывихе, импрессионное повреждение головки плечевой кости быстро прогрессирует, и может достигать 50% площади суставной поверхности. Ассоциированные с данной травмой повреждение суставной губы лопатки, разрыв мышц ротаторной манжеты, появление нестабильности плечевого сустава после устранения вывиха, выраженный болевой синдром требуют серьезного подхода к лечению данной патологии. В представленном клиническом случае у пациента кроме заднего вывиха был срастающийся со смещением перелом анатомической шейки плечевой кости. Чтобы избежать субакромиального импинджмента вместо исправления положения головки мы отказались от репозиции и произвели остеотомию с перемещением большого бугорка плечевой кости дистально.

Ключевые слова: задний вывих плеча, переломовывих плеча, хирургия плечевого сустава

Вклад авторов: все авторы внесли равнозначный вклад в проведение исследования и подготовку статьи.

Соблюдение этических стандартов: исследование одобрено этическим комитетом РНИМУ им. Н. И. Пирогова (протокол № 202 от 23 ноября 2020 г.), выполнено в соответствии с этическими стандартами Хельсинской декларации; пациент дал согласие на обработку и публикацию персональных данных.

✉ **Для корреспонденции:** Денис Айдарович Бадриев
ул. Островитянова, д. 1, г. Москва, 117997, Россия; ill1dan@mail.ru

Статья получена: 09.04.2022 **Статья принята к печати:** 15.04.2022 **Опубликована онлайн:** 29.04.2022

DOI: 10.24075/vrgmu.2022.022

Posterior dislocations of the shoulder are rare and account for 2–5% of all cases of shoulder dislocation. Posterior dislocations complicated by a fracture of the proximal metaphysis of the humerus are exceptionally rare and constitute about 0.9% of fracture-dislocations of the shoulder, corresponding to 0.6 cases per 100,000 people [1, 2].

At initial medical attendance, posterior dislocations of the shoulder escape correct diagnosis in 60% of the cases. Meanwhile, after 6 weeks of the humeral head dislocation the injury becomes chronic [3]. The median interval between the injury and final diagnosis constitutes 8 months [4].

Here we report a clinical case of chronic non-treated posterior dislocation of the shoulder with a reverse Hill-Sachs lesion involving about 25% of the articular surface, accompanied by a fracture of the anatomical neck of the humerus with varus displacement, in order to illustrate the complexity of diagnostics and treatment for such conditions.

Clinical case

Patient S., 37 years old, was admitted to our clinic. Two months before, he was injured by falling off a scooter. Immediately after the accident, the patient consulted an emergency room, where they performed clinical examination and a routine X-ray of the right shoulder joint in frontal projection (Fig. 1). The X-ray image revealed a fracture of the proximal humerus with minimal displacement of the fragments. The right upper limb was immobilized in a cast; the patient was advised to continue limb immobilization for 3 weeks and released with a recommendation to consult a local traumatologist at his place of residence. Next day, the patient attempted to visit the local trauma center, but there was no reception that day. The patient called an ambulance, which took him to one of the city hospitals, where they re-performed clinical examination and X-ray of the right shoulder joint in the same one frontal projection. Other

projections (lateral, etc.) were ignored, multispiral computed tomography (MSCT) was not performed either, so the correct diagnosis was missed again. Finally, as late as 3 weeks after the accident, another traumatologist recommended computed tomography (Fig. 2).

After receiving the results of instrumental examination, the patient re-applied to the doctor who recommended MSCT of the shoulder joint. However, the trauma center was not equipped with a computer, and the patient was re-addressed for a consultation in a hospital. Few days later, the patient was able to get to the hospital, where, on the MSCT basis, the posterior fracture-dislocation of the shoulder was finally identified; however, they recommended him to wait another few days until a specialist from another institution with appropriate experience would pay a visit. Under these unsatisfactory circumstances, the patient decided to independently consult at the Pirogov City Clinical Hospital No. 1, where, after clinical re-examination and study of the X-ray data, he was offered emergency hospitalization to prepare for surgical treatment.

At the time of admission to our clinic, the patient experienced significant limitations in the range of motion of the right shoulder joint: abduction — 25°, external rotation — 10°, internal rotation — 70°, and flexion — 65° (Fig. 3). No acute neurocirculatory reactions in the right upper limb were encountered.

The analysis of X-ray and MSCT data revealed the following features: a reverse Hill-Sachs lesion involving 25% of the total articular surface area of the humeral head; a fracture of the anatomical neck of the humerus with varus displacement; a fracture of the greater tubercle with proximal displacement (the tubercle protruded significantly above the articular surface). On top of that, all fractured areas showed distinct osseous consolidation, whereas the humerus had long remained in a position of fixed posterior dislocation.

In such injuries, the area of impacted fracture is one of the main factors predisposing to subsequent recurrence of shoulder dislocation [5]. Cases with > 25% of the articular surface affected usually require surgical treatment to restore the shoulder joint "stability" [2, 6].

Known surgical options for this pathology include transfer of the lesser tubercle (McLaughlin procedure); filling the defect in articular surface of the head with the subscapularis muscle tendon (Neer's modified method); subcapital rotational osteotomy (Weber's procedure); and shoulder arthroplasty (implants) [3]. Our selection of surgical tactics involved an algorithm proposed by Paparoidamis et al. on the basis of systematic literature review [7].

In accordance with the algorithm, given that in our patient the impaction area reached 25% of the humeral articular surface, a decision was made to eliminate the dislocation and reconstruct the proximal humerus. After preoperative preparation, a standard deltopectoral approach to the shoulder joint was performed under general anesthesia in the beach chair position. At the first stage, an osteotomy of the lesser tubercle was performed with an oscillating saw. At the second stage, the long head tendon of the biceps was dissected from the scapula and sutured to the pectoralis major muscle, and the shoulder joint scars were removed; we further performed a soft tissue release for the rotator cuff muscles and an open reduction of the dislocation. At the third stage, in order to prevent subacromial impingement, we performed an oblique slide osteotomy of the greater tubercle and brought it down 10 mm distally. The decision to relocate the tubercle was made in connection with the increased risk of aseptic necrosis of the humeral head due to possible damage to the posterior circumflex humeral artery



Fig. 1. X-ray of the right shoulder joint on the day of injury

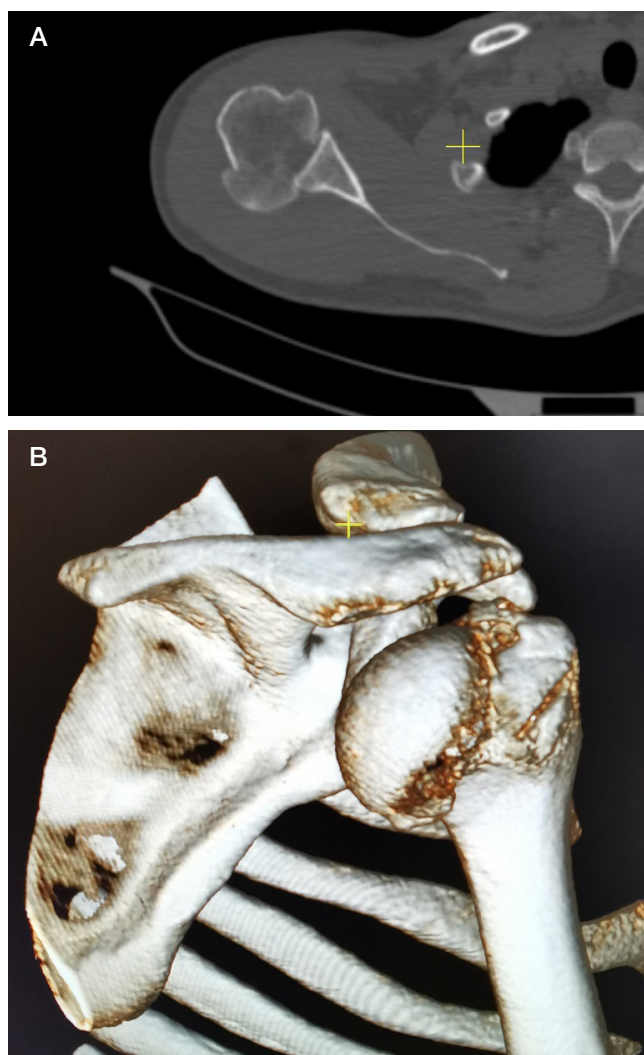


Fig. 2. Axial computed tomography scan of the right shoulder joint 3 weeks after injury (A). Volumetric reconstruction of the proximal part of the right humerus 3 weeks after injury (B)

upon the attempt to eliminate the varus displacement of the head [8]. At the fourth stage, the fragments of the humeral head and the reduced greater tubercle were fixed with a premodeled plate for osteosynthesis of the proximal humerus. The fifth stage consisted of a modified McLaughlin procedure: the lesser tubercle was relocated and fixed with a screw in place of the impaction defect in the articular surface of the humeral head. The wounds were sutured in layers. Aseptic dressings were applied. The right upper limb was immobilized with an abductor splint in the external rotation position.

The postoperative period proceeded smoothly. The sutures were removed on day 14. The immobilization of the upper limb in the abduction splint lasted 4 weeks, and the patient wore a standard arm sling for another 2 weeks. The patient received physiotherapy and physical rehabilitation with a coach starting from day 1 after surgery. The rehabilitation protocol emphasized strict immobilization of the right upper limb in the position of abduction to 60° in neutral rotation during the first 4 weeks after surgery. After that, passive recovery of the right shoulder joint mobility was carried out for 2 weeks, accompanied by immobilization of the right arm in a standard sling. The active locomotor rehabilitation of the operated limb was commenced 6 weeks after surgery.

Control X-rays performed 12 weeks, 6 months, and 1 year after surgery revealed progressive consolidation of the humeral neck fracture, preserved congruence of the articular surfaces in the shoulder joint, and no signs of aseptic necrosis in the humeral head (Fig. 4).

The function of the shoulder joint was assessed using the Constant Shoulder Score: the indicators increased from 24/100 at the time of admission to 88/100 at 12 months of observation, which corresponds to an excellent treatment outcome. The DASH and ASES scores at 12 months of observation were also interpreted as excellent [9] (Fig. 5).

Discussion

Fracture-dislocation of the shoulder occurs rarely and tends to escape correct primary diagnosis both clinically and radiographically, even in patients who seek medical help



Fig. 3. The patient before surgery

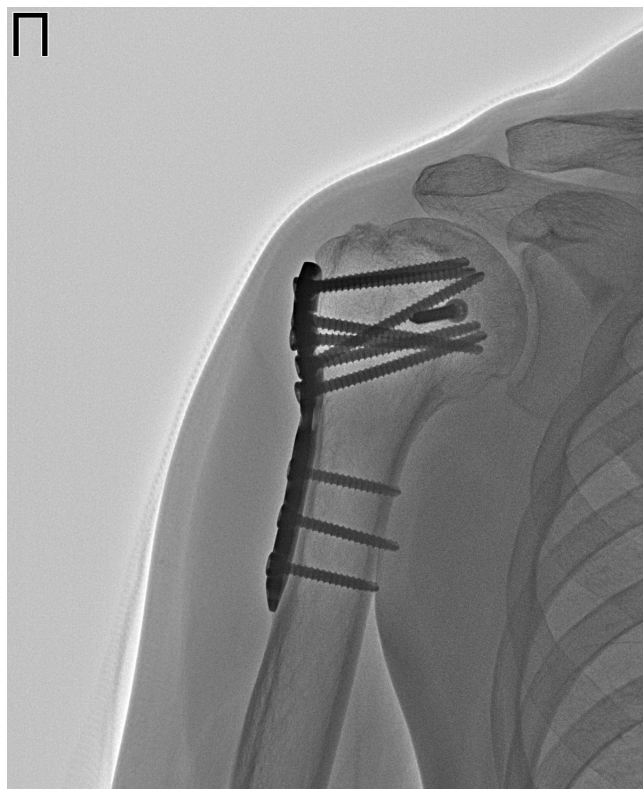


Fig. 4. X-ray of the right shoulder joint 12 months after surgery



Fig. 5. The patient 12 months after surgery

joint. The quality of long-term functional results crucially depends on the earliest possible diagnosis of fracture-dislocation and its urgent surgical treatment. [10, 11].

The most common types of fracture encountered in fracture-dislocations of the shoulder are impression injury to the articular surface of the head (the so-called reverse Hill-Sachs fracture; 29%) and fractures of the surgical neck (18.5%), the lesser tubercle (14.3%), and the greater tubercle (7.8%) of the humerus [12]. Fractures of the humeral diaphysis, scapula, or clavicle are encountered in 6% of the patients.

CONCLUSION

Routine X-ray radiography of the shoulder joint in frontal projection does not afford reliable determination of the humeral head dislocation. The lack of complementary projections poses

a threat of misdiagnosis. Delayed application for medical help, as well as conservative treatment because of incorrect diagnosis, significantly impairs the long-term functional outcome. Our report demonstrates the need for mandatory X-ray radiography of the shoulder joint in at least two projections.

The choice of surgical tactics for such cases requires careful planning, accounting for the time elapsed since the dislocation, the volume of defect in the articular surface of the humerus, the presence of concomitant injuries in the glenoid and the ligamentous-tendon complex, as well as the patient's age and functional requirements for the shoulder joint. Our clinical example illustrates options for the treatment of posterior fracture-dislocation, including preservation of the varus displacement of the humeral articular surface and distalization of the greater tubercle. Our choice of treatment tactics led to an excellent functional outcome in the patient.

References

1. Robinson CM, Akhtar A, Mitchell M, Beavis C. Complex posterior fracture-dislocation of the shoulder: epidemiology, injury patterns, and results of operative treatment. *J Bone Jt Surg.* 2007; 89 (7): 1454–66.
2. Kowalsky MS, Levine WN. Traumatic posterior glenohumeral dislocation: classification, pathoanatomy, diagnosis, and treatment. *Orthop Clin North Am.* 2008; 39 (4): 519–33.
3. Schliemann B, Muder D, Gebmann J, Schildhauer TA, Seybold D. Locked posterior shoulder dislocation: treatment options and clinical outcomes. *Arch Orthop Trauma Surg.* 2011; 131 (8): 1127–34.
4. Hill NA, McLaughlin HL. Locked posterior dislocation simulating a 'frozen shoulder'. *J Trauma.* 1963; 3: 225–34.
5. Cicak N. Posterior dislocation of the shoulder. *J Bone Jt Surg.* 2004; 86 (3): 9.
6. Sheehan SE, Gaviola G, Gordon R, Sacks A, Shi LL, Smith SE. Traumatic Shoulder Injuries: A force mechanism analysis — glenohumeral dislocation and instability. *Am J Roentgenol.* 2013; 201 (2): 378–93.
7. Paparoidamis G, Iliopoulos E, Narvani AA, Levy O, Tsiridis E, Polyzois I. Posterior shoulder fracture-dislocation: A systematic review of the literature and current aspects of management. *Chin J Traumatol.* 2021; 24 (1): 18–24.
8. Egiazyan KA, Ratyev AP, Ershov DS, Kuruch EA, Kuznetsov VN, Ovcharenko NV. Srednesrochnye rezul'taty xirurgicheskogo lecheniya pacientov s perelomovvixami plechevoj kosti. *Travmatologiya i ortopediya Rossii.* 2020; 26 (4): 68–79.
9. Lipina MM, Lychagin AV, Archipov SV, Kalinsky EB, Aliev RI, Yavliyva RH et al. Adaptaciya osnovnyx oprosnikov, primenyaemyx dlya ocenki sostoyaniya i funkci plechevogo sustava pri boli v sustave razlichnoj ehtiologii. *Kafedra travmatologii i ortopedii.* 2018; 34 (4): 44–50.
10. Egiazyan KA, Lazishvili GD, Ratyev AP, Danilov MA, Otvetchikova DI. Operativnoe lechenie povrezhdenij vrashhatel'noj manzhety plechevogo sustava. *Kafedra travmatologii i ortopedii.* 2017; 22 (2): 15–18.
11. Egiazyan KA, Ratyev AP, Gordienko DI, Grigoriev AV, Ovcharenko NV. Srednesrochnye rezul'taty lecheniya perelomov proksimal'nogo otdela plechevoj kosti metodom vnutrikostnogo osteosinteza. *Travmatologiya i ortopediya Rossii.* 2018; 24 (4): 81–88.
12. Dikic ID, Ganic ZD, Blagojevic ZD, Nho SJ, Romeo AA. Treatment of locked chronic posterior dislocation of the shoulder by reconstruction of the defect in the humeral head with an allograft. *J BONE Jt Surg.* 2010; 92 (1): 6.

Литература

1. Robinson CM, Akhtar A, Mitchell M, Beavis C. Complex posterior fracture-dislocation of the shoulder: epidemiology, injury patterns, and results of operative treatment. *J Bone Jt Surg.* 2007; 89 (7): 1454–66.
2. Kowalsky MS, Levine WN. Traumatic posterior glenohumeral dislocation: classification, pathoanatomy, diagnosis, and treatment. *Orthop Clin North Am.* 2008; 39 (4): 519–33.
3. Schliemann B, Muder D, Gebmann J, Schildhauer TA, Seybold D. Locked posterior shoulder dislocation: treatment options and clinical outcomes. *Arch Orthop Trauma Surg.* 2011; 131 (8): 1127–34.
4. Hill NA, McLaughlin HL. Locked posterior dislocation simulating a 'frozen shoulder'. *J Trauma.* 1963; 3: 225–34.
5. Cicak N. Posterior dislocation of the shoulder. *J Bone Jt Surg.* 2004; 86 (3): 9.
6. Sheehan SE, Gaviola G, Gordon R, Sacks A, Shi LL, Smith SE. Traumatic Shoulder Injuries: A force mechanism analysis — glenohumeral dislocation and instability. *Am J Roentgenol.* 2013; 201 (2): 378–93.
7. Paparoidamis G, Iliopoulos E, Narvani AA, Levy O, Tsiridis E, Polyzois I. Posterior shoulder fracture-dislocation: A systematic review of the literature and current aspects of management. *Chin J Traumatol.* 2021; 24 (1): 18–24.
8. Егизарян К. А., Ратьев А. П., Ершов Д. С., Куруч Е. А., Кузнецов В. Н., Овчаренко Н. В. Среднесрочные результаты хирургического лечения пациентов с переломами плечевой кости. *Травматология и ортопедия России.* 2020; 26 (4): 68–79.
9. Липина М. М., Лычагин А. В., Архипов С. В., Калинин Е. Б., Алиев Р. И., Явлиева Р. Х. и др. Адаптация основных опросников, применяемых для оценки состояния и функции плечевого сустава при боли в суставе различной этиологии. *Кафедра травматологии и ортопедии.* 2018; 34 (4): 44–50.
10. Егизарян К. А., Лазишвили Г. Д., Ратьев А. П., Данилов М. А., Ответчикова Д. И. Оперативное лечение повреждений вращательной манжеты плечевого сустава. *Кафедра травматологии и ортопедии.* 2017; 22 (2): 15–18.
11. Егизарян К. А., Ратьев А. П., Гордиенко Д. И., Григорьев А. А., Овчаренко Н. В. Среднесрочные результаты лечения переломов проксимального отдела плечевой кости методом внутрикостного остеосинтеза. *Травматология и ортопедия России.* 2018; 24 (4): 81–88.
12. Dikic ID, Ganic ZD, Blagojevic ZD, Nho SJ, Romeo AA. Treatment of locked chronic posterior dislocation of the shoulder by reconstruction of the defect in the humeral head with an allograft. *J BONE Jt Surg.* 2010; 92 (1): 6.

THE IMPACT OF IMAGE ORIENTATION ON DISTRIBUTION OF VISUAL FIXATIONS WHILE SOLVING SIMPLE COGNITIVE PROBLEMS

Nikishina VB¹, Petrash EA¹✉, Prirodova OF¹, Akhramenko RS¹, Danilova AV², Kuznetsova AA²

¹ Pirogov Russian National Research Medical University, Moscow, Russia

² Kursk State Medical University, Kursk, Russia

Optimization of the educational process, including distance learning, requires orderly arrangement of the information presented, which translates into the need to factor in oculomotor reactions accompanying the search for solutions to simple cognitive tasks. This need supports the relevance of the present study, which aimed to investigate the age-dependent parameters of the oculomotor reactions occurring in solving a simple cognitive task. The sample included 97 persons, 47 males and 50 females, ages 21 to 36. For the purpose of rating the oculomotor reactions, the sample was divided into age groups: 21–26 years ($n = 34$); 27–32 years ($n = 29$); 33–36 years ($n = 34$). The methodology that governed the rating procedures was developed by the authors of the study and relied on the Tobii EyeX eye tracking hardware and software solution (GazeControl software). The study revealed a significant correlation between orientation of the image (presentation angle) and distribution of the visual fixations: regardless of the image presentation angle and its properties (schematic monochrome or full color image), the fixations tend to fall predominantly into the top and left parts of the image (the first quadrant). Other findings include a) a significant dependence of the capability to solve simple cognitive tasks and recognize the contents of the image on the spatial orientation of the presented stimuli, and b) the number of errors made in image contents recognition increasing with age, this dependence being significant and observed for both the schematic monochrome image ($p_1 = 0.014$; $p_2 = 0.016$; $p_3 = 0.014$) and the full-color image ($p_1 = 0.015$; $p_2 = 0.015$; $p_3 = 0.017$). The researchers have also identified the significant angles of rotation of the presented face images that stably caused recognition errors.

Keywords: rating, oculomotor reactions, visual fixation, gaze fixation

Compliance with ethical standards: the study was approved by the Ethics Committee of Pirogov Russian National Research Medical University (minutes #211 of October 18, 2021) and conducted in conformity with the requirements of the Framework Legislation "On the Protection of Health of the Citizens." All participants signed the informed consent form agreeing to undergo examination

✉ **Correspondence should be addressed:** Ekaterina A. Petrash
Ostrovityanova st., 1, Moscow, 117997, Russia; petrash@mail.ru

Received: 07.02.2022 **Accepted:** 28.02.2022 **Published online:** 18.03.2022

DOI: 10.24075/brsmu.2022.011

ВЛИЯНИЕ ОРИЕНТАЦИОННЫХ ХАРАКТЕРИСТИК ИЗОБРАЖЕНИЯ НА РАСПРЕДЕЛЕНИЕ ЗРИТЕЛЬНЫХ ФИКСАЦИЙ ПРИ РЕШЕНИИ ПРОСТЫХ КОГНИТИВНЫХ ЗАДАЧ

В. Б. Никишина¹, Е. А. Петраш¹ ✉, О. Ф. Природова¹, Р. С. Ахраменко¹, А. В. Данилова², А. А. Кузнецова²

¹ Российский национальный исследовательский медицинский университет имени Н. И. Пирогова, Москва, Россия

² Курский государственный медицинский университет, Курск, Россия

Актуальность исследования обусловлена необходимостью организации предъявляемой информации с учетом параметров глазодвигательных реакций при решении простых когнитивных задач, что позволит оптимизировать процессы обучения, в том числе с использованием дистанционных образовательных технологий. Целью работы было изучить параметры глазодвигательных реакций при решении простой когнитивной задачи на узнавание по возрастной группе. Объем выборки составил 97 человек (47 мужчин и 50 женщин) в возрасте 21–36 лет. Нормирование показателей глазодвигательных реакций осуществляли по возрастным группам: 21–26 лет — 34 человека; 27–32 года — 29 человек; 33–36 лет — 34 человека, с использованием разработанной авторской методики и программно-аппаратного комплекса Tobii EyeX (ПО «GazeControl»). Показано, что ориентационные характеристики изображения (угол предъявления) статистически значимо соотносимы с показателями распределения фиксации взгляда. Распределение фиксации взгляда происходит преимущественно в верхней и в левой половинах изображения (первый квадрант) вне зависимости от угла наклона изображения и его характеристики (схематичное монохромное или полноцветное изображение). Выявлены значимая зависимость решения простых когнитивных задач и узнавания от пространственной ориентации предъявляемых стимулов и статистически значимое увеличение числа ошибок с увеличением возраста при узнавании как схематичного монохромного изображения ($p_1 = 0.014$; $p_2 = 0.016$; $p_3 = 0.014$), так и полноцветного изображения ($p_1 = 0.015$; $p_2 = 0.015$; $p_3 = 0.017$). Определены достоверно значимые углы поворота предъявляемых изображений лиц, приводящих к устойчивым ошибкам узнавания.

Ключевые слова: нормирование, глазодвигательные реакции, фиксации взгляда

Соблюдение этических стандартов: исследование одобрено этическим комитетом РНИМУ им. Н. И. Пирогова (протокол № 211 от 18 октября 2021 г.), проведено в соответствии с требованиями Основ законодательства «Об охране здоровья граждан»; все участники подписали информированное согласие на обследование.

✉ **Для корреспонденции:** Екатерина Анатольевна Петраш
ул. Островитянова, д. 1, г. Москва, 117997, Россия; petrash@mail.ru

Статья получена: 07.02.2022 **Статья принята к печати:** 28.02.2022 **Опубликована онлайн:** 18.03.2022

DOI: 10.24075/vrgmu.2022.011

Tracking of oculomotor reactions is a non-invasive technique employed to look into a wide range of cognitive and regulatory processes: attention, mnemonic activities, thinking categorization [1–3].

The technique enabling evaluation of the characteristics of oculomotor reactions in the context of a search for solutions to simple cognitive problems facilitates optimization of the educational processes, including those relying on the distance

learning technology [4–7]. A cognitive task triggers a number of activities: invoking initial representations, subsequent clarification, expansion, concretization, systematization, differentiation and generalization of knowledge. For the purpose of this study, we selected image recognition as a simple cognitive task. The object to be recognized is a face of a person, which is a complex social stimulus of perception [8–14]. The complexity of this object stems from the multiplicity

of details organized in a single symmetrical space that factors in the pre-determined location of each element. The social characteristics of the object allow identification of its species (human being) and gender.

We searched the Elibrary and Web of Science databases (using keywords "глазодвигательные реакции" (Russian for "oculomotor reactions") and "eye movements", respectively) covering papers published from 2015 to 2020). The results of this bibliometric analysis show that Russian researchers are less interested in the subject matter than their foreign counterparts. Oculomotor reactions were studied as part of research efforts in neurosciences, psychology, medical fields (ophthalmology and psychiatry), computer science, engineering. Papers dedicated to oculomotor reactions make up 29% of the total amount of the relevant scientific reports. Foreign studies focus on the many dimensions and diverse aspects of oculomotor reactions, which proves the technique selected for studying them is highly informative and universally applicable in the context of investigation of the processes of cognition and finding solutions to practical tasks, which rely on thinking and visual perception as such.

The attitude to the perceived stimuli and their categorization affects characteristics of oculomotor reactions, which means that oculomotor activity enables person's interactions with the world. Eye movements, acquiring the status of operations and actions, form integral oculomotor structures. Each of the formed oculomotor structures is associated with certain motives and conditions that govern how the person performs this or that activity [8, 9]. Eye tracking also allows measuring variables that are difficult to capture with other research methods, such as the exact spot looked at when receiving static or dynamic visual stimuli and instantaneous activation of the cognitive resources as required by the task [14].

The rating of oculomotor reactions in the context of visual perception activity is considered to be a statistical procedure that describes distribution of the studied parameters within an age group, and the subjects of such a rating should have no somatic and mental pathologies (be generally healthy). Optimization of the educational process, including distance learning, requires orderly arrangement of the information presented while factoring in the oculomotor reactions that accompany the search for solutions to simple cognitive tasks.

A study that aimed to determine how the number of gaze fixations affects face image recognition found that two fixations make the chances of successful recognition significantly better compared to a single fixation, regardless of whether the face in the image is familiar or not. Besides, the researchers have established that the greater number of fixations does not translate into better quality of recognition [15]. As a key takeaway, the authors concluded that two gaze fixations are enough to recognize a person's face in an image. The face scanning direction — left to right — should also be mentioned here as an observed general trend, same as the significant differences in localization of the gaze at the tutorial and actual identification stages of the experiment.

Studies of oculomotor reactions conducted by the Russian scientists support the aforementioned conclusion: a successful recognition of a person's face in an image takes two visual fixations [16].

The two factors affecting the parameters of oculomotor reactions are the task, which can alter the distribution of gaze fixations on the stimulus image, and the format of the image shown. We assessed the impact of these two factors on the oculomotor reactions in a set of two experiments. Both had the same task (recognize faces on the images) but different

formats of the images shown and varying angle at which they were presented. Studying the specific features of oculomotor reactions associated with contemplation of a face, researchers mainly focus on the number of gaze fixations in the substantial areas of the face image, those around eyes, mouth and nose [11–13]. However, they disregard spatial and orientational characteristics, i.e., directions (right-left, top-bottom) and angle of inclination of the image. Researchers also point to the significance of age as a factor affecting visual-spatial functions (field of visual perception, measurement by eye, etc). In adulthood, as opposed to the ages preceding it, correlations between the coordinate axes of visual sensory field are either unidentifiable or selective. Functional connections between the boundaries of the field of view in certain directions grow significantly weaker with age. In the perceptual visual field, on the contrary, structure of the perception becomes better pronounced with age, the improvement pattern coinciding with that of the spatial-discriminative capability of a person. Thus, the clearly shaped structure of visual perception enables maturation of this visual-spatial function and its maintenance at the optimal level throughout life [17].

Trying to identify the dominant characteristics (related to content or orientation) that affect the perception of a visual stimulus, we assumed that a change in the angle of inclination will condition distribution and number of fixations on the image. If content-related characteristics dominate the patterns of perception of an image of a face, the distribution of gaze fixations will remain relatively constant and concentrate in the areas of eyes, nose and mouth. If it is orientation that governs the perception, visual fixations will be predominantly registered in one of the four quadrants of the image, regardless of the angle at which it is shown.

The purpose of this study was to investigate the parameters of oculomotor reactions (number of fixations required to solve a simple cognitive task (recognition); distribution of fixations on specific areas of the image) associated with the process of solving simple cognitive tasks and assessed through the lens of age.

METHODS

The sample included 97 persons, 47 males and 50 females, ages 21 to 36 (early adulthood). For the purpose of rating the oculomotor reactions, the sample was divided into age groups: 21–26 years ($n = 34$); 27–32 years ($n = 29$); 33–36 years ($n = 34$). Forty-nine percent of the participants used vision correction aids (glasses or lenses).

The methodology that governed the rating procedures was developed by the authors of the study and relied on the Tobii EyeX eye tracking hardware and software solution (GazeControl software) [18]. The image recording frequency of a Tobii EyeX Controller is 90 Hz. The working distance of the eye tracker is 50–95 cm, the dimensions of the tracked space are 40–30 cm at a distance of 75 cm.

According to the methodology, the participants had to determine whether the two sequentially presented images showed faces of two different people or if both contained the face of the same person. The answers were registered for each pair of images presented.

The sets of stimuli included images of two types, schematic monochrome (Fig. 1A) and full-color. There were 45 pairs of face images of each type. They were divided into two groups: 15 pairs that had the face images central axis uninclined (0° angle), and 30 pairs that had the paired images differing from each other in the face's central axis inclination angle.

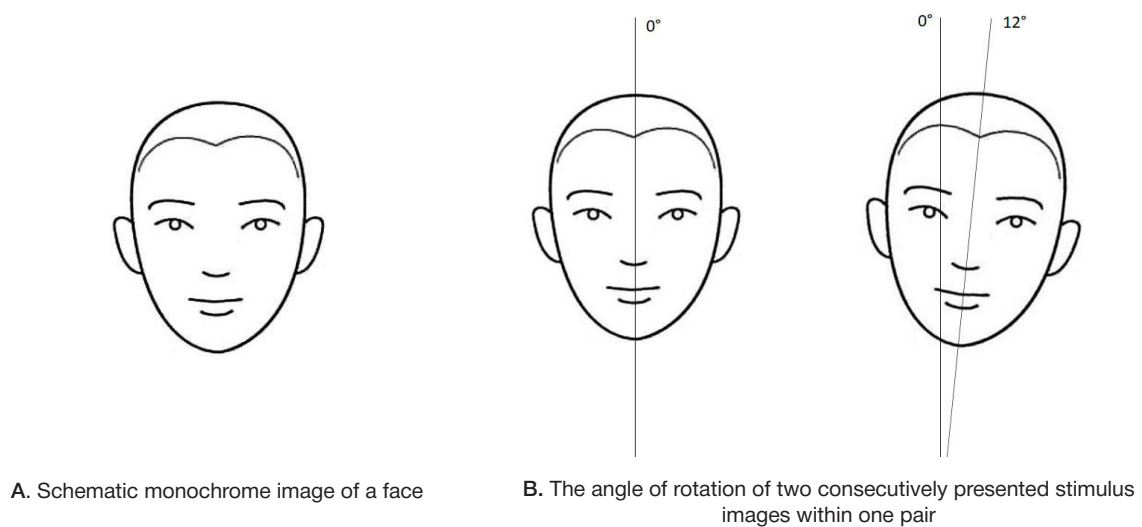


Fig. 1. Stimuli presented to the participants

Regardless of the direction, the inclination increment within a pair was 12°. This value was chosen based on the results of the earlier studies [19].

The resolution of all stimulus images was 1600–900 pixels, the files were .jpg. The monochrome images were made up of black lines showing the facial contours, hairline, ears, eyebrows, eyes, nose, mouth on a white background; the full-color face images were photographs of a man's face against a white background. Each image (including the interference images) was shown for 3 seconds, the duration of presentation of one pair of faces (including the interference) was 15 seconds; it took 7 minutes and 30 seconds to show one set of stimuli, and the total time of presentation of monochrome and full-color stimulus sets amounted to 15 minutes.

Between presentations of monochrome and full-color images, the participants rested for 2 min and could freely examine the environment and speak.

The number of errors made in judgments about the similarity or difference between the two face images enables assessment of the visual perception process specifics peculiar to the situations when the angle of the center line of one image differs from that of another image in a pair. The analysis of erroneous answers offered for a simple cognitive task (recognition) allowed identifying the shown face image's center line inclination angles that made recognition of the faces more difficult.

The study yielded heatmaps showing gaze distribution for each presented stimulus. The red zones on these maps, which were obtained based on the methodology developed by the study authors, are the registered and counted gaze fixations. The counting factored in the quadrants of the presented face.

For the purposes of statistical processing of the results we employed the methods of comparative statistics (Mann–Whitney U-test, use restrictions observed; Wilcoxon T-test, single sample and two sets of values obtained under different conditions). The three groups were compared in pairs.

RESULTS

The first step was the sample-wide analysis of the number of correctly recognized pairs of monochrome and full-color face images. Among the first findings was the fact that gender had no significant effect on the rate of recognition: both male and female participants have shown approximately similar results for schematic monochrome ($U = 246$; $p = 0.453$) and full-color ($U = 278$; $p = 0.887$) images. Same is true about vision correction: the participants that used vision correction aids were as likely to answer the experimental question correctly as their counterparts that did not rely on glasses or lenses ($U = 272$, $p = 0.597$ for monochrome images; $U = 264.5$, $p = 0.505$ for full-color images). These findings allow concluding

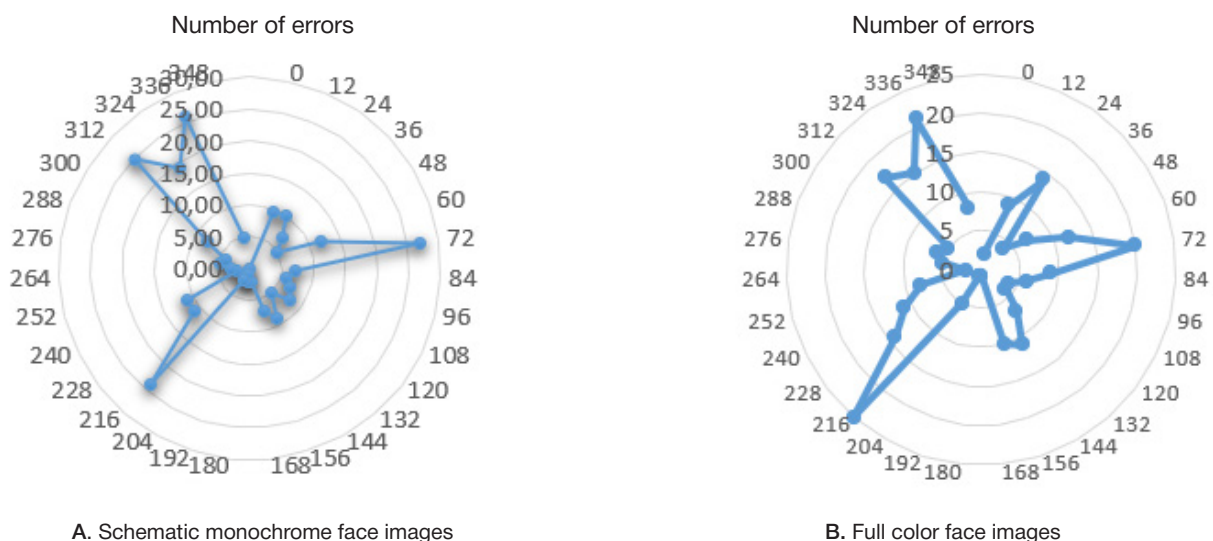


Fig. 2. Error distribution diagrams, sample-wide, recognition of monochrome and full-color face images depending on the angle of inclination of the image

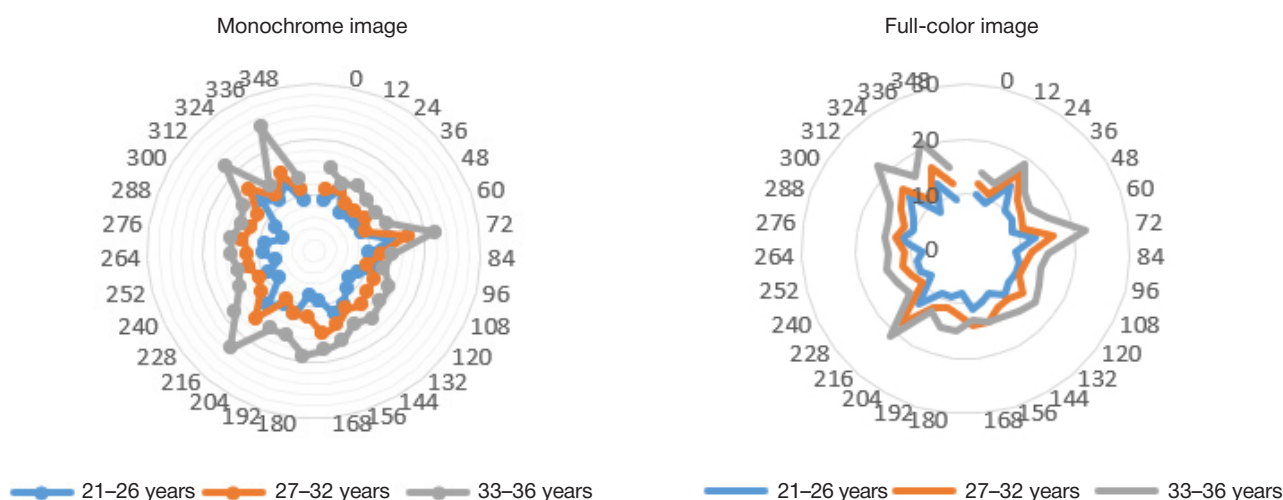


Fig. 3. Error distribution diagrams, by age groups, recognition of monochrome and full-color face images (simple cognitive task) depending on the angle of inclination of the image

that neither gender of the participants nor their level of visual acuity (and subsequent need for vision correction aids or lack thereof) influence the effectiveness of solving a simple cognitive task of recognizing face images significantly. Therefore, gender and vision correction aids are not the factors that have a significant effect on the process of recognition.

The next step was the analysis of effectiveness of solving a simple cognitive task (face recognition), which we conducted by calculating the indicators of the total number of errors and the total number of fixations (fixations were distributed over four

image quadrants). As a result, we identified the face inclination angles associated with the majority of errors (sample-wide, both monochrome and full-color images). Figure 2 shows these angles.

The presented face image center line angles that complicated solution of the simple cognitive task of face recognition (both monochrome and full-color images) were 72°, 216°, 312°, 324° and 336°. When the center axis of the second face image of a shown pair was rotated relative to the first one within the specified angles, the frequency of recognition



Fig. 4. Gaze fixation distribution diagrams, presentation of monochrome and full-color face images, depending on the angle of inclination of the image

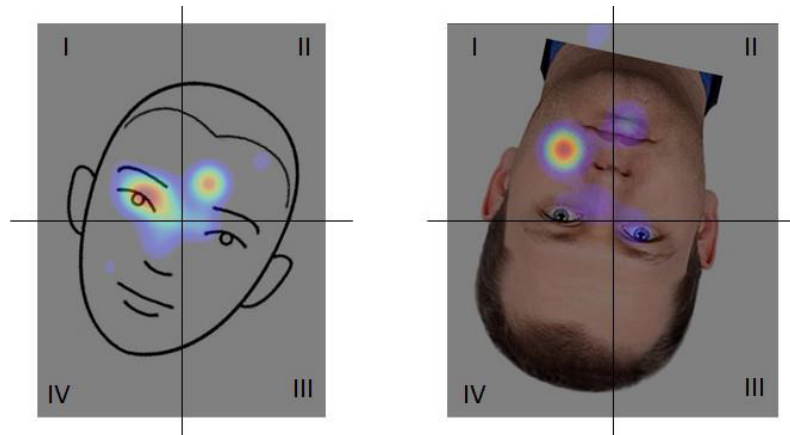


Fig. 5. Heat maps of gaze fixations, schematic monochrome and full-color images

errors averaged at 57.6%. It was also established that full-color images shown with their center lines at an angle of 24° (Fig. 2B) were recognized erroneously in a considerable number of cases, but this phenomenon was not observed for monochrome images (Fig. 2A).

The results of comparison of errors made in the three age groups allow drawing a conclusion that the amount of errors grows significantly with age (p_1 — indicator of significance of differences between age groups 21–26 and 27–32; p_2 — indicator of significance of differences between age groups 27–32 and 33–36; p_3 — indicator of significance of differences between age groups 21–26 and 33–36), this statement being relevant for both monochrome ($p_1 = 0.014$; $p_2 = 0.016$; $p_3 = 0.014$) and a full-color images ($p_1 = 0.015$; $p_2 = 0.015$; $p_3 = 0.017$) (Fig. 3).

Probably, the number of errors made progresses with age because of the growing reliance on stereotypes in visual perception and fading ability to perceive finer details. The nature of the errors made by the participants supports this assumption. The mistakes made by the members of the first age group (21–26 years old) had to do with the level of perceived details: shown same image several times in a sequence, each time at a different angle, they claimed that these were images of different faces. On the contrary, members of the third age group (33–36 years old), when shown images of different faces sequentially and with different central axis angles, claimed that the see one and the same image, i.e., their errors were associated with stereotyping of perception. Second group, ages 27 through 32, made errors of both types with equal frequency: they did not recognize similar face, thus making the error associated with

the level of perceived details, and they failed to recognize two images of the same face as such, which means the error has to do with perception stereotyping.

The paired comparison of the numbers of gaze fixations registered in the groups (using the Mann–Whitney U-test, $p < 0.05$) revealed no significant differences. Therefore, by this indicator the participants were united into a common research sample.

The errors quantity comparative analysis that aimed to investigate the difference between schematic monochrome and full-color image tasks (done using the Wilcoxon test, $p < 0.05$) revealed no significant differences ($T = 605$; $p = 0.763$). These findings allow concluding that the quality of the stimulus image (schematic monochrome or full-color) does not affect the effectiveness of solving a simple cognitive task of recognizing face images significantly. Recognition relies on gaze fixations on the key points of the face image, regardless of whether it is schematic monochrome or full-color. The gaze fixation points are concentrated on the eye line, nose and mouth.

At the next stage of the study we sought to investigate the number of gaze fixations by face quadrants, differentiating between schematic monochrome and realistic full-color images but disregarding age as a factor. In case of monochrome images, the quadrants received the maximum number of gaze fixations when the image was shown at the following angles: first quadrant — 24–96°; second quadrant — 216–348°; third quadrant — 192–228°; fourth quadrant — 108–180° (Fig. 4).

The results for full-color images were same as for monochrome images. Participants concentrated most on the first quadrant when shown the image with the central

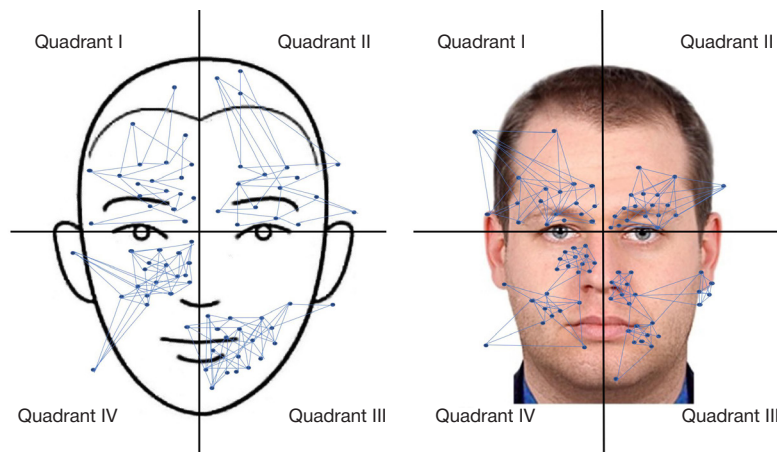


Fig. 6. An example of the trajectory of gaze movement, schematic monochrome and full-color images, regardless of age. * — dots indicate gaze fixations, lines — saccades

Table. Rated numbers of gaze fixations and the number of errors made in solving a simple cognitive task of face image recognition

Image inclination angle	Number of gaze fixations ($\bar{x} \pm \sigma$)	Number of errors (33–36 y. o.)	
		Recognition of schematic monochrome images ($\bar{x} \pm \sigma$)	Recognition of full color realistic images ($\bar{x} \pm \sigma$)
0	19.7 ± 4.66	–	–
12	20.1 ± 4.64	–	–
24	21.0 ± 4.26	–	–
36	15.4 ± 3.82	–	–
48	18.0 ± 5.41	–	–
60	21.4 ± 6.81	–	–
72	24.4 ± 5.86	27.04 ± 5.18	20.12 ± 4.29
84	18.5 ± 3.64	–	–
96	22.0 ± 4.10	–	–
108	18.3 ± 3.92	–	–
120	18.8 ± 3.08	–	–
132	19.6 ± 9.21	–	–
144	20.3 ± 4.98	–	–
156	19.0 ± 3.04	–	–
168	16.3 ± 3.78	–	–
180	15.4 ± 4.91	–	–
192	17.5 ± 3.08	–	–
204	17.6 ± 4.21	–	–
216	23.0 ± 5.02	24.37 ± 3.51	25.44 ± 5.07
228	16.4 ± 4.94	–	–
240	19.1 ± 4.60	–	–
252	18.3 ± 3.86	–	–
264	17.4 ± 3.71	–	–
276	15.3 ± 2.62	–	–
288	17.4 ± 3.73	–	–
300	16.5 ± 4.02	–	–
312	21.1 ± 4.59	25.26 ± 4.87	–
324	21.1 ± 3.59	–	–
336	24.8 ± 4.85	26.17 ± 6.09	21.09 ± 3.15
348	19.9 ± 3.88	–	–

axis inclined in the range between 0 and 84°, for the second quadrant the range was 240–324°, for the third — 192–276°, the fourth — 96–168 ° (Fig. 3).

In this study, we have experimentally confirmed that, in the context of solving a simple cognitive task, the distribution of gaze fixations depends on spatial orientation (center line inclination angle) characteristics of the face image, the differences registered being significant and statement applicable to both both schematic monochrome and full-color images. The general area that attracts gaze fixations regardless of the angle inclination of the central axis is the top left part of the face image, as illustrated by in heat maps (Fig. 5).

The uneven distribution of gaze fixations across the quadrants, as well as the multiple repetition of movement trajectories, should be noted as a general trend. The fixation points are concentrated in the area of the eye line, and the participants repeatedly returned their gaze to those points. For both schematic monochrome and full-color images we have also registered repeated fixations around the left zygomatic part (fourth quadrant) and the region of the mouth on the right (third quadrant) (Fig. 6).

Multiple gaze fixations in the nose area on the right (third quadrant) is a specific feature recorded for full-color images only. This spot attracts no fixations on a schematic monochrome image. The reason is that the orientational characteristics of a face image, i.e., eye shape, shape and size of nose, shape and size of lips, etc., determine the trajectory of eye movement and the areas of gaze fixations in the context a search for solutions to a simple cognitive task.

DISCUSSION

The rating procedure involves standardization; we found that neither gender nor vision correction aids (or lack thereof) have any significant effect.

Based on the results of the study, ranges of normative values for the number of gaze fixations were established. They factor in angle of inclination of the central axis of the presented face image and the number of errors made (as an indicator of the average number of fixations and standard deviation with confidence intervals). It should be noted that the rated numbers of fixations disregard age and quality of the stimulus (monochrome or full-color image) as factors, since

the comparative analysis revealed no significant differences imposed by them (see Table).

Based on the experimental data, the ranges of rated values were compiled for the third group (33–36 years) only, since this is the only group where the amount of errors exceeded 75% of the total number of cognitive tasks solved, with 75% being the threshold between likely random mistakes (below 75%) and a registerable pattern (above 75%). Moreover, the number of errors goes above 75% only at certain angles of the presented face image's central axis.

Thus, the age factor becomes significant for the simple cognitive task of face image recognition (both schematic monochrome and full-color images): the recognition success rate goes down as age goes up. The format of the presented image plays no significant part in the process of solving a simple cognitive problem of face image recognition. Repetition of the research procedure does not affect the results obtained.

The results of this study are consistent with findings of the previous studies. Earlier, it was proven that recognition effectiveness does not depend on the number of fixations provided there are at least two of them [20], which was also confirmed in our study. We have also confirmed the dependence of recognition success rate on the spatial-orientational characteristics of the stimulus image, the former, being a simple cognitive task, changing with the latter.

CONCLUSIONS

This study reliably establishes the effect orientational characteristics of the image have on distribution of gaze

fixations. Regardless of the angle of the image's center line and its properties (schematic monochrome or full color image), gaze fixations tend to amass in the first quadrant of the image, which is due to the cultural and historical traditions of reading and writing left to right and top to bottom. It can be assumed that people with different cultural and historical traditions will exhibit a different distribution of gaze fixations: Arab peoples read right to left, so the gaze fixations in their case will predominantly occupy the upper right part of the image (second quadrant). At the same time, the format of the presented image does not affect the distribution of gaze fixations. We have identified the angles of inclination of the presented image that complicate the search for solution to a simple cognitive task (comparison and recognition of two images). The maximum number of errors in image recognition (schematic monochrome and full color face images) was registered when the images were shown at the angles of 72°, 216°, 312°, 336°. The angle of 24° makes recognition of full-color images more difficult but has not such effect in case of schematic monochrome images; this fact is the result of a more complex structure of a full-color image in comparison with a schematic monochrome one. In addition to the eye lines and lips, gaze fixations were also registered in the areas of nose, forehead and ears when participants looked at full-color images. These elements are the criteria for comparison; the pattern did not repeat for schematic monochrome images. The practical significance of the results is that gaze fixation in the upper left part of the image allows avoiding erroneous characterization based on the interpretation of the relationship between the meaningful areas of the image and the parameters of oculomotor activity.

References

- Barabanshnikov VA, redaktor. *Ajtreking v psihologicheskoy nauke i praktike* M.: Kogito-Centr, 2015; 410 s. Russian.
- Belyaev RV, Grachev VI, Kolesov VV, Menshikova GYa, Popov AM, Ryabenkov VI. Okulomotornye reakcii v fiksacijah i sakkadah pri vizual'nom vosprijatii informacii. *Radioelektronika. Nanosistemy. Informacionnye tehnologii*. 2020; 12 (2): 263–74. DOI: 10.17725/rensit.2020.12.263. Russian.
- Ognev AS. *Ajtrekery v okulometricheskoy psihodiagnostike*. M.: Sputnik +, 2020; 134 s. Russian.
- Klimenskih MV, Lebedeva YuV, Malcev AV, Savelev VV. Psihologicheskie faktory jeffektivnogo onlajn-obuchenija studentov. *Perspektivy nauki i obrazovanija*. 2019; 6 (42): 312–21. Russian.
- Colliot T, Jamet É. Understanding the effects of a teacher video on learning from a multimedia document: an eye-tracking study. *Educational Technology Research and Development*. 2018; 66: 1415–33. DOI: 10.1007/s11423-018-9594-x.
- Hsieh R, Sato H. Evaluation of avatar and voice transform in programming e-learning lectures. *J Multimodal User Interfaces*. 2021; 15: 121–9. DOI: 10.1007/s12193-020-00349-5.
- Kaakinen JK. What Can Eye Movements Tell us about Visual Perception Processes in Classroom Contexts? Commentary on a Special Issue. *Educational Psychology Review*. 2021; 33 (4): 169–79. DOI: 10.1007/s10648-020-09573-7.
- Barabanshnikov VA. *Ajtreking. Metody registracii dvizhenij glaz v psihologicheskikh issledovanijah i praktike*. M.: Kogito-centr, 2014; 128 s. Russian.
- Barabanshnikov VA. *Okulomotornye struktury vosprijatija*. M.: Institut psihologii RAN, 1997; 380 s. Russian.
- Barabanshnikov VA, Ananeva KI, Haritonov VN. *Organizacija dvizhenij glaz pri vosprijatii izobrazhenij lica. Jeksperimental'naja psihologija*. 2009; 2 (2): 31–60. Russian.
- Demidov AA. Osobennosti okulomotornoj aktivnosti pri ocenke individual'no-psihologicheskikh osobennostej kommunikantov raznyh jetnosov po vyrazheniju ih lica. *Jeksperimental'naja psihologija*. 2020; 13 (1): 159–70. Russian.
- Dalton KM. Gaze fixation and the neural circuitry of face processing in autism. *Nature neuroscience*. 2005; 8 (4): 519–26. DOI: 10.1038/nn1421.
- Pelphrey KA. Visual scanning of faces in autism. *Autism Dev Disord*. 2002; 32 (4): 249–61.
- Tiadi A, Gérard CL, Peyre H., Bui-Quoc E, Bucci MP. Immaturity of Visual Fixations in Dyslexic Children. *Front Hum Neurosci*. 2016; 10: 58. DOI: 10.3389/fnhum.2016.00058.
- Hsiao JW, Cottrell G. Two fixations suffice in face recognition. *Psychological Science*. 2008; 19 (10): 998–1006.
- Rozhkova GI, Vasileva NN, Ognivov VV. Fiksacionnye dvizhenija glaz v estestvennyh uslovijah zritel'nogo vosprijatija. *Biomehanika glaza. Sb. trudov konferencii*. M.: MNIIGB im. Gelmgolca, 2009; s. 18–24. Russian.
- Rybalko EF. *Vozrastnaja i differencial'naja psihologija*. SPb.: Piter, 2001; 224 s. Russian.
- Prirodova OF, Nikishina VB, Morgun AN, Reznik-Orskaja MA, Petrash EA. Programma dlja apparatnogo kompleksa registracii i ocenki glazodvigatel'noj reakcii pri vypolnenii professional'no-kognitivnyh zadach (PAKROGR). *Svidetel'stvo o registracii programmy dlja JeVM* 2021614304, 23.03.2021. Zajavka # 2021610404 ot 18.01.2021. Russian.
- Hjuel D. *Glaz, mozg, zrenie*. M.: Mir, 1990; 239 s. Russian.
- Hsiao JW, Cottrell G. Two fixations suffice in face recognition. *Psychological Science*. 2008; 19 (10): 998–1006.

Литература

1. Барабанщиков В. А., редактор. Айттрекинг в психологической науке и практике М.: Когито-Центр, 2015; 410 с.
2. Беляев Р. В., Грачев В. И., Колесов В. В., Меньшикова Г. Я., Попов А. М., Рябенков В. И. Окуломоторные реакции в фиксации и саккадах при визуальном восприятии информации. Радиоэлектроника. Наносистемы. Информационные технологии. 2020; 12 (2): 263–74. DOI: 10.17725/rensit.2020.12.263.
3. Огнев А. С. Айттрекеры в окулометрической психодиагностике. М.: Спутник +, 2020; 134 с.
4. Клименских М. В., Лебедева Ю. В., Мальцев А. В., Савельев В. В. Психологические факторы эффективного онлайн-обучения студентов. Перспективы науки и образования. 2019; 6 (42): 312–21.
5. Colliot T, Jamet É. Understanding the effects of a teacher video on learning from a multimedia document: an eye-tracking study. Educational Technology Research and Development. 2018; 66: 1415–33. DOI: 10.1007/s11423-018-9594-x.
6. Hsieh R, Sato H. Evaluation of avatar and voice transform in programming e-learning lectures. J Multimodal User Interfaces. 2021; 15: 121–9. DOI: 10.1007/s12193-020-00349-5.
7. Kaakinen JK. What Can Eye Movements Tell us about Visual Perception Processes in Classroom Contexts? Commentary on a Special Issue. Educational Psychology Review. 2021; 33 (4):169–79. DOI: 10.1007/s10648-020-09573-7.
8. Барабанщиков В. А. Айттрекинг. Методы регистрации движений глаз в психологических исследованиях и практике. М.: Когито-центр, 2014; 128 с.
9. Барабанщиков В. А. Окуломоторные структуры восприятия. М.: Институт психологии РАН, 1997; 380 с.
10. Барабанщиков В. А., Ананьева К. И., Харитонов В. Н. Организация движений глаз при восприятии изображений лица. Экспериментальная психология. 2009; 2 (2): 31–60.
11. Демидов А. А. Особенности окуломоторной активности при оценке индивидуально-психологических особенностей коммуникантов разных этносов по выражению их лица. Экспериментальная психология. 2020; 13 (1): 159–70.
12. Dalton KM. Gaze fixation and the neural circuitry of face processing in autism. Nature neuroscience. 2005; 8 (4): 519–26. DOI: 10.1038/nn1421.
13. Pelphrey KA. Visual scanning of faces in autism. Autism Dev Disord. 2002; 32 (4): 249–61.
14. Tiadi A, Gérard CL, Peyre H., Bui-Quoc E, Bucci MP. Immaturity of Visual Fixations in Dyslexic Children. Front Hum Neurosci. 2016; 10: 58. DOI: 10.3389/fnhum.2016.00058.
15. Hsiao JW, Cottrell G. Two fixations suffice in face recognition. Psychological Science. 2008; 19 (10): 998–1006.
16. Рожкова Г. И., Васильева Н. Н., Огников В. В. Фиксационные движения глаз в естественных условиях зрительного восприятия. Биомеханика глаза. Сб. трудов конференции. М.: МНИИГБ им. Гельмгольца, 2009; с. 18–24
17. Рыбалко Е. Ф. Возрастная и дифференциальная психология. СПб.: Питер, 2001; 224 с.
18. Природова О. Ф., Никишина В. Б., Моргун А. Н., Резник-Орская М. А., Петраш Е. А. Программа для аппаратного комплекса регистрации и оценки глазодвигательной реакции при выполнении профессионально-когнитивных задач (ПАКРОГР). Свидетельство о регистрации программы для ЭВМ 2021614304, 23.03.2021. Заявка № 2021610404 от 18.01.2021.
19. Хьюбел Д. Глаз, мозг, зрение. М.: Мир, 1990; 239 с.
20. Hsiao JW, Cottrell G. Two fixations suffice in face recognition. Psychological Science. 2008; 19 (10): 998–1006.